A Complete Atlas of Recalibrated HST FOS Spectra of Active Galactic Nuclei and Quasars — Paper I: Pre-COSTAR Spectra

Ian N. Evans

Smithsonian Astrophysical Observatory, 60 Garden Street, MS-29, Cambridge, MA 02138

ievans@cfa.harvard.edu

and

Anuradha P. Koratkar

Goddard Earth Sciences and Technology Center, 3.002 South Campus, University of Maryland Baltimore County, 1000 Hilltop Circle, Baltimore, MD 21250

koratkar@umbc.edu

ABSTRACT

We have recalibrated all non-polarimetric, pre-*COSTAR*, archival *Hubble Space Telescope Faint Object Spectrograph* UV and optical spectrophotometry of active galaxies and quasars in order to extract uniformly calibrated spectrophotometric data for further detailed scientific investigations. The raw archival spectra have been recalibrated using the latest algorithms and calibration data. Spectral data contaminated by intermittent noisy diodes and cosmic ray events have been identified manually and eliminated. Wherever possible we have combined multiple observations of the same source to produce a single spectrum per object with the highest possible signal-to-noise ratio and covering the widest wavelength range, scaling the individual datasets to the same photometric scale where necessary. Detailed quality assurance has been performed to ensure that the merged object spectra are of the highest quality consistent with the limitations of the individual datasets and calibrations.

The recalibrated, merged object spectra are available in electronic form from http://hea-www.harvard.edu/FOSAGN/ and in the electronic edition.

We use this dataset to present statistics of the photometric accuracy in the wavelength overlap regions for observations spanning multiple gratings.

Subject headings: atlases—galaxies:active—galaxies:nuclei—galaxies:Seyfert—quasars:general—ultraviolet:galaxies

1. Introduction

Studies of Active Galactic Nuclei (AGN), especially the need to better understand the physics of the central engine, have progressed rapidly in recent years. Many of these investigations have exploited the characteristic emission-line spectra of the nucleus to elucidate the physics and energetics of the line emitting regions, which in turn constrain models of the ionizing source and thus provide important clues as to the nature of the central engine.

The technique of using emission-line intensity ratios to classify objects and investigate their ionization mechanisms is enhanced significantly by combining high quality UV and optical spectrophotometry. The *Hubble Space Telescope/Faint Object Spectrograph (HST/FOS)* data archive is a rich source of excellent high quality UV and optical spectrophotometric data that can be used for various scientific problems associated with individual objects or classes of objects. To effectively use these spectra to obtain meaningful scientific results, it is essential that the data be compared consistently and be calibrated as uniformly as possible.

As a first step in our study of AGN emission lines, we have recalibrated all pre-*COSTAR* (Corrective Optics Space Telescope Axial Replacement) archival *FOS* UV and optical spectrophotometry of AGNs and quasars, and are in the process of doing the same for the post-*COSTAR* data. In this paper we present the results of the recalibration of these large number of datasets from the pre-*COSTAR* era. A preliminary version of the data (Pesto et al. 1997) that comprise this atlas has recently been used by Kuraszkiewicz et al. (2002) to investigate the relationships between AGN emission-line equivalent widths and luminosity and redshift. These authors have performed multicomponent fits to the line profiles and present measured equivalent widths and FWHM for 28 UV and optical emission-lines.

1.1. The sample

We have obtained all *HST* pre-*COSTAR* (UV and optical) *FOS* spectrophotometric data for AGNs and quasars. The selection of observations to be retrieved from the *HST* data archive was made using the *Starview* interface to the archive. All *FOS* observations of targets that included one or more of the words "active," "AGN," "BL Lac," "BLR," "LINER," "Markarian," "Mkn," "Mrk," "NLR," "quasar," "QSO," "QSR," or "Seyfert" (irrespective of character case) in the target description were selected. In addition, a search of all targets that included the word "galaxy" in the target description was performed to identify any additional AGNs that were not listed using the above criteria. The search was restricted to observation dates prior to 1994 January 1 to select only pre-*COSTAR* observations (the data archive "*COSTAR*-deployed" flag was not used to select pre-*COSTAR*

observations, since this flag was not always populated correctly for some early observations.)

The resulting sample includes 964 spectra. Of these, 78 were rejected because of failed target acquisitions or other deficiencies (typically, lack of signal or gross inconsistency with other spectra of the same object, suggesting that the target was badly mis-centered or not included in the aperture). The remaining 886 datasets include observations of 221 distinct sources.

The data presented in this atlas were obtained using the *FOS* spectroscopic (`ACCUM`) and rapid readout (`RAPID`) observing modes. All the observations were conducted using standard substepping and overscanning, and the individual dispersed spectra therefore have a size of 2064 pixels. The `ACCUM` mode data in this atlas were read out every 2 minutes for the `FOS/RD` configuration and every 4 minutes for the `FOS/BL` configuration. The `RAPID` mode data have proposer specified readout times.

In a future paper, we will present a complete atlas of *FOS* spectra of AGN obtained after the installation of *COSTAR*.

Spectropolarimetry mode data are not included in this sample. Such data are not calibrated using the "average inverse sensitivity" (*AIS*) technique, and are not scaled to the white dwarf photometric reference scale that is employed for data obtained using other observing modes. The complexities inherent in deriving the reference data that are needed to calibrate existing spectropolarimetry mode datasets in a manner that is photometrically consistent with the `ACCUM` and `RAPID` mode datasets were deemed to outweigh the advantages of integrating the former data with the latter, especially since only a very limited volume of spectropolarimetry mode data is available.

2. FOS Instrument Description

Prior to its removal on 1997 February 13 during the *HST* second servicing mission, the *FOS* provided the only wide wavelength coverage spectrographic capability during the first 7 years of the *HST* mission.

The *FOS* employs independent optical paths for each of the two detectors in the instrument. Each optical path from the telescope included (in order) a set of wheel-mounted defining apertures, an optional waveplate assembly for polarization measurements, a grazing incidence mirror, an order sorting filter (if required), a collimating mirror, a set of wheel-mounted dispersers (high and low dispersion gratings, a prism, and a mirror for target acquisition), and finally the *Digicon* detectors.

Each *Digicon* incorporates a two-dimensional transmissive photocathode selected to maximize the quantum efficiency over a particular waveband. For the *FOS* blue side (`FOS/BL`) a bi-alkali (Na_2KSb) coating provided acceptable response from 1150 Å to 5400 Å, while a tri-alkali (Na_2KSbCs) coating covers the wavelength region 1620–8500 Å on the *FOS* red side (`FOS/RD`). Electrons emitted by the photocathode are deflected magnetically without magnification onto a linear array of 512 silicon diodes, where the electron pulses are counted. Prior to the installation of *COSTAR*, the size of a single *FOS* diode projected onto the sky is $\sim 0\farcs35$ in X (along the dispersion direction) and $\sim 1\farcs43$ in Y (perpendicular to the dispersion direction.)

The *FOS* accumulates photon counts by repeatedly executing a data acquisition cycle termed an *int*. Each *int* consists of a fixed period, called a *livetime* (typically ~ 0.5 s) during which signal counts from the diode array are accumulated, followed by a *deadtime* (typically ~ 0.01 s) during which no data are gathered and the instrument processes the data and performs other housekeeping operations.

To minimize the possible effects of instrumental problems on the science data, routine data-taking *substeps* and *overscans* the photoelectron beam by deflecting the electrons magnetically onto different locations on the diode array between successive *int*s in a predetermined pattern. Substepping improves the wavelength sampling of the spectrum by successively stepping the spectrum by a fraction (usually 1/4) of a diode width. Overscanning steps the spectrum by integer multiples of the diode width, thus smoothing out diode-to-diode sensitivity variations and insuring against lost data due to faulty or disabled diodes. Because of substepping and overscanning, a typical *FOS* spectrum contains 2064 pixels. For such spectra, the 16 pixels at each edge of the data have lower exposure times and the sensitivity of these pixels is more uncertain.

Since the *Digicon* detectors use magnetic deflection of electrons to determine which region of the photocathode is imaged onto the diode array, shielding the detectors from external magnetic fields is essential for proper operation. Unfortunately, the magnetic shielding was not adequate, so variations of the detector orientation relative to the Earth's geomagnetic field alter the magnetic deflection in the detectors. The effect, known as "geomagnetically-induced image motion" (GIM) is particularly pronounced for the `FOS/RD` side data, but is present also in `FOS/BL` data. For data obtained prior to 1993 April 05, a *post facto* correction algorithm that steps spectral data by integer pixel offsets in the *FOS* X (dispersion) direction to minimize image motion is applied during science data calibration. After that date, most science data were obtained with an on-board software patch that ameliorated GIM in both detector X and Y coordinates. However, residual GIM is still present in data calibrated using the standard instrument processing and the *STSDAS calfos* task. Residual

GIM is corrected in data calibrated using the *stpoa poa_calfos* task (see section 4) developed by the *Space Telescope European Coordinating Facility* (ST-ECF) *Post-Operational Archive* group.

The dispersed image for each aperture/disperser/detector combination is located on a different region of the *Digicon* photocathode. To calibrate the observed spectrum for the photocathode granularity and local sensitivity each aperture/disperser/detector combination requires individual flat field and inverse sensitivity calibration data. Due to changes over the lifetime of the *FOS* the location of the dispersed image on the photocathode varies and there are time dependent variations in the flat field structure. Although calibration data were obtained periodically during the life of the instrument, each science observation was not accompanied by individual calibration observations. Consequently, any calibrated science observation may have small ($<\sim 5\%$) photometric errors introduced due to time dependent variations of the instrument characteristics between the science observation and the calibration observations used during data processing.

3. FOS Target Acquisition

Although the blind pointing capability of *HST* is excellent, celestial target coordinate uncertainties, inherent limitations of the accuracy of the *Guide Star Catalog* (*GSC*) reference frame, and the small sizes of the *FOS* science apertures generally mandate that the target be acquired into the selected aperture by the *FOS* prior to obtaining scientifically useful data. This is particularly true if a reliable photometric scale is needed. Nearly all the targets described in this atlas were acquired by the *FOS* using either the binary search or peakup target acquisition modes. However, in order to save time, a handful of observations used the spacecraft blind pointing rather than acquiring the target with the *FOS*. Table 1 indicates the target acquisition strategy used for each observation.

The *FOS* binary search (`ACQ/BINARY`) target acquisition mode functions by first obtaining images of the center, lower ($-Y$), and upper ($+Y$) thirds of the `4.3` target acquisition aperture (the *FOS* aperture normally used for target acquisition, and the largest aperture available for science observations, subtended approximately $4\farcs3 \times 4\farcs3$ on the sky prior to the installation of *COSTAR*) by applying magnetic deflections in the *Digicon* to image the appropriate region of the photocathode onto the diode array. To locate the target in Y, the aperture region including the brightest source is then scanned up to 8 more times in a binary pattern using magnetic deflections that decrease by a factor of two in each step. This procedure should ultimately place the target on the $+Y$ or $-Y$ edge of the diode array. In the X direction (*i.e.*, along the diode array) the target position is identified by means of a

simple centroid above a threshold. Once the target location in X and Y is determined, the appropriate offset is computed and the telescope performs a small angle maneuver to center the target in the aperture.

Although the binary search target acquisition mode is quite efficient, the target search algorithm has limited dynamic range. If more than five target peaks are identified in either of the first three images, the acquisition fails. In the pre-*COSTAR* era this was a common failure mode because of the nature of the telescope point spread function resulting from the aberrated primary mirror. Additionally, if the binary search procedure could not place the target on the edge of the aperture after 8 steps, the acquisition failed and the telescope remained at its blind pointing position. In such cases, the target acquisition accuracy cannot be determined, and depends heavily on the accuracy of the target coordinates provided by the observer. This failure mode is common prior to the implementation on 1993 April 05 of the on-board GIM correction. A modification to the flight software to maneuver the telescope to the position of the final scan step after 8 steps regardless of whether or not the acquisition was successful was implemented on 1993 June 01. Since the final Y step size is 1/256 of the diode height ($\sim$5.5 milliarcseconds), the revised behavior generally leaves the target well centered in the aperture, and is significantly better than using the blind pointing position.

Studies by Caganoff, Tsvetanov, & Armus (1992) and Vassiliadis et al. (1994) indicate that successful pre-*COSTAR* era binary search target acquisitions of point sources are repeatable to better than $0\farcs1$, but with a systematic offset from the image center of order $0\farcs1$ primarily in the X direction. Prior to 1993 April 05, an additional uncertainty of up to $0\farcs15$ must be added in quadrature to the target location because of the uncorrected GIM.

Unlike binary search, which identifies the target position within the `4.3` aperture and then maneuvers the telescope to the correct pointing, the peakup (`ACQ/PEAK`) target acquisition mode scans the telescope in a user specified raster pattern to locate the target. This technique typically has the advantage of locating the target with the aperture actually used for the science observation, rather than identifying the target in the `4.3` aperture and then switching to the science aperture (although peaking-up in one aperture and then moving to another aperture is not prohibited). After the raster scan is completed, the telescope performs a small angle maneuver to the location of the raster scan point with the greatest number of counts. Accurately centering a target in a small aperture often requires a multi-stage peakup sequence, where successive peakups are performed to acquire the target in successively smaller apertures. There is no interpolation between the scan points. Therefore, the pointing accuracy of the peakup target acquisition mode depends on the details of the scan pattern used. Observations obtained in the pre-*COSTAR* era tend to have less

than optimal scan patterns, and less well designed target acquisition strategies in general, than post-*COSTAR* when a better understanding of the behavior of the target acquisition responses became available.

Besides acquiring the target directly using either the binary search or peakup acquisition modes described above, the acquisition procedure used for many targets includes some form of *blind offset*. There are two possible forms of blind offset. The first involves using one of the standard target acquisition modes to acquire a target other than the intended science target, and then performing a small angle maneuver to the science target. This would typically be done if there is good reason to believe that the morphology of the target may such that the target acquisition might not be successful, and there is a nearby star that could be acquired readily. The accuracy with which the science target will be centered in the aperture depends on both the target acquisition strategy and the knowledge of the relative positions of the science target and the offset star. If a *HST* image is available, then the latter can often be determined to better than $0\farcs01$.

The other form of blind offset involves acquiring the science target in one aperture and then performing a small angle maneuver to center the target in another (often larger) aperture. If the target is acquired by one detector and then an offset is performed to place the target in an aperture for the other detector, then the offset is termed a *sideswitch*. A sideswitch may be performed if the expected colors or morphology of the target make target acquisition unlikely to succeed in the detector used for the science observation. Another case where a sideswitch may be used is if observations using both detectors are required, but a high pointing accuracy is not needed for the "secondary" detector (*e.g.*, because a larger aperture is used). The accuracy of this form of blind offset depends on the knowledge of the relative aperture positions, which was of order $0\farcs1$ for most of the apertures, other than the `4.3` target acquisition aperture, that were recommended for use in the pre-*COSTAR* era.

4. Data Reduction and Analysis

Consistent and uniform calibrations are fundamental for addressing any observationally analyzed problem that requires access to an extensive set of spectrophotometric data. The original calibrations applied to the *FOS* archival data were neither consistently nor uniformly calibrated, for several reasons: (1) the *FOS* routine science data processing pipeline calibrations used early in the *HST* mission did not consider many instrumental effects that were later identified and quantified; (2) although the pipeline calibrations used the best calibration data available at the time, further analyses have enabled the calibration data to be refined, rendering the prior calibrations obsolete; (3) time varying calibrations are re-

quired to correctly model the behavior of the instrument, but earlier versions of the pipeline did not incorporate such capabilities; and (4) the pipeline photometric reference scale was changed from the mean UV reference flux system to a white dwarf model for G191-B2B in 1994, affecting the derived photometry dramatically. These problems are especially acute for pre-*COSTAR FOS* spectrophotometric data, and all spectropolarimetric data.

More recently, the *HST* archive at the ST ScI has begun providing on-the-fly recalibrated *FOS* data using the average inverse sensitivity calibration technique and the latest calibration data available from the ST ScI. The *FOS* chapters of the *HST Data Handbook* (Keyes 1998) provide a comprehensive discussion of the calibration status of the instrument using these data.

Although the on-the-fly recalibration does a good job, on average, for a given observation, several calibration improvements are still possible. In particular, data obtained using the most common *FOS* blue detector configurations benefit significantly from an enhanced version of the *FOS* calibration pipeline (*poa_calfos*) and associated calibration data developed by the ST-ECF *Post-Operational Archive* group. When compared to the *STSDAS calfos* task, the *poa_calfos* task improves both the photometric and dispersion calibrations by applying corrections for *FOS* optical bench temperature, Y-base errors, and residual GIM. The *stpoa* package that includes the *poa_calfos* task and associated software is described by Alexov et al. (2001), and is available from http://www.stecf.org/poa/FOS/.

Even though these tasks provide the best available automated routine calibrations of *individual FOS* spectra, they do not produce the best calibrated spectra of a given object for several reasons. First, there is no mechanism to tie together individual spectra obtained using multiple dispersers and apertures, even though comparison of the overlap regions of individual spectra can reduce the overall uncertainty in the photometric calibration of the source spectrum. Second, the standard calibrations do not eliminate hot pixels (for example, due to cosmic rays), and in many cases transient noisy diodes are not handled either. Noisy diodes typically evolve with time, so that often these can be identified only by careful visual inspection of the data products. Finally, to extract maximum information from the *FOS* data one must also investigate the data log for each spectrum to assess the impact on the data of observational problems, such as a failed target acquisition, and apply appropriate corrections as necessary. Full details of the recalibration process are included below in section 4.2.

The merged UV-optical AGN spectra presented here are based on individual observations that are recalibrated using current calibration data, and that include the additional processing steps described above. They are both more uniformly and more carefully calibrated than spectra extracted directly from the *HST* data archive.

4.1. "Average Inverse Sensitivity" Calibration

FOS data, other than spectropolarimetry mode data, that are processed using current versions of the *STSDAS* tool *calfos* and the *stpoa* tool *poa_calfos* are calibrated using the average inverse sensitivity method. This technique employs a photometric calibration that is generated by spline fits to *FOS* inverse sensitivity data derived from the average of many observations of several spectrophotometric standard stars (the white dwarf photometric reference scale).

Corrections for temporal, wavelength dependent, and aperture dependent variations of the instrumental response are predicted using empirical models. These models consider effects such as time-dependent telescope focus changes due to thermal heating ("breathing") of the optical telescope assembly as a function of orbital position, long term focus changes due to structural outgassing and mechanical shrinkage, time-dependent detector sensitivity degradation, and variations in aperture throughput due to the degraded pre-*COSTAR* point spread function. Decoupling these effects allows the instrumental inverse sensitivity to be determined more accurately by combining data from a large number of standard star observations, thus enhancing the photometric accuracy of the instrumental calibration.

As the *AIS* calibrations were developed over a period of several years, improvements have been applied progressively to correct for deficiencies and/or photometric discrepancies identified in recalibrated datasets. For example, detailed investigation of the photometric scales in the wavelength overlap regions between adjacent gratings for the set of data used to construct this atlas have been used to improve significantly the quality of the spline fits to the inverse sensitivity data near the grating edges.

4.2. Recalibration Steps

The uncalibrated data files for all of the datasets were retrieved from the *HST* archive. Observational datasets obtained prior to the development of the AIS calibration did not include all of the header keywords necessary to recalibrate the data. These keywords were added using the *STSDAS* task *addnewkeys*. The dataset headers were updated to reference the latest calibration reference files with the *getreffile* and *upreffile* tasks in *STSDAS*. After the headers were updated, the data were recalibrated using the most current calibrations.

All of the datasets obtained using the red detector, and some of the datasets obtained using the blue detector, were calibrated using version 3.2 of *calfos*. Most of the blue detector datasets were calibrated using version 1.1 of the task *poa_calfos*, after first updating the dataset headers using the *poa_preproc_fos* task.

4.3. Generation of a Single Spectrum per Object

Where possible, the recalibrated spectra have been combined carefully to produce the high quality, complete wavelength coverage UV-optical spectra. Before combining any spectra the observational consistency of the datasets is investigated.

4.3.1. Noisy Channel Removal

Although a correction is applied during the calibration process for known disabled diodes, the calibrated spectra may be contaminated by intermittently noisy diodes. Some of these diodes were disabled during later observations because they were consistently adding noise to the data. The contributions of undetected noisy diodes is removed from the individual datasets prior to merging spectra.

To identify datasets containing noisy channels, we used two main methods. For all `RAPID-READOUT` observations and for *ACCUM* mode observations with multiple readouts, the raw counts in each channel of each data group (readout) are compared with the raw counts in the same channel for the remaining groups. If the raw counts exceed the mean of the remaining groups by $5\,\sigma$ (assuming Poisson statistics), then the dataset is considered a candidate for further investigation. The purpose of this test is to identify datasets containing time-variable noisy diodes.

The second test compares the raw counts in each data group with a version of the data smoothed using a 4th order Savitzky-Golay filter with a width 9 channels (1 diode = 4 channels). Once again, if the raw counts exceed the smoothed version by $5\,\sigma$, then the dataset is considered a candidate for further investigation. This test is applied to all data groups of all datasets, and is intended to identify datasets with noisy diodes that are not time-variable.

Each candidate dataset is then inspected visually to determine whether the channels/groups identified by the automated tests are in-fact noisy. This visual inspection is needed because strong, narrow emission lines can sometimes fool the automated tests. Channels that are determined to be noisy based on the visual inspection are excluded when all of the calibrated data groups that comprise a single dataset are combined to produce a single spectrum. The corresponding data quality for intermittently noisy channels that have been corrected is set to 140 if the sampling is at least 50% of nominal after the noisy groups have been removed. If there is still some exposure but it is less than 50% of nominal sampling, then the data quality is set to 150. Finally, the data quality is set to 500 if the channel is noisy in all data groups. In all cases where the data quality of a channel is modified,

the larger of the previous and the new values is assigned, always preserving the worst data quality for that channel.

If the same intermittently noisy channels are identified in consecutive observations that were obtained using the same detector, then the preceding and succeeding observations are checked visually to determine whether the noisy channels persist, even if those datasets were not flagged by either of the automated checks.

4.3.2. Merging Individual Data Readouts

The first step involved in merging datasets to form a single spectrum per observation is to combine the data from the individual readouts that comprise a single dataset. For `RAPID-READOUT` observations each data group in the calibrated dataset is the flux-calibrated spectrum obtained during the corresponding readout, and is independent of the data obtained during other readouts. For these datasets the average spectrum during the observation is determined by computing the mean flux over all readouts. This is done on a per-channel basis, and excludes those groups for which a channel is identified as being intermittently noisy.

A similar process is used for *ACCUM* mode observations. In these calibrated datasets, each data group contains the flux-calibrated spectrum corresponding to the sum of the current and all previous readouts. An additional step is applied to remove the contribution of the previous readouts to each data group, after which the individual groups are combined using the procedure described above for the `RAPID-READOUT` observations.

After constructing a single spectrum per dataset, observations with the same instrumental configuration that were split across consecutive orbits are combined. An exposure-weighted mean spectrum of the datasets is computed after first verifying that the spectra are similar. If the data are not consistent, then this is usually indicative of an on-board problem such as a guide star reacquisition failure, and the anomalous dataset is discarded.

Whenever datasets are combined, the errors are propagated by assuming that 100% of the error is due to Poisson noise (photon statistical errors). Error contributions arising from uncertainties in calibration reference data are not propagated by the *calfos* tasks. If the data quality of any channel is revised, this is done by setting the output data quality equal to the maximum (worst) data quality of the input channels that contribute flux to that channel.

4.3.3. Merging Data from Multiple Dispersers

Observations with the same pointing (a single target acquisition, but which may be spread over several consecutive orbits) that are obtained using the same detector and aperture, but with different dispersers, are merged next.

Spectra obtained using the red detector are truncated blueward of 1610 Å because of the very rapid fall-off in the quantum efficiency of the red detector tri-alkali photocathode. Similarly, spectra obtained using the `G160L` grating are truncated redward of 2300 Å to eliminate contamination from second-order geocoronal Lyα.

Resampling to a common set of bins in wavelength space is used to merge data in the wavelength region where adjacent spectra from two dispersers overlap. The resampled wavelength bins in the overlap region are chosen so that their widths vary linearly from the the channel width of the one disperser at the start of the overlap region to the channel width of the adjacent disperser at the end of the overlap region. For example, consider adjacent UV spectra obtained with the `G130H` and `G190H` gratings. The resampled wavelength bins will have a width that is nearly the same as the channel width of the `G130H` spectrum at the blue end of the overlap region. At the red end of the overlap region, the bin width will be nearly the same as the channel width of the `G190H` spectrum. The number of resampled wavelength bins in the overlap region is chosen to be approximately equal to the arithmetic mean of the number of channel bins that span the overlap region in the adjacent spectra.

The contribution to a resampled wavelength bin of each channel of a spectrum being merged is determined by calculating the fractional width of the channel that overlaps the resampled wavelength bin, and assuming that within a single channel the flux is uniformly distributed. To provide a smooth transition over the edges of the wavelength overlap region, the final flux in each resampled wavelength bin is the mean of the resampled fluxes from the overlapping spectra, weighted linearly according to the bin position in the overlap region. The resampled flux from the blue spectrum is weighted by 100% at the extreme blue edge of the overlap region, and the red spectrum receives zero weighting. At the extreme red edge of the overlap region the weights are reversed. In the center of the overlap region the two overlapping spectra are weighted equally. Channels in the overlap region that have fluxes computed by interpolating and combining datasets have their data quality set to 70.

4.3.4. Data Scaling

The mean and standard deviation of the ratio of the individual fluxes from the overlapping datasets in the resampled channels is computed as part of the merging process. These

statistics and visual inspection of plots of the individual and combined fluxes are used to determine whether a photometric correction should be applied as part of the merging process. In general, the overlapping spectra have fluxes that agree within $3\,\sigma$, and no significant photometric shift is discernable in the overlap plots. This should not be surprising, since statistics gained through processing preliminary versions of the complete dataset presented in this atlas were used to constrain the photometric response of the AIS calibrations in the grating overlap regions.

Generally the mean flux ratios in the overlap regions agree within of order 5–10% (Table 2; see also Koratkar et al. (1997)), but occasionally deviations larger than $3\,\sigma$ are seen. If visual inspection of the overlap plots also indicates a clear and consistent photometric shift between the datasets being combined, then a correction is applied to one of the datasets to bring the fluxes into agreement. We assume that the higher flux is correct, and the dataset with the lower flux is scaled by a multiplicative factor so that the overlap regions agree. This is roughly equivalent to assuming that some fraction of the flux is lost, either due to less precise centering of the target in the aperture after a reacquisition, or due to loss of flux off the edge of the diode array because of errors positioning the dispersed spectrum on the array (Y-base errors). Both of these types of errors can result in flux losses of order 10% (Bohlin 1993; Evans 1993; Koratkar & Taylor 1993). Although the photometric loss due to these effects is, in principle, non-gray, detailed modeling of the flux loss versus wavelength requires precise knowledge of the source morphology and position within the aperture for each disperser that is in general not available. The error resulting from using a single multiplicative scale factor to correct the flux should be of order a few percent if the mean correction is of order 10%. Channels that have a scale factor applied are assigned a data quality of 60.

The value of the multiplicative factor applied to scale the dataset with the lower flux is the value of the mean flux ratio in the overlap region, excluding wavelength regions (a) with poor signal-to-noise ratio (S/N), typically a few channels near the very blue wavelength end of the grating spectrum; and (b) near strong emission or absorption lines, where the flux is a strong function of wavelength. The wavelength ranges that are included in the scale factor determination are selected by visual inspection of the overlap plots. However because only smoothly varying spectral regions with adequate S/N are used, the value of the mean flux ratio is only very weakly dependent on the exact wavelength ranges chosen.

In some cases, the overlap statistics indicate that a much larger scale factor is required to match two datasets. Such large corrections are needed only for datasets where a target acquisition failed and the target is partially out of the aperture. These datasets are excluded from consideration *unless* they provide the only available information for a particular object and spectral region. The photometric and spectral uncertainties are likely significant in the

wavelength regions spanned by datasets identified in Table 1 as having applied corrections $\gtrsim$ 30%. If the source is extended, then a different region of the source was sampled during the observation for which the target acquisition failed.

4.3.5. Wavelength Scale

No attempt is made to correct the wavelength scales of the spectra being merged to align precisely spectral features that are visible in the wavelength overlap region. Spectral features that are suitable for determining the relative shift between the grating wavelength zero-points are not present in the overlap regions for the vast majority of datasets in this sample.

Several sources contribute to the overall uncertainty of the wavelength scale zero-point for a given observation. These include mechanical effects, such as the repeatability of both the filter and grating wheel assembly (Koratkar & Martin 1995) and the aperture wheel (Dahlem & Koratkar 1994), and the accuracy and repeatability of the target acquisition strategy used when acquiring the data (Caganoff, Tsvetanov, & Armus 1992; Vassiliadis et al. 1994). Typically, the mechanical subsystems are repeatable with a root-mean-square (RMS) error of order 0.5 channels, and peak variations about 3–4 times larger. For point sources, target miscentering due to limitations in the pre-*COSTAR* target acquisition alignments may contribute twice this error, and observers often employed inadequate target acquisition strategies that further degrade the absolute wavelength reference. Koratkar et al. (1997) find that the ($1\,\sigma$) uncertainty of the absolute wavelength scale zero-point, referenced to galactic absorption lines, is of order 0.5 channels for contemporaneous observations of three bright Seyfert nuclei observed with the FOS. Near the ends of the individual grating spectra the uncertainty can be several times larger. Measurements of the long-term repeatability of the absolute wavelength scale zero-point using geocoronal Lyα also yield similar errors (Koratkar & Evans 1995).

To preclude the possibility of introducing spurious features into the output spectrum arising from differences between the wavelength scales of the spectra being merged, the overlap region is chosen carefully to exclude emission or absorption lines, or edges, *unless* visual inspection of the resampled input spectra indicates that the spectra are well matched. This ensures that the profile of any feature is not distorted in the merged spectrum. If multiple strong features are present (for example, a series of absorption lines) then the overlap region is chosen so that the entire set of features is treated together, *wherever possible*.

It is important to stress here that the separation in wavelength space between spectral

features that do not all fall on a single grating may be uncertain at a level of 2–3 channels. If precise velocity information is required with high accuracy, then detailed analysis of the individual spectra is essential.

4.3.6. Final Data Merging Steps

The next step applied to create the merged spectra is to combine observations with the same pointing that are obtained using the same aperture, but with different detectors. The operations performed are identical to those described above, and the same caveats apply. These single-pointing, single-aperture spectra are used as fiducials for determining whether additional spectra of the same target can be merged directly. We therefore designate these merged spectra *"reference spectra"*.

If multiple spectra were obtained during the same pointing, but with *different* apertures, then these will be merged next. The reference spectra for the different apertures being merged are first compared. If the reference spectra agree statistically ($3\,\sigma$) then the spectra can be combined. Rather than interpolate between the reference spectra, however, the individual readouts for all of the datasets that share a unique grating plus detector configuration are independently merged, using the procedure described earlier for combining multiple readouts for a single dataset. The resulting datasets are then reprocessed through the subsequent steps of the overall merging procedure.

Finally, spectra obtained at different times are merged, if appropriate. The procedure employed is exactly analogous to that used to merge spectra obtained with different apertures. The result is a single merged dataset that is the highest-quality spectrum of the target, covering the total observed wavelength range.

4.4. Disperser Overlap Region Statistics

Multiple disperser observations were obtained for approximately 2/3 objects in the present sample. In these cases, we define the *overlap ratio* between adjacent dispersers as the mean ratio of the fluxes measured by the two dispersers in the wavelength overlap region. The ratio is determined after the spectra in the overlap region are resampled to a common wavelength scale, as described in section 4.3.3, and is always computed by dividing the individual flux values from the dataset with the longer center wavelength by the corresponding flux values from the dataset with the shorter center wavelength. No data scaling is applied to the flux values used to compute the overlap ratios.

Histograms of the overlap ratio distributions are plotted for several different disperser combinations in Figures 1–7. The statistical mean, standard deviation, and median values corresponding to these figures are presented in Table 2. Note that in this table, the primary values quoted are computed from the set of overlap ratios in the range $0.8 \leq \text{ratio} \leq 1.25$ (the values for the entire set of data are given in parentheses). The reason for restricting the range of overlap ratios considered is that the most discrepant values, which significantly impact the determination of the mean and standard deviation, arise from datasets which suffer from target acquisition or guide star problems. Inspection of the figures indicates that the overlap ratio distributions are adequately characterized by considering only data within the chosen limits.

As can be seen from Table 2, in the wavelength overlap regions, spectra obtained using adjacent dispersers agree photometrically to a few percent accuracy, with deviations of order 5–7%. Photometric consistency is largely independent of detector and disperser, although cross-detector (blue/red) overlaps and overlaps involving the low resolution dispersers are marginally worse than same detector overlaps and those that include only high resolution dispersers. The slight increase in scatter in the cross-detector case is likely because the apertures for the two detectors are physically separated, so that either separate target acquisitions are required for each side, or a blind offset is required to move the target from one aperture to the other. In either case, there is an additional contribution to the scatter from target centering that is generally not present in the same detector case. For overlaps involving the low resolution dispersers, we note that most of the datasets use the `G160L` grating with the `FOS/BL` detector and the `4.3` aperture, and the overlaps include both a detector change and an aperture change.

Although a photometric uncertainty of order 5–10% may be present in the wavelength overlap regions, the overall photometric accuracy is expected to be somewhat better than this, since the spline fits to the inverse sensitivity data near the ends of the wavelength coverage of a disperser are not as well constrained as the fits in the center of the wavelength region. Consequently, the photometric accuracy near the center of the disperser's wavelength coverage may be significantly better than near the extremes.

Approximately 74% of datasets obtained as part of the same observation have fluxes in the wavelength overlap regions that are consistent to within 10%. The overlap statistics suggest that the photometric accuracy of our sample datasets is slightly worse than one might expect based on observations of calibration standard stars (Keyes 1998). This should not be surprising, since the standard star observations employ highly accurate (and time consuming) target acquisition strategies that were almost never used for routine (non-calibration) observations. In addition to less accurate target acquisition procedures, other calibration

uncertainties degrade the photometric accuracy of these datasets. For example, scattered light corrections for many AGNs with strong continua are much less well determined that is the case for photometric standard stars that have extremely well modeled UV–IR spectra.

We have included in Figure 7 and Table 2 overlap ratio data for a series of 39 monitoring observations of the nucleus of NGC 5548 obtained on successive days in 1993 April–May. All of the observations were identical, and consisted of a 3 stage peakup target acquisition followed by observations in with the `FOS/BL` detector and the `G130H` and `G190H` gratings in the `4.3` aperture. The overlap ratios of this very homogeneous dataset agree within a few percent, as expected, except for two outliers that are associated with observations that had target acquisition problems. These data are probably representative of the best that can be achieved using routine target acquisition strategies during the pre-*COSTAR* phase of the mission.

5. The Atlas

Where possible we have combined multiple observations to produce a single spectrum for each object with the highest possible signal-to-noise ratio and covering the widest wavelength range. The recalibrated spectra are available in electronic form from http://hea-www.harvard.edu/FOSAGN/ and in the electronic edition. They include calibrated wavelength, flux, error, and data quality files stored in FITS format.

In addition to providing electronic access as described above, in Figure 8 we present plots of the merged spectra that are further processed in a uniform way to display the salient features of each spectrum. Note that the processing described in this section is performed during the creation of the plots, and is *not* applied to the recalibrated spectra available in electronic form. The merged spectrum is split into two wavelength intervals, 1140–3300 Å and 3240–6820 Å, which are plotted separately. These wavelength ranges were chosen so that high resolution grating spectra for `G130H`, `G190H`, and `G270H` fall entirely on the first plot, irrespective of detector, and `G400H`, `G570H`, and `G780H` spectra fall entirely on the second plot.

Each plot is split further into three panels that are stacked vertically. The fluxed object spectrum is displayed in the upper panel. Prior to plotting, any noisy channels at the ends of the flux spectrum are removed. Spectra obtained using the *FOS* red detector are generally trimmed below 1610 Å since in almost all cases the spectra blueward of this wavelength are extremely noisy because of the rapidly decreasing photocathode sensitivity. If the S/N ratio around 1610 Å is either particularly good or particularly poor, the wavelength cutoff may

be varied based on visual inspection of the resulting plot. Spectra obtained using the `G160L` grating are trimmed redward of 2300 Å to ensure that second order geocoronal Lyα does not confuse the flux plot.

To maximize the visual detectability of features in the flux spectrum, where necessary we have smoothed the data prior to plotting. This is done by evaluating the local S/N ratio of the flux spectrum, and locally smoothing the data with an n-point boxcar filter when the S/N ratio is less than 3 : 1. For the first pass, n is set equal to 3 channels. If the local S/N ratio of the resulting smoothed data is still less than 3 : 1, then the filter length is increased to 5 channels and this new filter is applied locally to the original (unsmoothed) data. The iterative process is repeated until a maximum filter length of 9 channels is reached.

Locations of prominent emission-lines commonly observed in AGN spectra are marked at the top of the upper panel. The line positions are corrected to the rest frame of the source by scaling according to the redshift, which is printed in the upper right-hand corner of the plot, and is generally taken from Veron-Cetty & Veron (2000). Note that the presence of a marker for a particular line is not intended to imply that the line is detected in the object spectrum. Rather, the marker indicates where the line centroid would appear in the rest frame of the object. Similarly, locations of prominent geocoronal and galactic absorption lines are marked at the bottom of this plot panel.

The propagated statistical error is presented in the middle panel of each plot as a percentage of the calibrated flux value.

The bottom panel of each plot includes two sets of information. First, the wavelength coverage of each individual disperser contributing to the merged spectrum is marked. Note that this is not necessarily equal to the entire spectral range of the disperser and detector combination used in the observation, since the wavelength limits of the overlap regions may be have been modified as described in section 4.3.3. Second, the smoothing length of the local boxcar filter applied to the plotted data is shown in this panel.

6. Conclusions

Although individual *FOS* datasets can be retrieved from the *HST* data archive at the ST ScI, and are subject to on-the-fly reprocessing, high quality complete *per-object* spectra must be constructed by combining multiple datasets, and are thus not readily available.

To assist observers who need consistent, uniformly calibrated UV and optical spectrophotometry of AGNs and quasars, we have recalibrated all non-polarimetric, pre-*COSTAR*,

archival *FOS* datasets using the latest calibration data and software from both the ST ScI and the ST-ECF. We are currently recalibrating the complete set of post-*COSTAR FOS* AGN spectra, and the results of this work will be published in a future paper.

Multiple observations of the same source using different instrumental configurations (for example, using different detectors, dispersers, and apertures) are merged to form single per-object spectra. Observations of the same source obtained at different epochs are combined if the data are statistically matched (*i.e.*, there is no evidence of time-dependent variability in the data).

Extensive manual processing is required on a case-by-case basis to ensure that the merged object spectra are of the highest possible quality consistent with the limitations of the individual datasets. In each dataset, spectral channels contaminated by intermittent noisy diodes and cosmic ray events are identified and removed. Differences between the photometric scales of individual observations of the same source are identified and corrected as appropriate. Such differences arise typically because of failed or inadequate target acquisition strategies.

The recalibrated, merged object spectra are available in electronic form at http://hea-www.harvard.edu/FOSAGN/ and in the electronic edition. We present plots of each merged spectra that are further processed via adaptive smoothing. These plots allow the user to identify significant features of each spectrum quickly.

We thank Anne Gonnella, Sharon Pesto, and Elisa Blitz for retrieving archival data data and calibrating many of the data sets for preliminary versions of this atlas. The results of these early calibrations were ultimately fed back into the *FOS* calibration program to refine the photometric scales in the disperser overlap regions.

The authors would also like to thank our *FOS* colleagues Ralph Bohlin and Charles ("Tony") Keyes for numerous energetic discussions about all aspects of *FOS* calibrations.

We thank Paul Green and the H/RCULES collaboration for continuing to push us to complete and publish this atlas!

Finally, we would like to thank an anonymous referee for carefully considered comments and suggestions that have materially improved the quality of this paper.

Based on observations made with the NASA/ESA Hubble Space Telescope, obtained from the data archive at the Space Telescope Science Institute. ST ScI is operated by the Association of Universities for Research in Astronomy, Inc. under the NASA contract NAS 5-26555. Support for this work was provided by NASA through grant number AR-4364 from

the Space Telescope Science Institute, which is operated by AURA, Inc., under NASA contract NAS 5-26555. Publication of this work was supported in part by NASA through grant number NAG 5-8958.

This research has made use of the NASA/IPAC Extragalactic Database (NED) which is operated by the Jet Propulsion Laboratory, California Institute of Technology, under contract with the National Aeronautics and Space Administration.

REFERENCES

Alexov, A., Bristow, P. D., Kerber, F., & Rosa, M. R. 2001, POA/FOS Technical Report POA-FOS-2001-08, Garching: ST-ECF

Baldwin, J. A., Phillips, M. M., and Terlevich, R. 1981, PASP, 93, 5

Bohlin, R. C. 1993, FOS Instrument Science Report CAL/FOS-97, Baltimore: ST ScI

Caganoff, S., Tsvetanov, Z., & Armus, L. 1992, FOS Instrument Science Report CAL/FOS-81, Baltimore: ST ScI

Dahlem, M. & Koratkar, A. P. 1994, FOS Instrument Science Report CAL/FOS-131, Baltimore: ST ScI

Evans, I. N. 1993, FOS Instrument Science Report CAL/FOS-107, Baltimore: ST ScI

Keyes, C. D. 1998, HST Data Handbook, Version 3.1, Baltimore: ST ScI

Koratkar, A. P. & Evans, I. N. 1995, FOS Instrument Science Report CAL/FOS-142, Baltimore: ST ScI

Koratkar, A. P., Evans, I. N., Pesto, S., & Taylor, C. J. 1997, ApJ, 491, 536

Koratkar, A. P. & Martin, S. 1995, FOS Instrument Science Report CAL/FOS-145, Baltimore: ST ScI

Koratkar, A. P. & Taylor, C. J. 1993, FOS Instrument Science Report CAL/FOS-96, Baltimore: ST ScI

Kuraszkiewicz J. K., Green, P. J, Forster, K., Aldcroft, T. L., Evans, I. N., & Koratkar, A. 2002, ApJS, 143, in press

Pesto, S., Koratkar, A., Blitz, E., & Evans, I. N. 1997, in ASP Conf. Ser. 113: IAU Colloq. 159: Emission Lines in Active Galaxies: New Methods and Techniques, ed. B. M. Peterson, F. Cheng, & A. S. Wilson (San Francisco: ASP), 134

Vassiliadis, E., Bolhin, R. C., Koratkar, A. P., & Evans, I. N. 1994, FOS Instrument Science Report CAL/FOS-122, Baltimore: ST ScI

Veilleux, S. & Osterbrock, D. 1989, ApJS, 63, 295

Veron-Cetty, M. P. & Veron, P. 2000, ESO Sci. Rep., 19, 1

This preprint was prepared with the AAS LaTeX macros v5.0.

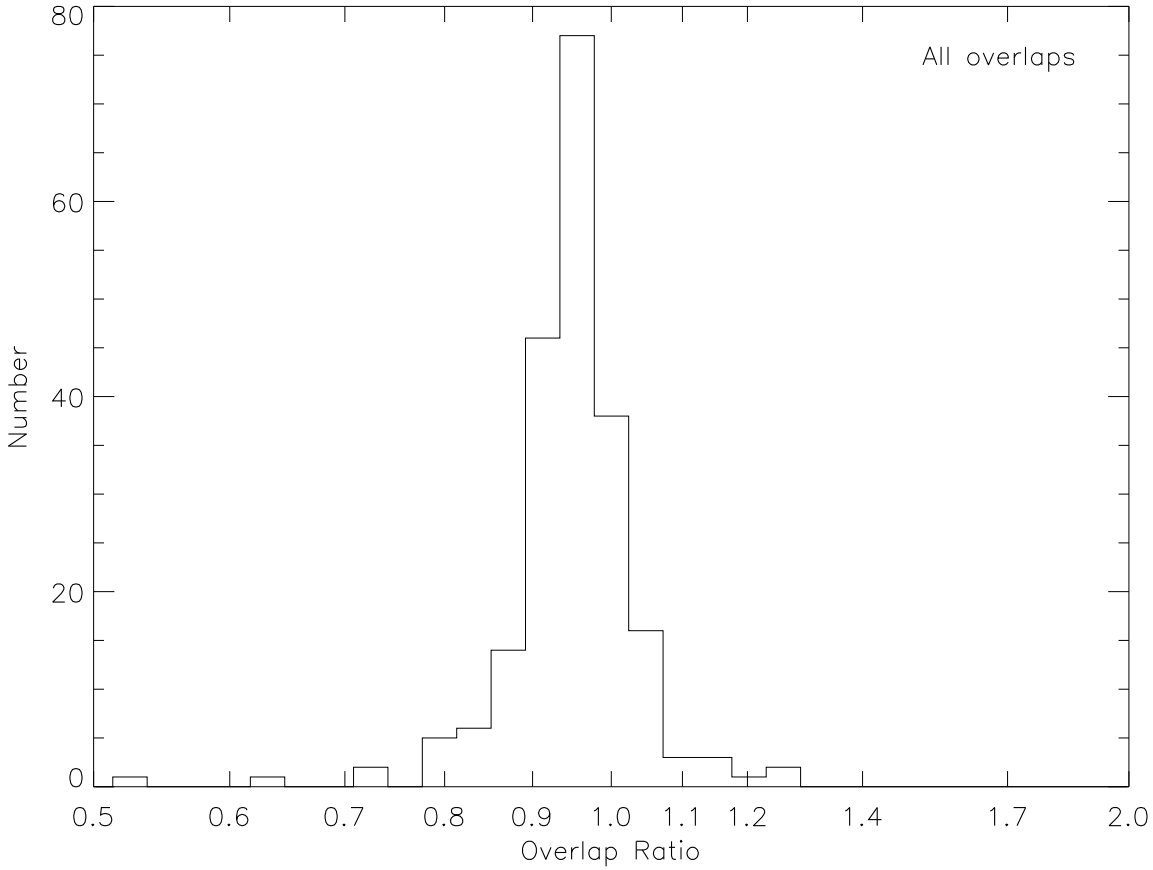

Fig. 1.— Disperser overlap statistics for all dataset overlaps.

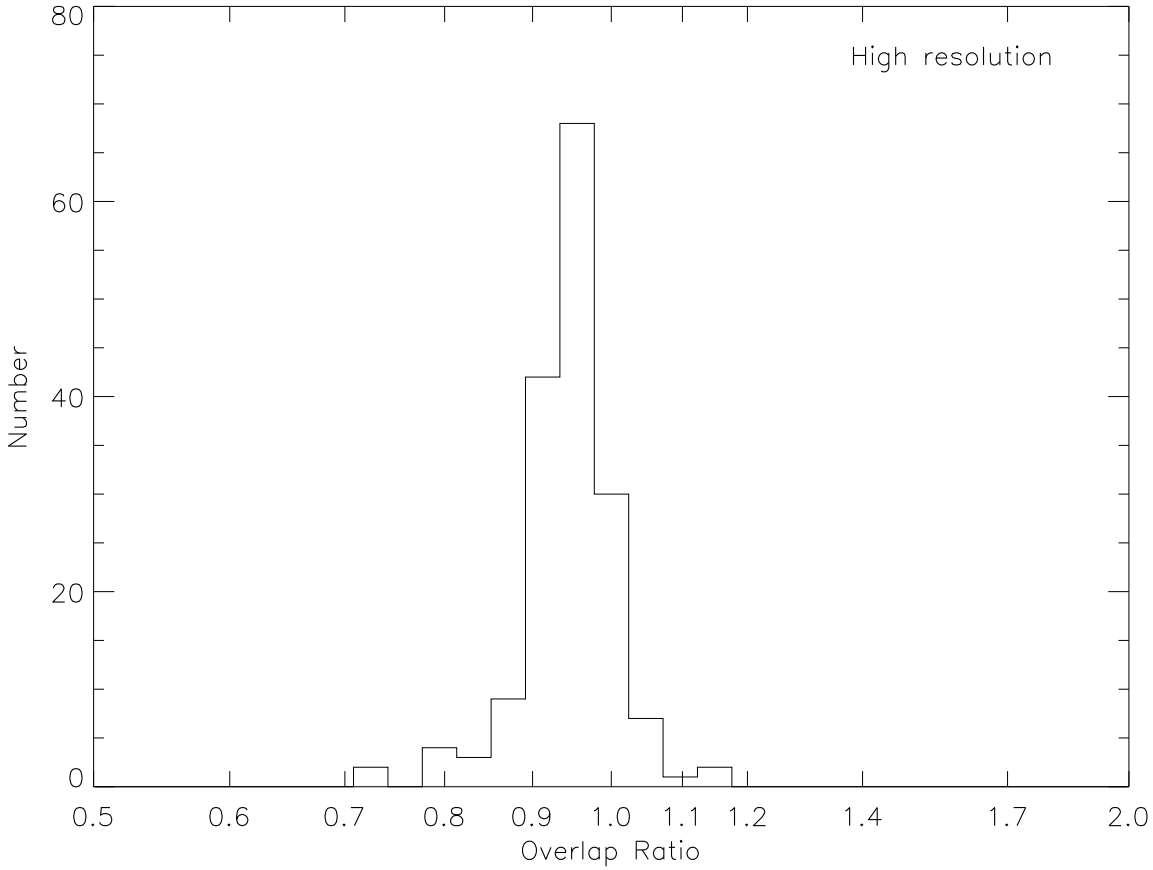

Fig. 2.— As Fig. 1, but for all high dispersion grating datasets only.

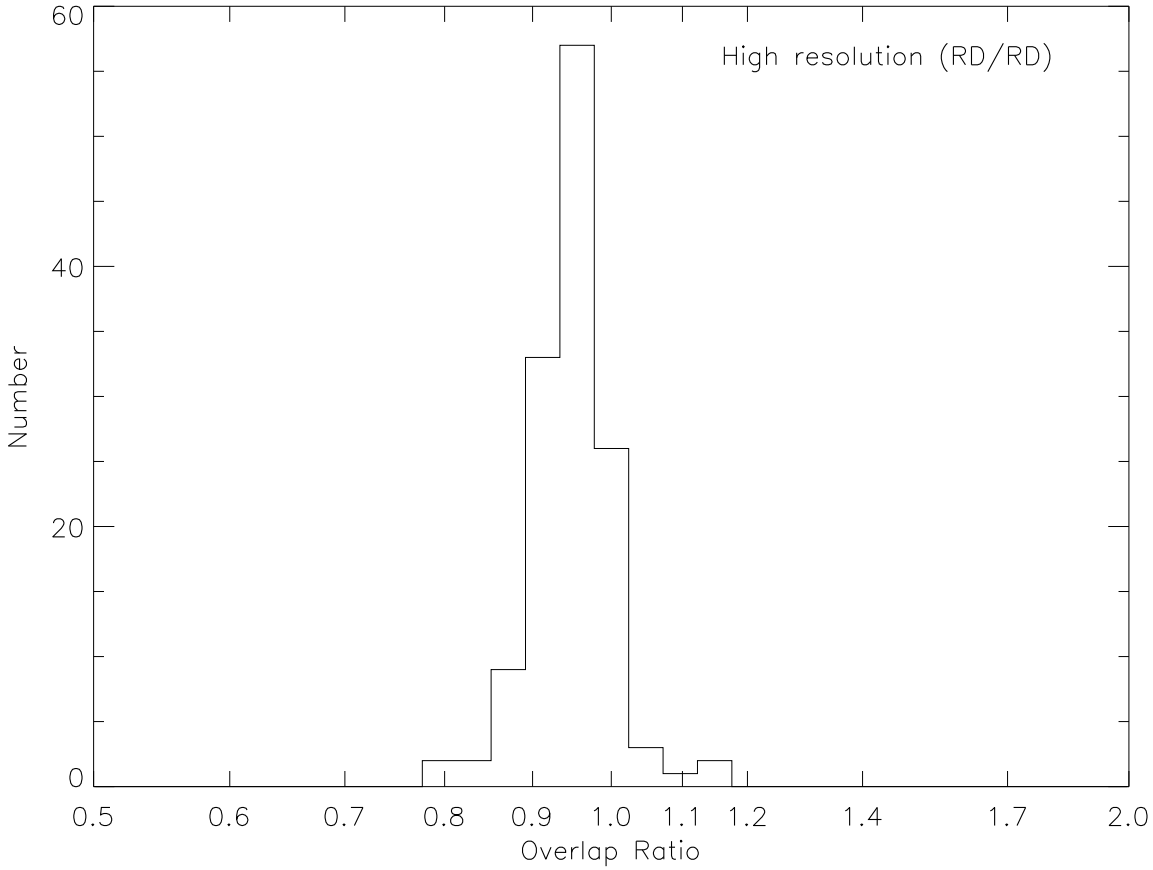

Fig. 3.— As Fig. 1, but for high dispersion grating datasets both obtained with the FOS/RD detector only.

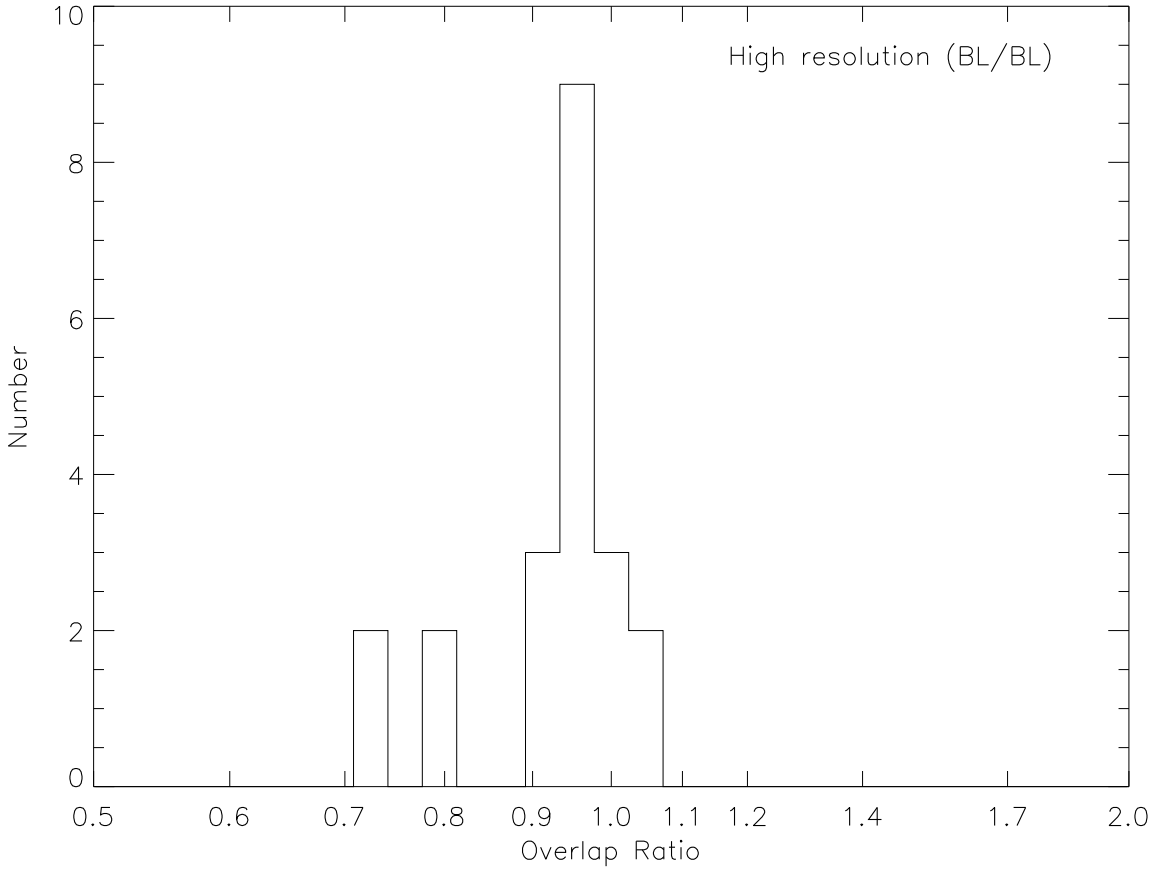

Fig. 4.— As Fig. 1, but for high dispersion grating datasets both obtained with the FOS/BL detector only.

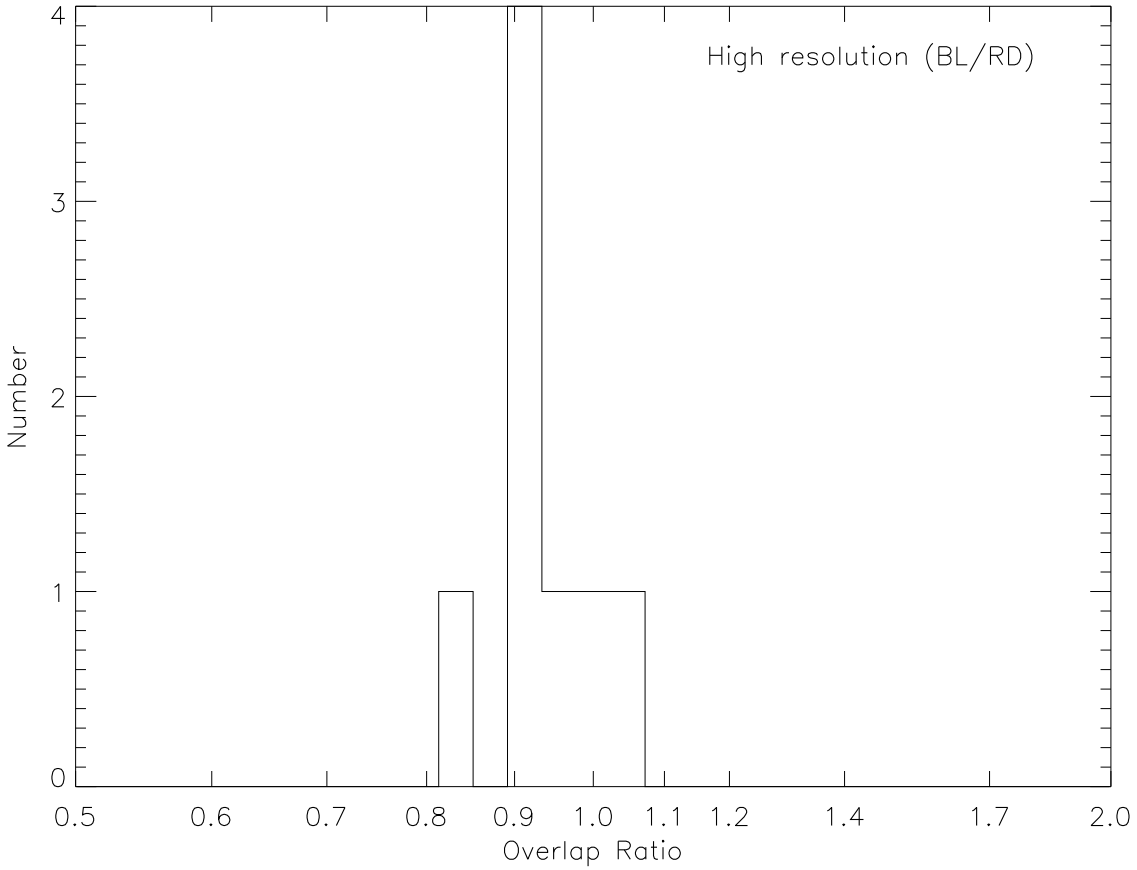

Fig. 5.— As Fig. 1, but for cross-detector (`FOS/BL`+`FOS/RD`) high dispersion grating datasets only.

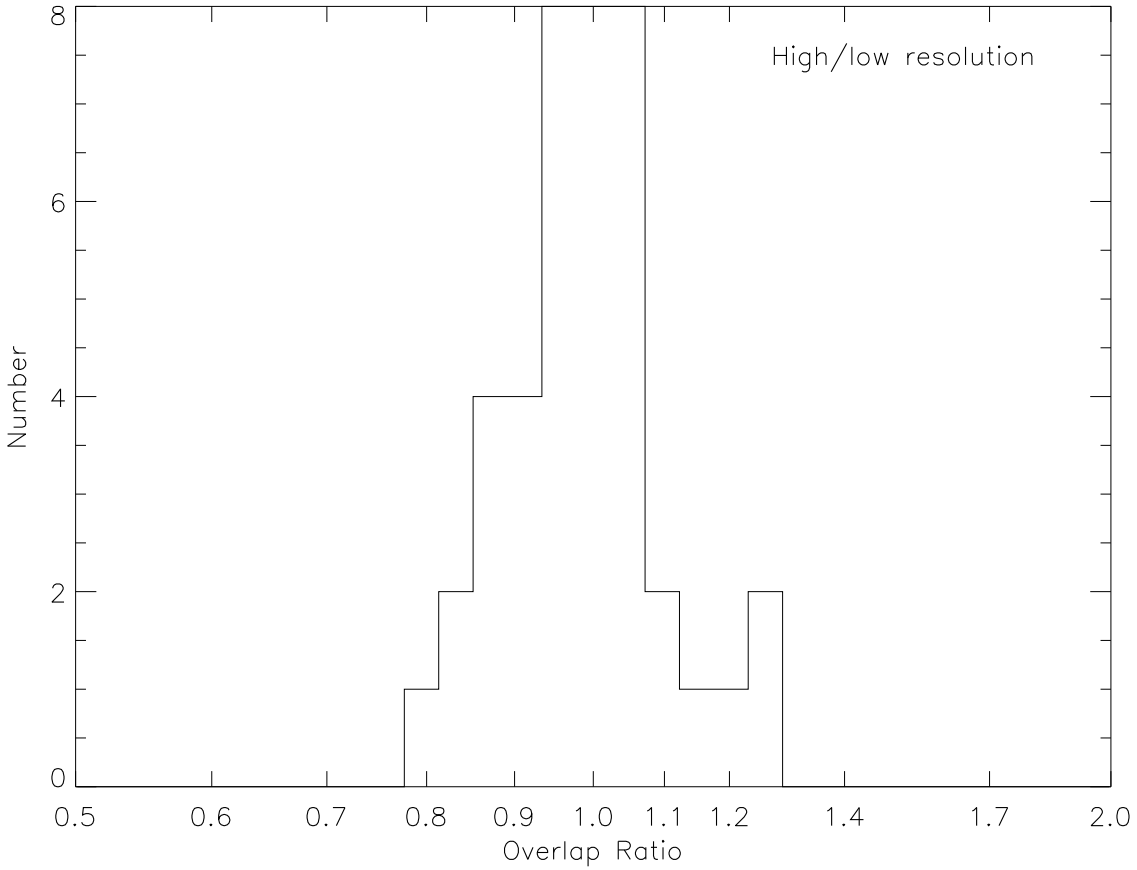

Fig. 6.— As Fig. 1, but for high-resolution+low-resolution disperser dataset overlaps only.

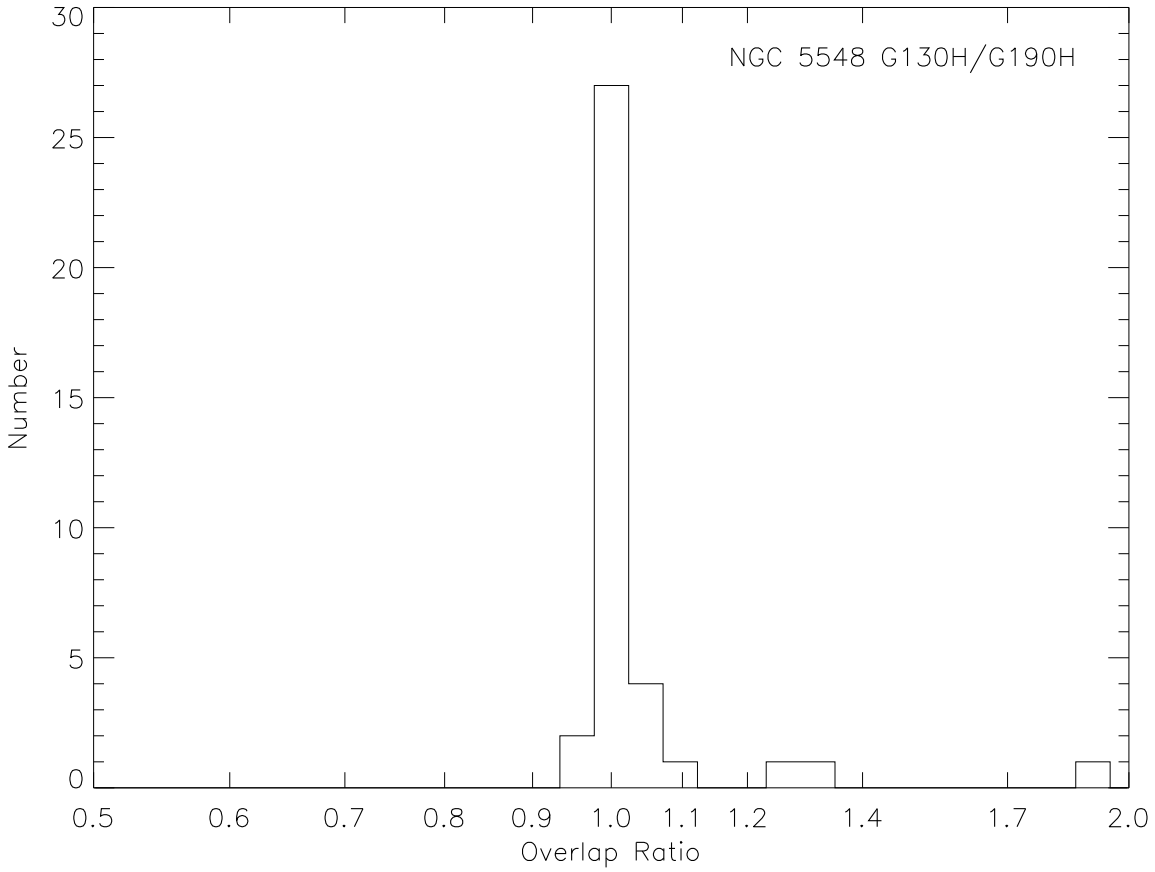

Fig. 7.— As Fig. 1, but for a uniform sample of 39 `G130H` and `G190H` observations of the nucleus of NGC 5548 obtained with the *FOS* blue detector.

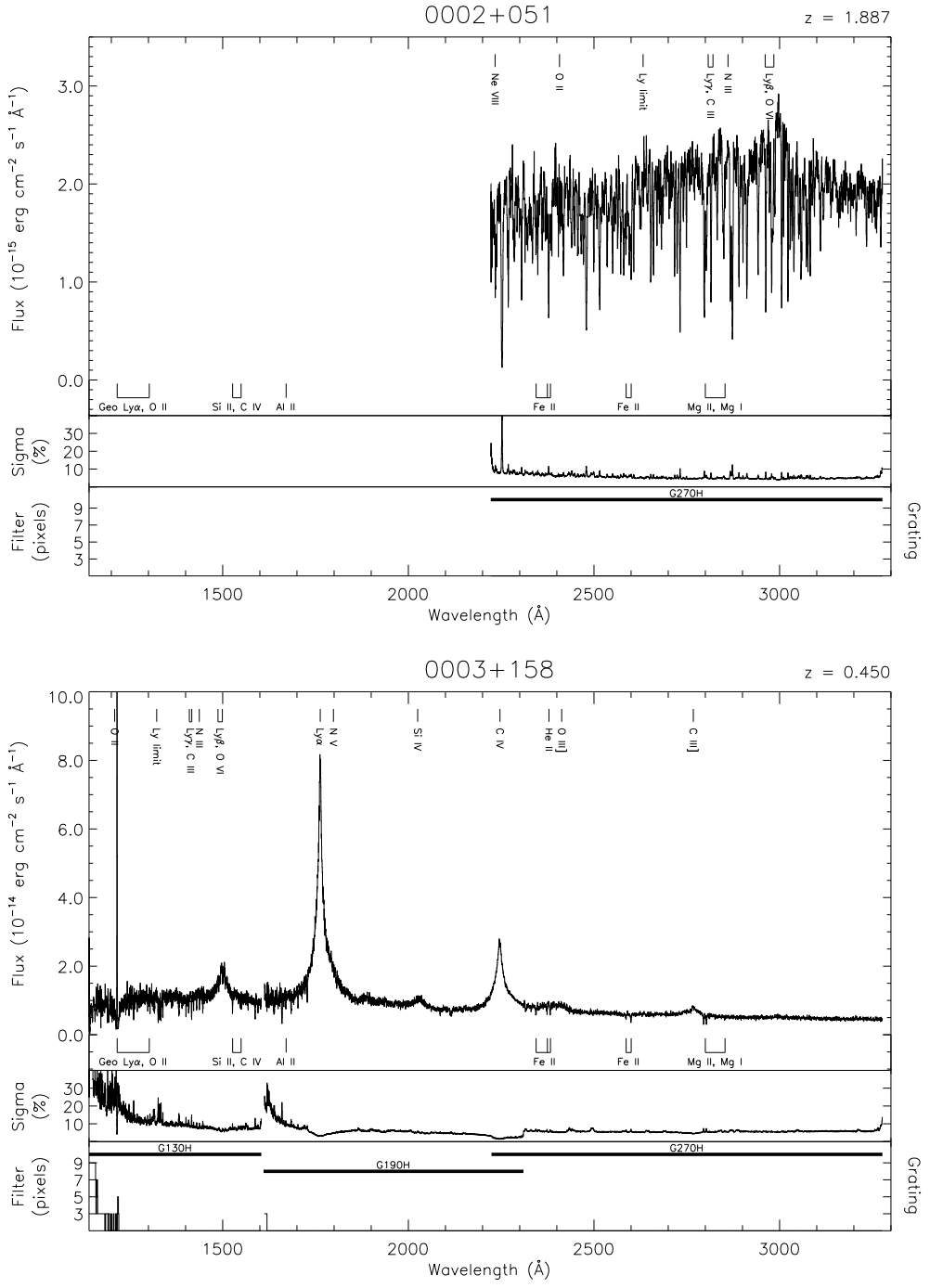

Fig. 8.— Merged spectra of all objects included in this atlas.

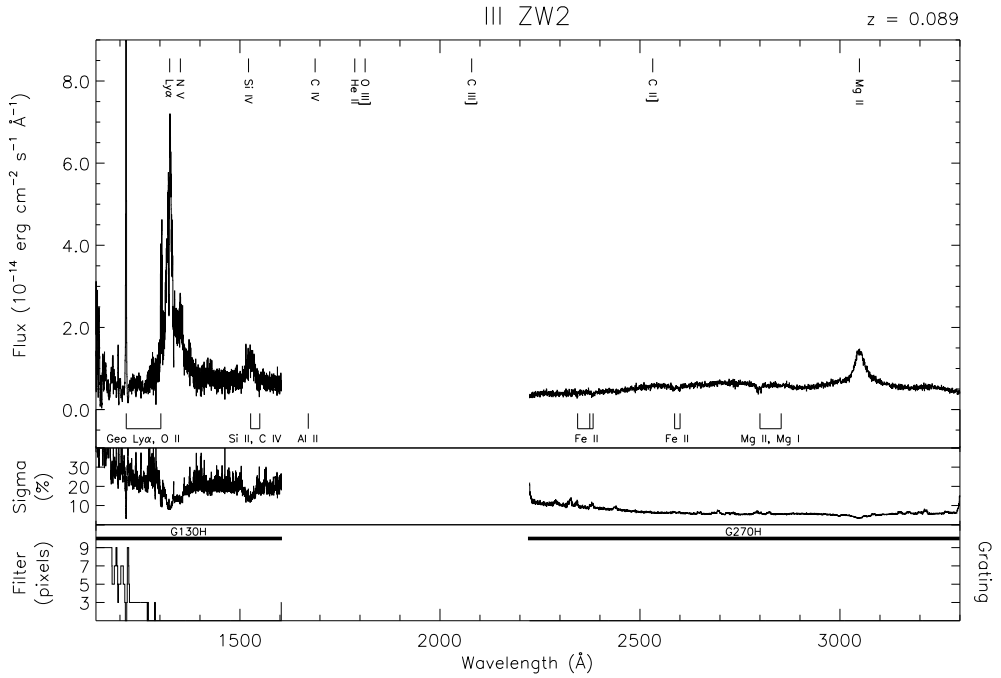
III ZW2
z = 0.089
Flux (10^{-14} erg cm^{-2} s^{-1} Å^{-1})
Lyα, N V
Si IV
C IV
He II, O III]
C III]
C II]
Mg II
Geo Lyα, O II
Si II, C IV
Al II
Fe II
Fe II
Mg II, Mg I
Sigma (%)
G130H
G270H
Filter (pixels)
Grating
Wavelength (Å)

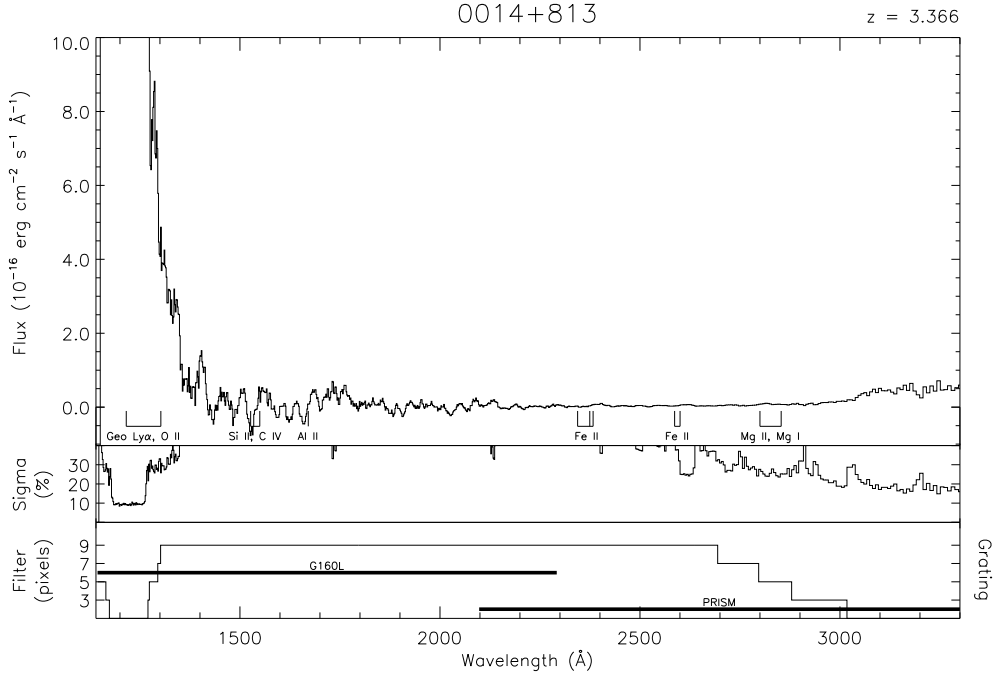
0014+813
z = 3.366
Flux (10^{-16} erg cm^{-2} s^{-1} Å^{-1})
Geo Lyα, O II
Si II, C IV
Al II
Fe II
Fe II
Mg II, Mg I
Sigma (%)
G160L
PRISM
Filter (pixels)
Grating
Wavelength (Å)

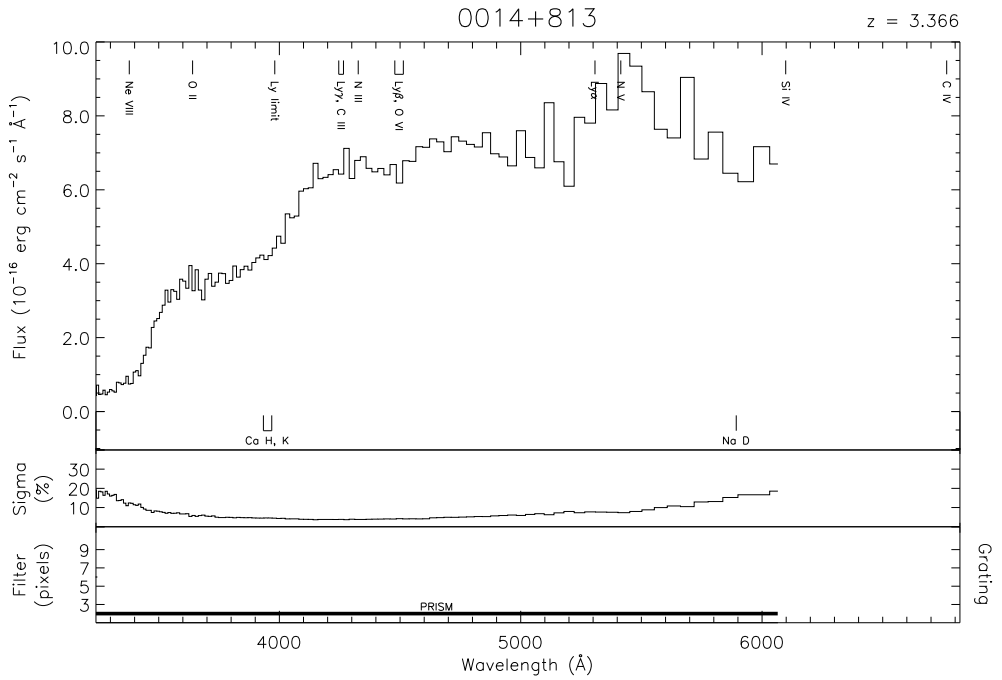
0014+813
z = 3.366
Flux (10^{-16} erg cm^{-2} s^{-1} Å^{-1})
Ne VIII
O II
Ly limit
N III
Lyγ, C III
Lyβ, O VI
Lyα
N V
Si IV
C IV
Ca H, K
Na D
Sigma (%)
Filter (pixels)
PRISM
Grating
Wavelength (Å)

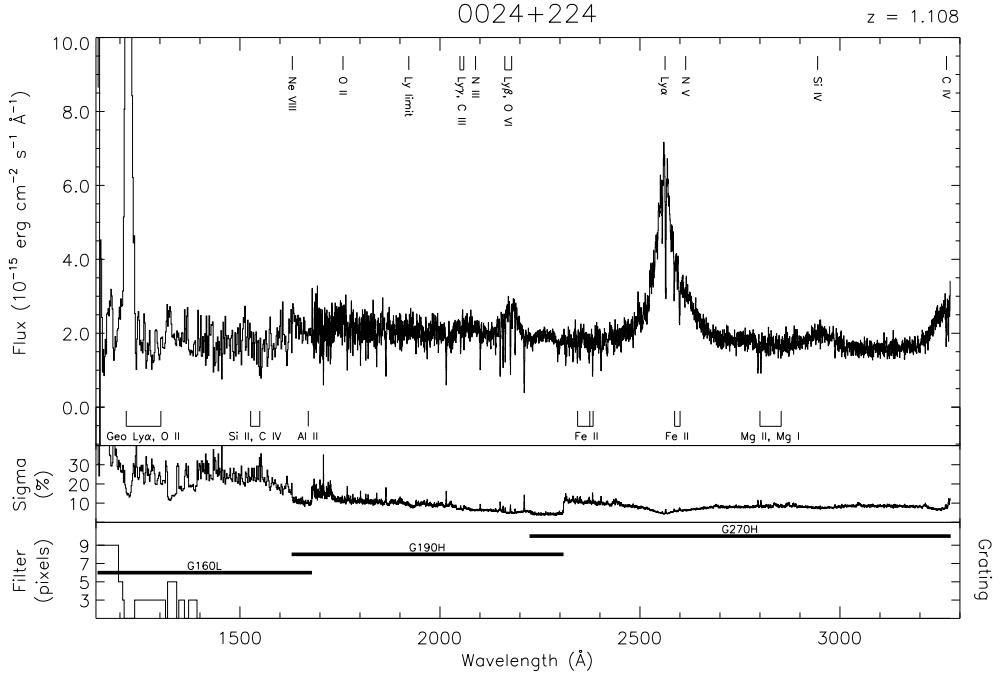
0024+224
z = 1.108
Flux (10^{-15} erg cm^{-2} s^{-1} Å^{-1})
Ne VIII
O II
Ly limit
N III
Lyγ, C III
Lyβ, O VI
Lyα
N V
Si IV
C IV
Geo Lyα, O II
Si II, C IV
Al II
Fe II
Fe II
Mg II, Mg I
Sigma (%)
Filter (pixels)
G270H
G190H
G160L
Grating
Wavelength (Å)

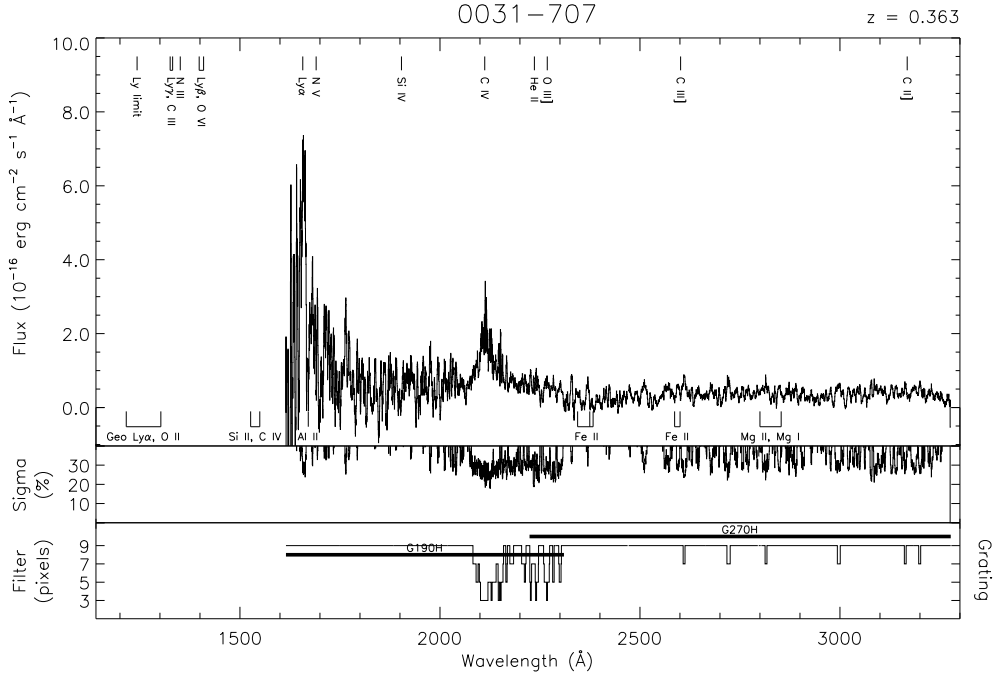
0031−707
z = 0.363
Flux (10^{-16} erg cm^{-2} s^{-1} Å^{-1})
Ly limit
N III
Lyγ, C III
Lyβ, O VI
N V
Lyα
Si IV
C IV
O III]
He II
C III]
C II]
Geo Lyα, O II
Si II, C IV
Al II
Fe II
Fe II
Mg II, Mg I
Sigma (%)
G270H
G190H
Filter (pixels)
Grating
Wavelength (Å)

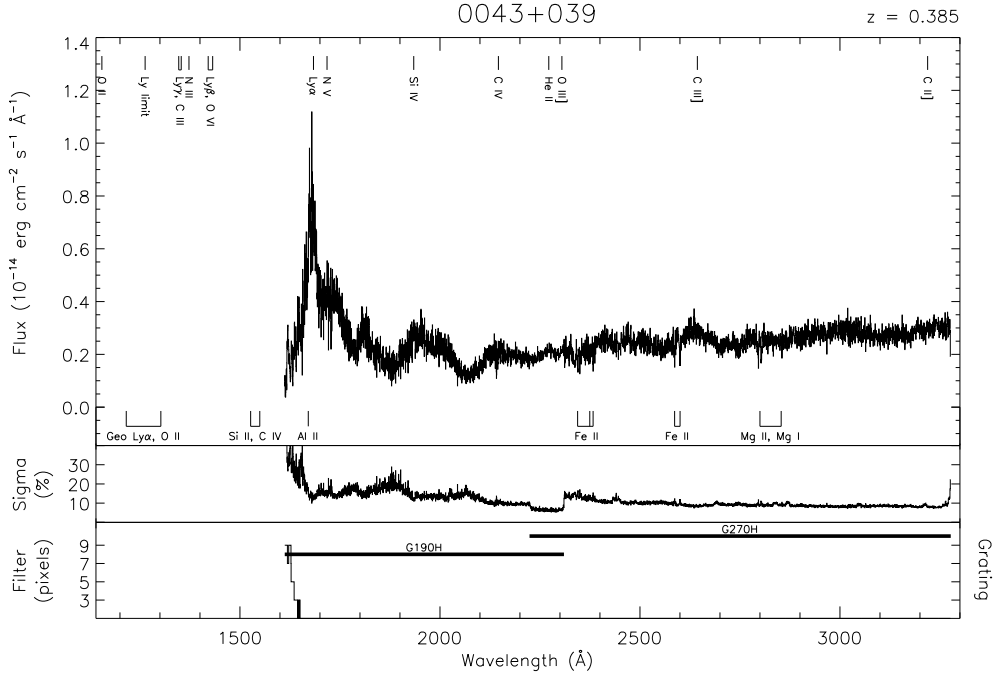
0043+039
z = 0.385
Flux (10^{-14} erg cm^{-2} s^{-1} Å^{-1})
Ly limit
N III
Lyγ, C III
Lyβ, O VI
N V
Lyα
Si IV
C IV
O III]
He II
C III]
C II]
Geo Lyα, O II
Si II, C IV
Al II
Fe II
Fe II
Mg II, Mg I
Sigma (%)
G270H
G190H
Filter (pixels)
Grating
Wavelength (Å)

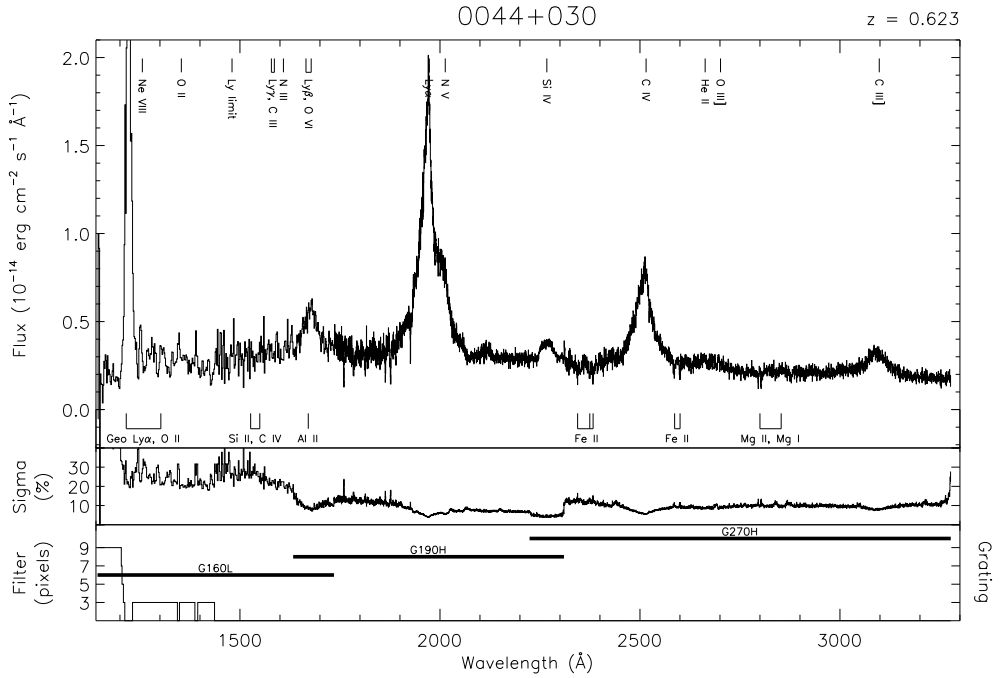
0044+030
z = 0.623
Flux (10^{-14} erg cm^{-2} s^{-1} Å^{-1})
Ne VIII
O II
Ly limit
N III
Lyγ, C III
Lyβ, O VI
Lyα
N V
Si IV
C IV
He II
O III]
C III]
Geo Lyα, O II
Si II, C IV
Al II
Fe II
Fe II
Mg II, Mg I
Sigma (%)
G270H
G190H
G160L
Filter (pixels)
Grating
Wavelength (Å)

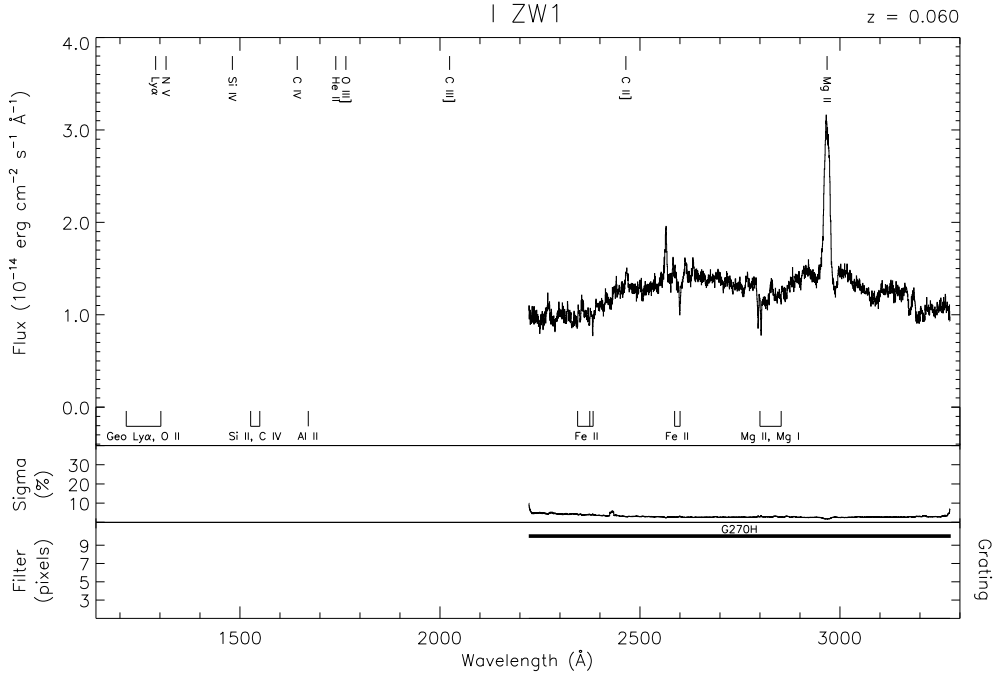
I ZW1
z = 0.060
Flux (10^{-14} erg cm^{-2} s^{-1} Å^{-1})
N V Lyα
Si IV
C IV
He II O III]
C III]
C II]
Mg II
Geo Lyα, O II
Si II, C IV
Al II
Fe II
Fe II
Mg II, Mg I
Sigma (%)
G270H
Filter (pixels)
Grating
Wavelength (Å)

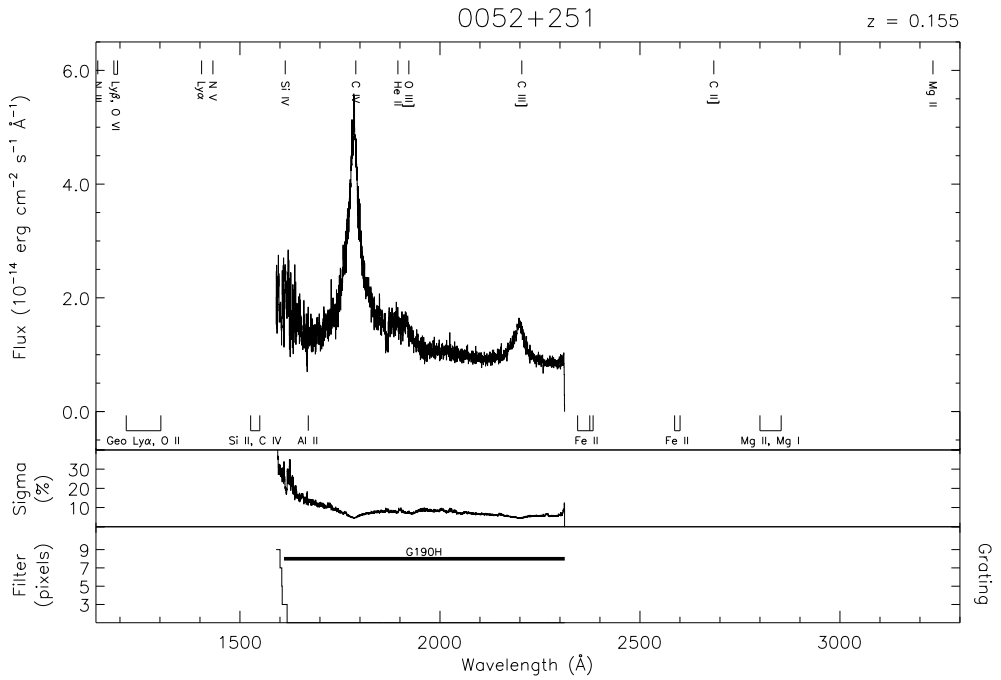
0052+251
z = 0.155
Flux (10^{-14} erg cm^{-2} s^{-1} Å^{-1})
N III
Lyβ, O VI
Lyα
N V
Si IV
C IV
He II
O III]
C III]
C II]
Mg II
Geo Lyα, O II
Si II, C IV
Al II
Fe II
Fe II
Mg II, Mg I
Sigma (%)
Filter (pixels)
G190H
Grating
Wavelength (Å)

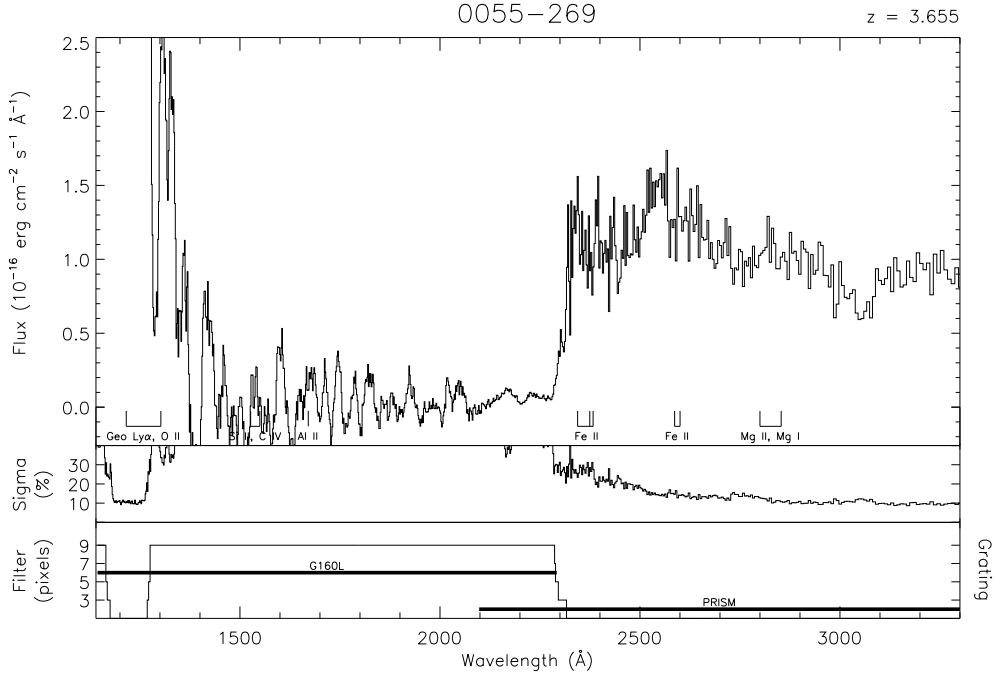
0055−269
z = 3.655
Flux (10^{-16} erg cm^{-2} s^{-1} Å^{-1})
Geo Lyα, O II
Si II, C IV
Al II
Fe II
Fe II
Mg II, Mg I
Sigma (%)
Filter (pixels)
G160L
PRISM
Grating
Wavelength (Å)

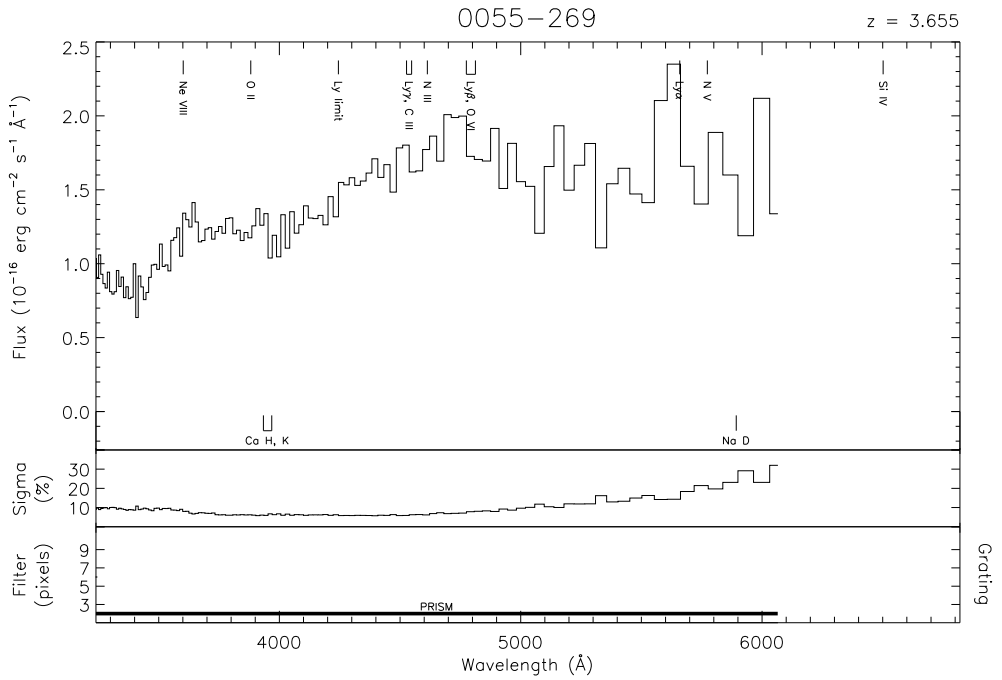
0055−269
z = 3.655
Flux (10^{-16} erg cm^{-2} s^{-1} Å^{-1})
Ne VIII
O II
Ly limit
Lyγ, C III
N III
Lyβ, O VI
Lyα
N V
Si IV
Ca H, K
Na D
Sigma (%)
Filter (pixels)
PRISM
Grating
Wavelength (Å)

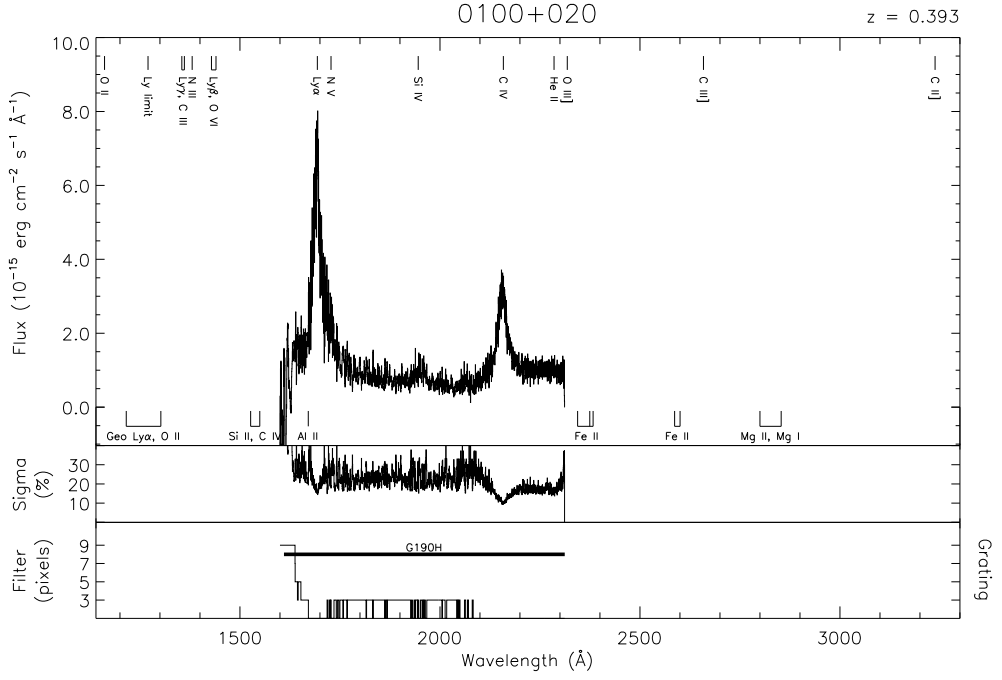
0100+020
z = 0.393
Flux (10^{-15} erg cm^{-2} s^{-1} Å^{-1})
O II
Ly limit
N III
Lyγ, C III
Lyβ, O VI
N V
Lyα
Si IV
C IV
O III]
He II
C III]
C II]
Geo Lyα, O II
Si II, C IV
Al II
Fe II
Fe II
Mg II, Mg I
Sigma (%)
Filter (pixels)
G190H
Grating
Wavelength (Å)

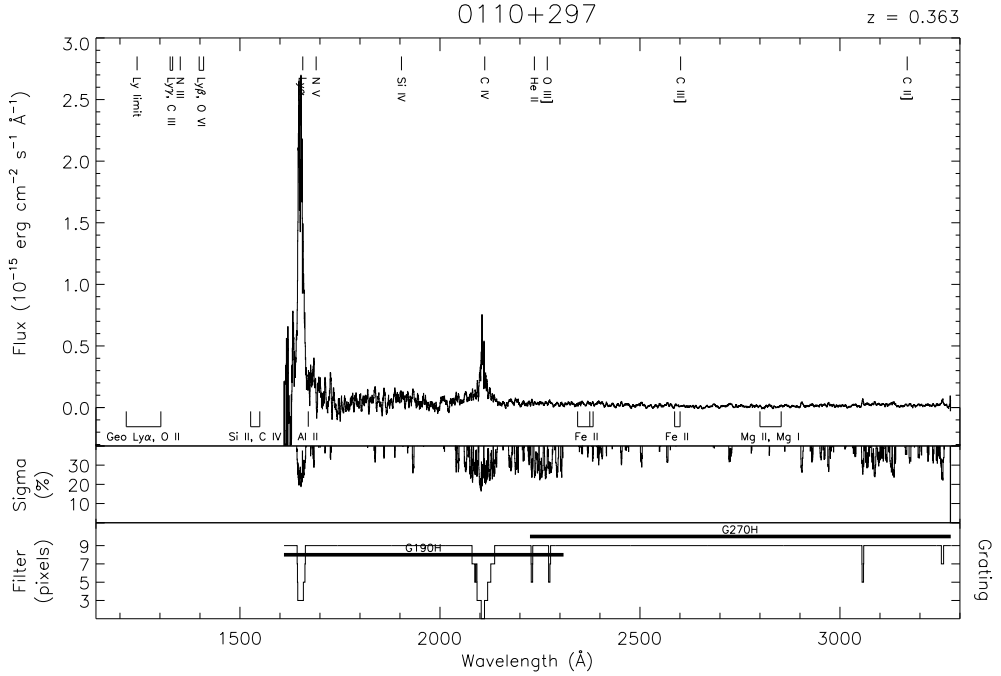
0110+297
z = 0.363
Flux (10^{-15} erg cm^{-2} s^{-1} Å^{-1})
Ly limit
N III
Ly7, C III
Lyδ, O VI
Lyα
N V
Si IV
C IV
He II
O III]
C III]
C II]
Geo Lyα, O II
Si II, C IV
Al II
Fe II
Fe II
Mg II, Mg I
Sigma (%)
G270H
G190H
Filter (pixels)
Grating
Wavelength (Å)

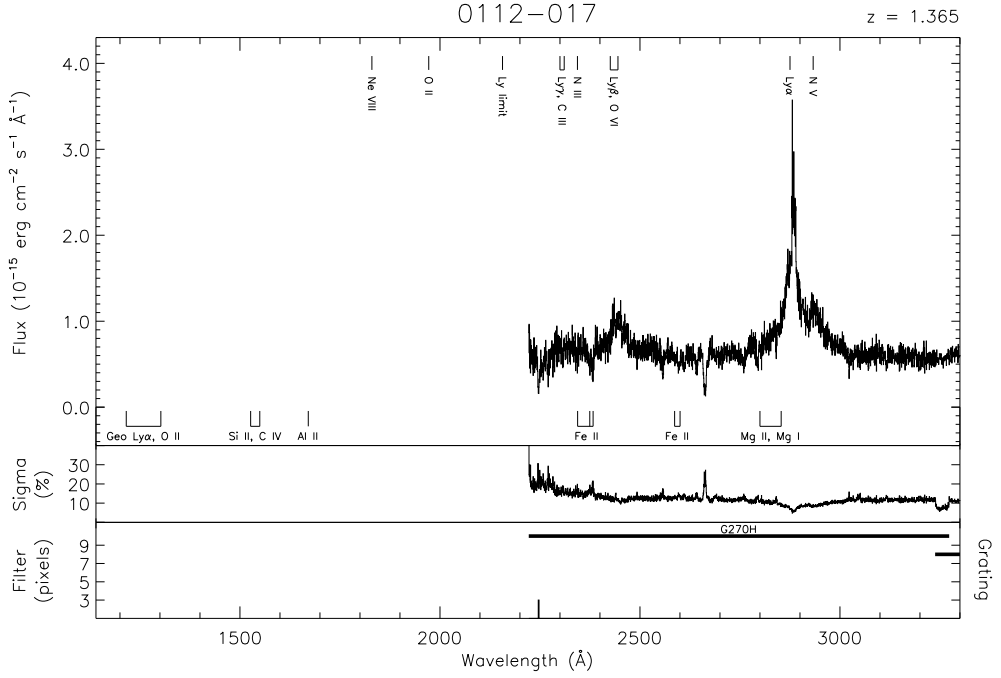
0112−017
z = 1.365
Flux (10^{-15} erg cm^{-2} s^{-1} Å^{-1})
Ne VIII
O II
Ly limit
N III
Ly7, C III
Lyδ, O VI
Lyα
N V
Geo Lyα, O II
Si II, C IV
Al II
Fe II
Fe II
Mg II, Mg I
Sigma (%)
G270H
Filter (pixels)
Grating
Wavelength (Å)

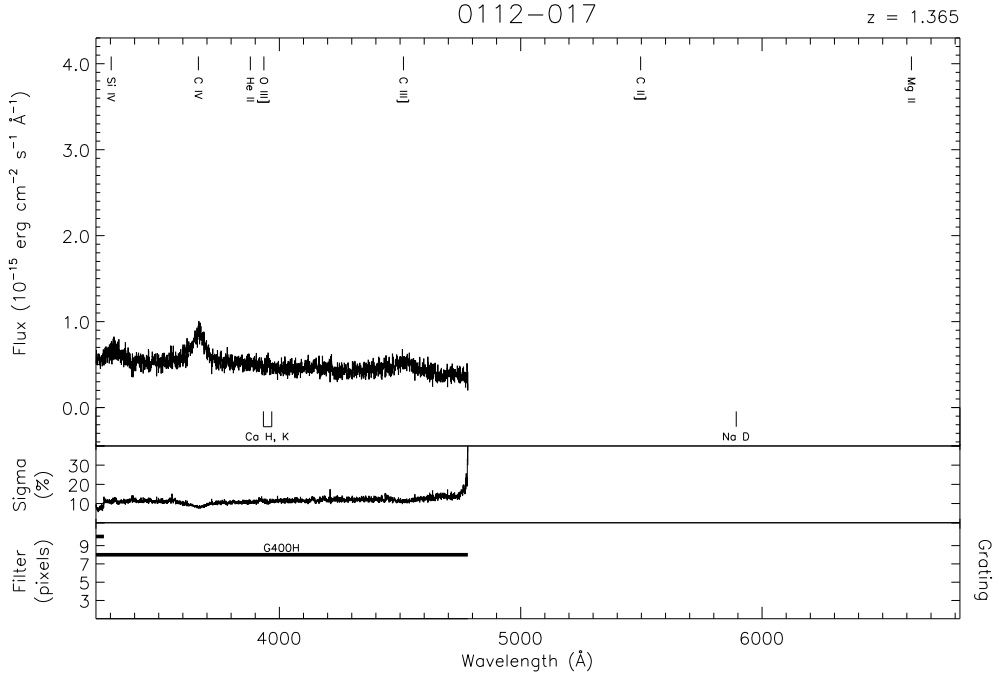
0112−017
z = 1.365
Si IV
C IV
He II
O III]
C III]
C II]
Mg II
Ca H, K
Na D
G400H
Flux (10^{-15} erg cm^{-2} s^{-1} Å^{-1})
Sigma (%)
Filter (pixels)
Grating
Wavelength (Å)

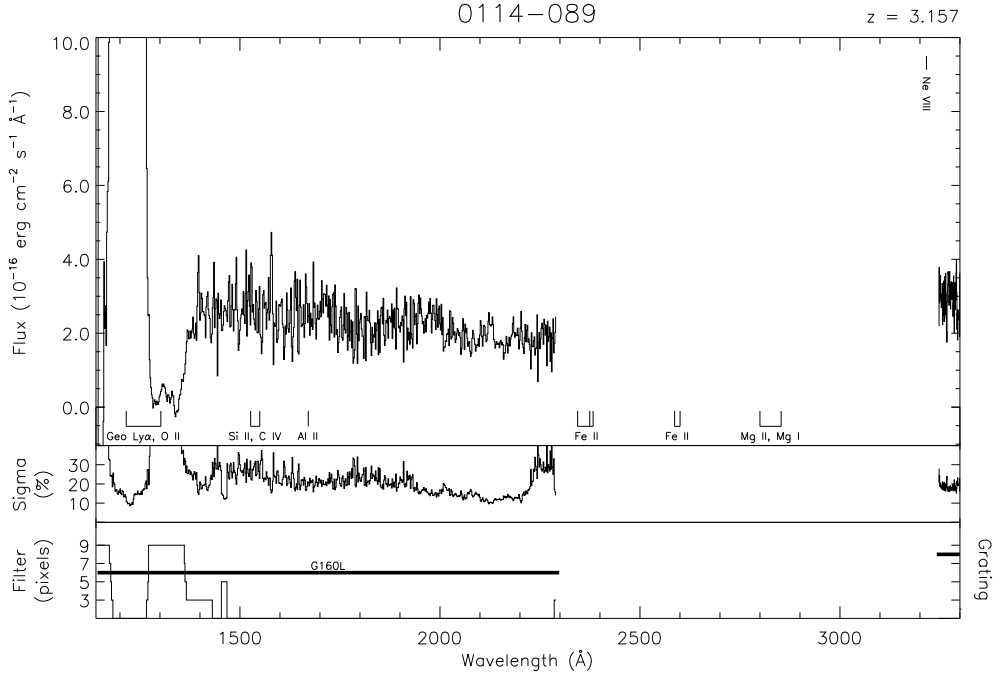
0114−089
z = 3.157
Ne VIII
Geo Lyα, O II
Si II, C IV
Al II
Fe II
Fe II
Mg II, Mg I
G160L
Flux (10^{-16} erg cm^{-2} s^{-1} Å^{-1})
Sigma (%)
Filter (pixels)
Grating
Wavelength (Å)

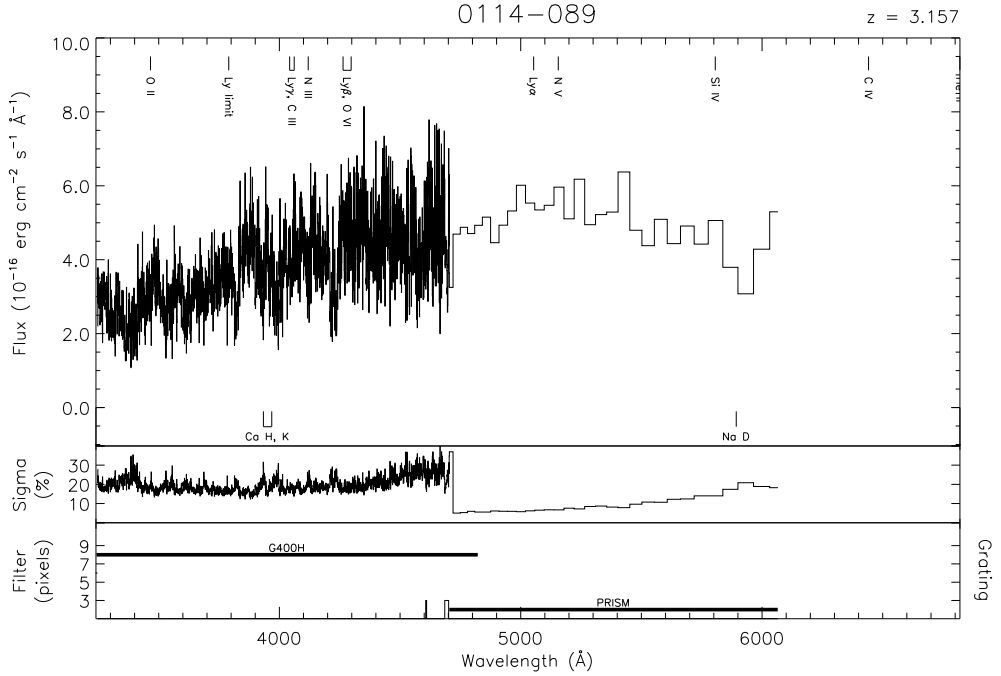
0114−089
z = 3.157
O II
Ly limit
Lyγ, C III
N III
Lyβ, O VI
Lyα
N V
Si IV
C IV
Ca H, K
Na D
Flux (10^{-16} erg cm^{-2} s^{-1} Å^{-1})
Sigma (%)
Filter (pixels)
G400H
PRISM
Grating
Wavelength (Å)

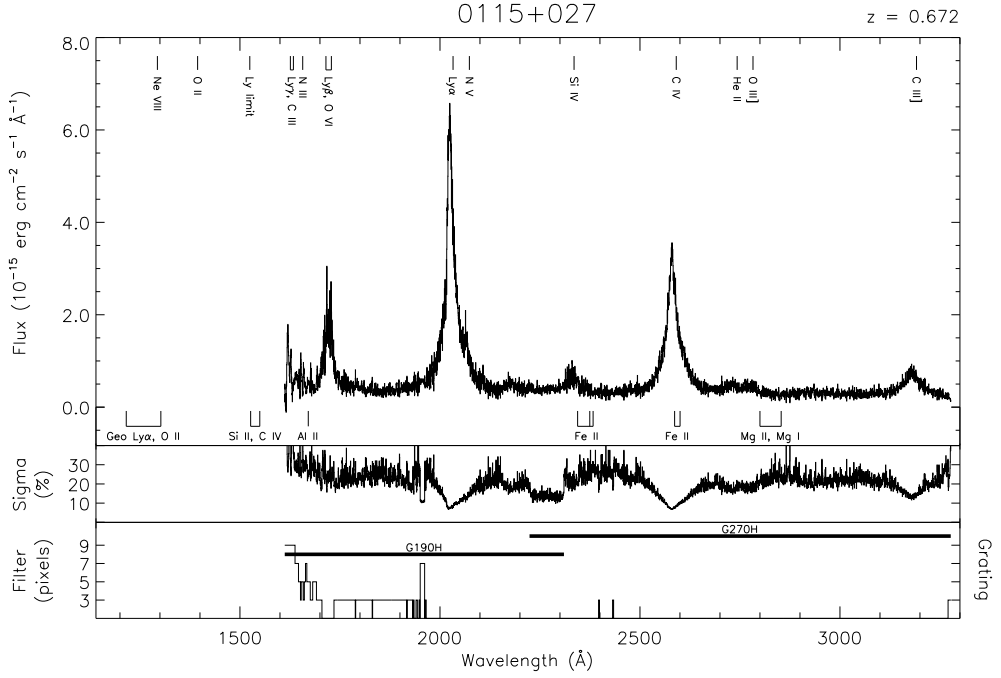
0115+027
z = 0.672
Ne VIII
O II
Ly limit
Lyγ, C III
N III
Lyβ, O VI
Lyα
N V
Si IV
C IV
He II
O III]
C III]
Geo Lyα, O II
Si II, C IV
Al II
Fe II
Fe II
Mg II, Mg I
Flux (10^{-15} erg cm^{-2} s^{-1} Å^{-1})
Sigma (%)
Filter (pixels)
G190H
G270H
Grating
Wavelength (Å)

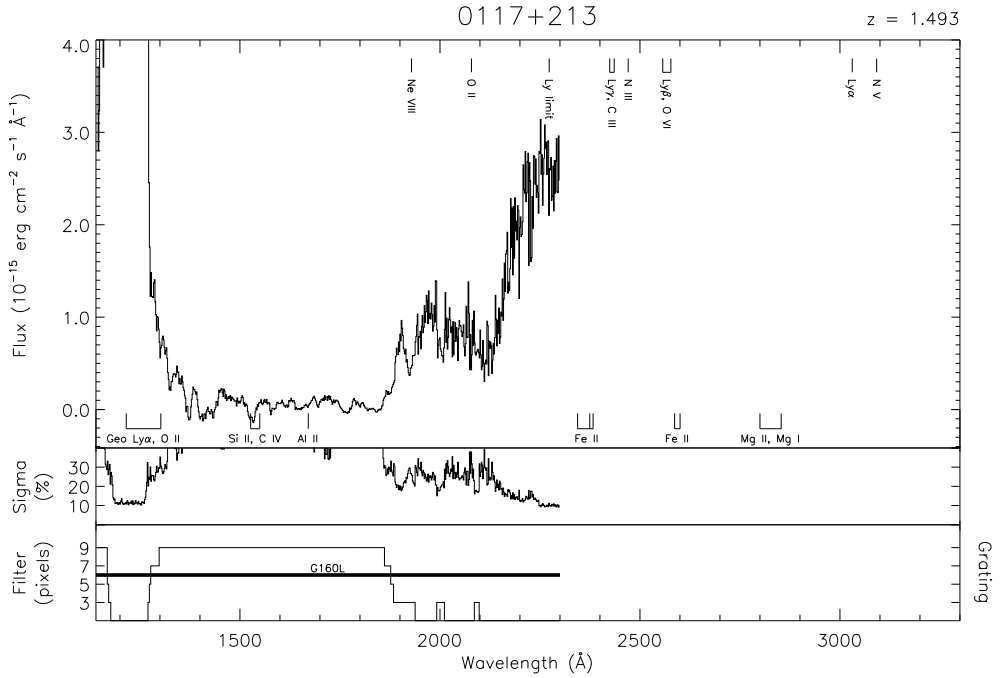
0117+213
z = 1.493
Flux (10^{-15} erg cm^{-2} s^{-1} Å^{-1})
Ne VIII
O II
Ly limit
Lyγ, C III
N III
Lyβ, O VI
Lyα
N V
Geo Lyα, O II
Si II, C IV
Al II
Fe II
Fe II
Mg II, Mg I
Sigma (%)
Filter (pixels)
G160L
Grating
Wavelength (Å)

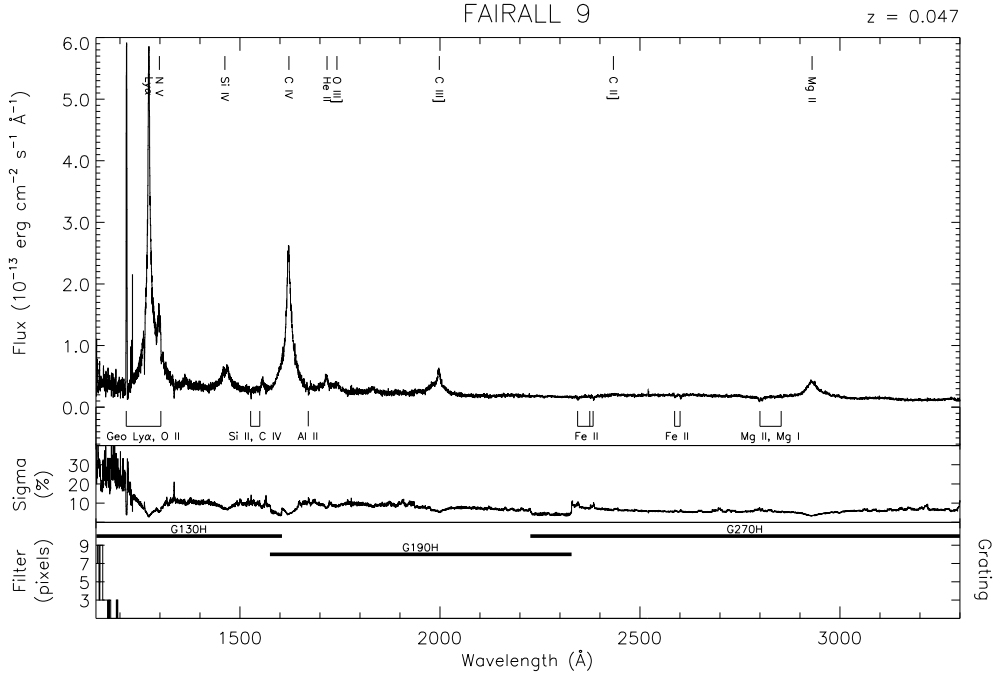
FAIRALL 9
z = 0.047
Flux (10^{-13} erg cm^{-2} s^{-1} Å^{-1})
Lyα
N V
Si IV
C IV
He II
O III]
C III]
C II]
Mg II
Geo Lyα, O II
Si II, C IV
Al II
Fe II
Fe II
Mg II, Mg I
Sigma (%)
G130H
G270H
G190H
Filter (pixels)
Grating
Wavelength (Å)

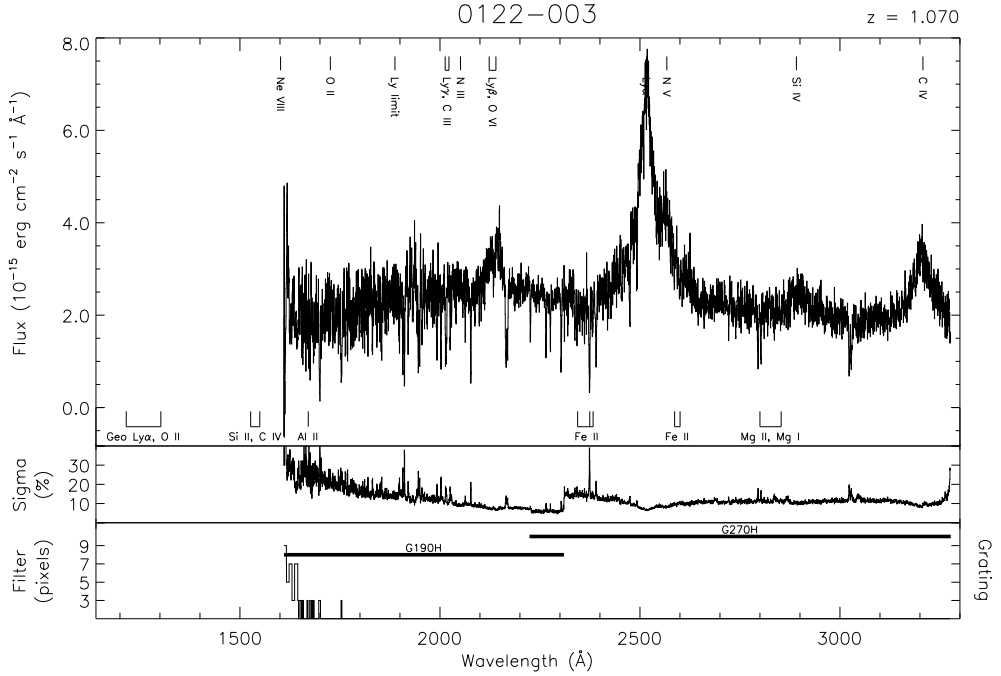
0122−003
z = 1.070
Flux (10^{-15} erg cm^{-2} s^{-1} Å^{-1})
Ne VIII
O II
Ly limit
N III
Lyγ, C III
Lyβ, O VI
Lyα
N V
Si IV
C IV
Geo Lyα, O II
Si II, C IV
Al II
Fe II
Fe II
Mg II, Mg I
Sigma (%)
Filter (pixels)
G270H
G190H
Grating
Wavelength (Å)

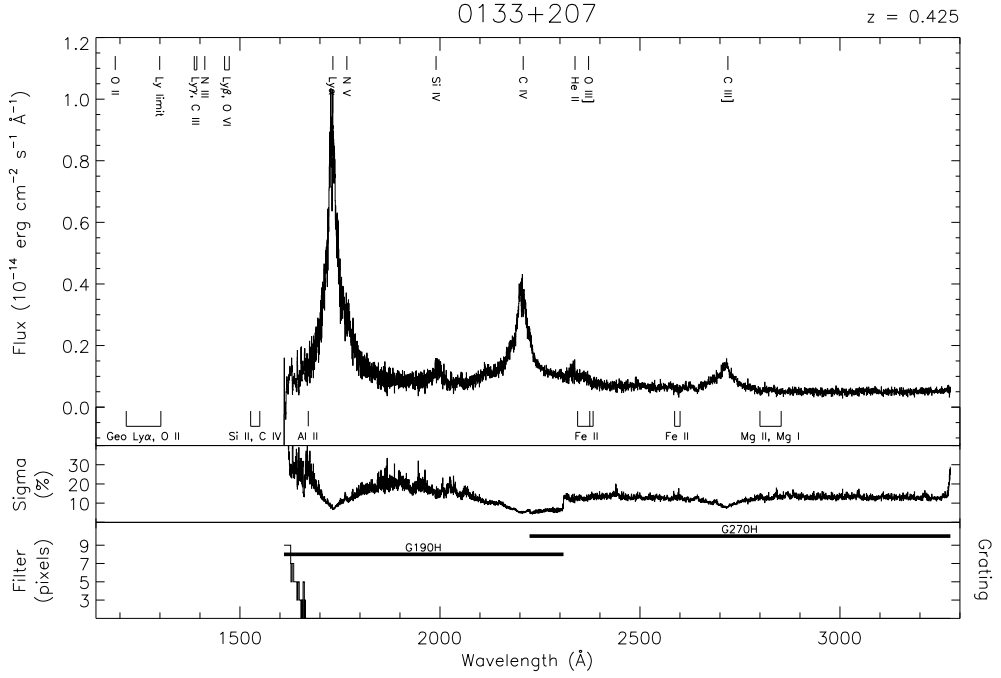
0133+207
z = 0.425
Flux (10^{-14} erg cm^{-2} s^{-1} Å^{-1})
O II
Ly limit
N III
Lyγ, C III
Lyβ, O VI
Lyα
N V
Si IV
C IV
He II
O III]
C III]
Geo Lyα, O II
Si II, C IV
Al II
Fe II
Fe II
Mg II, Mg I
Sigma (%)
Filter (pixels)
G270H
G190H
Grating
Wavelength (Å)

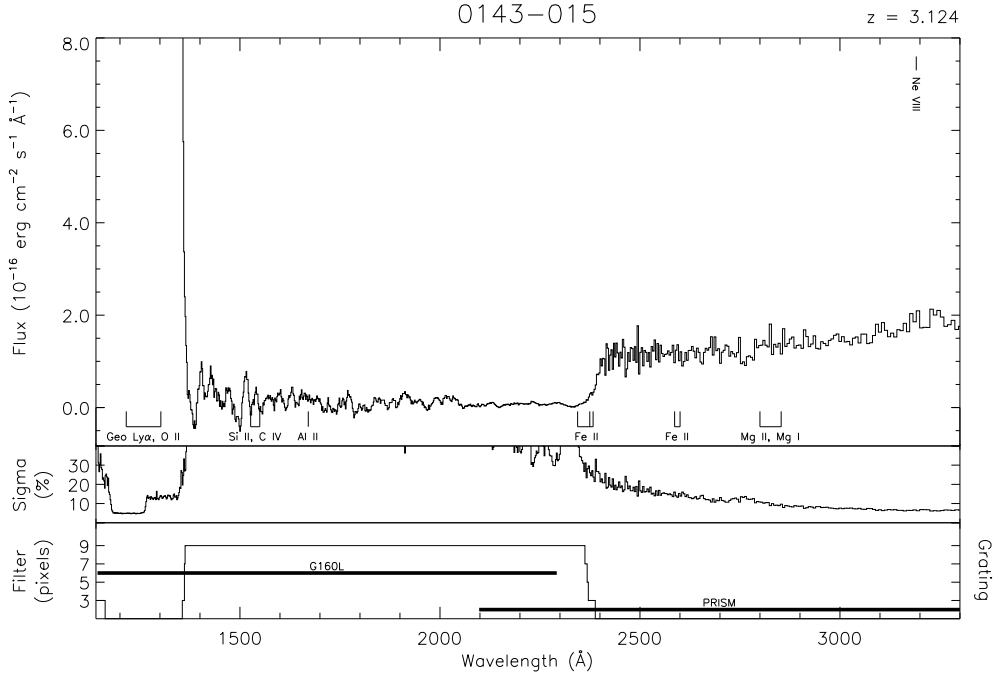
0143−015
z = 3.124
Flux (10^{-16} erg cm^{-2} s^{-1} Å^{-1})
Ne VIII
Geo Lyα, O II
Si II, C IV
Al II
Fe II
Fe II
Mg II, Mg I
Sigma (%)
Filter (pixels)
G160L
PRISM
Grating
Wavelength (Å)

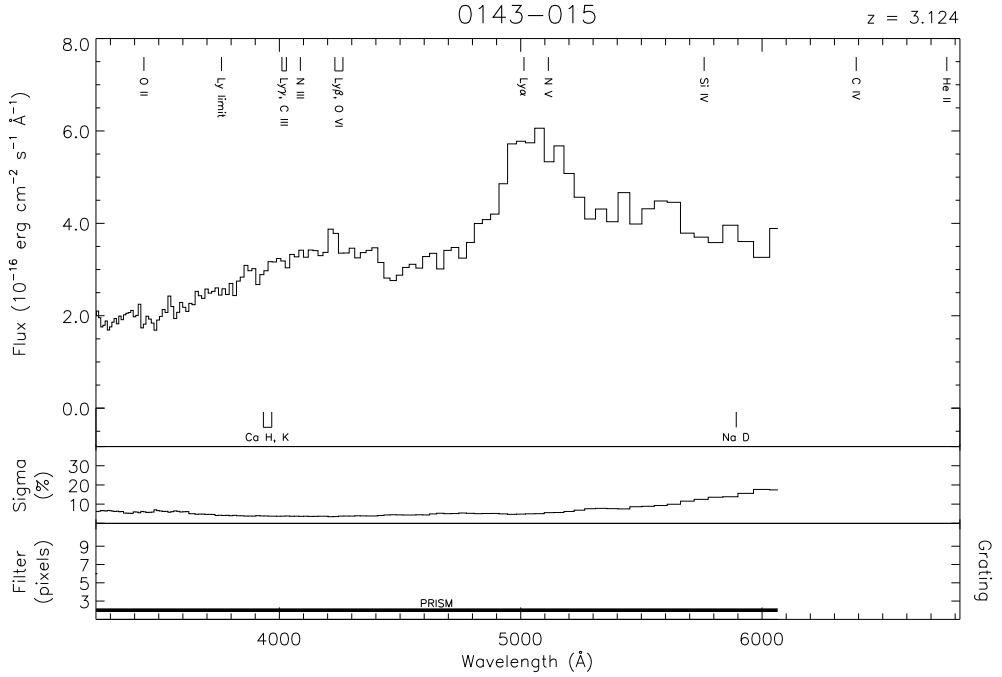
0143−015
z = 3.124
Flux (10^{-16} erg cm^{-2} s^{-1} Å^{-1})
O II
Ly limit
Lyδ, C III
N III
Lyβ, O VI
Lyα
N V
Si IV
C IV
He II
Ca H, K
Na D
Sigma (%)
Filter (pixels)
PRISM
Grating
Wavelength (Å)

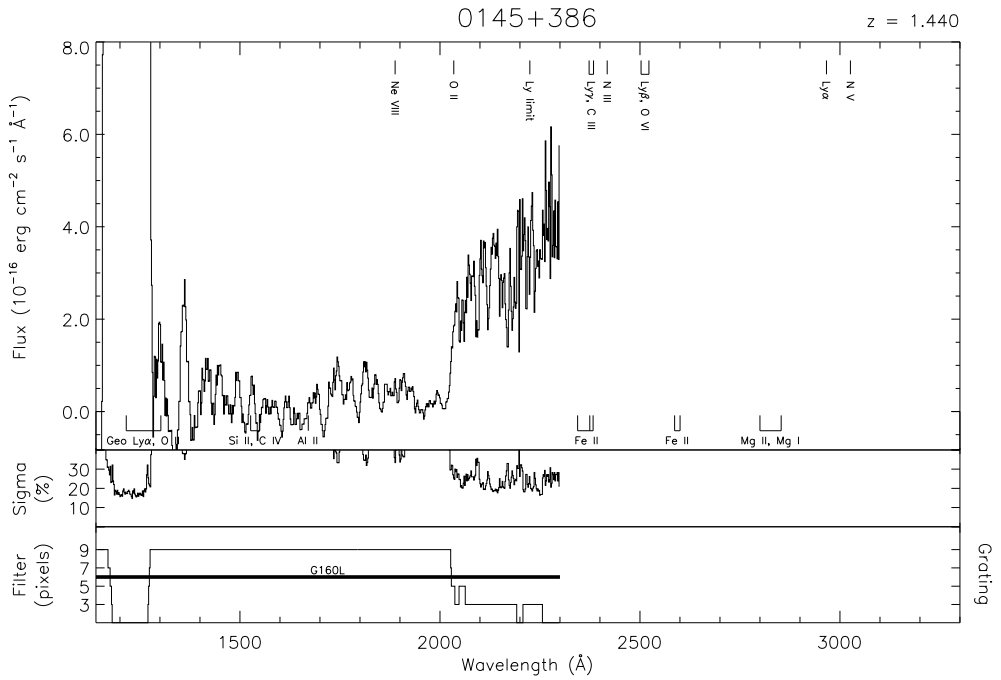
0145+386
z = 1.440
Flux (10^{-16} erg cm^{-2} s^{-1} Å^{-1})
Ne VIII
O II
Ly limit
Lyγ, C III
N III
Lyβ, O VI
Lyα
N V
Geo Lyα, O I
Si II, C IV
Al II
Fe II
Fe II
Mg II, Mg I
Sigma (%)
Filter (pixels)
G160L
Grating
Wavelength (Å)

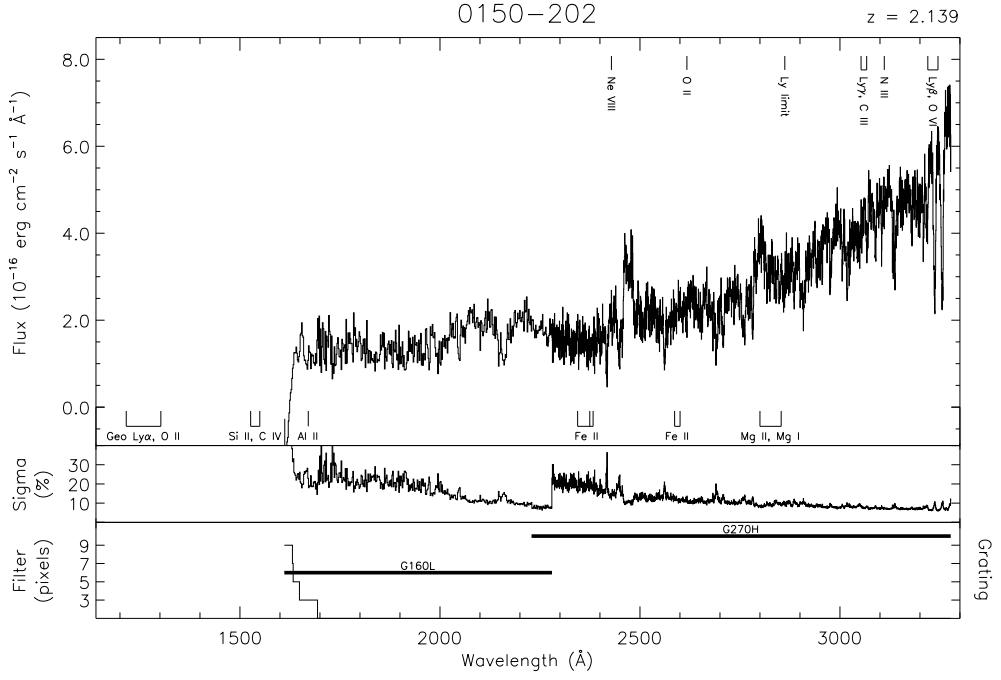
0150−202
z = 2.139
Flux (10^{-16} erg cm^{-2} s^{-1} Å^{-1})
Ne VIII
O II
Ly limit
Lyγ, C III
N III
Lyβ, O VI
Geo Lyα, O II
Si II, C IV
Al II
Fe II
Fe II
Mg II, Mg I
Sigma (%)
G270H
G160L
Filter (pixels)
Grating
Wavelength (Å)

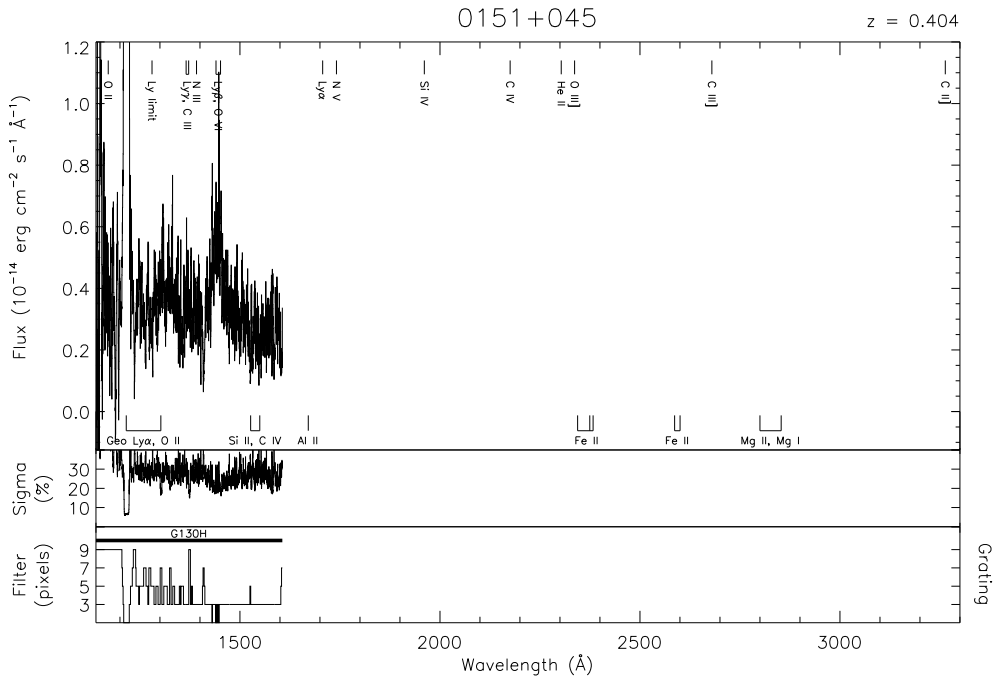
0151+045
z = 0.404
Flux (10^{-14} erg cm^{-2} s^{-1} Å^{-1})
O II
Ly limit
N III
C III
Ly β, O VI
Ly α
N V
Si IV
C IV
He II
O III]
C III]
C II]
Geo Lyα, O II
Si II, C IV
Al II
Fe II
Fe II
Mg II, Mg I
Sigma (%)
G130H
Filter (pixels)
Grating
Wavelength (Å)

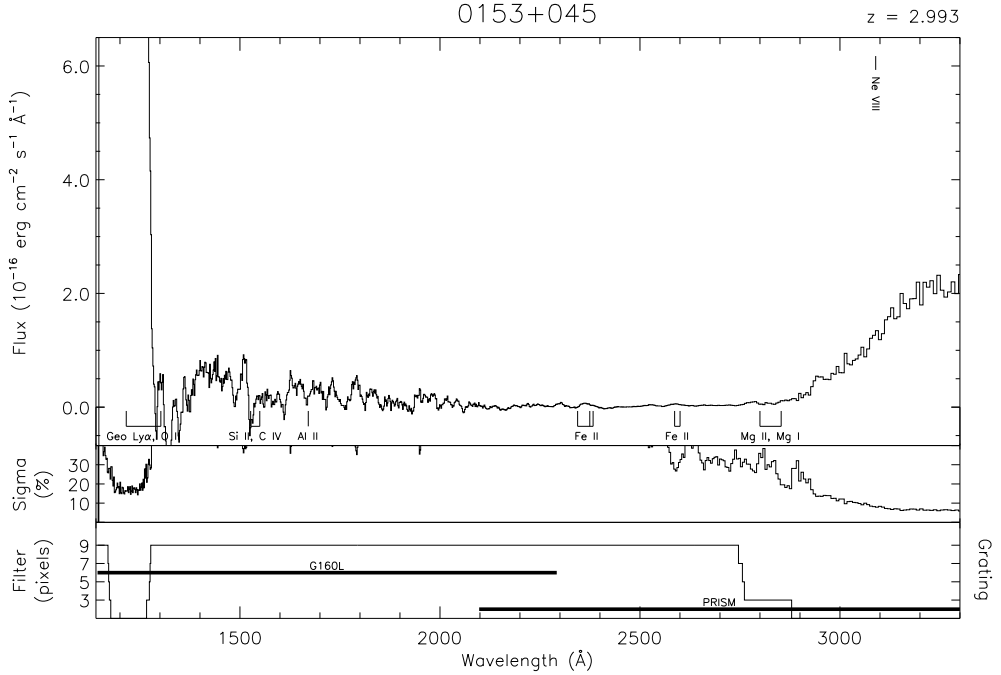
0153+045
z = 2.993
Flux (10^{-16} erg cm^{-2} s^{-1} Å^{-1})
Ne VIII
Geo Lyα, O II
Si II, C IV
Al II
Fe II
Fe II
Mg II, Mg I
Sigma (%)
G160L
PRISM
Filter (pixels)
Grating
Wavelength (Å)

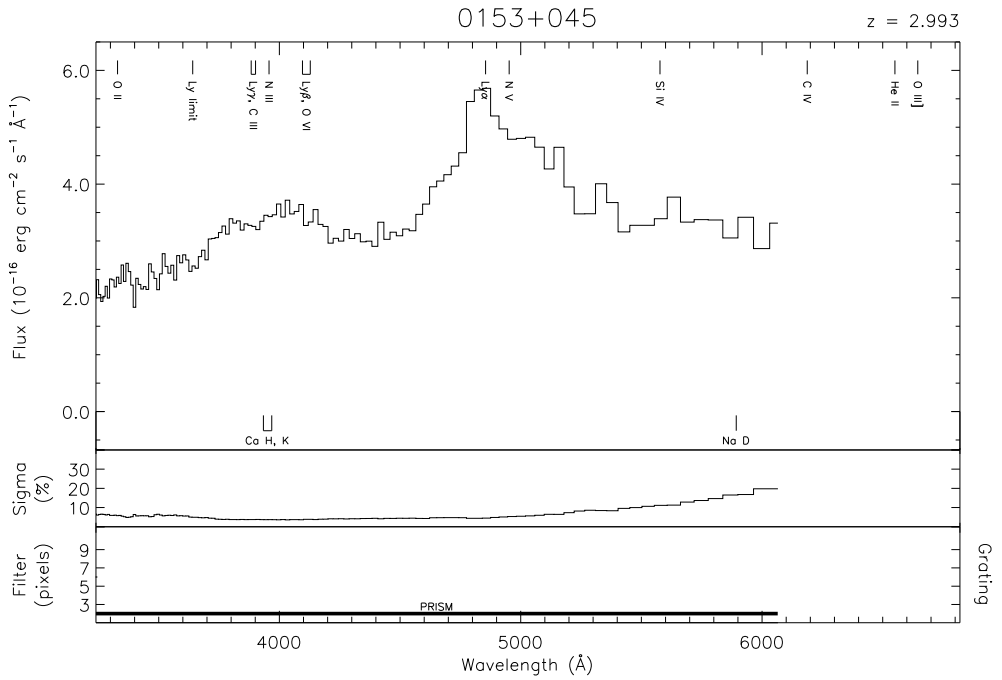
0153+045
z = 2.993
O II
Ly limit
Lyγ, C III
N III
Lyβ, O VI
Lyα
N V
Si IV
C IV
He II
O III]
Flux (10^{-16} erg cm^{-2} s^{-1} Å^{-1})
Ca H, K
Na D
Sigma (%)
Filter (pixels)
PRISM
Grating
Wavelength (Å)

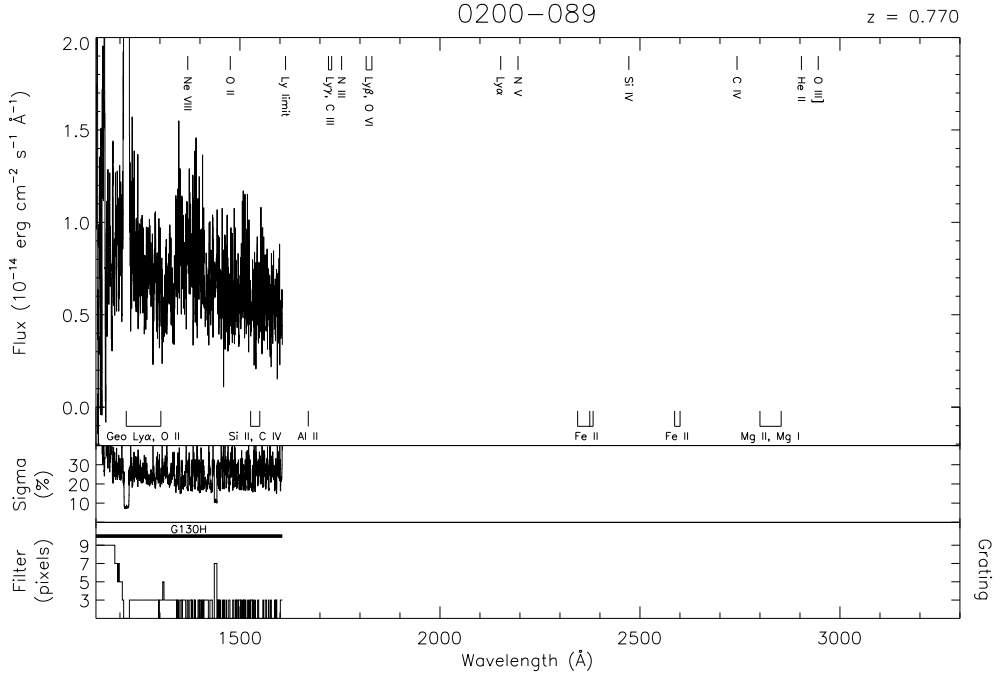
0200−089
z = 0.770
Ne VIII
O II
Ly limit
N III
Lyγ, C III
Lyβ, O VI
Lyα
N V
Si IV
C IV
He II
O III]
Flux (10^{-14} erg cm^{-2} s^{-1} Å^{-1})
Geo Lyα, O II
Si II, C IV
Al II
Fe II
Fe II
Mg II, Mg I
Sigma (%)
G130H
Filter (pixels)
Grating
Wavelength (Å)

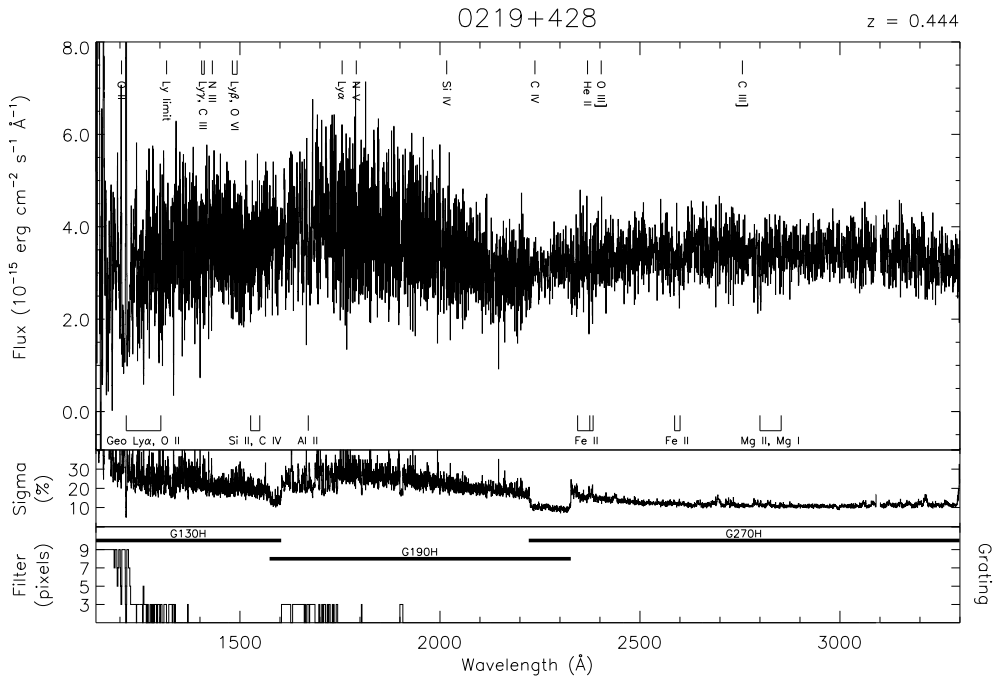
0219+428
z = 0.444
Flux (10^{-15} erg cm^{-2} s^{-1} Å^{-1})
Ly limit
N III
C III
Lyβ, O VI
Lyα
N V
Si IV
C IV
He II
O III]
C III]
Geo Lyα, O II
Si II, C IV
Al II
Fe II
Fe II
Mg II, Mg I
Sigma (%)
G130H
G190H
G270H
Filter (pixels)
Grating
Wavelength (Å)

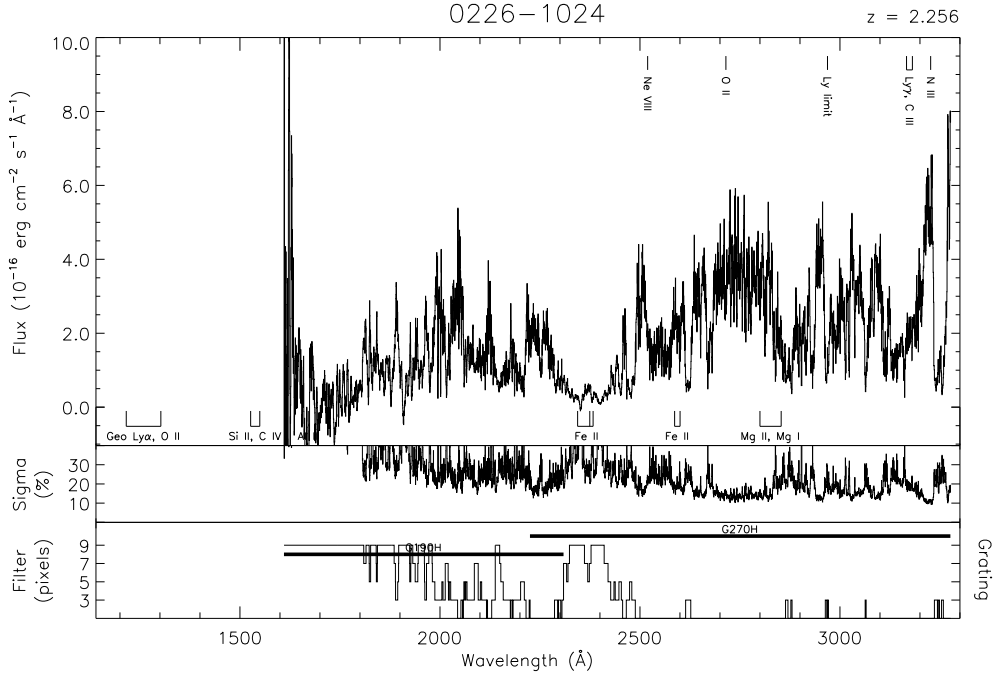
0226−1024
z = 2.256
Flux (10^{-16} erg cm^{-2} s^{-1} Å^{-1})
Ne VIII
O II
Ly limit
Lyγ, C III
N III
Geo Lyα, O II
Si II, C IV
Al II
Fe II
Fe II
Mg II, Mg I
Sigma (%)
G270H
G190H
Filter (pixels)
Grating
Wavelength (Å)

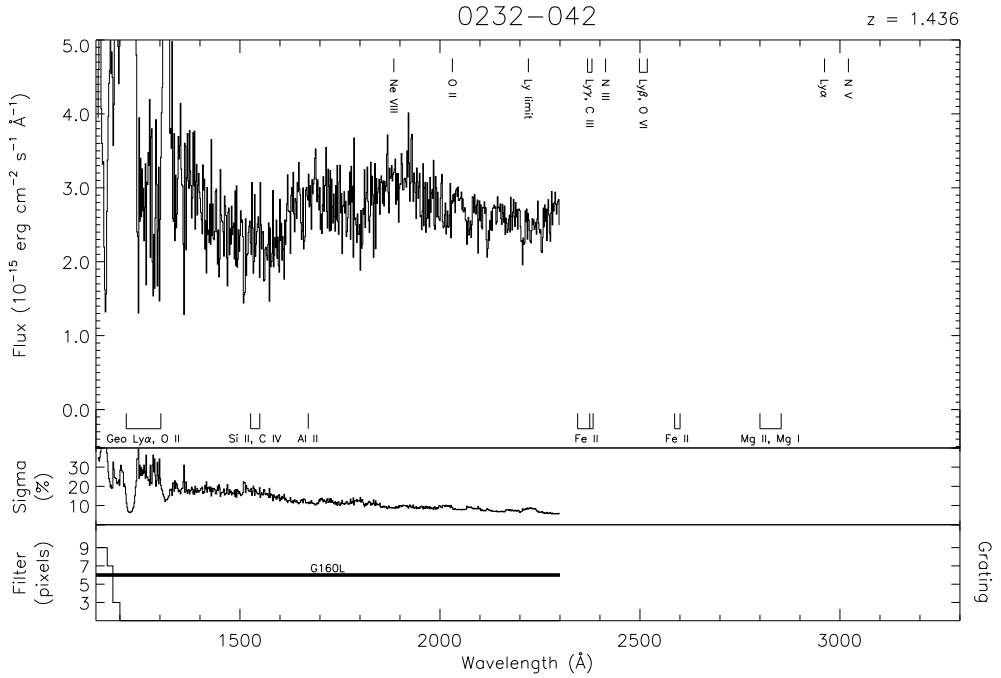
0232−042
z = 1.436
Flux (10^{-15} erg cm^{-2} s^{-1} Å^{-1})
Ne VIII
O II
Ly limit
Lyγ, C III
N III
Lyβ, O VI
Lyα
N V
Geo Lyα, O II
Si II, C IV
Al II
Fe II
Fe II
Mg II, Mg I
Sigma (%)
Filter (pixels)
G160L
Grating
Wavelength (Å)

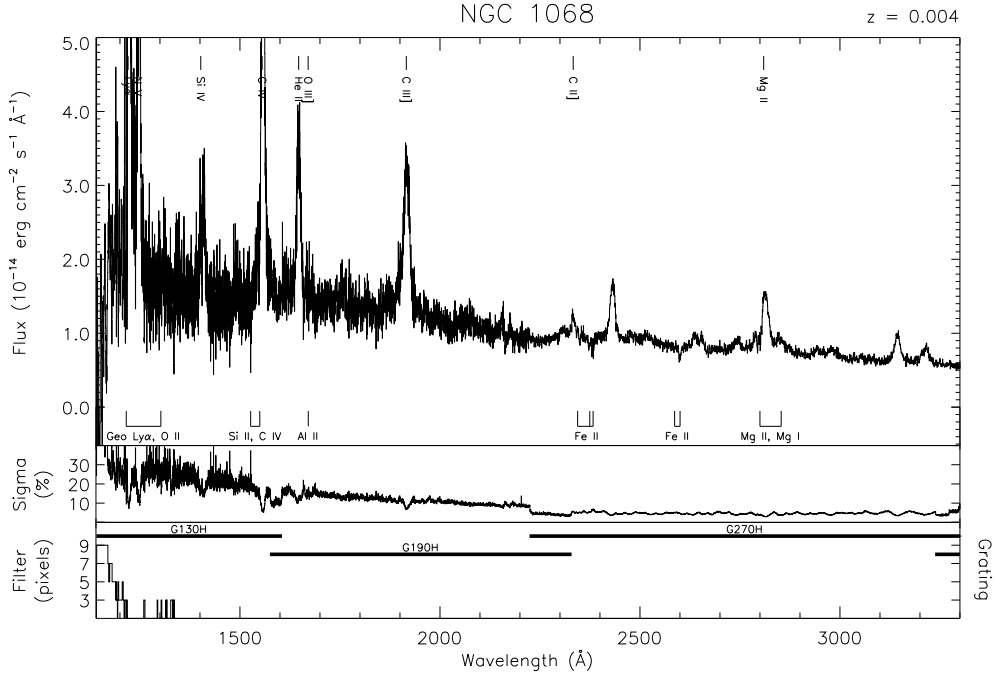
NGC 1068
z = 0.004
Flux (10^{-14} erg cm^{-2} s^{-1} Å^{-1})
Si IV
C IV
He II
O III]
C III]
C II]
Mg II
Geo Lyα, O II
Si II, C IV
Al II
Fe II
Fe II
Mg II, Mg I
Sigma (%)
G130H
G190H
G270H
Filter (pixels)
Grating
Wavelength (Å)

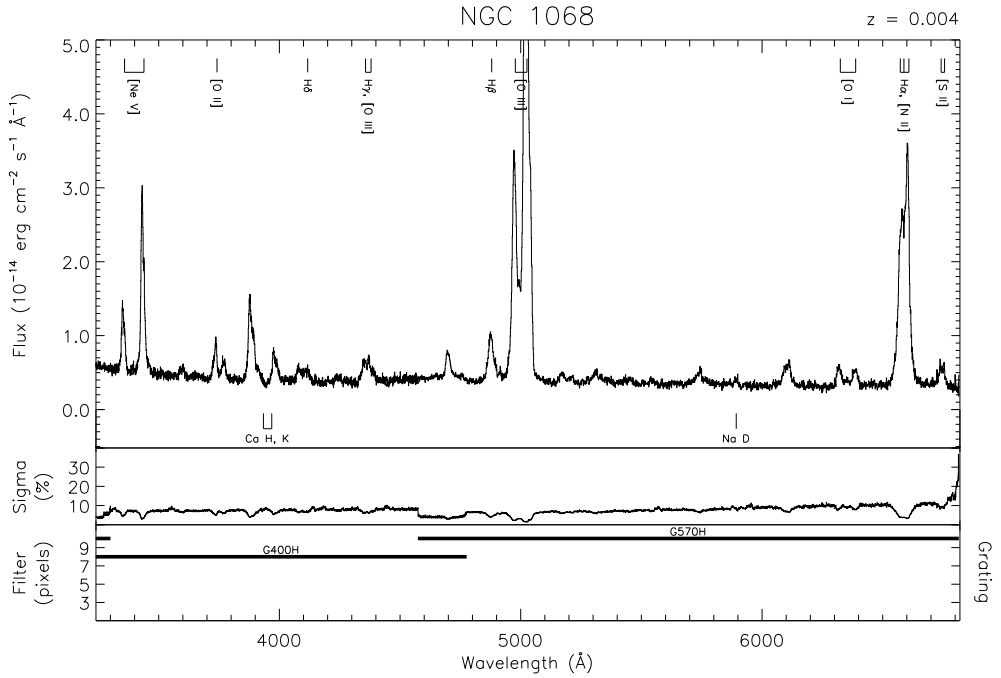
NGC 1068
z = 0.004
Flux (10^{-14} erg cm^{-2} s^{-1} Å^{-1})
[Ne V]
[O II]
Hδ
[Ne III], O III]
Hβ
[O III]
[O I]
Hα, [N II]
[S II]
Ca H, K
Na D
Sigma (%)
G570H
G400H
Filter (pixels)
Grating
Wavelength (Å)

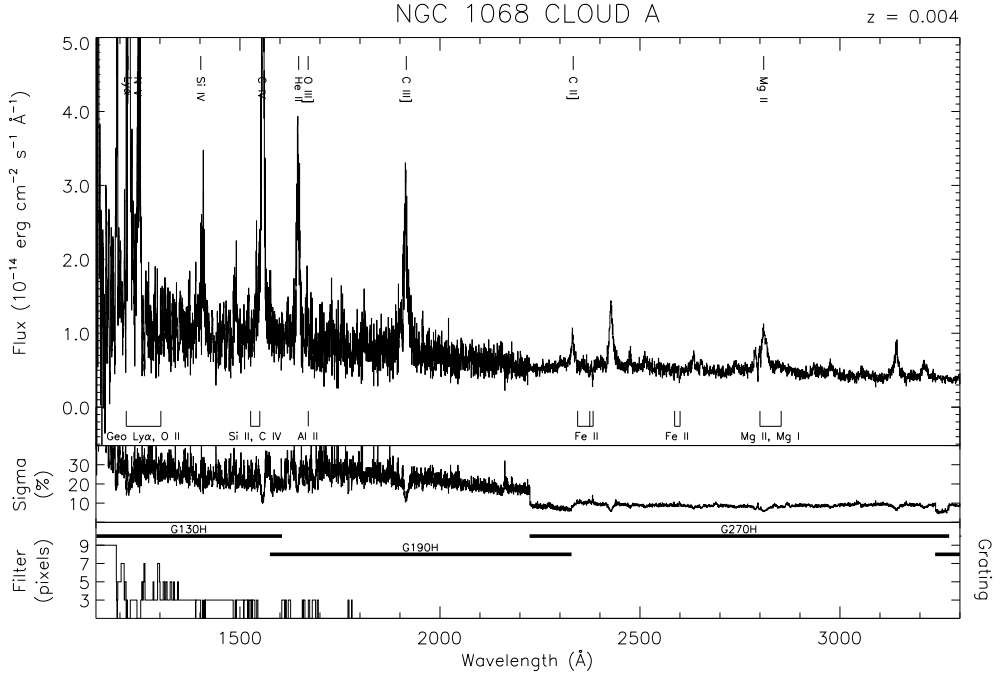
NGC 1068 CLOUD A
z = 0.004
Flux (10^{-14} erg cm^{-2} s^{-1} Å^{-1})
Si IV
C IV
He II
O III]
C III]
C II]
Mg II
Geo Lyα, O II
Si II, C IV
Al II
Fe II
Fe II
Mg II, Mg I
Sigma (%)
G130H
G190H
G270H
Filter (pixels)
Grating
Wavelength (Å)

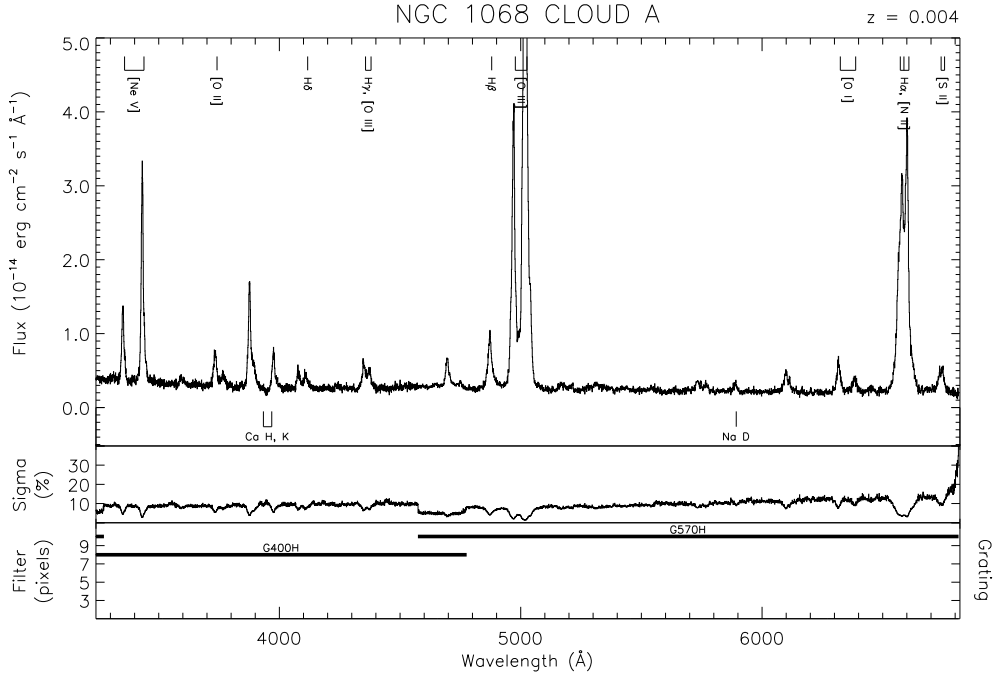
NGC 1068 CLOUD A
z = 0.004
Flux (10^{-14} erg cm^{-2} s^{-1} Å^{-1})
[Ne V]
[O II]
Hδ
[Ne III], [O III]
Hβ
[O III]
[O I]
Hα, [N II]
[S II]
Ca H, K
Na D
Sigma (%)
G570H
G400H
Filter (pixels)
Grating
Wavelength (Å)

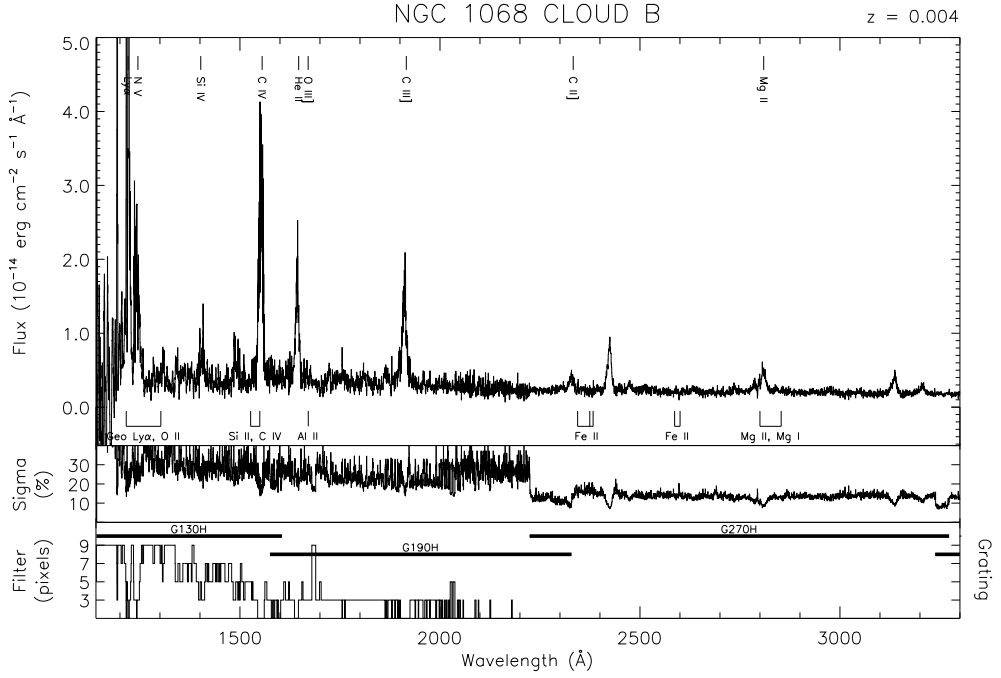
NGC 1068 CLOUD B
z = 0.004
Flux (10^{-14} erg cm^{-2} s^{-1} Å^{-1})
Lyβ
N V
Si IV
C IV
He II
O III]
C III]
C II]
Mg II
Geo Lyα, O II
Si II, C IV
Al II
Fe II
Fe II
Mg II, Mg I
Sigma (%)
G130H
G270H
G190H
Filter (pixels)
Grating
Wavelength (Å)

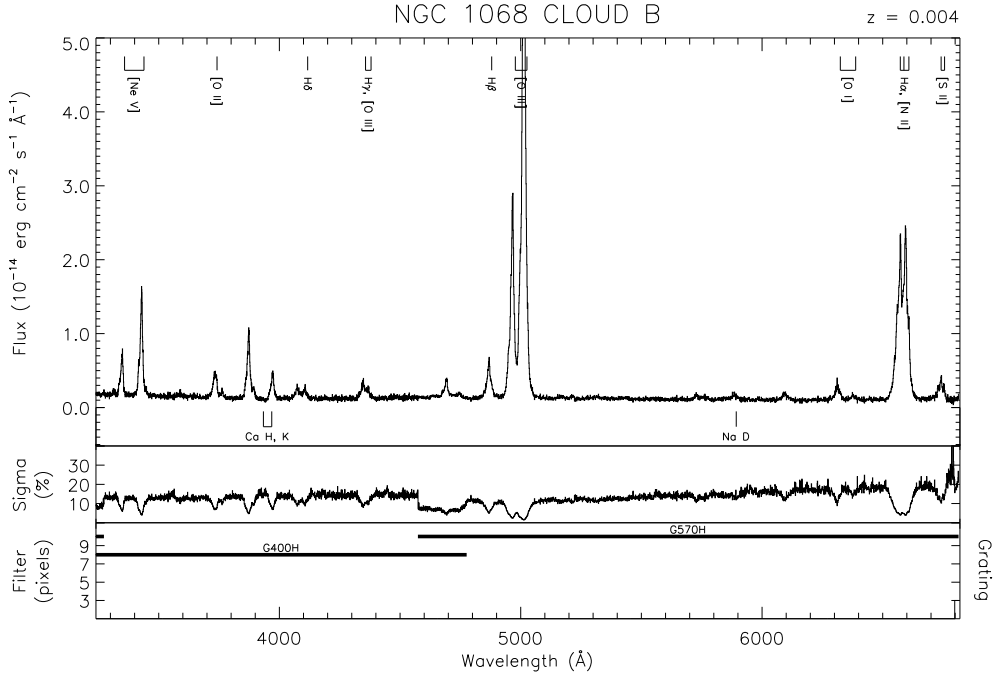
NGC 1068 CLOUD B
z = 0.004
Flux (10^{-14} erg cm^{-2} s^{-1} Å^{-1})
[Ne V]
[O II]
Hδ
[Ne III], O III]
Hε
[O III]
[O I]
Hα, [N II]
[S II]
Ca H, K
Na D
Sigma (%)
G570H
G400H
Filter (pixels)
Grating
Wavelength (Å)

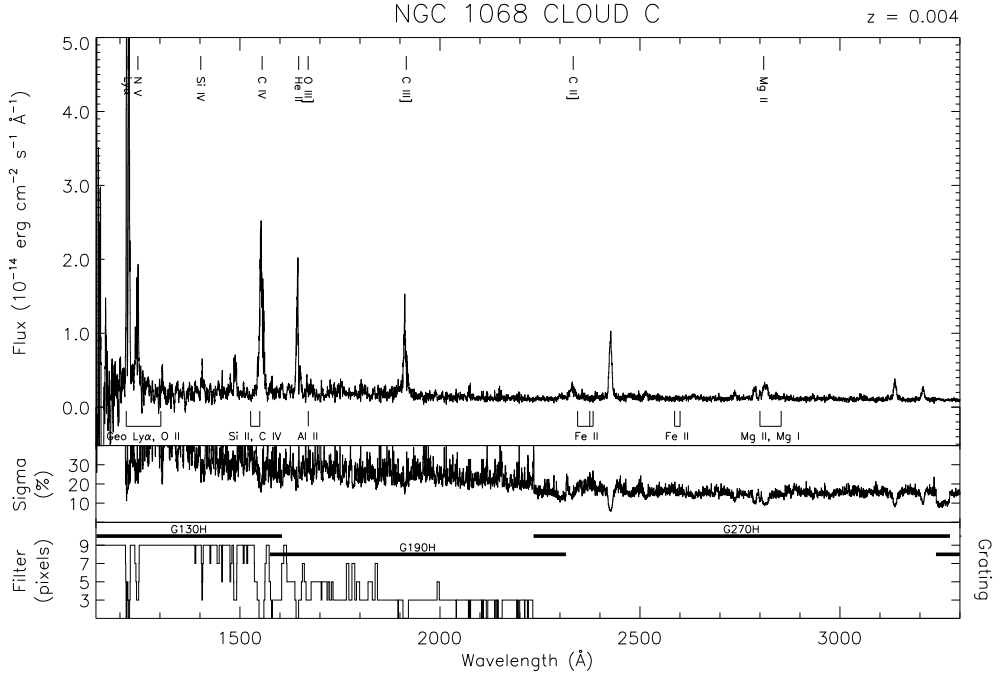
NGC 1068 CLOUD C
z = 0.004
Flux (10^{-14} erg cm^{-2} s^{-1} Å^{-1})
Lyβ
N V
Si IV
C IV
He II
O III]
C III]
C II]
Mg II
Geo Lyα, O II
Si II, C IV
Al II
Fe II
Fe II
Mg II, Mg I
Sigma (%)
G130H
G270H
G190H
Filter (pixels)
Grating
Wavelength (Å)

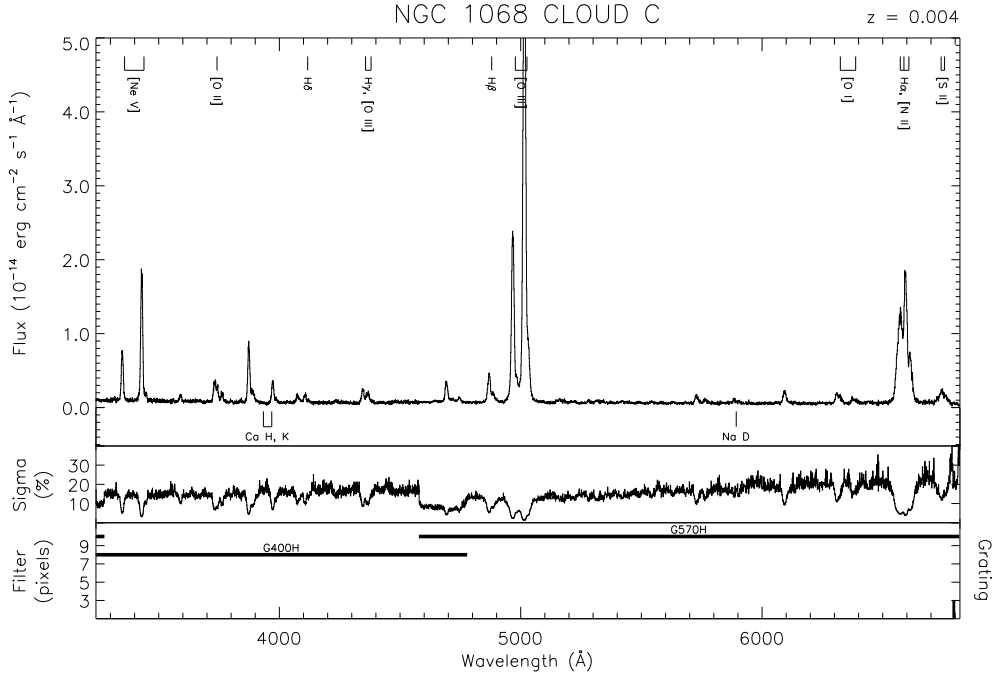
NGC 1068 CLOUD C
z = 0.004
Flux (10^{-14} erg cm^{-2} s^{-1} Å^{-1})
[Ne V]
[O II]
Hδ
[Ne III], O III]
Hγ
[O III]
[O I]
Hα, [N II]
[S II]
Ca H, K
Na D
Sigma (%)
G570H
G400H
Filter (pixels)
Grating
Wavelength (Å)

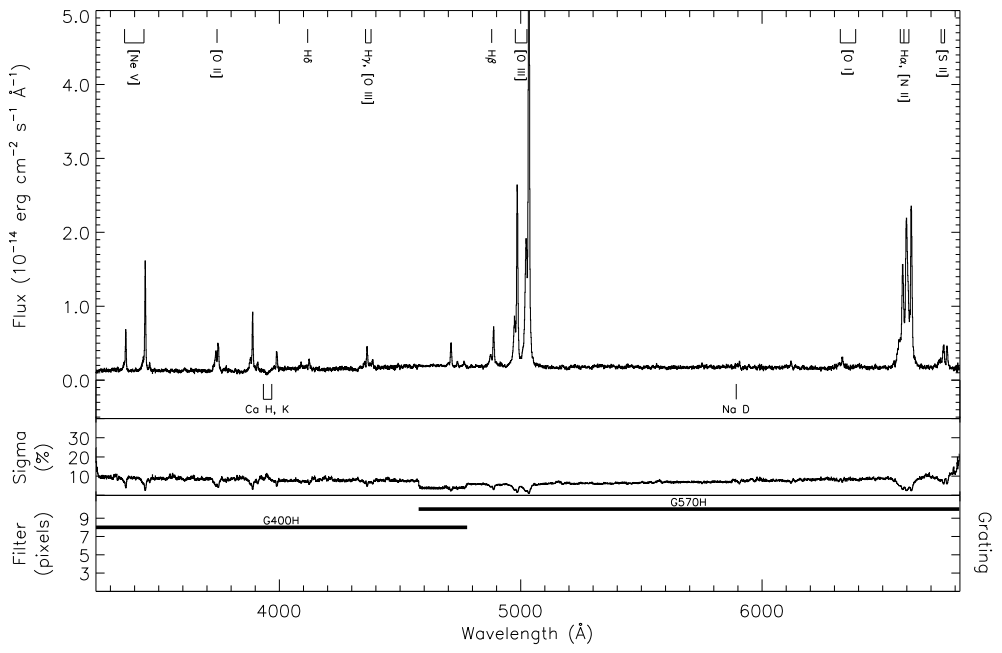
NGC 1068 CLOUD D
z = 0.004
Flux (10^{-14} erg cm^{-2} s^{-1} Å^{-1})
[Ne V]
[O II]
Hδ
[Ne III], O III]
Hγ
[O III]
[O I]
Hα, [N II]
[S II]
Ca H, K
Na D
Sigma (%)
G570H
G400H
Filter (pixels)
Grating
Wavelength (Å)

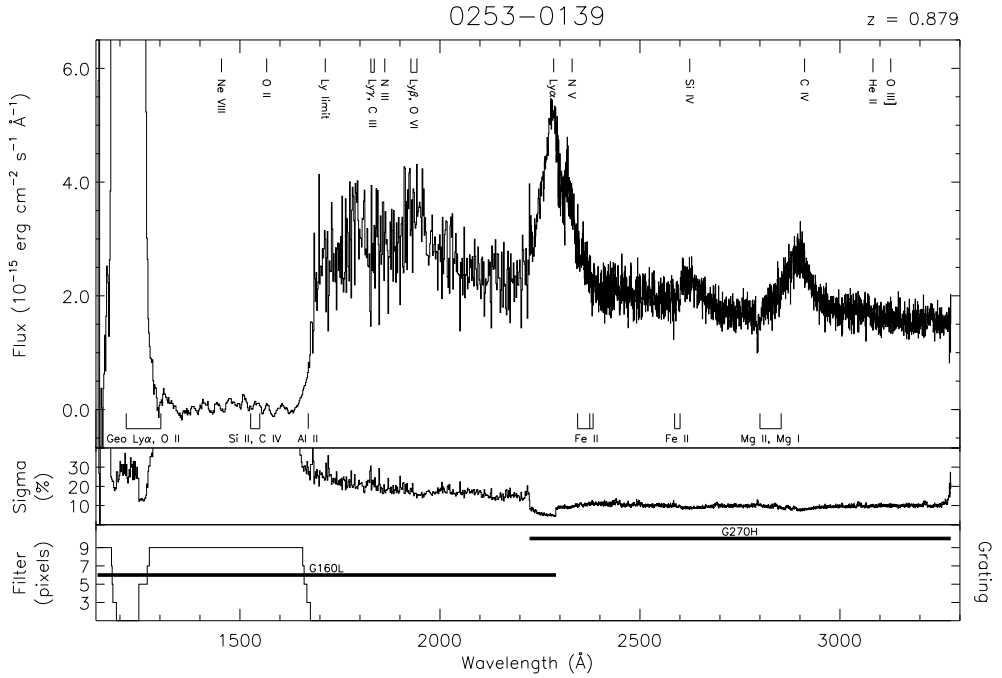
0253−0139
z = 0.879
Flux (10^{-15} erg cm^{-2} s^{-1} Å^{-1})
Ne VIII
O II
Ly limit
N III
Lyγ, C III
Lyβ, O VI
Lyα
N V
Si IV
C IV
He II
O III]
Geo Lyα, O II
Si II, C IV
Al II
Fe II
Fe II
Mg II, Mg I
Sigma (%)
G270H
G160L
Filter (pixels)
Grating
Wavelength (Å)

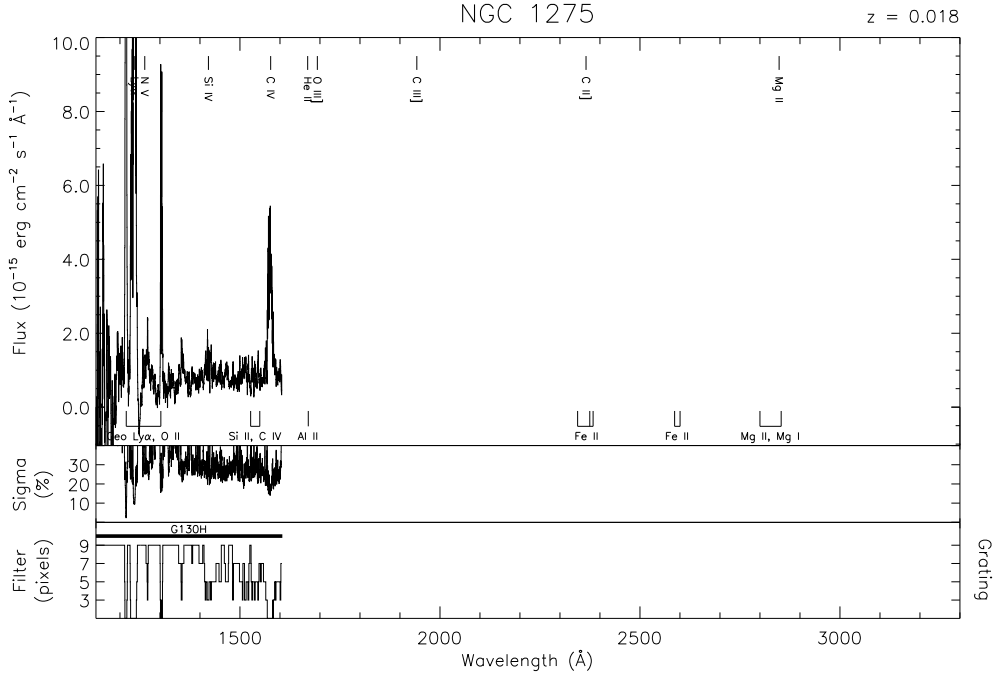
NGC 1275
z = 0.018
Flux (10^{-15} erg cm^{-2} s^{-1} Å^{-1})
Lyα
N V
Si IV
C IV
O III]
He II
C III]
C II]
Mg II
Geo Lyα, O II
Si II, C IV
Al II
Fe II
Fe II
Mg II, Mg I
Sigma (%)
G130H
Filter (pixels)
Grating
Wavelength (Å)

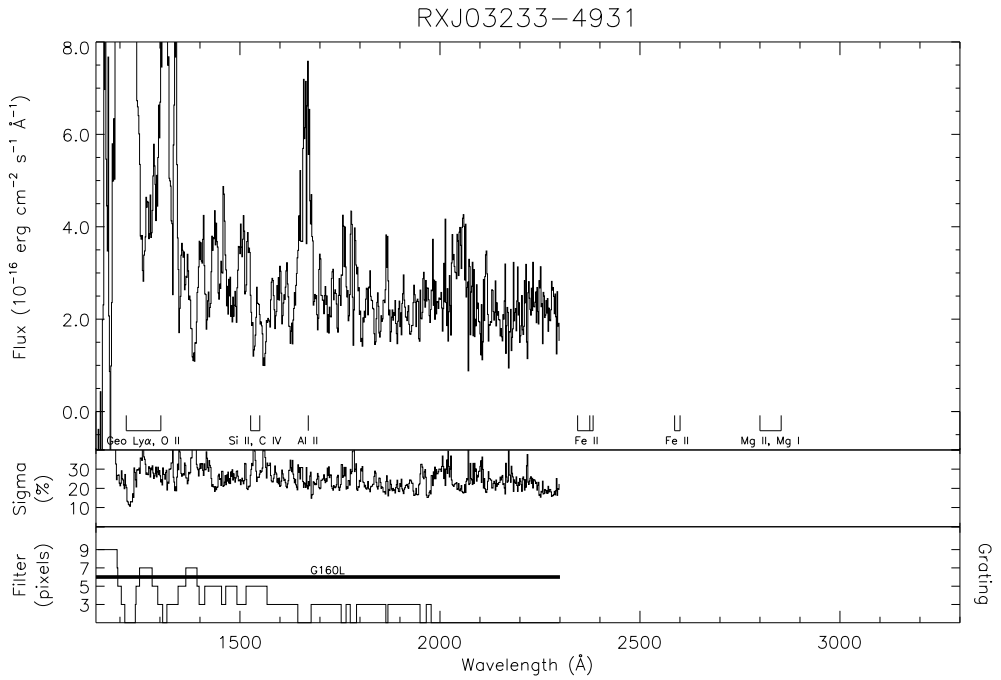
RXJ03233−4931
Flux (10^{-16} erg cm^{-2} s^{-1} Å^{-1})
Geo Lyα, O II
Si II, C IV
Al II
Fe II
Fe II
Mg II, Mg I
Sigma (%)
Filter (pixels)
G160L
Grating
Wavelength (Å)

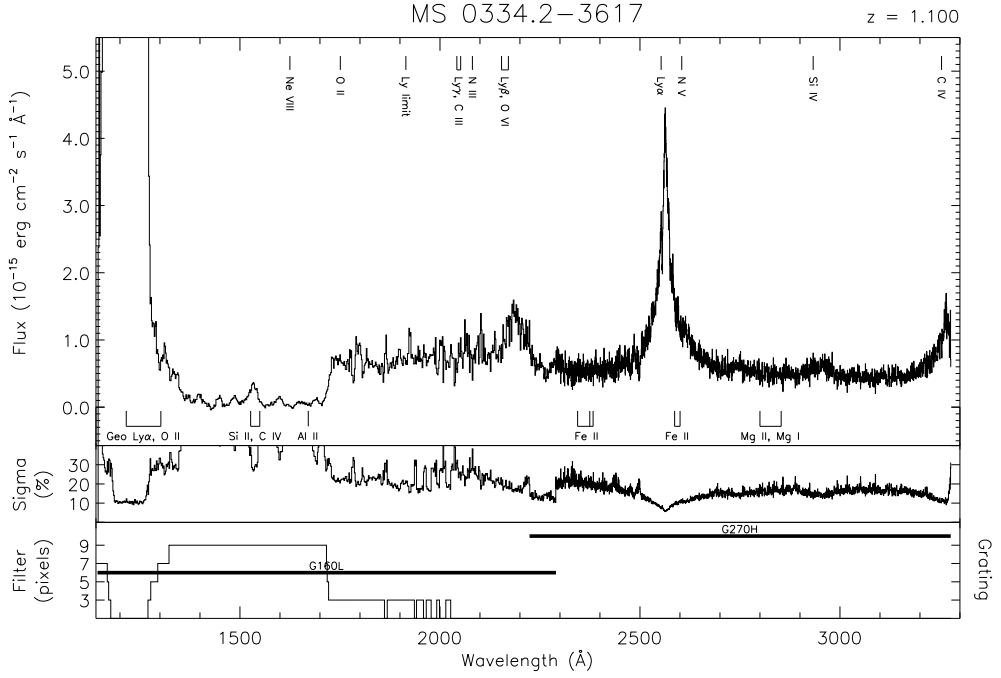
MS 0334.2−3617
z = 1.100
Flux (10^{-15} erg cm^{-2} s^{-1} Å^{-1})
Ne VIII
O II
Ly limit
Lyγ, C III
N III
Lyβ, O VI
Lyα
N V
Si IV
C IV
Geo Lyα, O II
Si II, C IV
Al II
Fe II
Fe II
Mg II, Mg I
Sigma (%)
G270H
G160L
Filter (pixels)
Grating
Wavelength (Å)

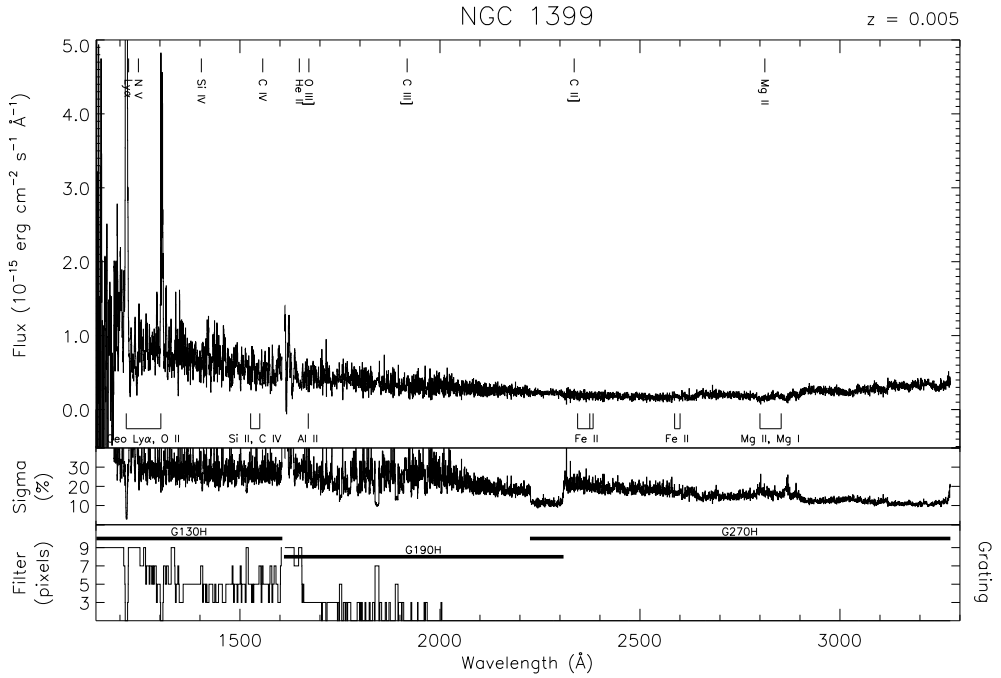
NGC 1399
z = 0.005
Flux (10^{-15} erg cm^{-2} s^{-1} Å^{-1})
Geo Lyα, O II
Si II, C IV
Al II
Fe II
Fe II
Mg II, Mg I
Sigma (%)
G130H
G190H
G270H
Filter (pixels)
Grating
Wavelength (Å)

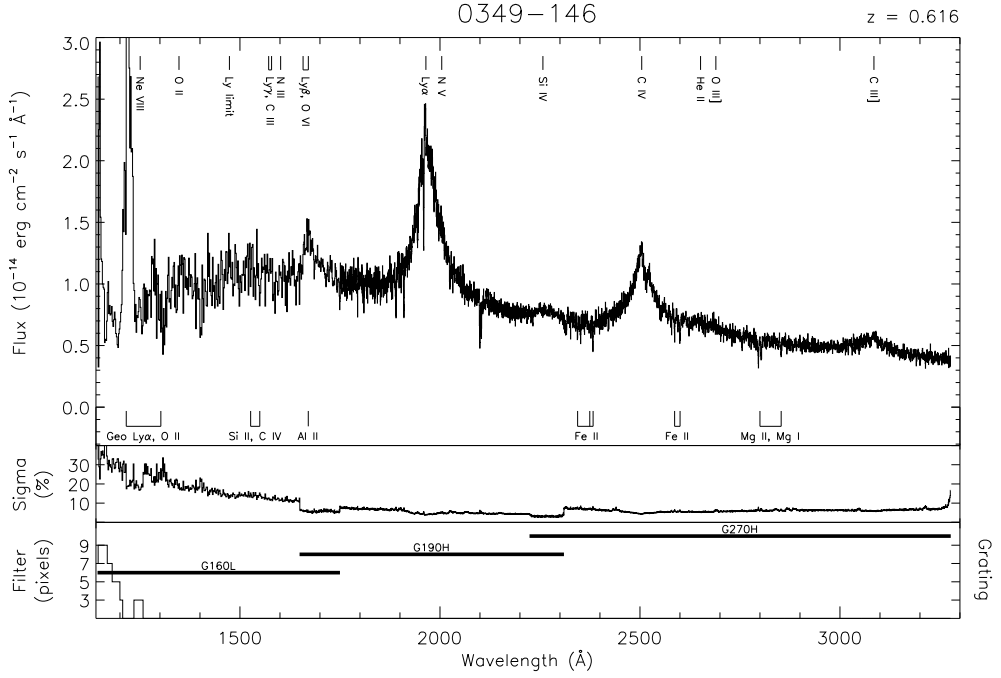
0349−146
z = 0.616
Flux (10^{-14} erg cm^{-2} s^{-1} Å^{-1})
Ne VIII
O II
Ly limit
N III
Lyγ, C III
Lyδ, O VI
Lyα
N V
Si IV
C IV
He II
O III]
C III]
Geo Lyα, O II
Si II, C IV
Al II
Fe II
Fe II
Mg II, Mg I
Sigma (%)
G160L
G190H
G270H
Filter (pixels)
Grating
Wavelength (Å)

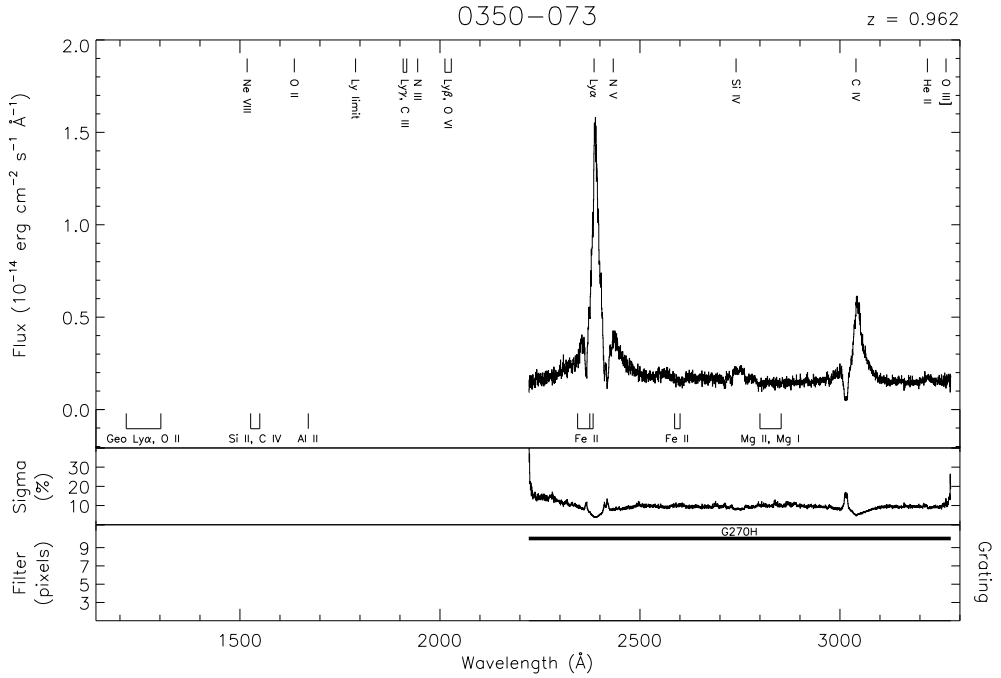
0350−073
z = 0.962
Flux (10^{-14} erg cm^{-2} s^{-1} Å^{-1})
Ne VIII
O II
Ly limit
N III
Lyγ, C III
Lyβ, O VI
Lyα
N V
Si IV
C IV
He II
O III]
Geo Lyα, O II
Si II, C IV
Al II
Fe II
Fe II
Mg II, Mg I
Sigma (%)
G270H
Filter (pixels)
Grating
Wavelength (Å)

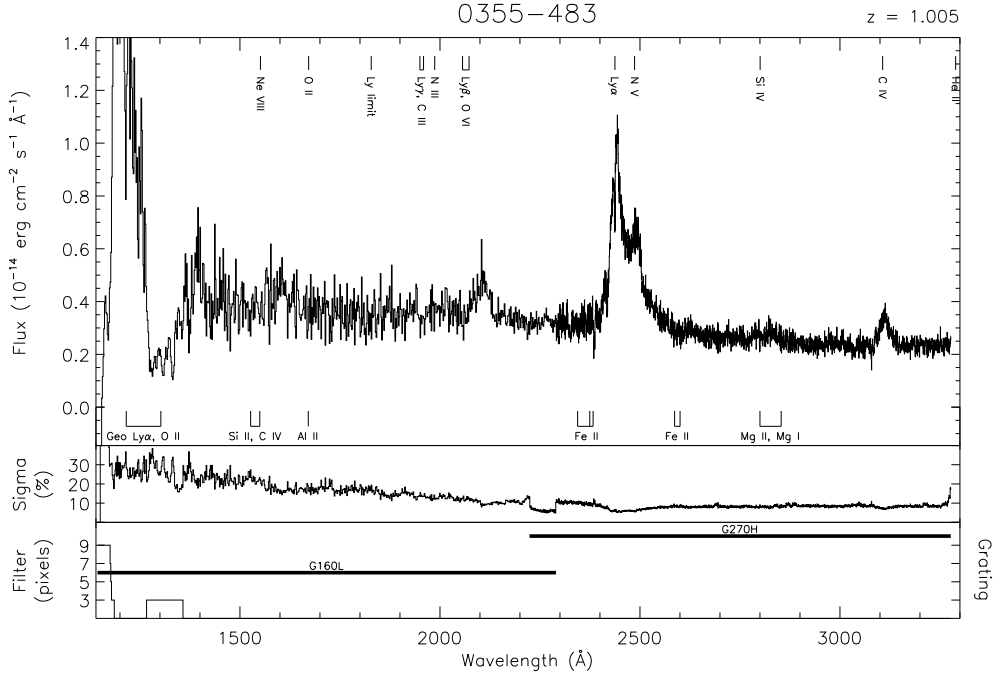
0355−483
z = 1.005
Flux (10^{-14} erg cm^{-2} s^{-1} Å^{-1})
Ne VIII
O II
Ly limit
N III
Lyγ, C III
Lyβ, O VI
Lyα
N V
Si IV
C IV
Hα II
Geo Lyα, O II
Si II, C IV
Al II
Fe II
Fe II
Mg II, Mg I
Sigma (%)
G270H
G160L
Filter (pixels)
Grating
Wavelength (Å)

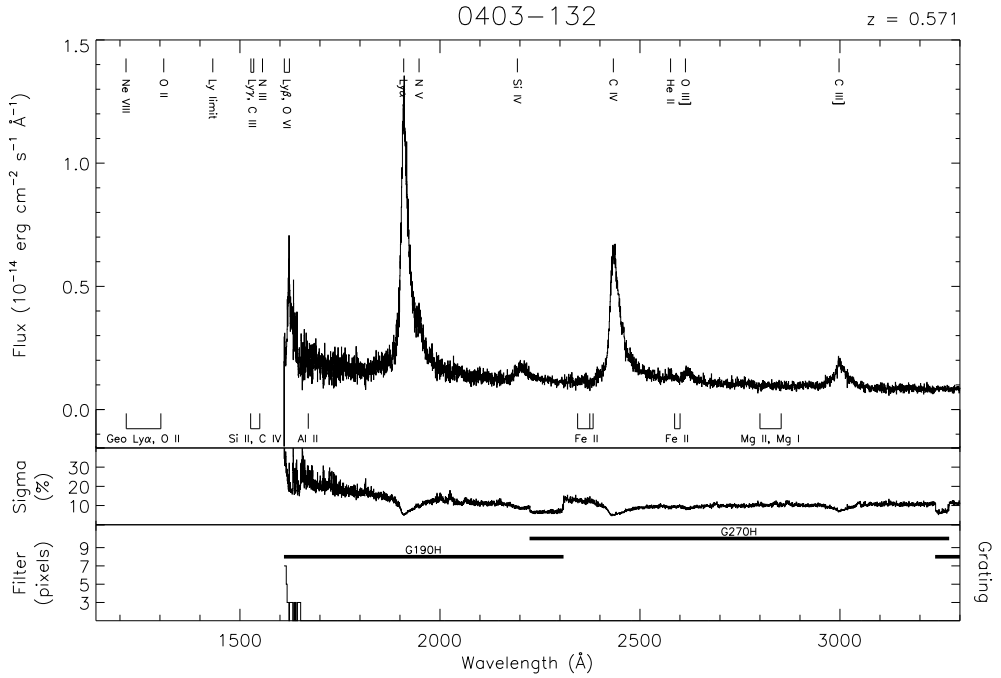
0403−132
z = 0.571
Flux (10^{-14} erg cm^{-2} s^{-1} Å^{-1})
Ne VIII
O II
Ly limit
N III
Lyγ, C III
Lyβ, O VI
Lyα
N V
Si IV
C IV
He II
O III]
C III]
Geo Lyα, O II
Si II, C IV
Al II
Fe II
Fe II
Mg II, Mg I
Sigma (%)
G270H
G190H
Filter (pixels)
Grating
Wavelength (Å)

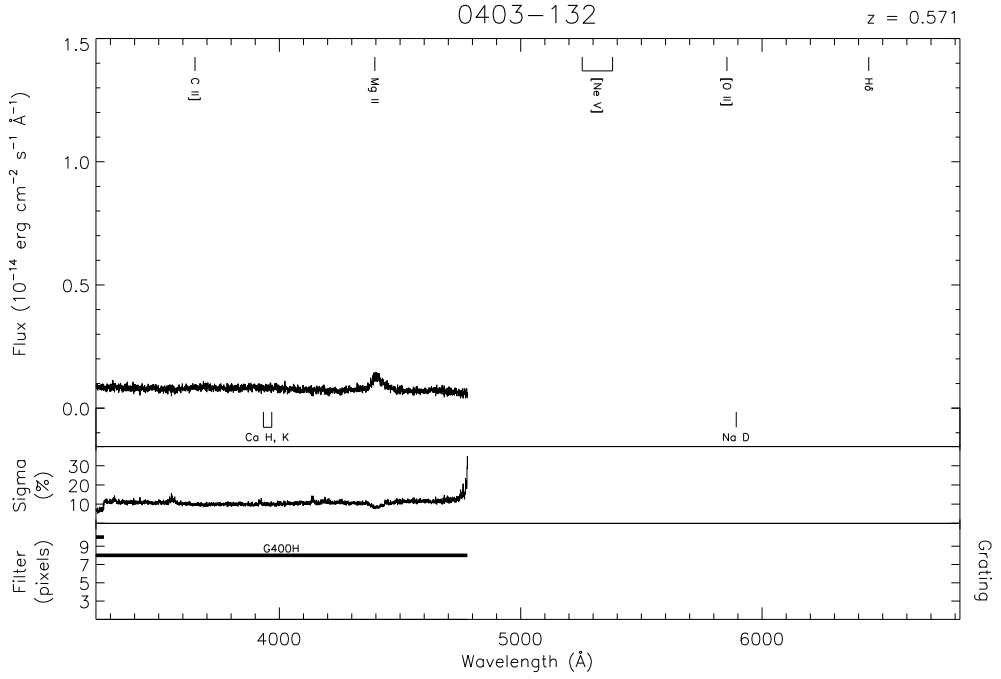
0403−132
z = 0.571
Flux (10^{-14} erg cm^{-2} s^{-1} Å^{-1})
C II]
Mg II
[Ne V]
[O II]
Hδ
Ca H, K
Na D
Sigma (%)
G400H
Filter (pixels)
Grating
Wavelength (Å)

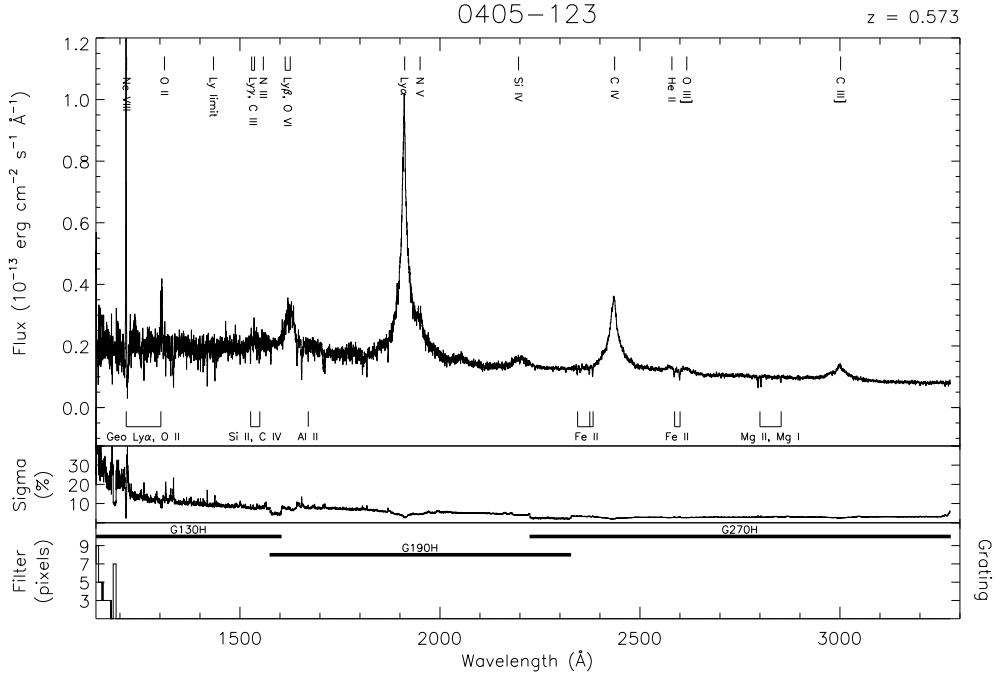
0405−123
z = 0.573
Flux (10^{-13} erg cm^{-2} s^{-1} Å^{-1})
Ne VIII
O II
Ly limit
N III
Lyγ, C III
Lyβ, O VI
N V
Lyα
Si IV
C IV
He II
O III]
C III]
Geo Lyα, O II
Si II, C IV
Al II
Fe II
Fe II
Mg II, Mg I
Sigma (%)
G130H
G270H
G190H
Filter (pixels)
Grating
Wavelength (Å)

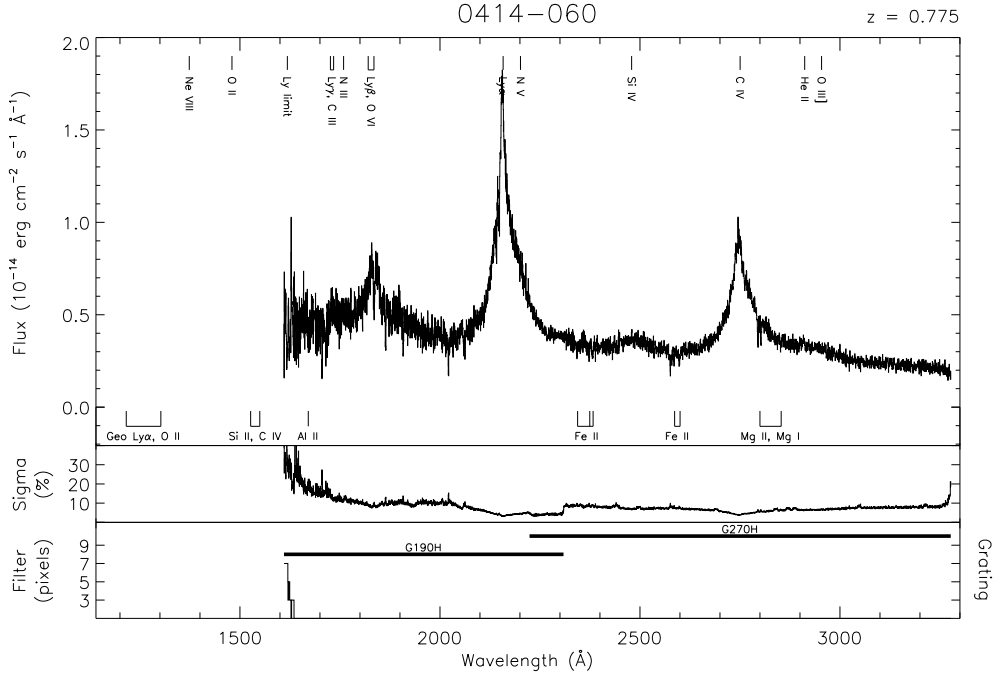
0414−060
z = 0.775
Flux (10^{-14} erg cm^{-2} s^{-1} Å^{-1})
Ne VIII
O II
Ly limit
N III
Lyγ, C III
Lyβ, O VI
N V
Lyα
Si IV
C IV
He II
O III]
Geo Lyα, O II
Si II, C IV
Al II
Fe II
Fe II
Mg II, Mg I
Sigma (%)
G270H
G190H
Filter (pixels)
Grating
Wavelength (Å)

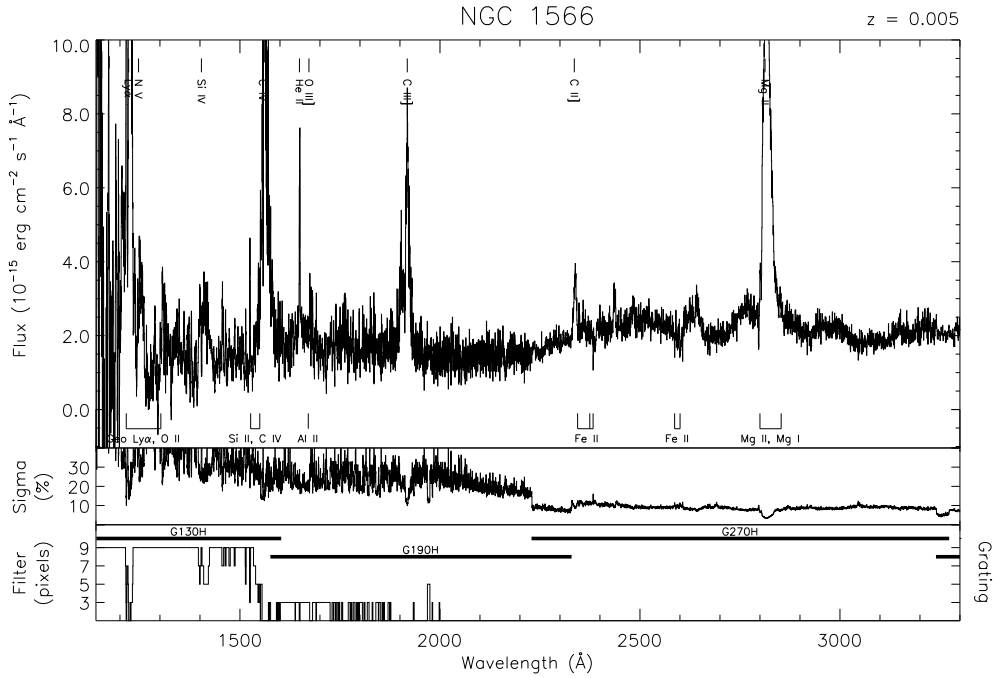
NGC 1566
z = 0.005
Flux (10^{-15} erg cm^{-2} s^{-1} Å^{-1})
Geo Lyα, O II
Si II, C IV
Al II
Fe II
Fe II
Mg II, Mg I
Sigma (%)
G130H
G190H
G270H
Filter (pixels)
Grating
Wavelength (Å)

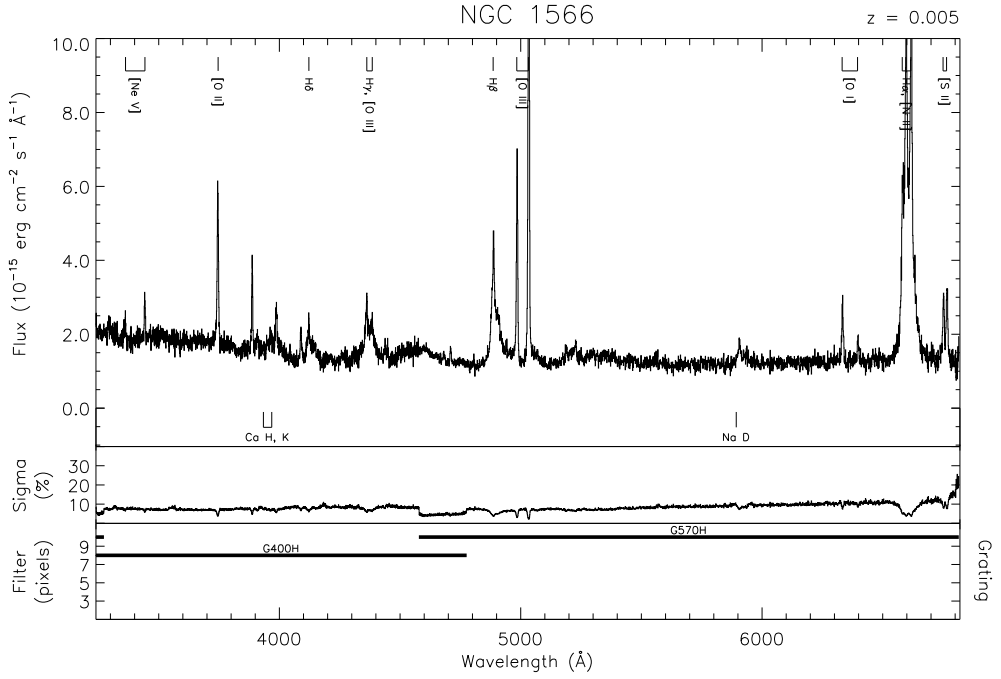
NGC 1566
z = 0.005
Flux (10^{-15} erg cm^{-2} s^{-1} Å^{-1})
Ca H, K
Na D
Sigma (%)
G400H
G570H
Filter (pixels)
Grating
Wavelength (Å)

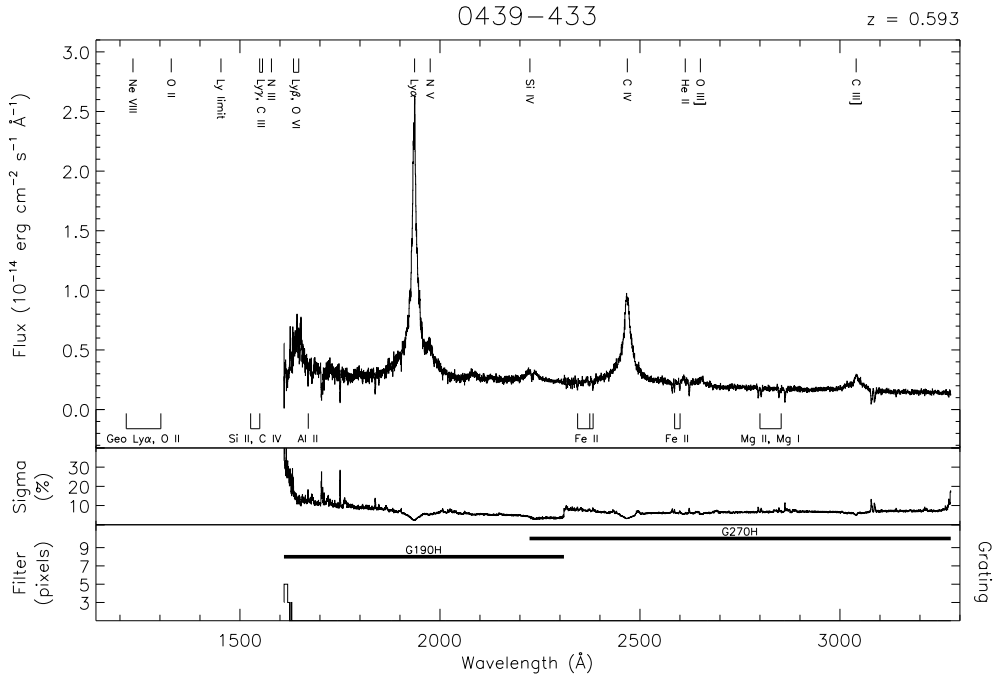
0439−433
z = 0.593
Flux (10^{-14} erg cm^{-2} s^{-1} Å^{-1})
Ne VIII
O II
Ly limit
N III
Lyγ, C III
Lyβ, O VI
Lyα
N V
Si IV
C IV
He II
O III]
C III]
Geo Lyα, O II
Si II, C IV
Al II
Fe II
Fe II
Mg II, Mg I
Sigma (%)
G270H
G190H
Filter (pixels)
Grating
Wavelength (Å)

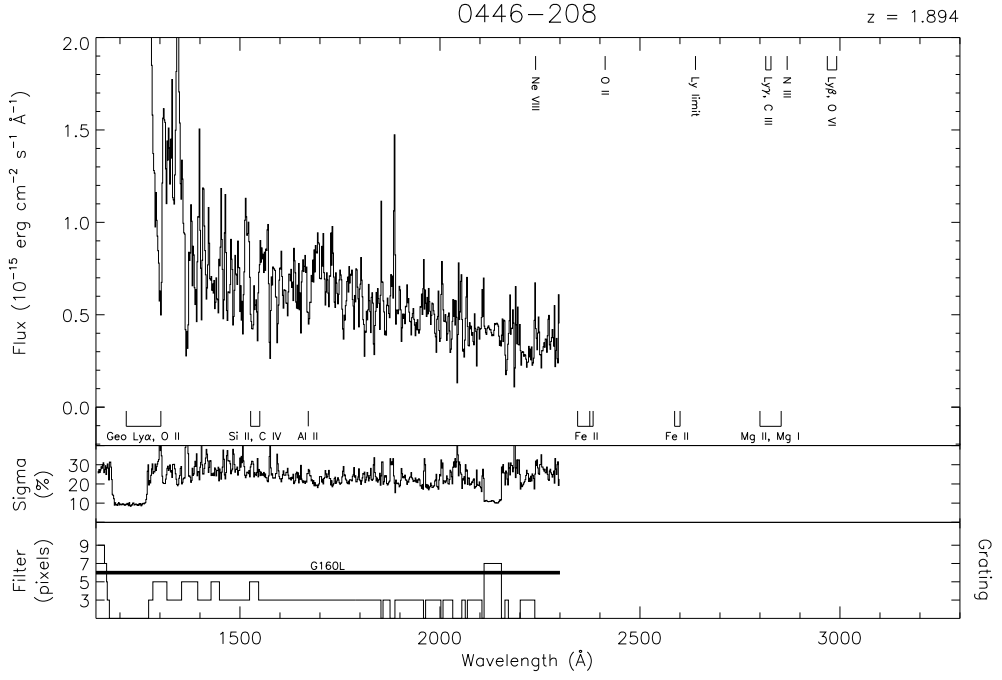
0446−208
z = 1.894
Flux (10^{-15} erg cm^{-2} s^{-1} Å^{-1})
Ne VIII
O II
Ly limit
N III
Lyγ, C III
Lyβ, O VI
Geo Lyα, O II
Si II, C IV
Al II
Fe II
Fe II
Mg II, Mg I
Sigma (%)
G160L
Filter (pixels)
Grating
Wavelength (Å)

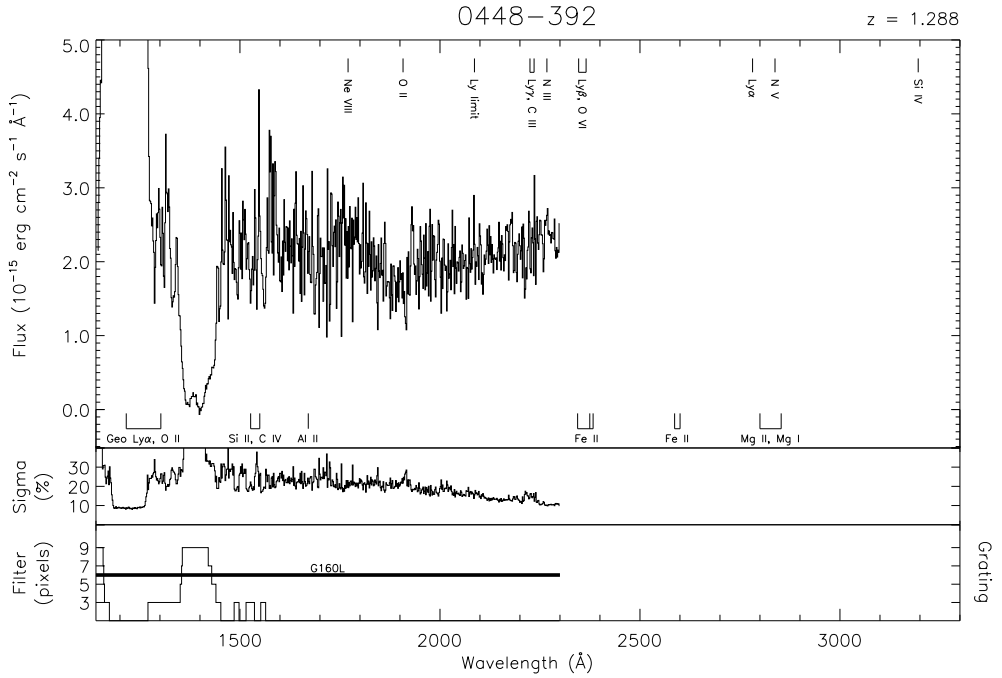
0448−392
z = 1.288
Flux (10^{-15} erg cm^{-2} s^{-1} Å^{-1})
Ne VIII
O II
Ly limit
N III
Lyγ, C III
Lyβ, O VI
Lyα
N V
Si IV
Geo Lyα, O II
Si II, C IV
Al II
Fe II
Fe II
Mg II, Mg I
Sigma (%)
Filter (pixels)
G160L
Grating
Wavelength (Å)

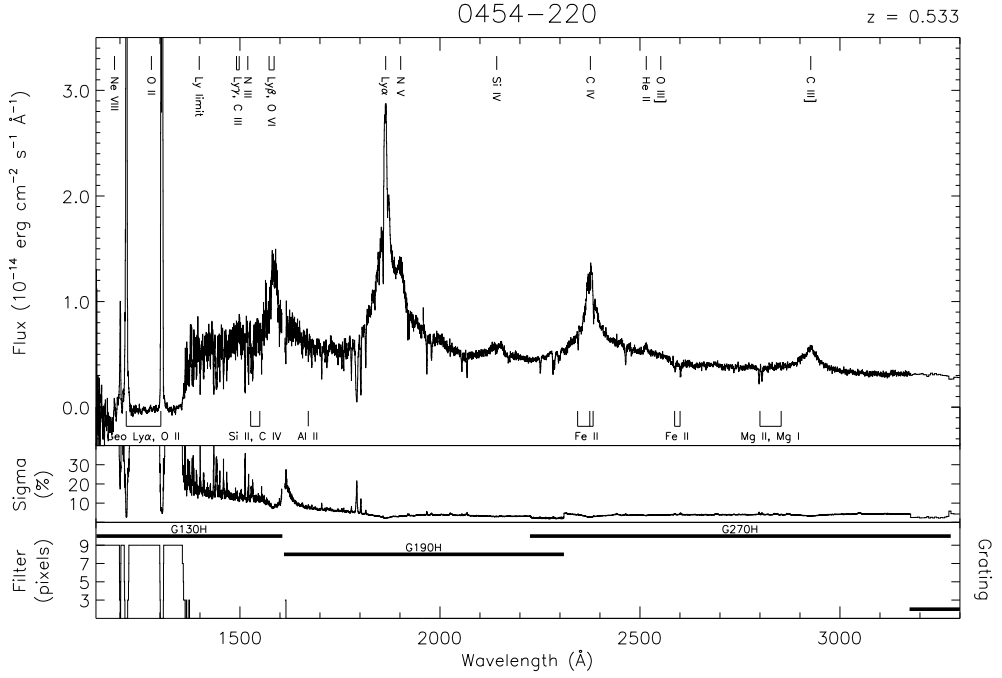
0454−220
z = 0.533
Flux (10^{-14} erg cm^{-2} s^{-1} Å^{-1})
Ne VIII
O II
Ly limit
N III
Lyγ, C III
Lyβ, O VI
Lyα
N V
Si IV
C IV
He II
O III]
C III]
Geo Lyα, O II
Si II, C IV
Al II
Fe II
Fe II
Mg II, Mg I
Sigma (%)
G130H
G190H
G270H
Filter (pixels)
Grating
Wavelength (Å)

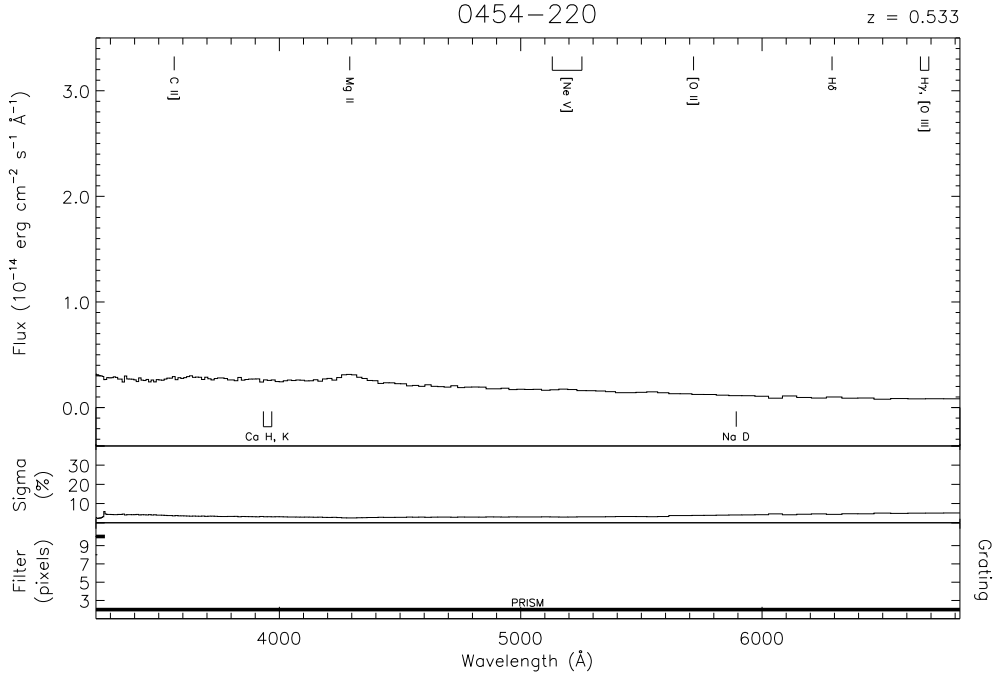
0454−220
z = 0.533
C II]
Mg II
[Ne V]
[O II]
Hδ
Hγ, [O III]
Flux (10^{-14} erg cm^{-2} s^{-1} Å^{-1})
Ca H, K
Na D
Sigma (%)
Filter (pixels)
PRISM
Grating
Wavelength (Å)

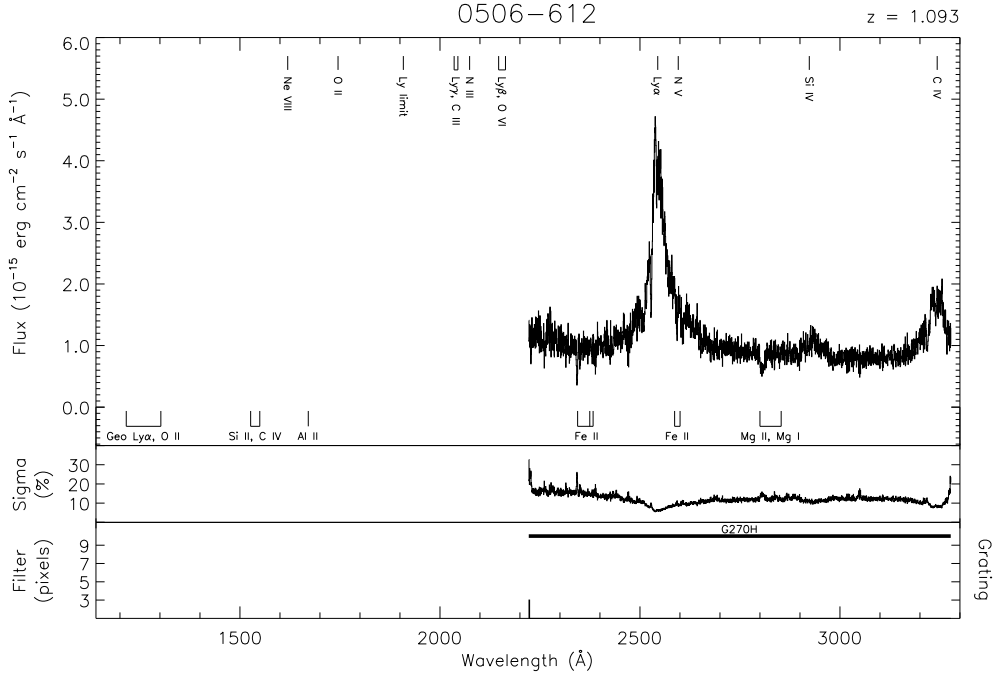
0506−612
z = 1.093
Ne VIII
O II
Ly limit
N III
Lyγ, C III
Lyβ, O VI
Lyα
N V
Si IV
C IV
Flux (10^{-15} erg cm^{-2} s^{-1} Å^{-1})
Geo Lyα, O II
Si II, C IV
Al II
Fe II
Fe II
Mg II, Mg I
Sigma (%)
G270H
Filter (pixels)
Grating
Wavelength (Å)

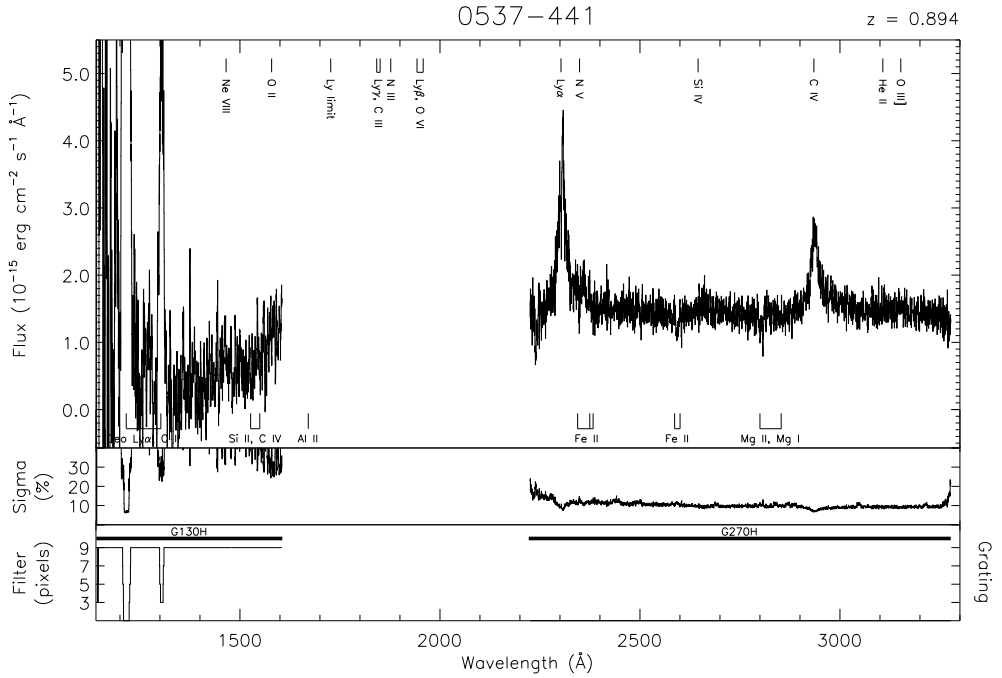
0537−441
z = 0.894
Flux (10^{-15} erg cm^{-2} s^{-1} Å^{-1})
Ne VIII
O II
Ly limit
N III
Lyγ, C III
Lyβ, O VI
Lyα
N V
Si IV
C IV
He II
O III]
Geo Lyα, O II
Si II, C IV
Al II
Fe II
Fe II
Mg II, Mg I
Sigma (%)
G130H
G270H
Filter (pixels)
Grating
Wavelength (Å)

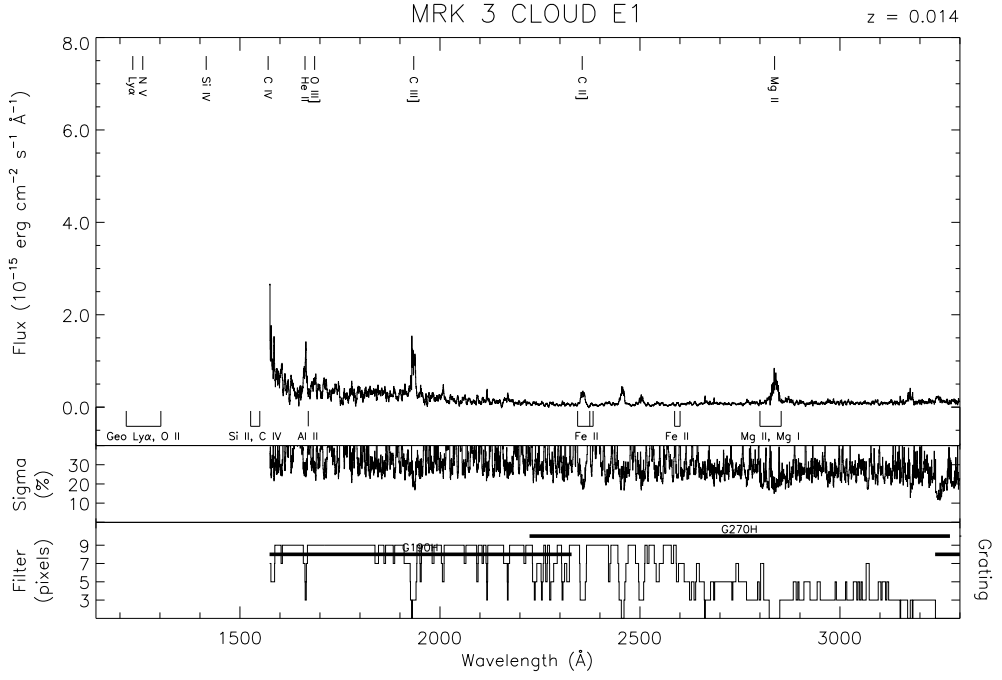
MRK 3 CLOUD E1
z = 0.014
Flux (10^{-15} erg cm^{-2} s^{-1} Å^{-1})
N V Lyα
Si IV
C IV
He II
O III]
C III]
C II]
Mg II
Geo Lyα, O II
Si II, C IV
Al II
Fe II
Fe II
Mg II, Mg I
Sigma (%)
G270H
G190H
Filter (pixels)
Grating
Wavelength (Å)

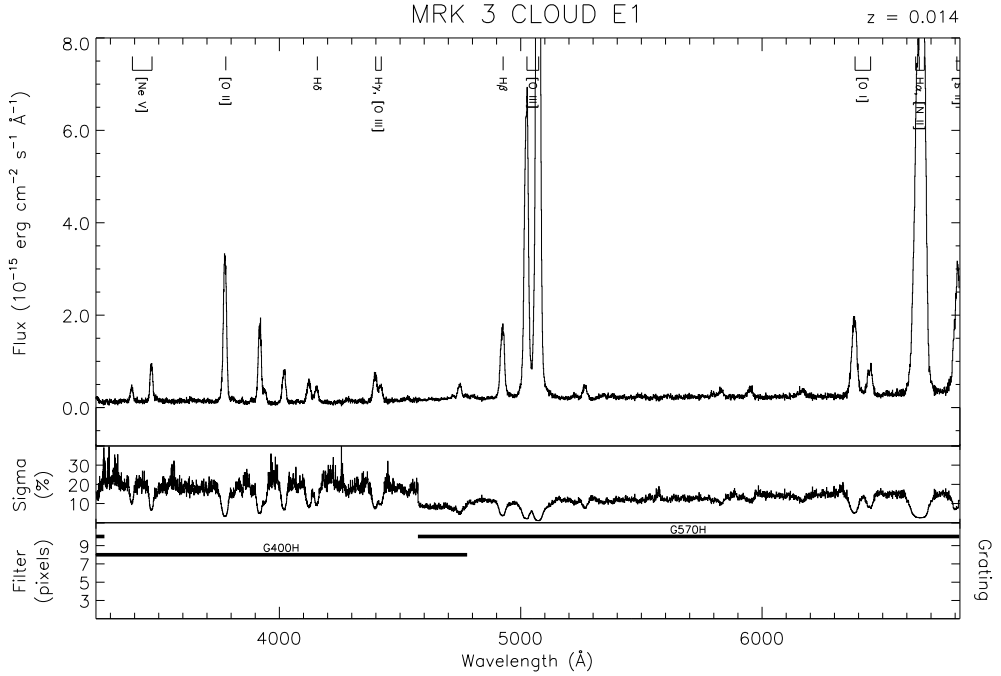
MRK 3 CLOUD E1
z = 0.014
Flux (10^{-15} erg cm^{-2} s^{-1} Å^{-1})
[Ne V]
[O II]
Hδ
[Ne III], Hγ
Hβ
[O III]
[O I]
[N II], Hα
[S II]
Sigma (%)
G570H
G400H
Filter (pixels)
Grating
Wavelength (Å)

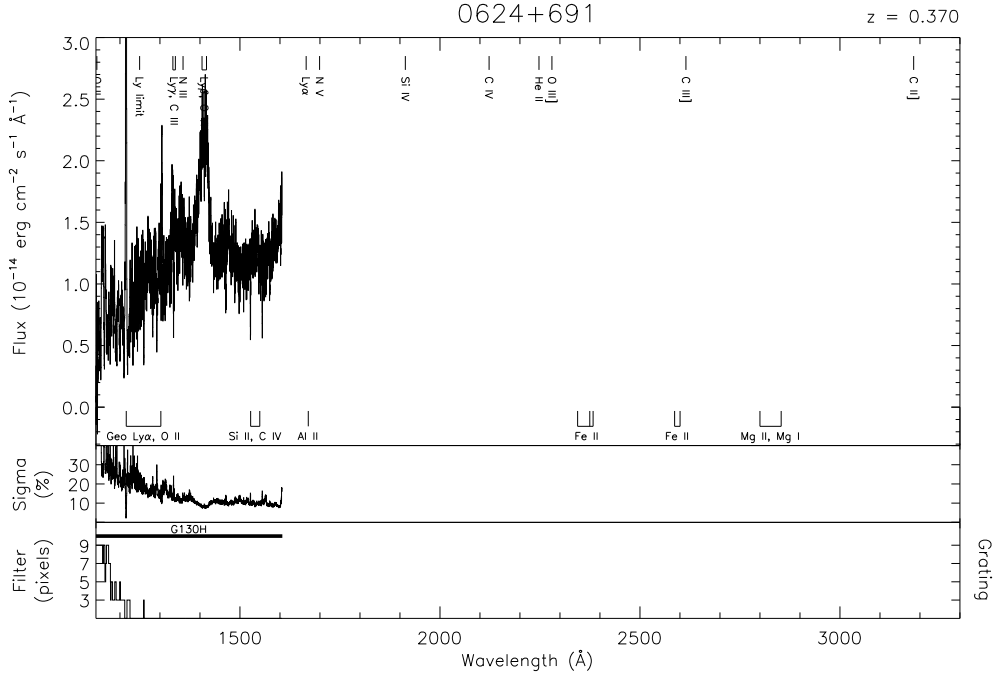
0624+691
z = 0.370
Flux (10^{-14} erg cm^{-2} s^{-1} Å^{-1})
Ly limit
N III, Lyγ, C III
Lyβ, O VI
N V, Lyα
Si IV
C IV
O III], He II
C III]
C II]
Geo Lyα, O II
Si II, C IV
Al II
Fe II
Fe II
Mg II, Mg I
Sigma (%)
G130H
Filter (pixels)
Grating
Wavelength (Å)

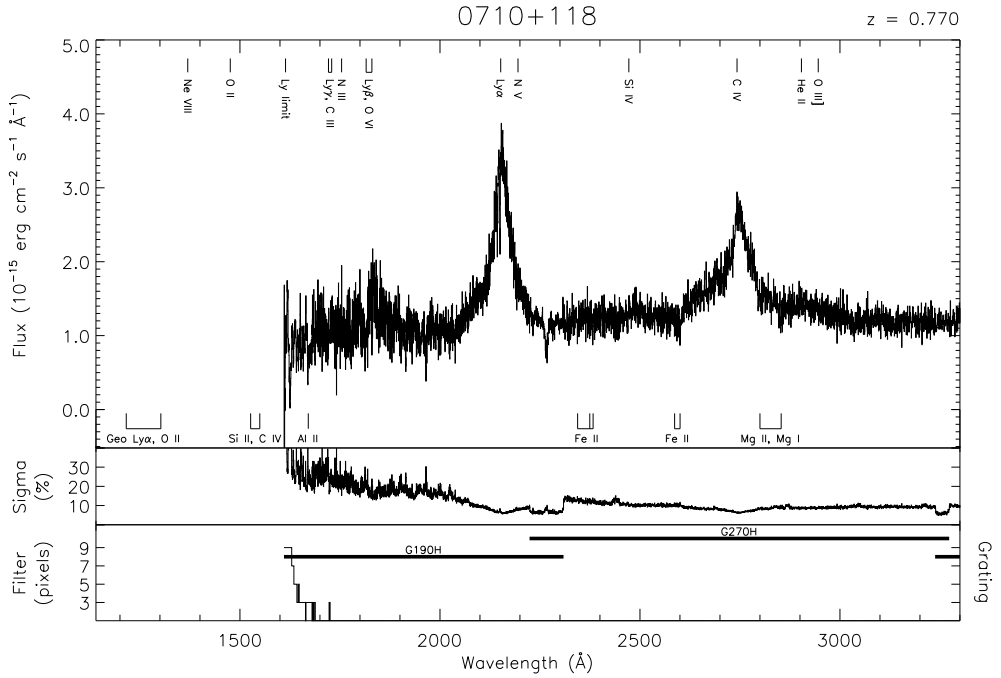
0710+118
z = 0.770
Flux (10^{-15} erg cm^{-2} s^{-1} Å^{-1})
Ne VIII
O II
Ly limit
N III
Lyγ, C III
Lyβ, O VI
Lyα
N V
Si IV
C IV
He II
O III]
Geo Lyα, O II
Si II, C IV
Al II
Fe II
Fe II
Mg II, Mg I
Sigma (%)
Filter (pixels)
G270H
G190H
Grating
Wavelength (Å)

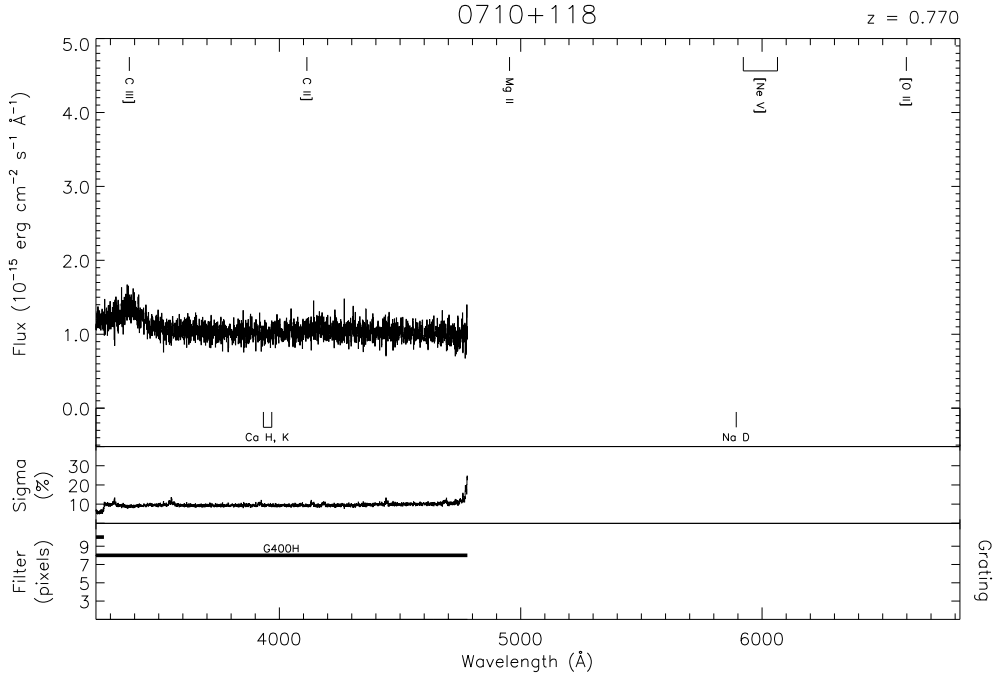
0710+118
z = 0.770
Flux (10^{-15} erg cm^{-2} s^{-1} Å^{-1})
C III]
C II]
Mg II
[Ne V]
[O II]
Ca H, K
Na D
Sigma (%)
Filter (pixels)
G400H
Grating
Wavelength (Å)

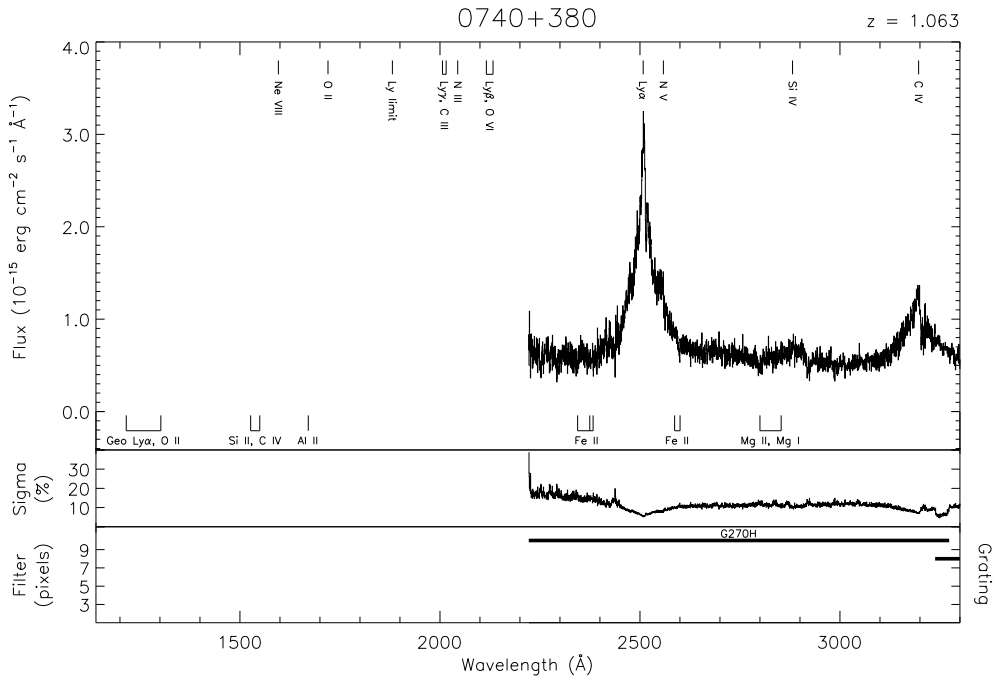
0740+380
z = 1.063
Flux (10^{-15} erg cm^{-2} s^{-1} Å^{-1})
Ne VIII
O II
Ly limit
Ly7, C III
N III
Ly6, O VI
Lyα
N V
Si IV
C IV
Geo Lyα, O II
Si II, C IV
Al II
Fe II
Fe II
Mg II, Mg I
Sigma (%)
G270H
Filter (pixels)
Grating
Wavelength (Å)

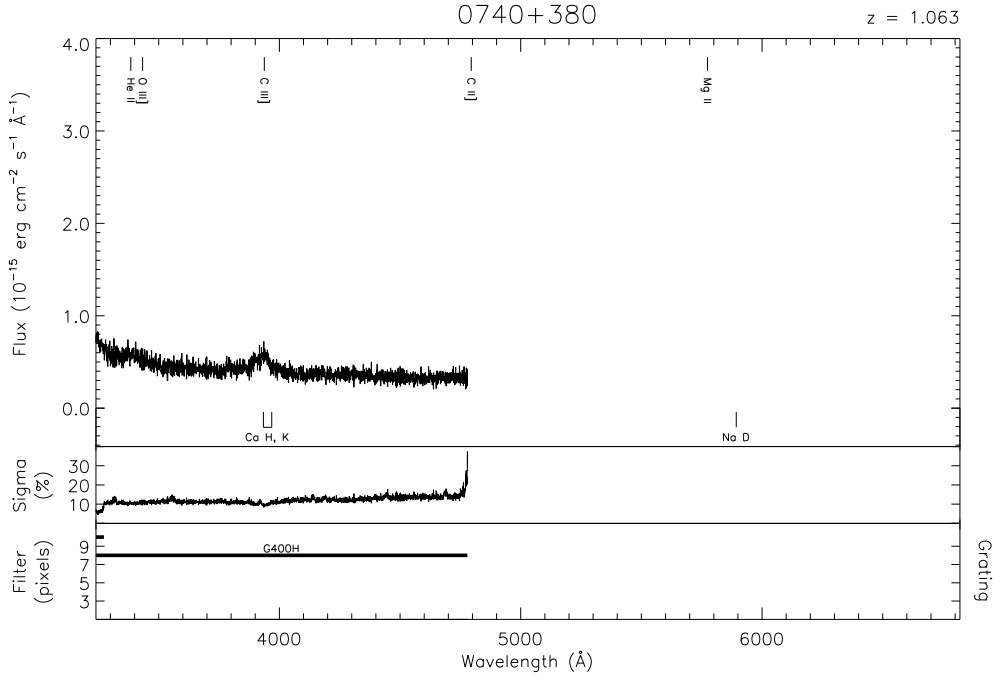
0740+380
z = 1.063
Flux (10^{-15} erg cm^{-2} s^{-1} Å^{-1})
He II
O III]
C III]
C II]
Mg II
Ca H, K
Na D
Sigma (%)
G400H
Filter (pixels)
Grating
Wavelength (Å)

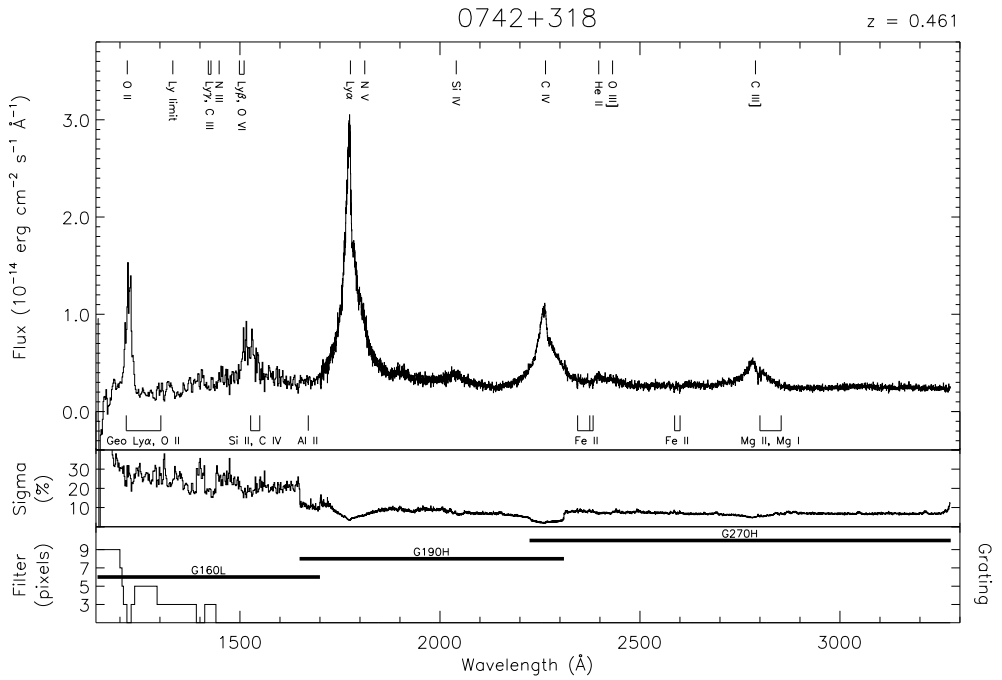
0742+318
z = 0.461
O II
Ly limit
N III
Lyγ, C III
Lyβ, O VI
Lyα
N V
Si IV
C IV
He II
O III]
C III]
Flux (10^-14 erg cm^-2 s^-1 Å^-1)
Geo Lyα, O II
Si II, C IV
Al II
Fe II
Fe II
Mg II, Mg I
Sigma (%)
G270H
G190H
G160L
Filter (pixels)
Grating
Wavelength (Å)

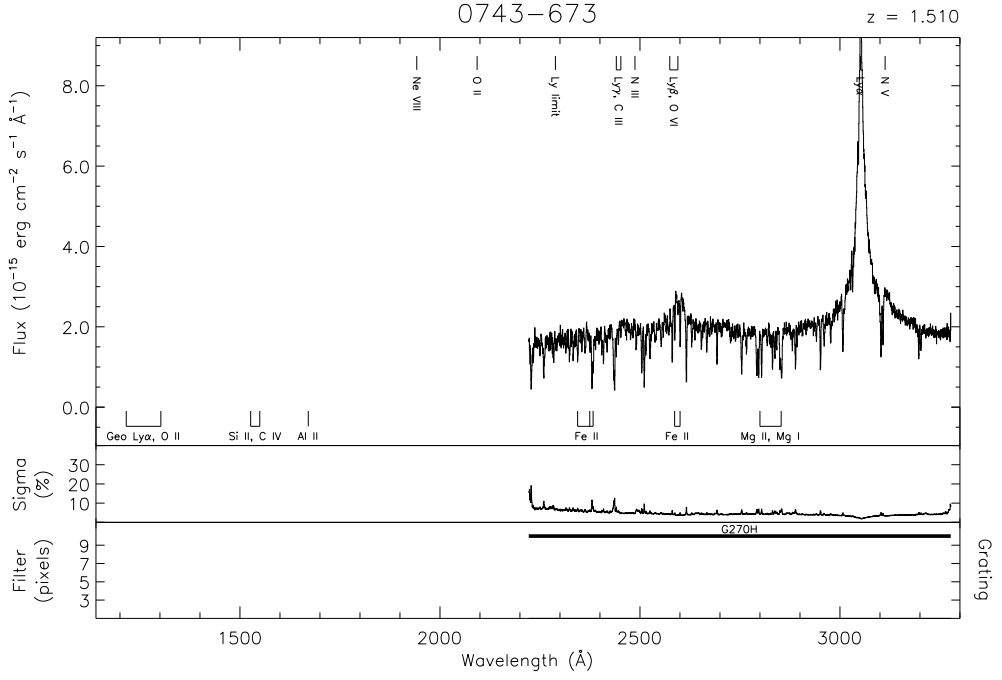
0743−673
z = 1.510
Ne VIII
O II
Ly limit
N III
Lyγ, C III
Lyβ, O VI
Lyα
N V
Flux (10^-15 erg cm^-2 s^-1 Å^-1)
Geo Lyα, O II
Si II, C IV
Al II
Fe II
Fe II
Mg II, Mg I
Sigma (%)
G270H
Filter (pixels)
Grating
Wavelength (Å)

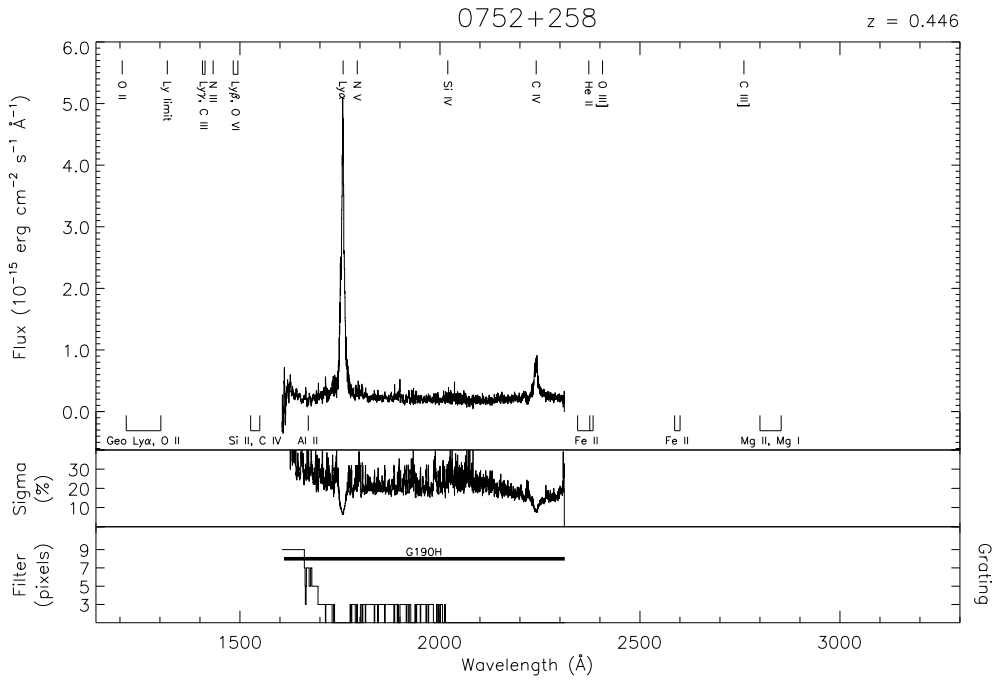
0752+258
z = 0.446
Flux (10^{-15} erg cm^{-2} s^{-1} Å^{-1})
O II
Ly limit
N III
Lyγ, C III
Lyβ, O VI
Lyα
N V
Si IV
C IV
He II
O III]
C III]
Geo Lyα, O II
Si II, C IV
Al II
Fe II
Fe II
Mg II, Mg I
Sigma (%)
Filter (pixels)
G190H
Grating
Wavelength (Å)

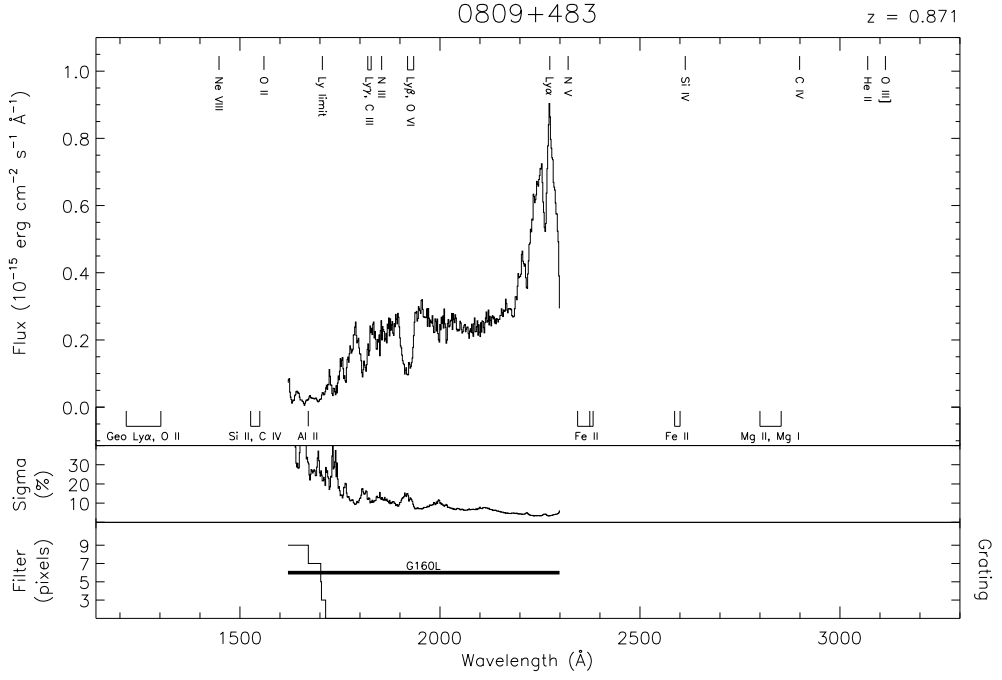
0809+483
z = 0.871
Flux (10^{-15} erg cm^{-2} s^{-1} Å^{-1})
Ne VIII
O II
Ly limit
N III
Lyγ, C III
Lyβ, O VI
Lyα
N V
Si IV
C IV
He II
O III]
Geo Lyα, O II
Si II, C IV
Al II
Fe II
Fe II
Mg II, Mg I
Sigma (%)
Filter (pixels)
G160L
Grating
Wavelength (Å)

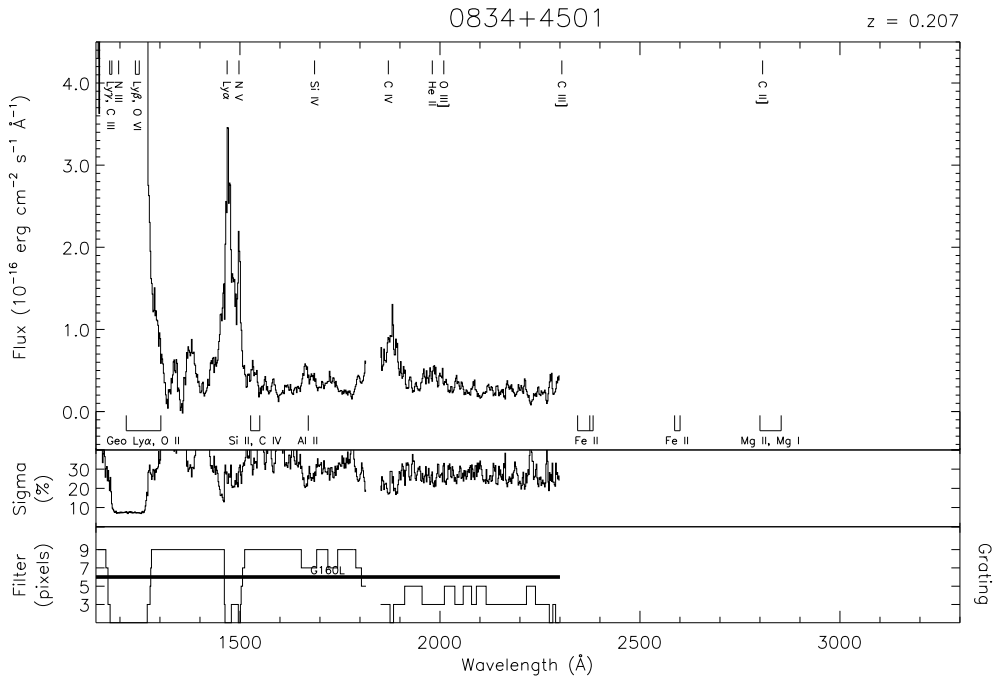
0834+4501
z = 0.207
Flux (10^{-16} erg cm^{-2} s^{-1} Å^{-1})
Lyγ, C III
Lyβ, O VI
N V
Lyα
Si IV
C IV
He II
O III]
C III]
C II]
Geo Lyα, O II
Si II, C IV
Al II
Fe II
Fe II
Mg II, Mg I
Sigma (%)
Filter (pixels)
G160L
Grating
Wavelength (Å)

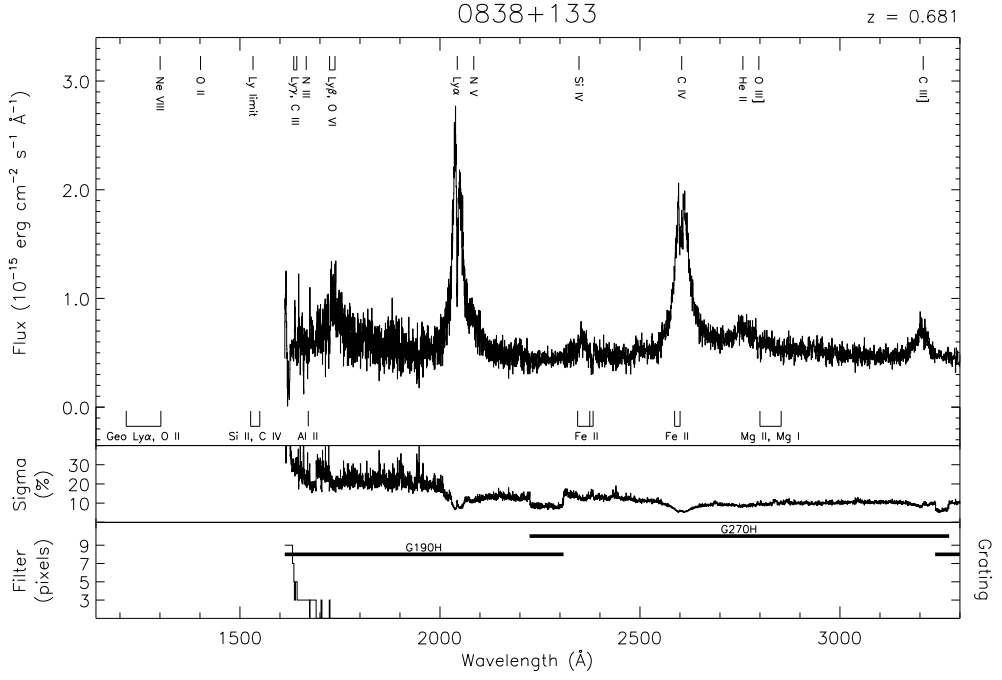
0838+133
z = 0.681
Flux (10^{-15} erg cm^{-2} s^{-1} Å^{-1})
Ne VIII
O II
Ly limit
N III
Lyγ, C III
Lyβ, O VI
N V
Lyα
Si IV
C IV
He II
O III]
C III]
Geo Lyα, O II
Si II, C IV
Al II
Fe II
Fe II
Mg II, Mg I
Sigma (%)
G270H
G190H
Filter (pixels)
Grating
Wavelength (Å)

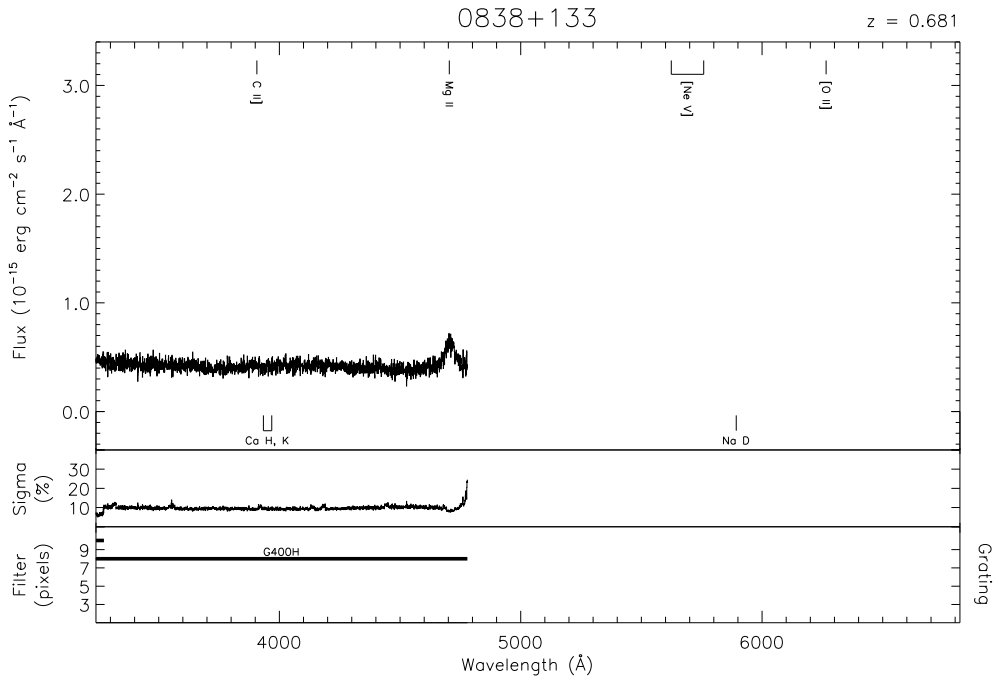
0838+133
z = 0.681
C II]
Mg II
[Ne V]
[O II]
Ca H, K
Na D
G400H
Flux (10^{-15} erg cm^{-2} s^{-1} Å^{-1})
Sigma (%)
Filter (pixels)
Grating
Wavelength (Å)

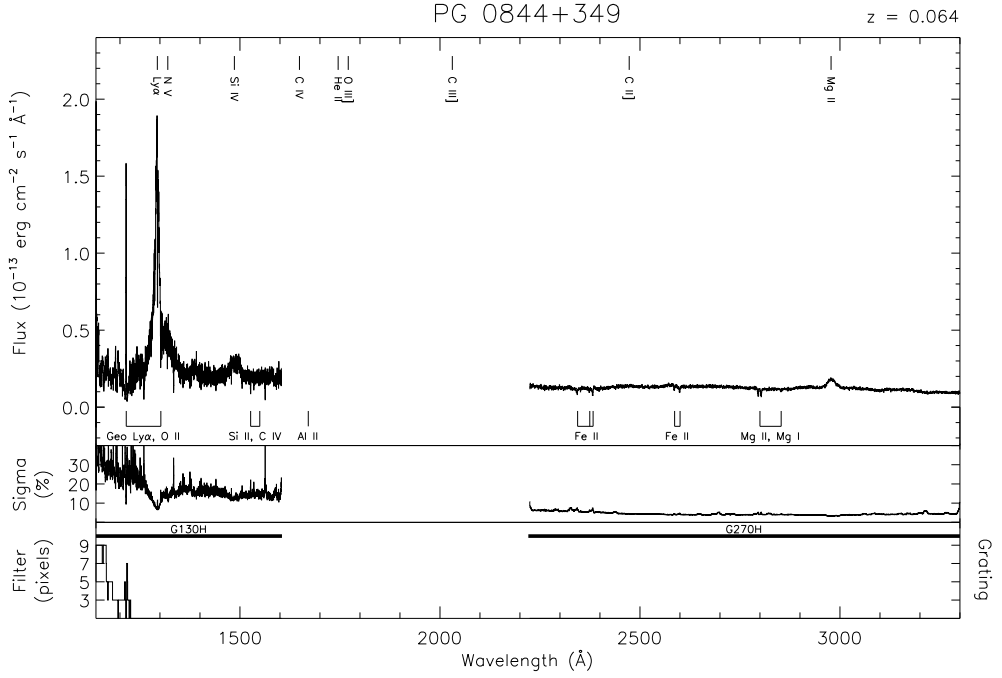
PG 0844+349
z = 0.064
N V Lyα
Si IV
C IV
He II
O III]
C III]
C II]
Mg II
Geo Lyα, O II
Si II, C IV
Al II
Fe II
Fe II
Mg II, Mg I
G130H
G270H
Flux (10^{-13} erg cm^{-2} s^{-1} Å^{-1})
Sigma (%)
Filter (pixels)
Grating
Wavelength (Å)

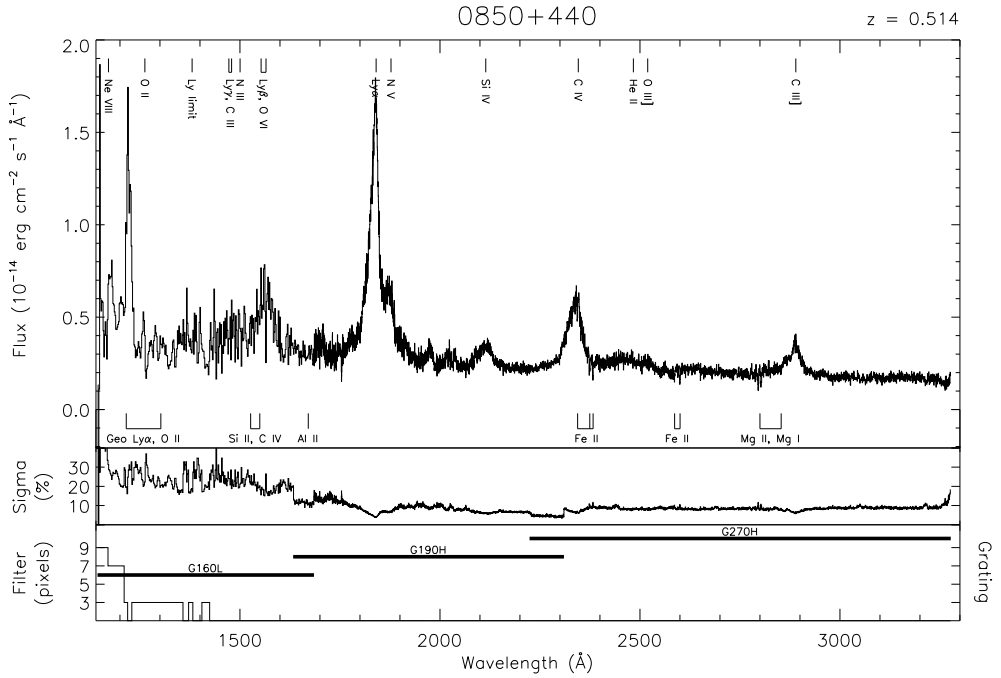
0850+440
z = 0.514
Flux (10^{-14} erg cm^{-2} s^{-1} Å^{-1})
Ne VIII
O II
Ly limit
N III, C III
Lyβ, O VI
Lyα
N V
Si IV
C IV
He II
O III]
C III]
Geo Lyα, O II
Si II, C IV
Al II
Fe II
Fe II
Mg II, Mg I
Sigma (%)
Filter (pixels)
G160L
G190H
G270H
Grating
Wavelength (Å)

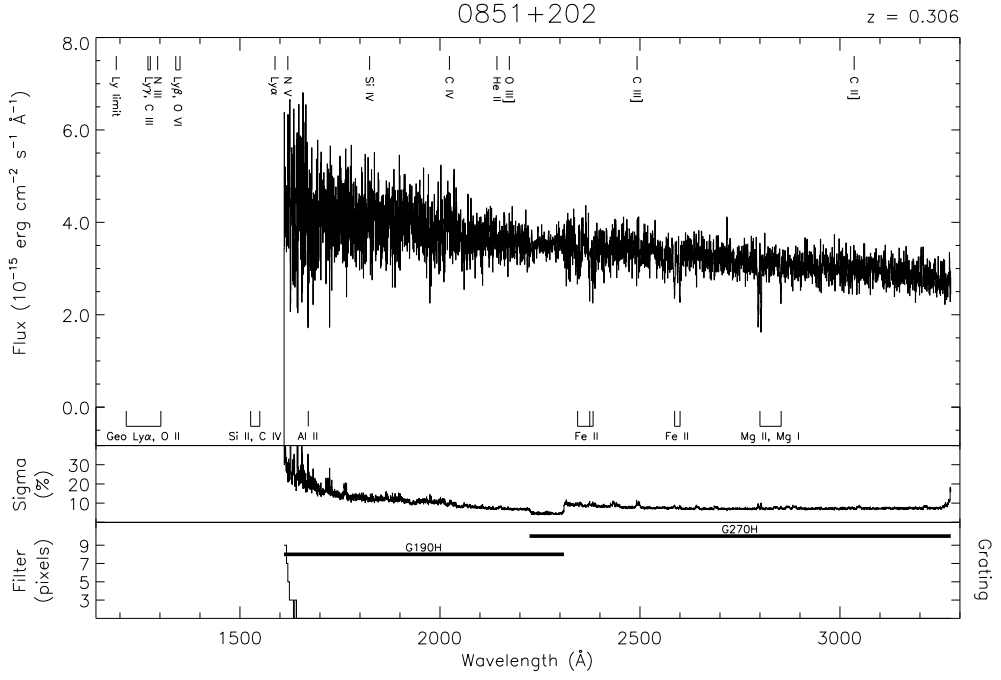
0851+202
z = 0.306
Flux (10^{-15} erg cm^{-2} s^{-1} Å^{-1})
Ly limit
N III, C III
Lyβ, O VI
Lyα
N V
Si IV
C IV
He II
O III]
C III]
C II]
Geo Lyα, O II
Si II, C IV
Al II
Fe II
Fe II
Mg II, Mg I
Sigma (%)
Filter (pixels)
G190H
G270H
Grating
Wavelength (Å)

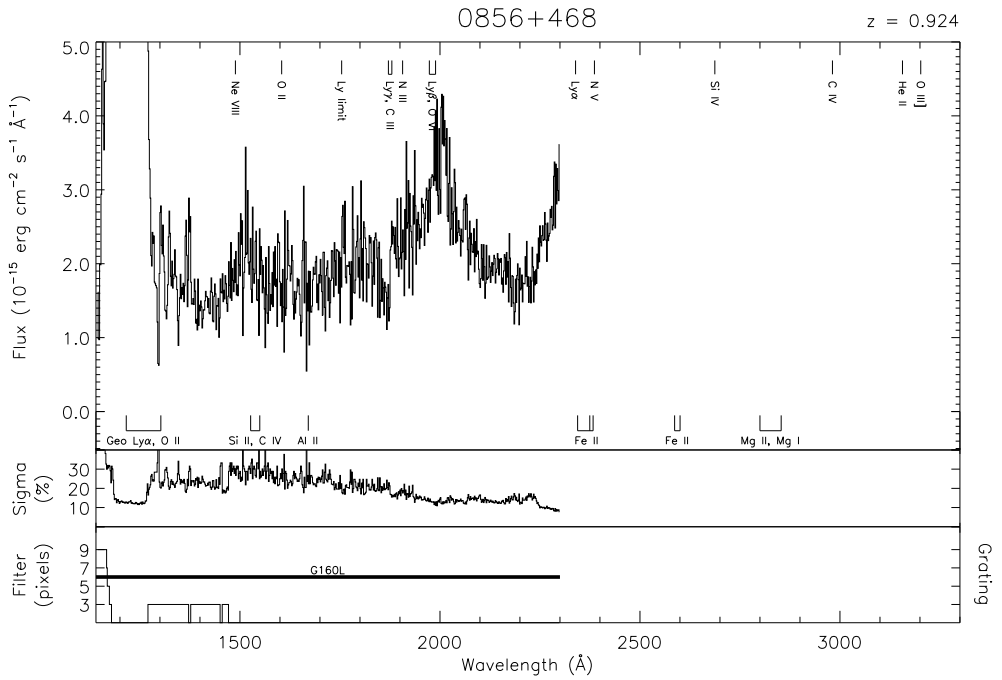
0856+468
z = 0.924
Flux (10^{-15} erg cm^{-2} s^{-1} Å^{-1})
Ne VIII
O II
Ly limit
N III
Lyγ, C III
Lyβ, O VI
Lyα
N V
Si IV
C IV
He II
O III]
Geo Lyα, O II
Si II, C IV
Al II
Fe II
Fe II
Mg II, Mg I
Sigma (%)
Filter (pixels)
G160L
Grating
Wavelength (Å)

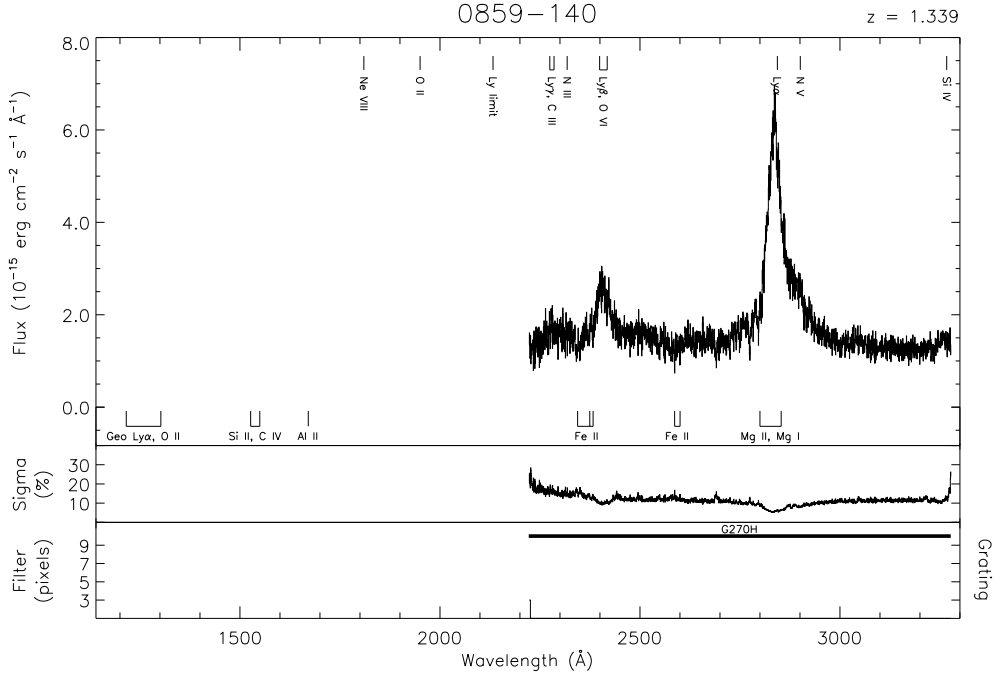
0859−140
z = 1.339
Flux (10^{-15} erg cm^{-2} s^{-1} Å^{-1})
Ne VIII
O II
Ly limit
N III
Lyγ, C III
Lyβ, O VI
Lyα
N V
Si IV
Geo Lyα, O II
Si II, C IV
Al II
Fe II
Fe II
Mg II, Mg I
Sigma (%)
Filter (pixels)
G270H
Grating
Wavelength (Å)

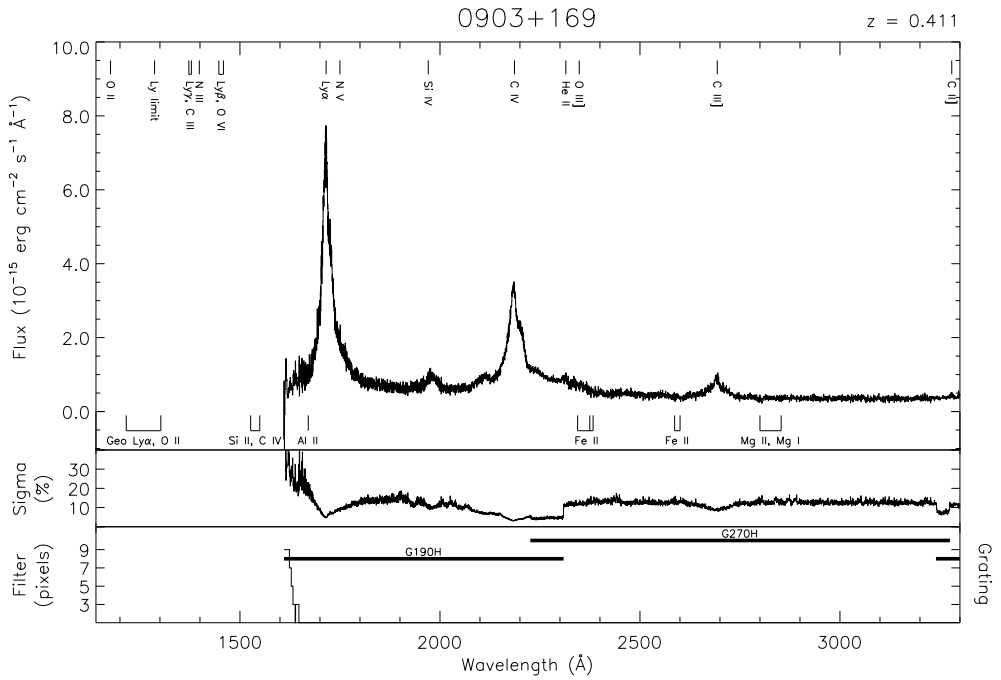
0903+169
z = 0.411
Flux (10^{-15} erg cm^{-2} s^{-1} Å^{-1})
O II
Ly limit
N III
Ly γ, C III
Lyβ, O VI
N V
Lyα
Si IV
C IV
He II
O III]
C III]
C I]
Geo Lyα, O II
Si II, C IV
Al II
Fe II
Fe II
Mg II, Mg I
Sigma (%)
Filter (pixels)
G270H
G190H
Grating
Wavelength (Å)

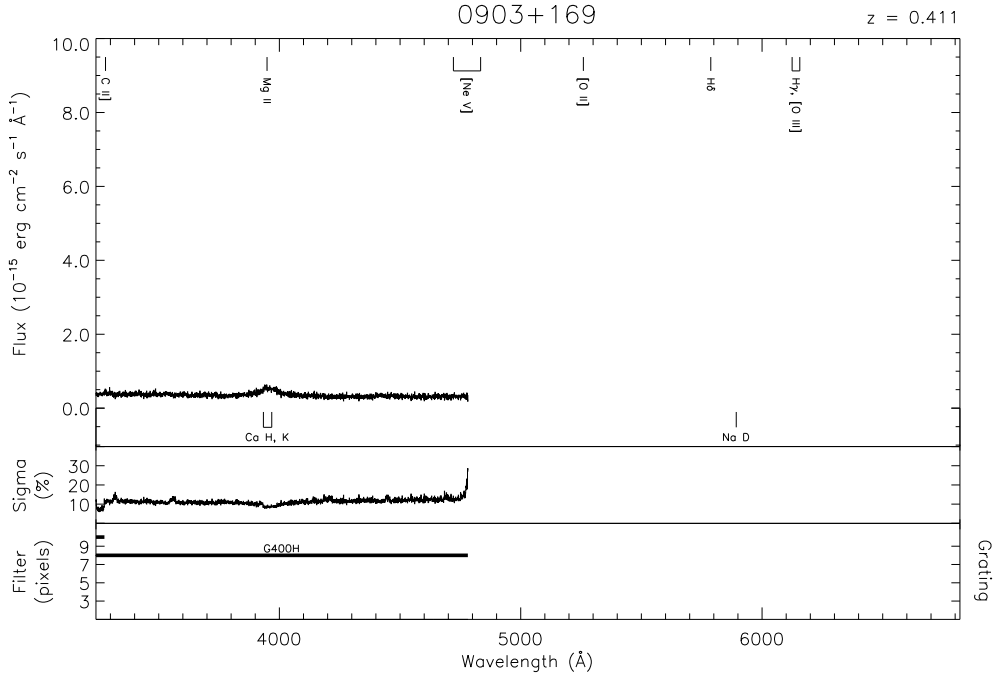
0903+169
z = 0.411
Flux (10^{-15} erg cm^{-2} s^{-1} Å^{-1})
C II]
Mg II
[Ne V]
[O II]
Hδ
Hγ, [O III]
Ca H, K
Na D
Sigma (%)
Filter (pixels)
G400H
Grating
Wavelength (Å)

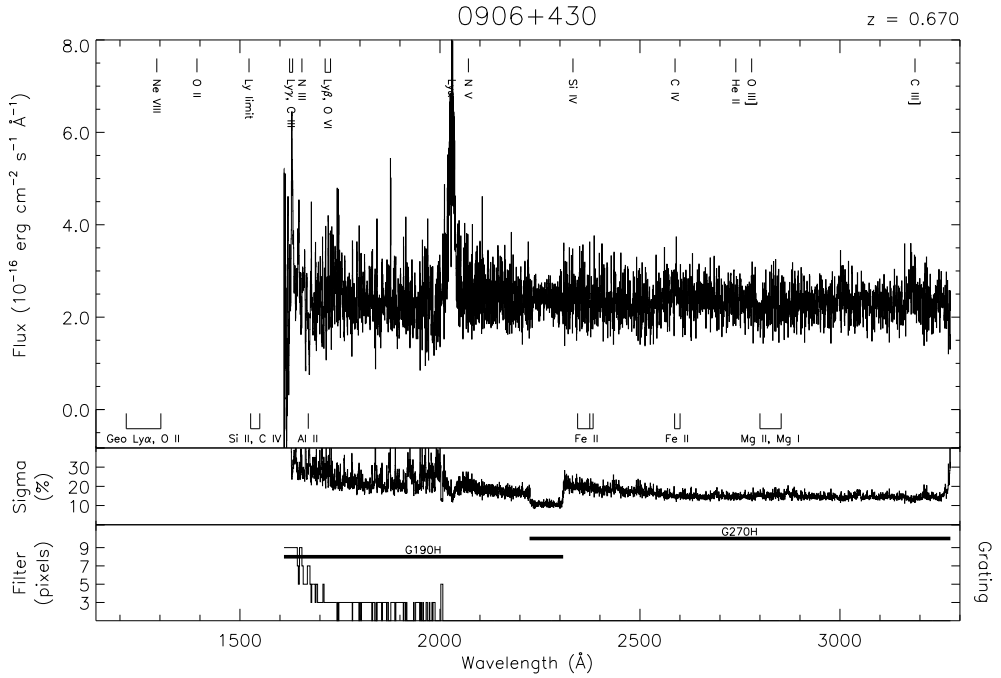
0906+430
z = 0.670
Flux (10^{-16} erg cm^{-2} s^{-1} Å^{-1})
Ne VIII
O II
Ly limit
N III, C III
Lyδ, O VI
Lyα
N V
Si IV
C IV
He II
O III]
C III]
Geo Lyα, O II
Si II, C IV
Al II
Fe II
Fe II
Mg II, Mg I
Sigma (%)
Filter (pixels)
G190H
G270H
Grating
Wavelength (Å)

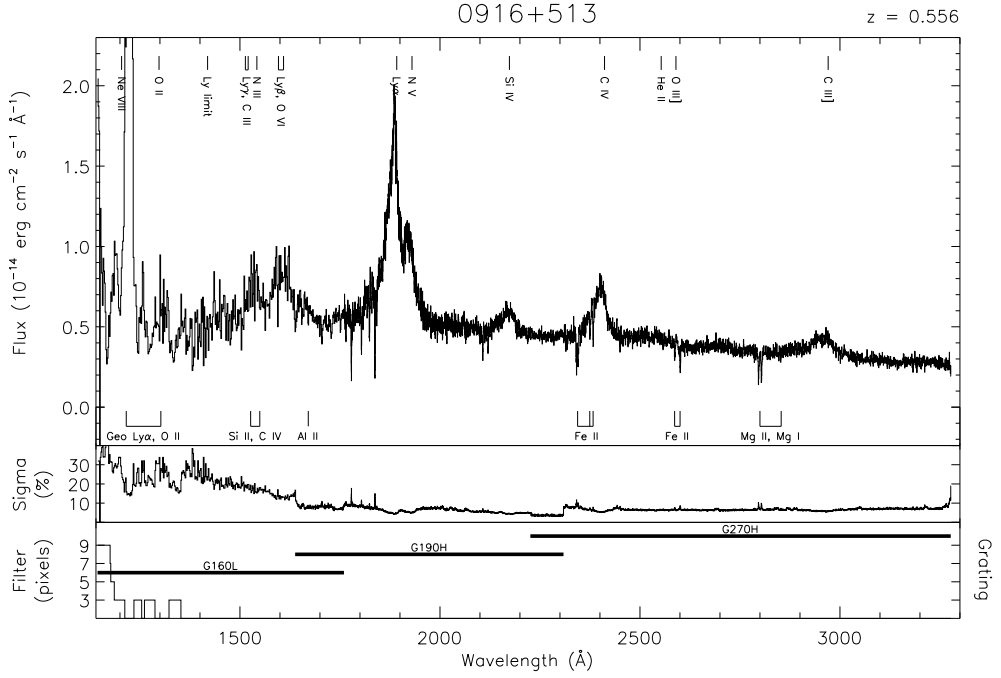
0916+513
z = 0.556
Flux (10^{-14} erg cm^{-2} s^{-1} Å^{-1})
Ne VIII
O II
Ly limit
N III, C III
Lyδ, O VI
Lyα
N V
Si IV
C IV
He II
O III]
C III]
Geo Lyα, O II
Si II, C IV
Al II
Fe II
Fe II
Mg II, Mg I
Sigma (%)
Filter (pixels)
G160L
G190H
G270H
Grating
Wavelength (Å)

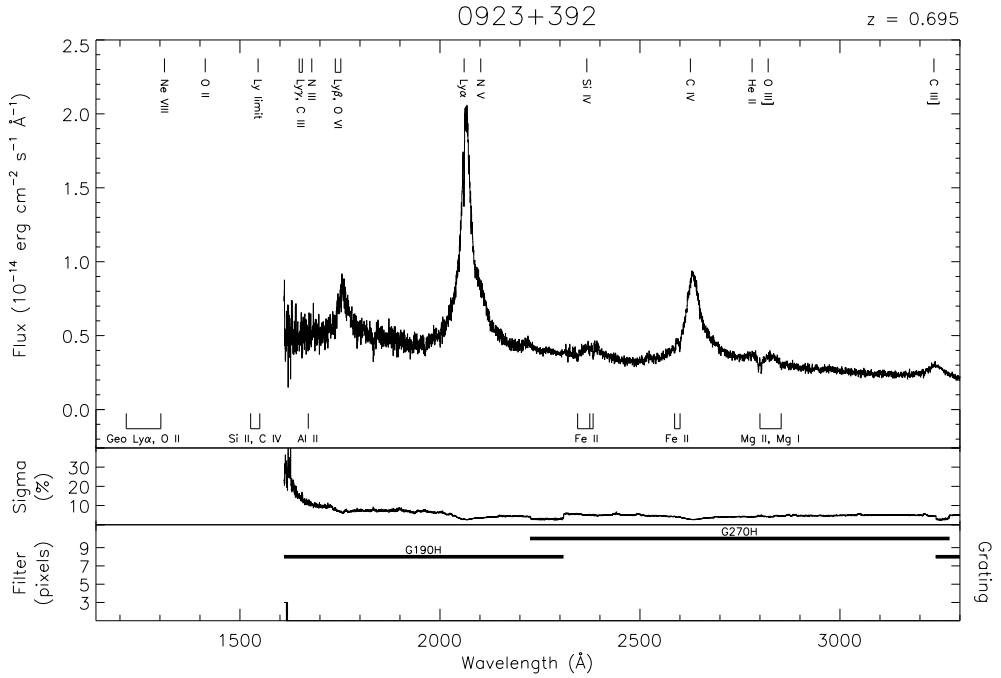
0923+392
z = 0.695
Flux (10^{-14} erg cm^{-2} s^{-1} Å^{-1})
Ne VIII
O II
Ly limit
N III
Lyγ, C III
Lyβ, O VI
Lyα
N V
Si IV
C IV
He II
O III]
C III]
Geo Lyα, O II
Si II, C IV
Al II
Fe II
Fe II
Mg II, Mg I
Sigma (%)
G270H
G190H
Filter (pixels)
Grating
Wavelength (Å)

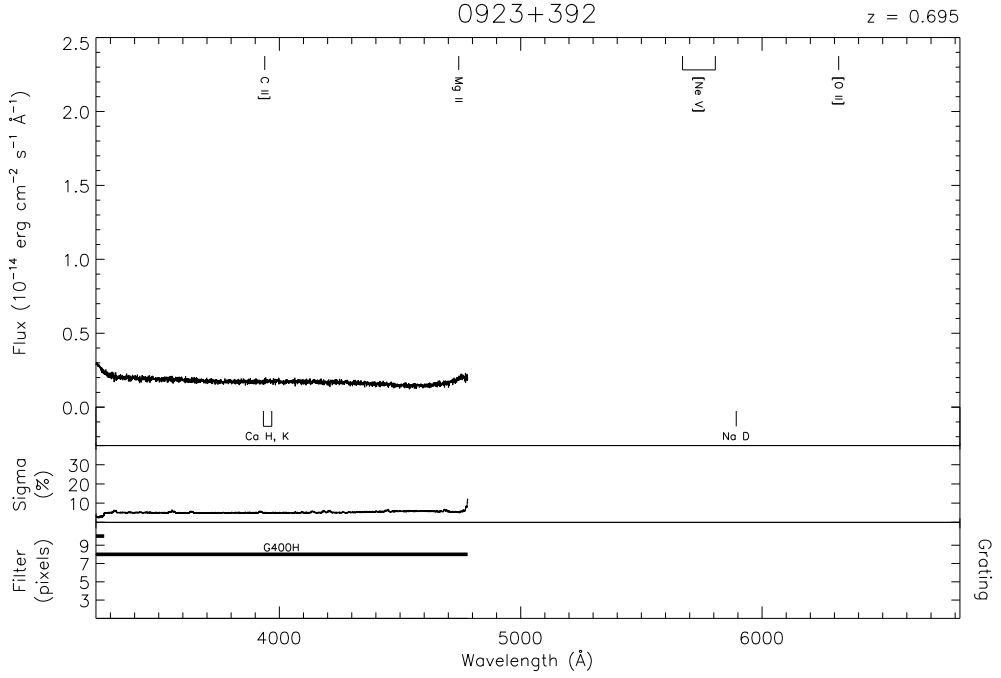
0923+392
z = 0.695
Flux (10^{-14} erg cm^{-2} s^{-1} Å^{-1})
C II]
Mg II
[Ne V]
[O II]
Ca H, K
Na D
Sigma (%)
G400H
Filter (pixels)
Grating
Wavelength (Å)

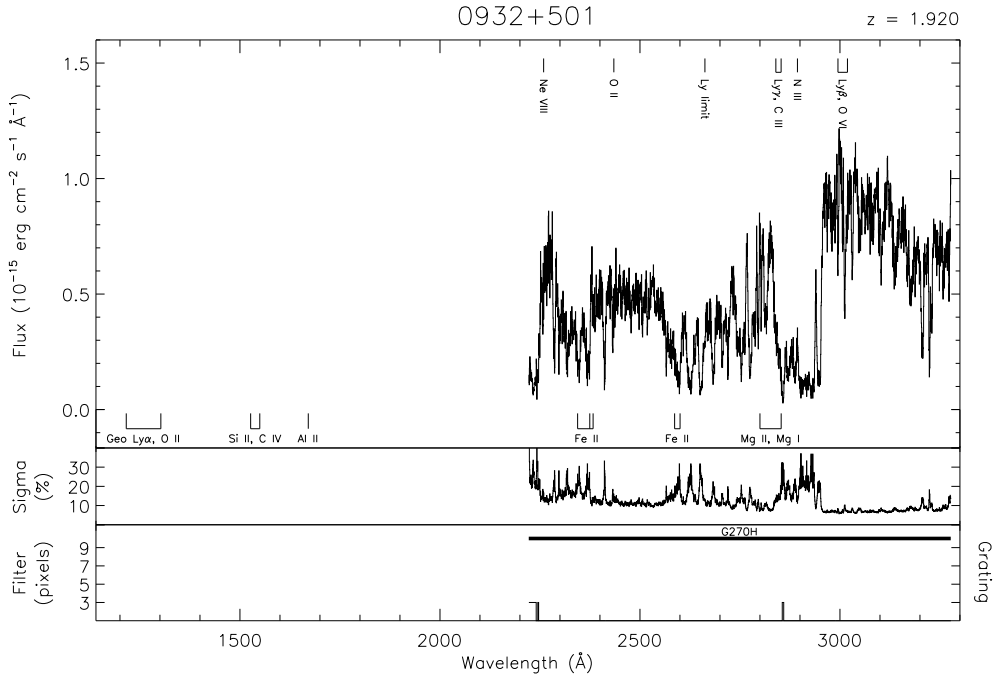
0932+501
z = 1.920
Flux (10^{-15} erg cm^{-2} s^{-1} Å^{-1})
Ne VIII
O II
Ly limit
N III
Lyγ, C III
Lyβ, O VI
Geo Lyα, O II
Si II, C IV
Al II
Fe II
Fe II
Mg II, Mg I
Sigma (%)
G270H
Filter (pixels)
Grating
Wavelength (Å)

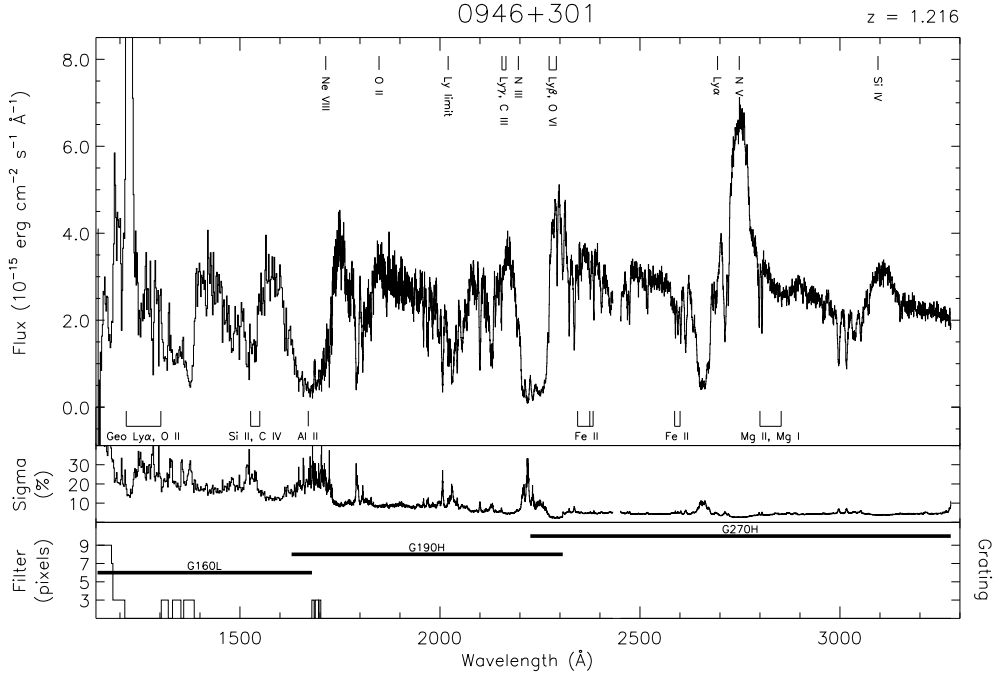
0946+301
z = 1.216
Flux (10^{-15} erg cm^{-2} s^{-1} Å^{-1})
Ne VIII
O II
Ly limit
N III
Lyγ, C III
Lyβ, O VI
Lyα
N V
Si IV
Geo Lyα, O II
Si II, C IV
Al II
Fe II
Fe II
Mg II, Mg I
Sigma (%)
G270H
G190H
G160L
Filter (pixels)
Grating
Wavelength (Å)

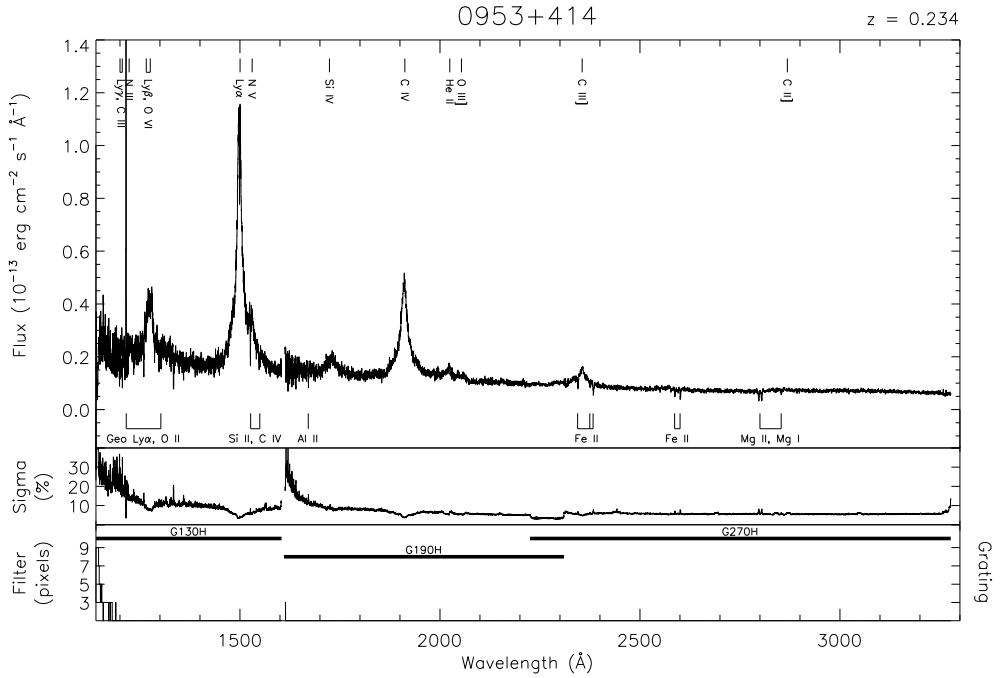
0953+414
z = 0.234
Flux (10^{-13} erg cm^{-2} s^{-1} Å^{-1})
N III, C III
Lyγ, C III
Lyβ, O VI
N V
Lyα
Si IV
C IV
He II
O III]
C III]
C II]
Geo Lyα, O II
Si II, C IV
Al II
Fe II
Fe II
Mg II, Mg I
Sigma (%)
G130H
G270H
G190H
Filter (pixels)
Grating
Wavelength (Å)

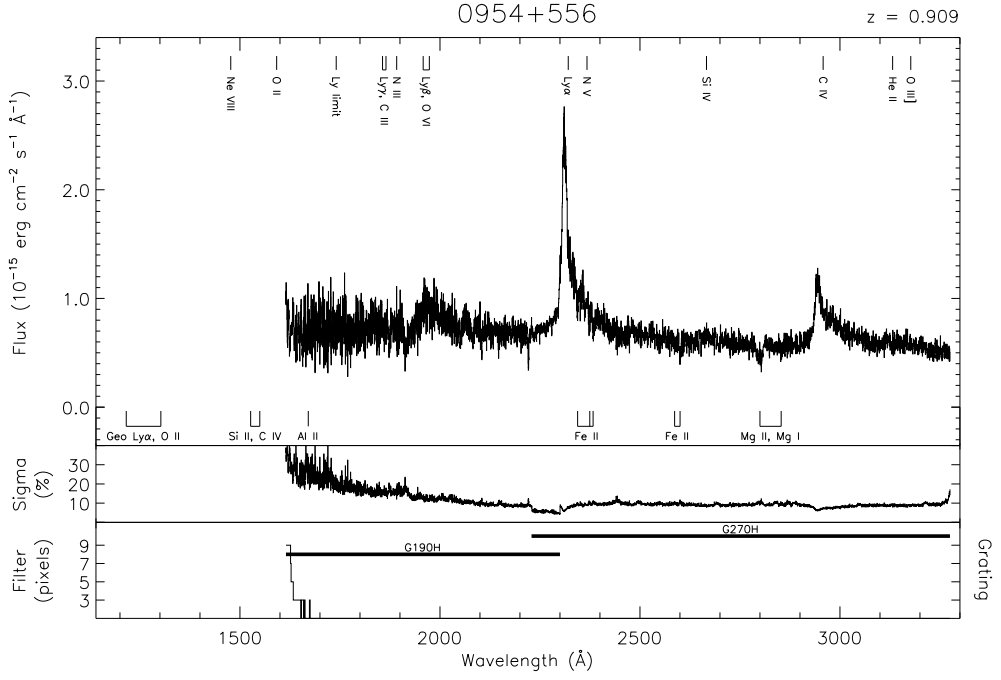
0954+556
z = 0.909
Flux (10^{-15} erg cm^{-2} s^{-1} Å^{-1})
Ne VIII
O II
Ly limit
N III
Lyγ, C III
Lyβ, O VI
N V
Lyα
Si IV
C IV
He II
O III]
Geo Lyα, O II
Si II, C IV
Al II
Fe II
Fe II
Mg II, Mg I
Sigma (%)
G270H
G190H
Filter (pixels)
Grating
Wavelength (Å)

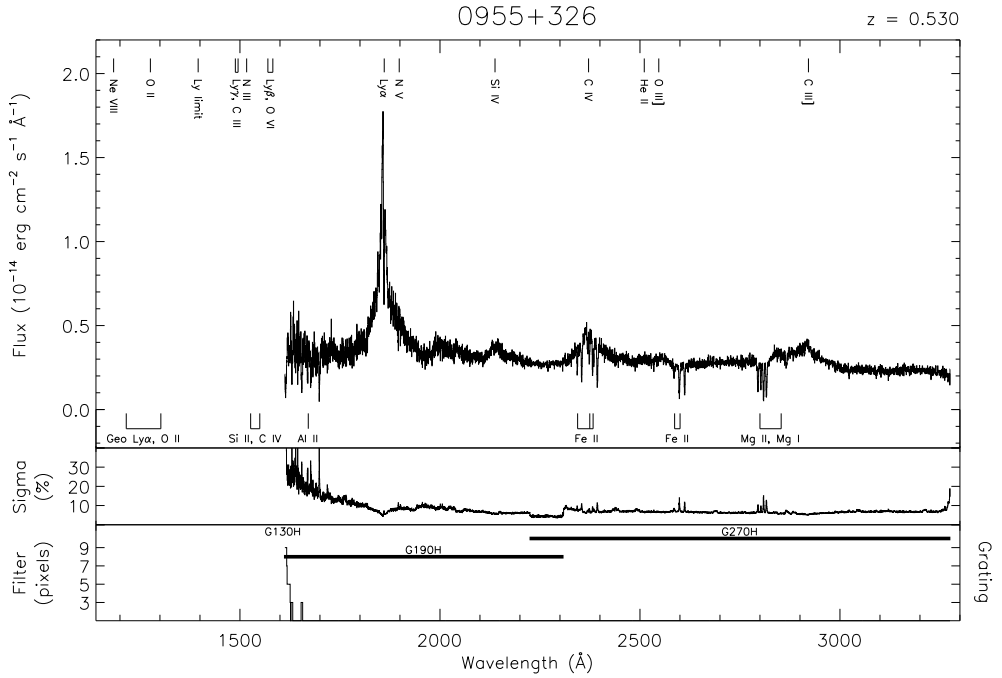
0955+326
z = 0.530
Ne VIII
O II
Ly limit
N III
Lyγ, C III
Lyβ, O VI
Lyα
N V
Si IV
C IV
He II
O III]
C III]
Geo Lyα, O II
Si II, C IV
Al II
Fe II
Fe II
Mg II, Mg I
Flux (10^-14 erg cm^-2 s^-1 Å^-1)
Sigma (%)
Filter (pixels)
G130H
G190H
G270H
Grating
Wavelength (Å)

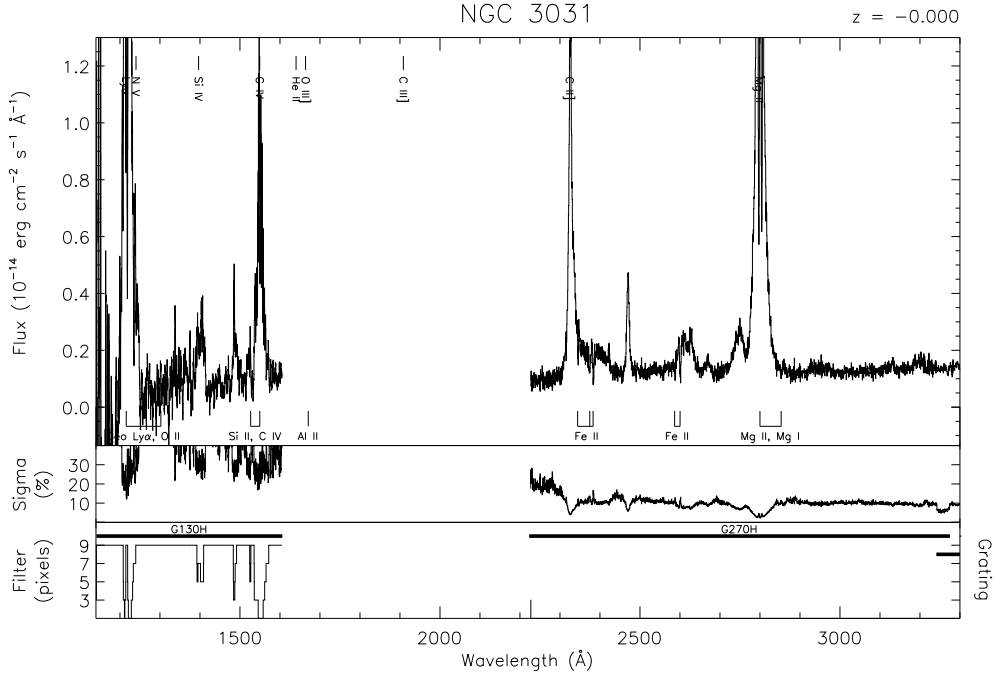
NGC 3031
z = −0.000
N V
Si IV
C IV
He II
O III]
C III]
Geo Lyα, O II
Si II, C IV
Al II
Fe II
Fe II
Mg II, Mg I
Flux (10^-14 erg cm^-2 s^-1 Å^-1)
Sigma (%)
Filter (pixels)
G130H
G270H
Grating
Wavelength (Å)

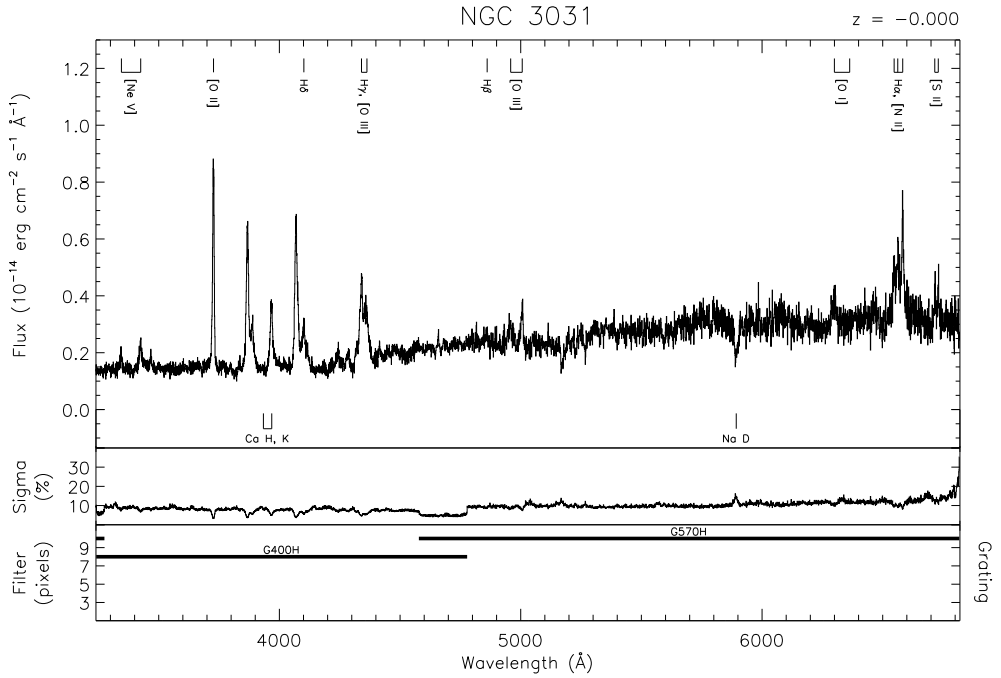
NGC 3031
z = −0.000
Flux (10^{-14} erg cm^{-2} s^{-1} Å^{-1})
[Ne V]
[O II]
Hδ
Hγ, [O III]
Hβ
[O III]
[O I]
Hα, [N II]
[S II]
Ca H, K
Na D
Sigma (%)
Filter (pixels)
G400H
G570H
Grating
Wavelength (Å)

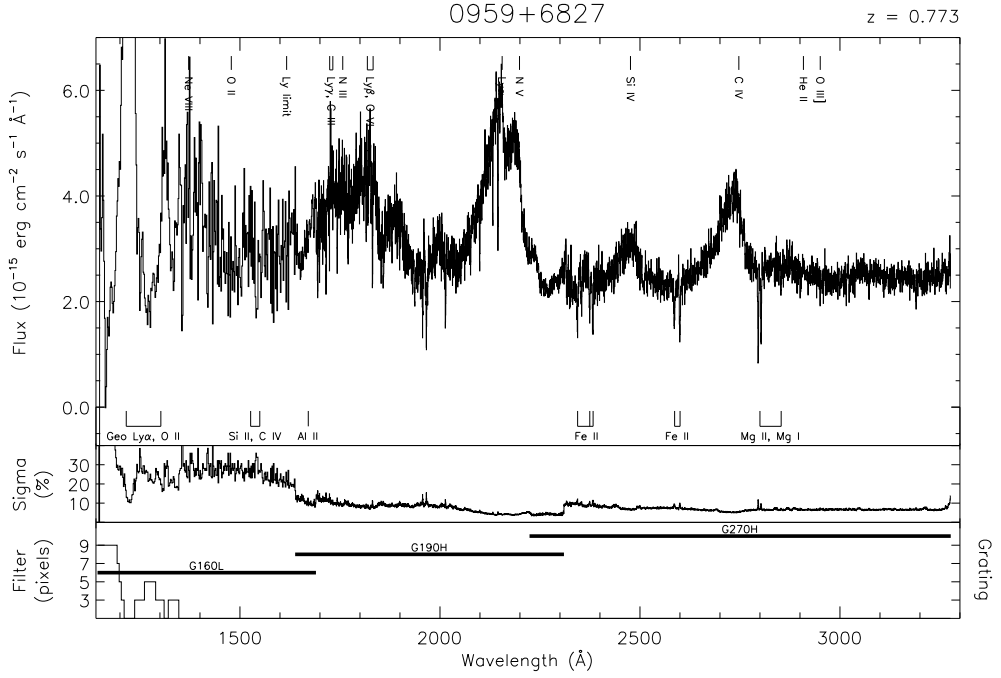
0959+6827
z = 0.773
Flux (10^{-15} erg cm^{-2} s^{-1} Å^{-1})
Ne VIII
O II
Ly limit
N III
Lyγ, Si III
Lyβ, O VI
C III
N V
Si IV
C IV
He II
O III]
Geo Lyα, O II
Si II, C IV
Al II
Fe II
Fe II
Mg II, Mg I
Sigma (%)
Filter (pixels)
G160L
G190H
G270H
Grating
Wavelength (Å)

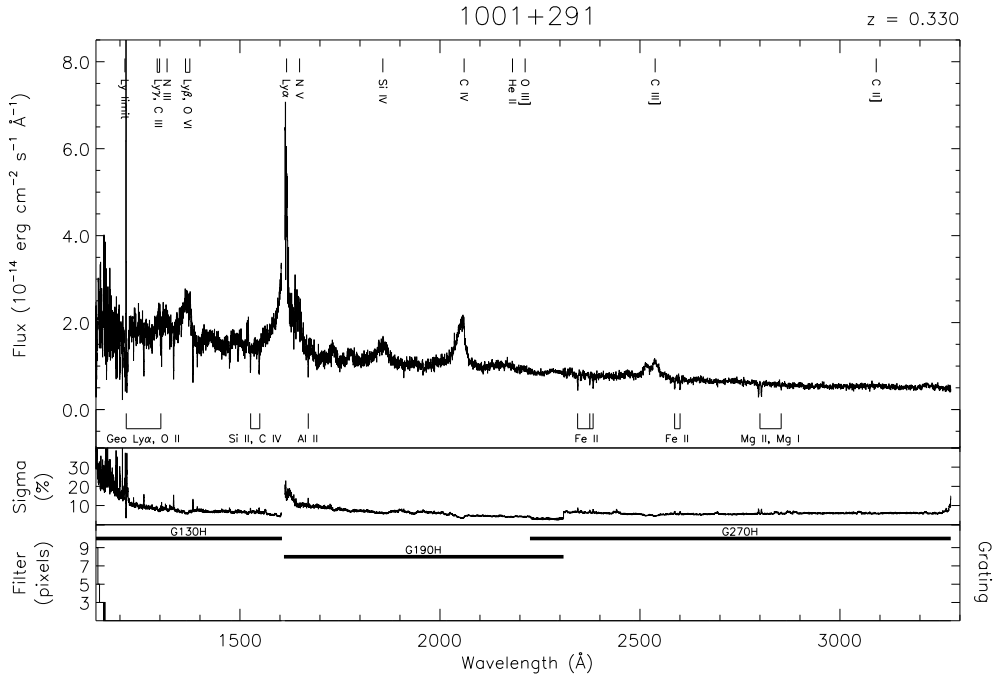
1001+291
z = 0.330
Flux (10^{-14} erg cm^{-2} s^{-1} Å^{-1})
Ly limit
N III, Ly γ, C III
Lyβ, O VI
Lyα
N V
Si IV
C IV
He II
O III]
C III]
C II]
Geo Lyα, O II
Si II, C IV
Al II
Fe II
Fe II
Mg II, Mg I
Sigma (%)
Filter (pixels)
G130H
G190H
G270H
Grating
Wavelength (Å)

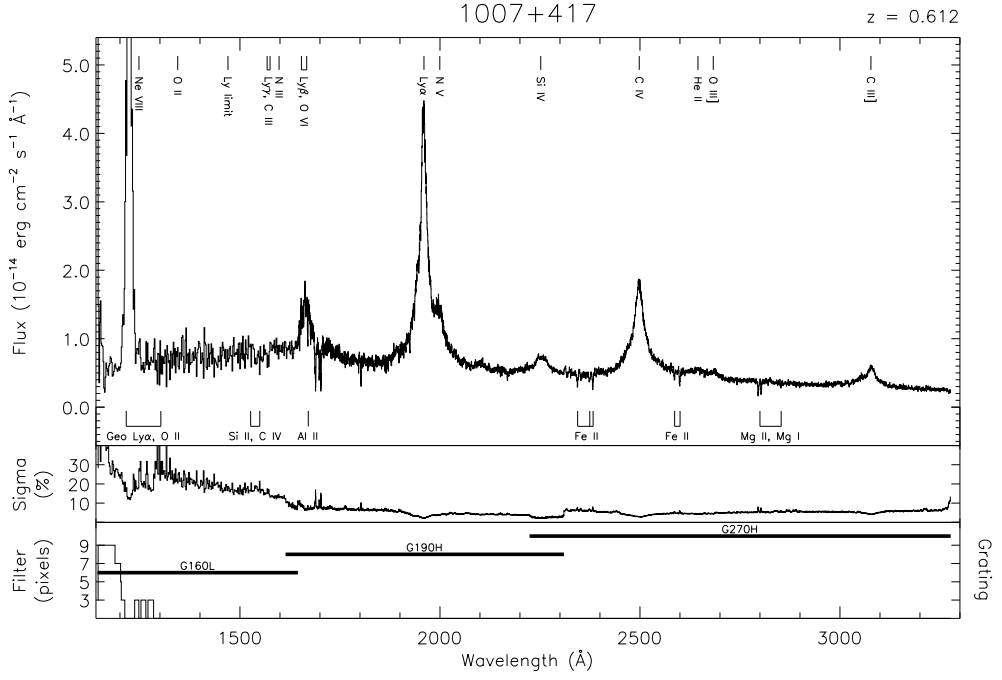
1007+417
z = 0.612
Flux (10^{-14} erg cm^{-2} s^{-1} Å^{-1})
Ne VIII
O II
Ly limit
N III, Ly γ, C III
Lyβ, O VI
Lyα
N V
Si IV
C IV
He II
O III]
C III]
Geo Lyα, O II
Si II, C IV
Al II
Fe II
Fe II
Mg II, Mg I
Sigma (%)
Filter (pixels)
G160L
G190H
G270H
Grating
Wavelength (Å)

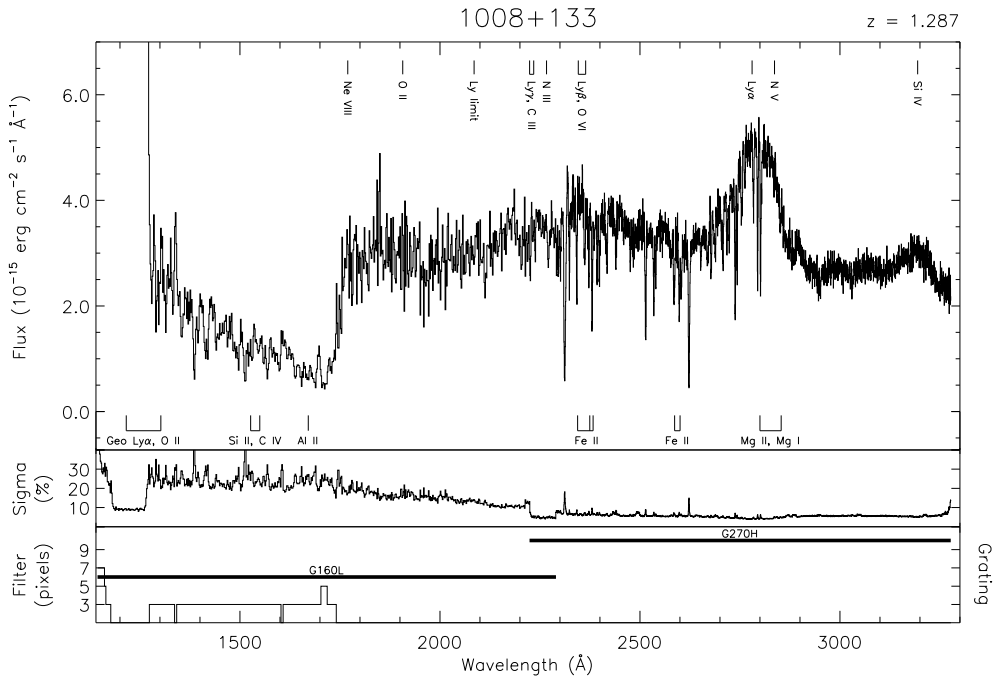
1008+133
z = 1.287
Flux (10^{-15} erg cm^{-2} s^{-1} Å^{-1})
Ne VIII
O II
Ly limit
N III
Lyγ, C III
Lyβ, O VI
Lyα
N V
Si IV
Geo Lyα, O II
Si II, C IV
Al II
Fe II
Fe II
Mg II, Mg I
Sigma (%)
G270H
G160L
Filter (pixels)
Grating
Wavelength (Å)

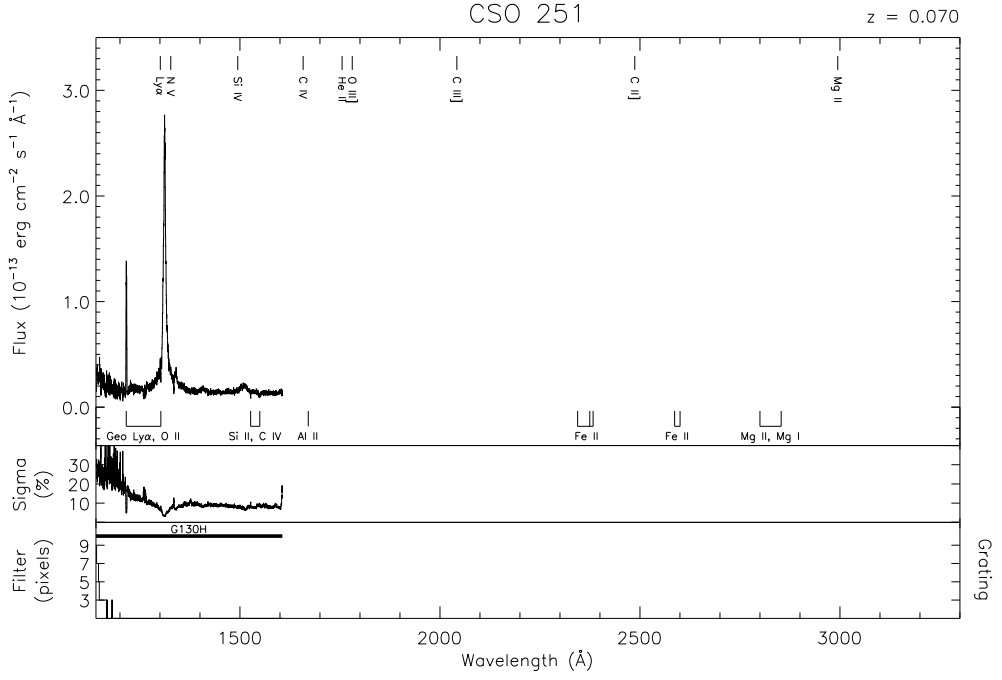
CSO 251
z = 0.070
Flux (10^{-13} erg cm^{-2} s^{-1} Å^{-1})
N V
Lyα
Si IV
C IV
O III]
He II
C III]
C II
Mg II
Geo Lyα, O II
Si II, C IV
Al II
Fe II
Fe II
Mg II, Mg I
Sigma (%)
G130H
Filter (pixels)
Grating
Wavelength (Å)

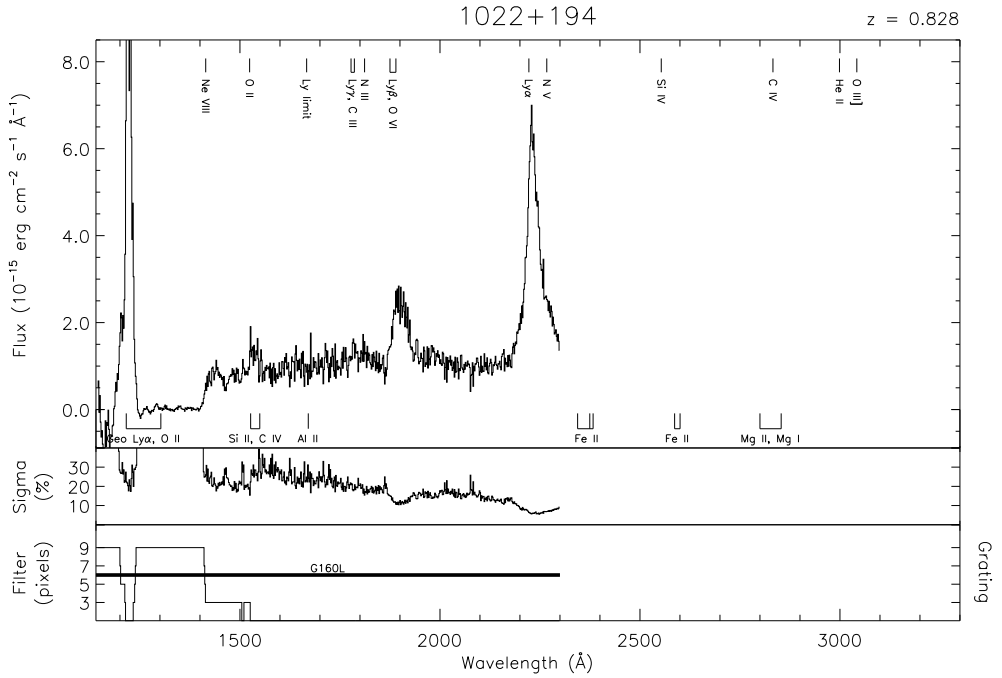
1022+194
z = 0.828
Flux (10^{-15} erg cm^{-2} s^{-1} Å^{-1})
Ne VIII
O II
Ly limit
N III
Lyγ, C III
Lyβ, O VI
Lyα
N V
Si IV
C IV
He II
O III]
Geo Lyα, O II
Si II, C IV
Al II
Fe II
Fe II
Mg II, Mg I
Sigma (%)
Filter (pixels)
G160L
Grating
Wavelength (Å)

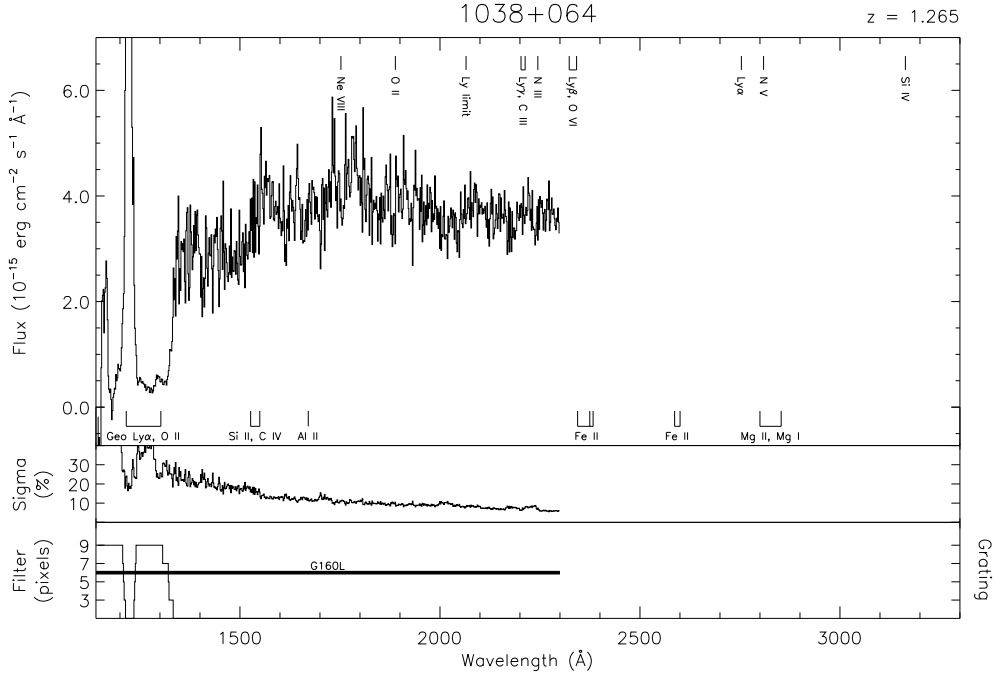
1038+064
z = 1.265
Flux (10^{-15} erg cm^{-2} s^{-1} Å^{-1})
Ne VIII
O II
Ly limit
N III
Lyγ, C III
Lyβ, O VI
Lyα
N V
Si IV
Geo Lyα, O II
Si II, C IV
Al II
Fe II
Fe II
Mg II, Mg I
Sigma (%)
Filter (pixels)
G160L
Grating
Wavelength (Å)

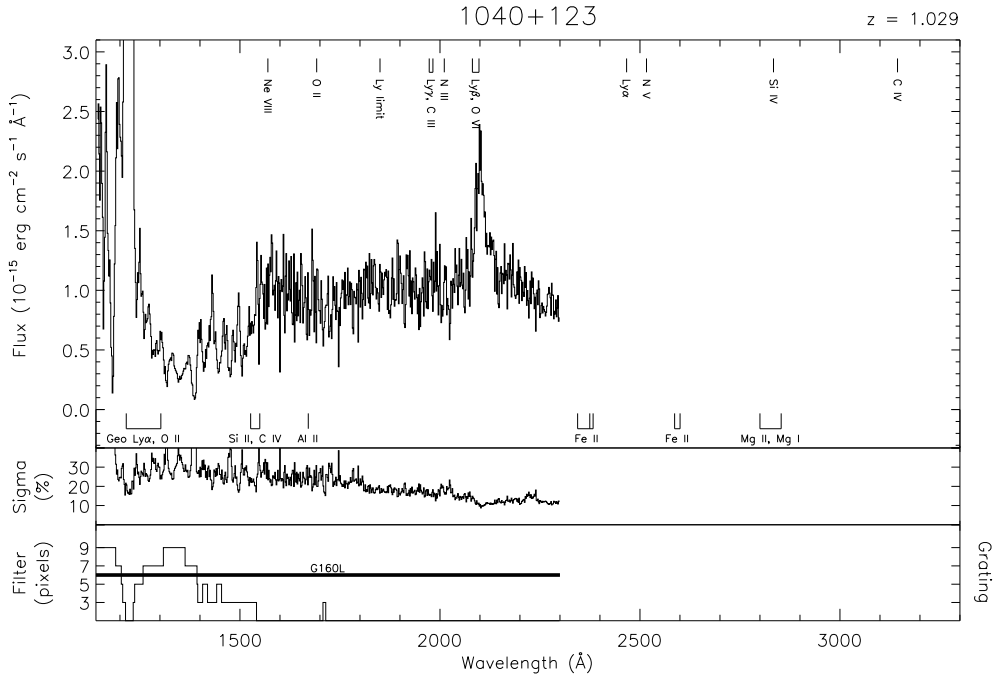
1040+123
z = 1.029
Flux (10^{-15} erg cm^{-2} s^{-1} Å^{-1})
Ne VIII
O II
Ly limit
Lyγ, C III
N III
Lyβ, O VI
Lyα
N V
Si IV
C IV
Geo Lyα, O II
Si II, C IV
Al II
Fe II
Fe II
Mg II, Mg I
Sigma (%)
Filter (pixels)
G160L
Grating
Wavelength (Å)

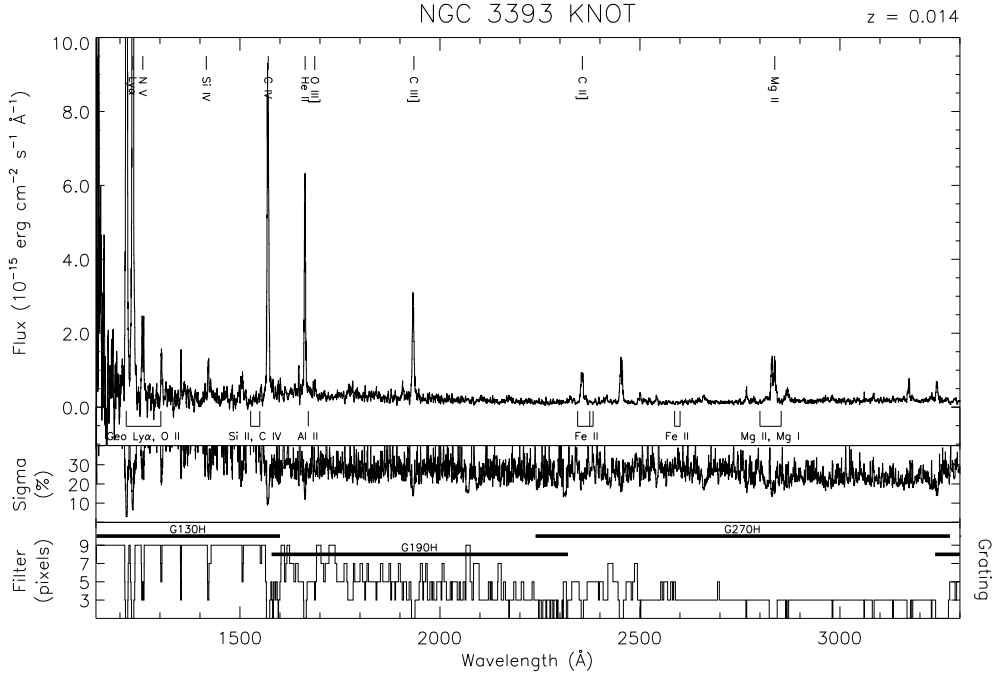
NGC 3393 KNOT
z = 0.014
Flux (10^{-15} erg cm^{-2} s^{-1} Å^{-1})
Lyβ
N V
Si IV
C IV
He II
O III]
C III]
C II]
Mg II
Geo Lyα, O II
Si II, C IV
Al II
Fe II
Fe II
Mg II, Mg I
Sigma (%)
G130H
G190H
G270H
Filter (pixels)
Grating
Wavelength (Å)

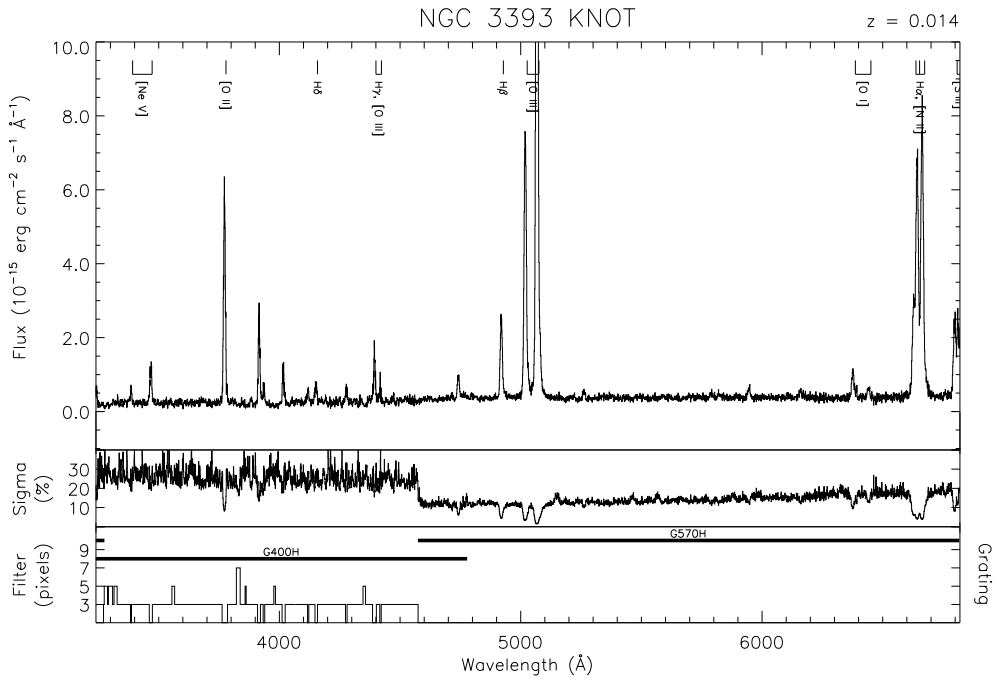
NGC 3393 KNOT
z = 0.014
Flux (10^{-15} erg cm^{-2} s^{-1} Å^{-1})
[Ne V]
[O II]
Hδ
Hγ, [O III]
Hβ
[O III]
[O I]
Hα, [N II]
[S II]
Sigma (%)
Filter (pixels)
G400H
G570H
Grating
Wavelength (Å)

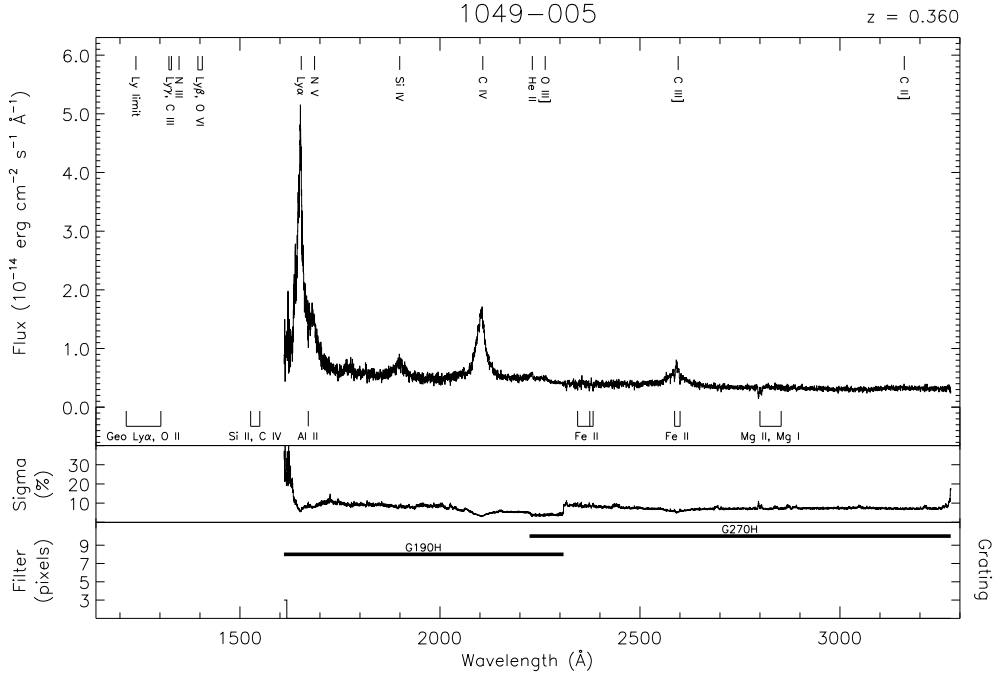
1049−005
z = 0.360
Flux (10^{-14} erg cm^{-2} s^{-1} Å^{-1})
Ly limit
Ly, C III
Lyβ, O VI
Lyα
N V
Si IV
C IV
He II
O III]
C III]
C II]
Geo Lyα, O II
Si II, C IV
Al II
Fe II
Fe II
Mg II, Mg I
Sigma (%)
Filter (pixels)
G190H
G270H
Grating
Wavelength (Å)

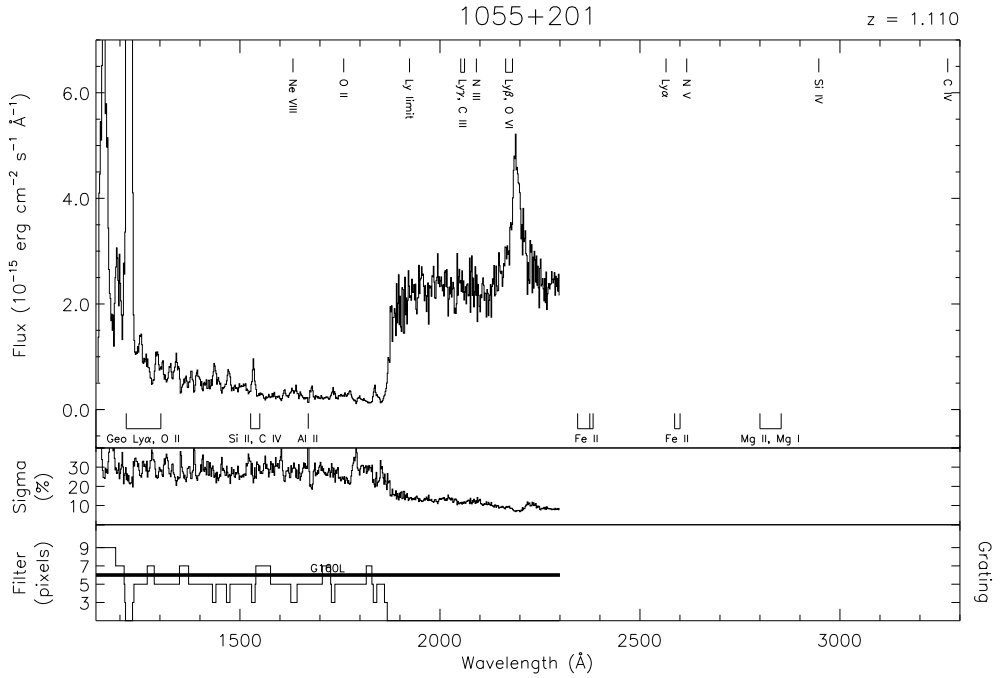
1055+201
z = 1.110
Flux (10^{-15} erg cm^{-2} s^{-1} Å^{-1})
Ne VIII
O II
Ly limit
N III
Lyγ, C III
Lyβ, O VI
Lyα
N V
Si IV
C IV
Geo Lyα, O II
Si II, C IV
Al II
Fe II
Fe II
Mg II, Mg I
Sigma (%)
Filter (pixels)
G160L
Grating
Wavelength (Å)

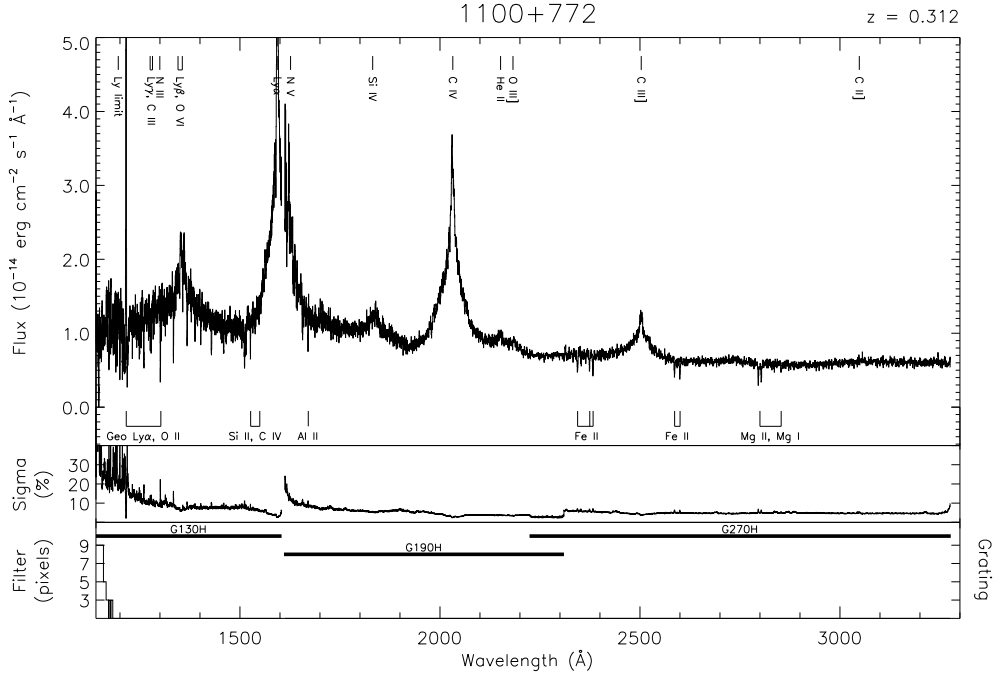
1100+772
z = 0.312
Flux (10^{-14} erg cm^{-2} s^{-1} Å^{-1})
Ly limit
N III
Lyγ, C III
Lyβ, O VI
Lyα
N V
Si IV
C IV
He II
O III]
C III]
C II]
Geo Lyα, O II
Si II, C IV
Al II
Fe II
Fe II
Mg II, Mg I
Sigma (%)
G130H
G190H
G270H
Filter (pixels)
Grating
Wavelength (Å)

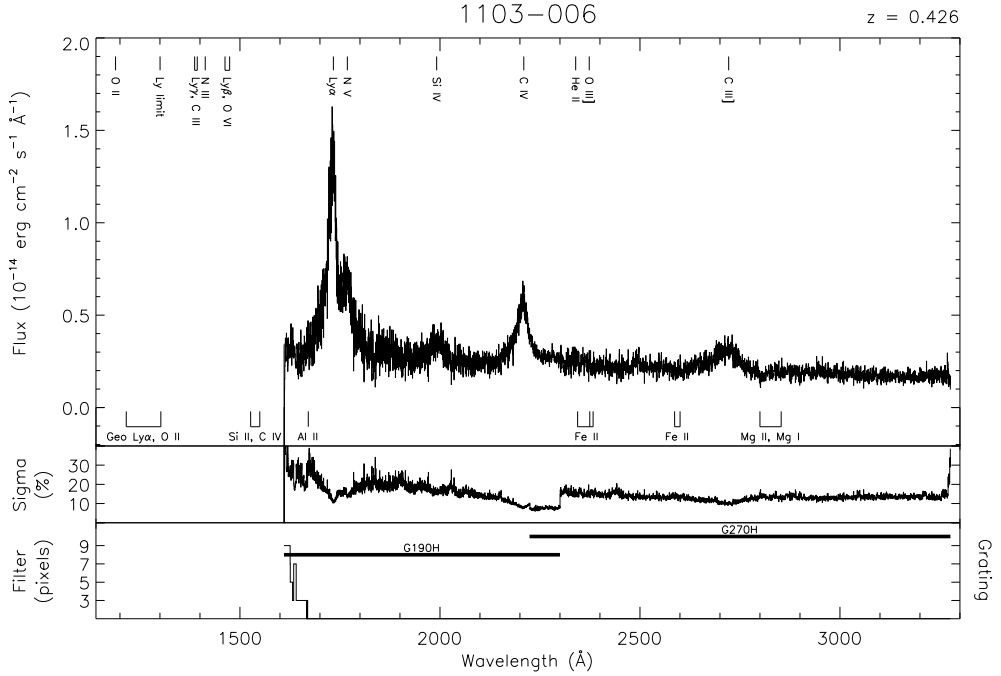
1103−006
z = 0.426
Flux (10^{-14} erg cm^{-2} s^{-1} Å^{-1})
O II
Ly limit
N III
Lyγ, C III
Lyβ, O VI
N V
Lyα
Si IV
C IV
He II
O III]
C III]
Geo Lyα, O II
Si II, C IV
Al II
Fe II
Fe II
Mg II, Mg I
Sigma (%)
G270H
G190H
Filter (pixels)
Grating
Wavelength (Å)

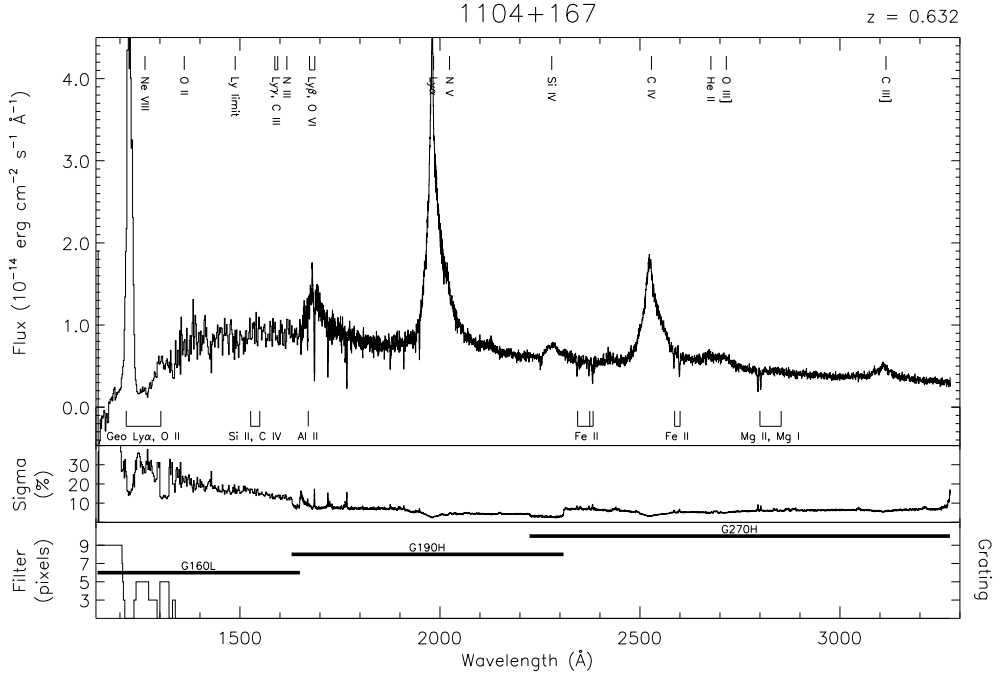
1104+167
z = 0.632
Flux (10^{-14} erg cm^{-2} s^{-1} Å^{-1})
Ne VIII
O II
Ly limit
N III
Lyγ, C III
Lyβ, O VI
N V
Lyα
Si IV
C IV
He II
O III]
C III]
Geo Lyα, O II
Si II, C IV
Al II
Fe II
Fe II
Mg II, Mg I
Sigma (%)
G270H
G190H
G160L
Filter (pixels)
Grating
Wavelength (Å)

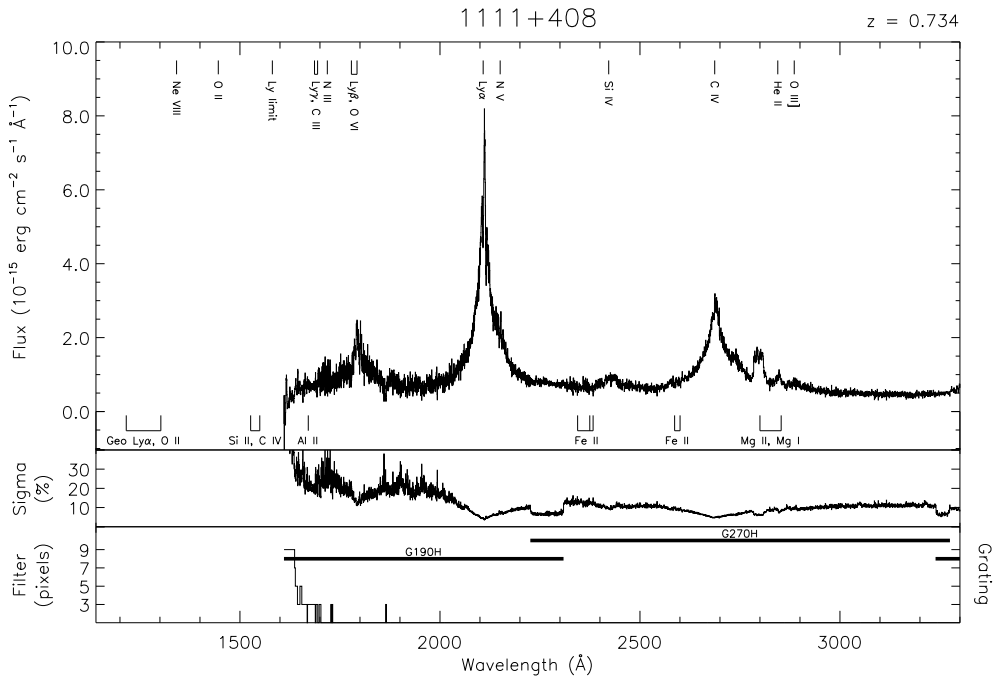
1111+408
z = 0.734
Flux (10^{-15} erg cm^{-2} s^{-1} Å^{-1})
Ne VIII
O II
Ly limit
N III
Lyγ, C III
Lyβ, O VI
Lyα
N V
Si IV
C IV
He II
O III]
Geo Lyα, O II
Si II, C IV
Al II
Fe II
Fe II
Mg II, Mg I
Sigma (%)
Filter (pixels)
G190H
G270H
Grating
Wavelength (Å)

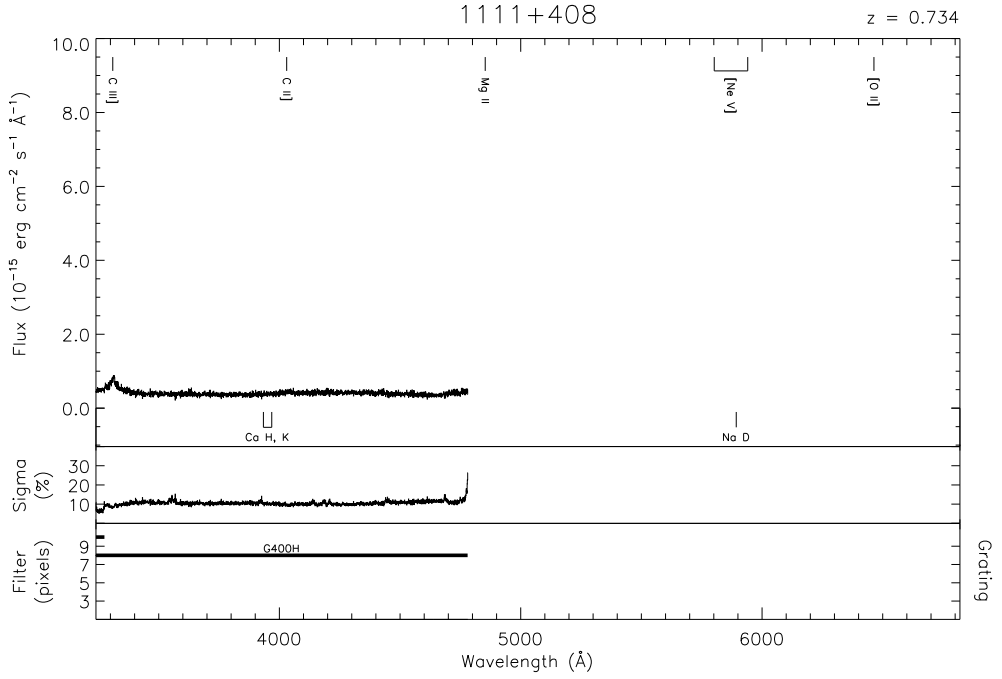
1111+408
z = 0.734
Flux (10^{-15} erg cm^{-2} s^{-1} Å^{-1})
C III]
C II]
Mg II
[Ne V]
[O II]
Ca H, K
Na D
Sigma (%)
Filter (pixels)
G400H
Grating
Wavelength (Å)

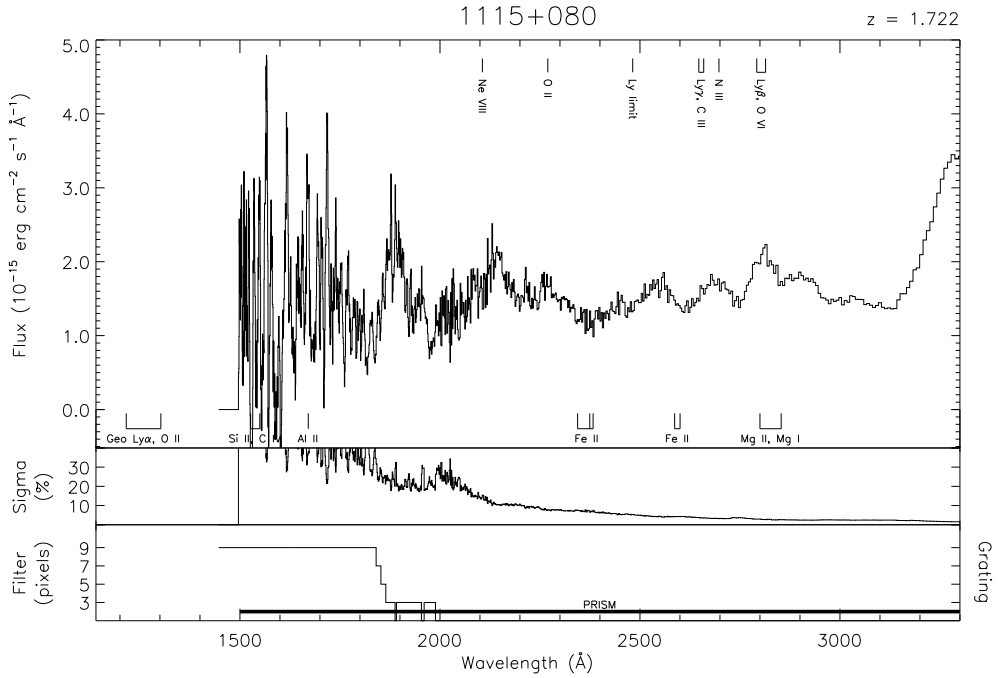
1115+080
z = 1.722
Flux (10^{-15} erg cm^{-2} s^{-1} Å^{-1})
Ne VIII
O II
Ly limit
Lyγ, C III
N III
Lyβ, O VI
Geo Lyα, O II
Si II, C I
Al II
Fe II
Fe II
Mg II, Mg I
Sigma (%)
Filter (pixels)
PRISM
Grating
Wavelength (Å)

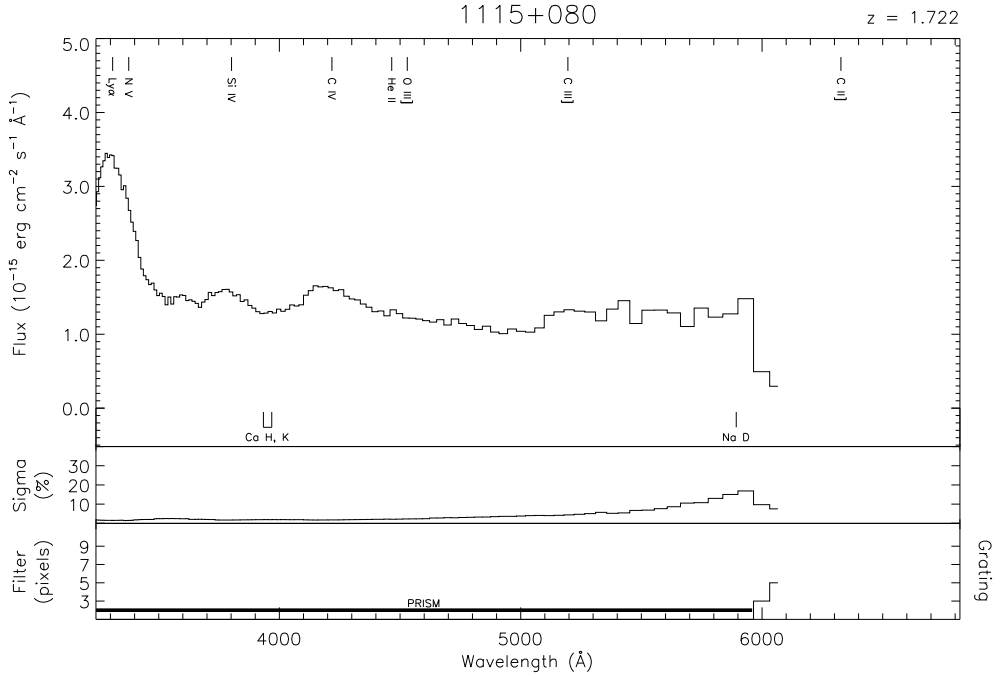
1115+080
z = 1.722
Flux (10^{-15} erg cm^{-2} s^{-1} Å^{-1})
Lyα
N V
Si IV
C IV
He II
O III]
C III]
C II]
Ca H, K
Na D
Sigma (%)
Filter (pixels)
PRISM
Grating
Wavelength (Å)

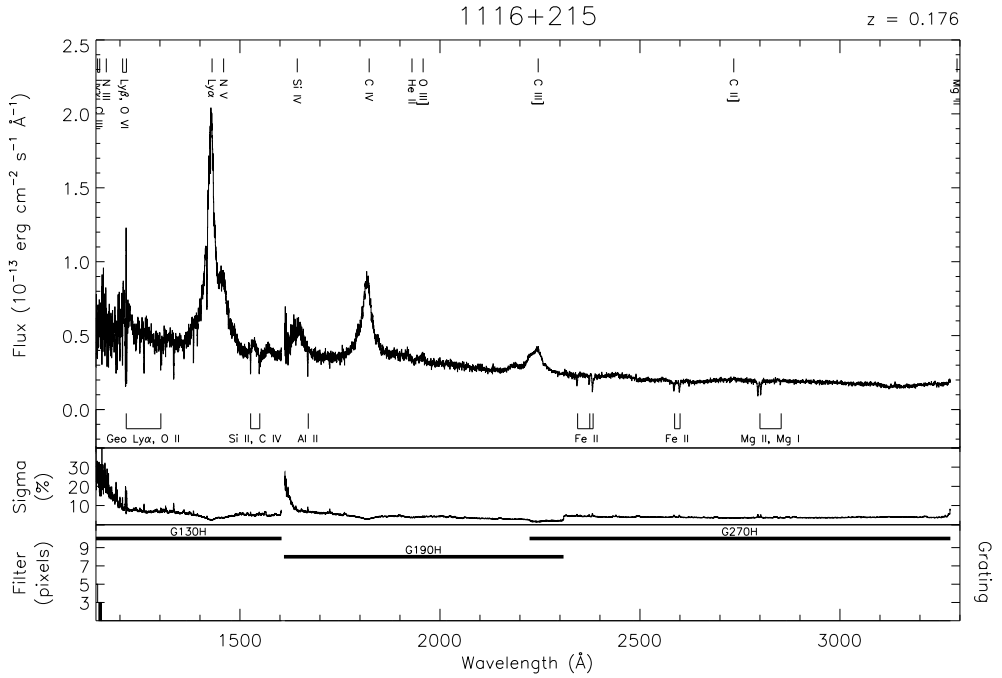
1116+215
z = 0.176
Flux (10^{-13} erg cm^{-2} s^{-1} Å^{-1})
N III] λ1909
Lyβ, O VI
N V
Lyα
Si IV
C IV
He II
O III]
C III]
C II]
Mg II
Geo Lyα, O II
Si II, C IV
Al II
Fe II
Fe II
Mg II, Mg I
Sigma (%)
G130H
G190H
G270H
Filter (pixels)
Grating
Wavelength (Å)

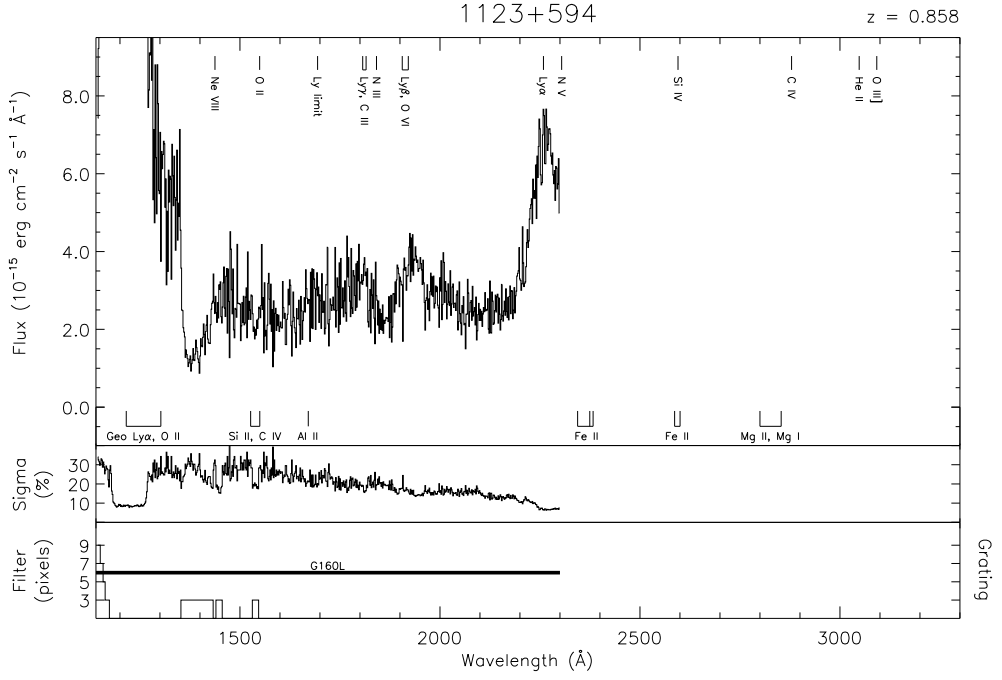
1123+594
z = 0.858
Flux (10^{-15} erg cm^{-2} s^{-1} Å^{-1})
Ne VIII
O II
Ly limit
N III
Lyγ, C III
Lyβ, O VI
N V
Lyα
Si IV
C IV
He II
O III]
Geo Lyα, O II
Si II, C IV
Al II
Fe II
Fe II
Mg II, Mg I
Sigma (%)
G160L
Filter (pixels)
Grating
Wavelength (Å)

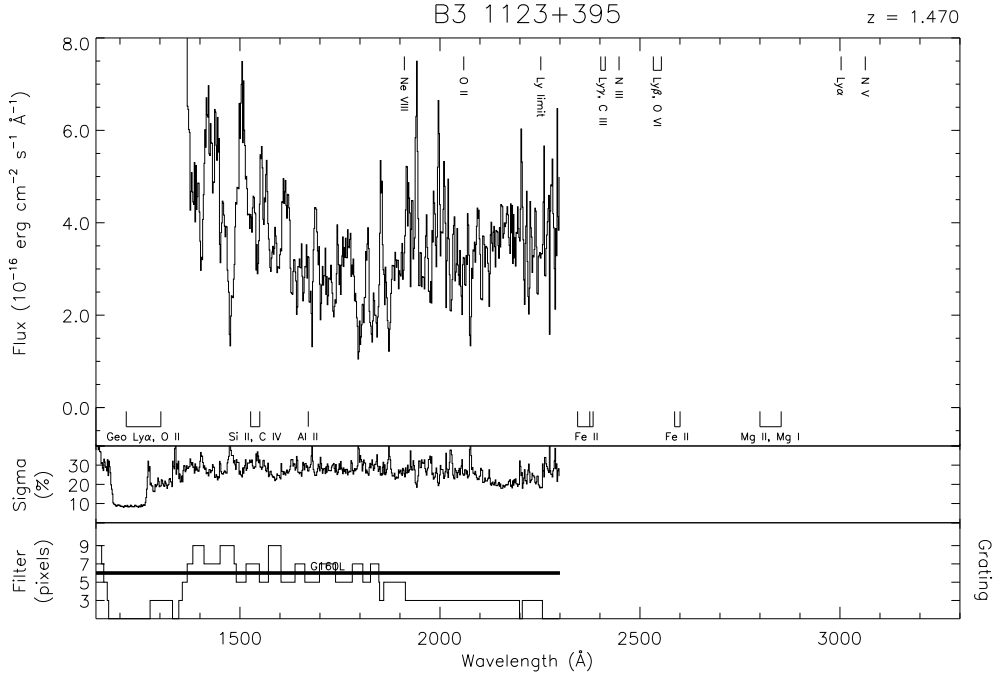
B3 1123+395
z = 1.470
Flux (10^{-16} erg cm^{-2} s^{-1} Å^{-1})
Ne VIII
O II
Ly limit
N III
Lyγ, C III
Lyβ, O VI
Lyα
N V
Geo Lyα, O II
Si II, C IV
Al II
Fe II
Fe II
Mg II, Mg I
Sigma (%)
Filter (pixels)
G160L
Grating
Wavelength (Å)

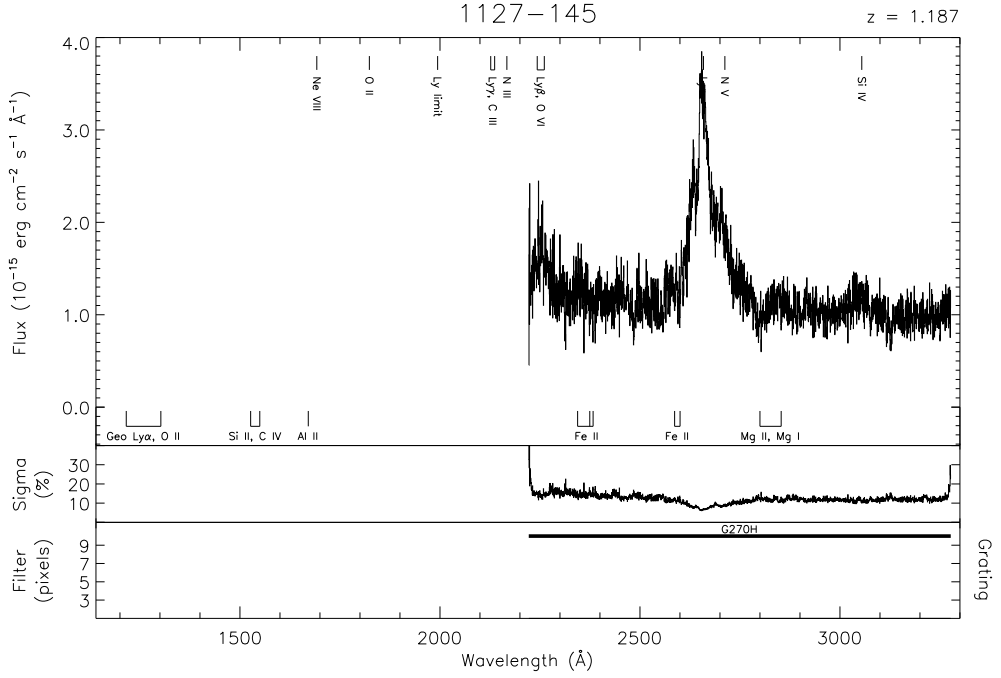
1127−145
z = 1.187
Flux (10^{-15} erg cm^{-2} s^{-1} Å^{-1})
Ne VIII
O II
Ly limit
N III
Lyγ, C III
Lyβ, O VI
N V
Si IV
Geo Lyα, O II
Si II, C IV
Al II
Fe II
Fe II
Mg II, Mg I
Sigma (%)
Filter (pixels)
G270H
Grating
Wavelength (Å)

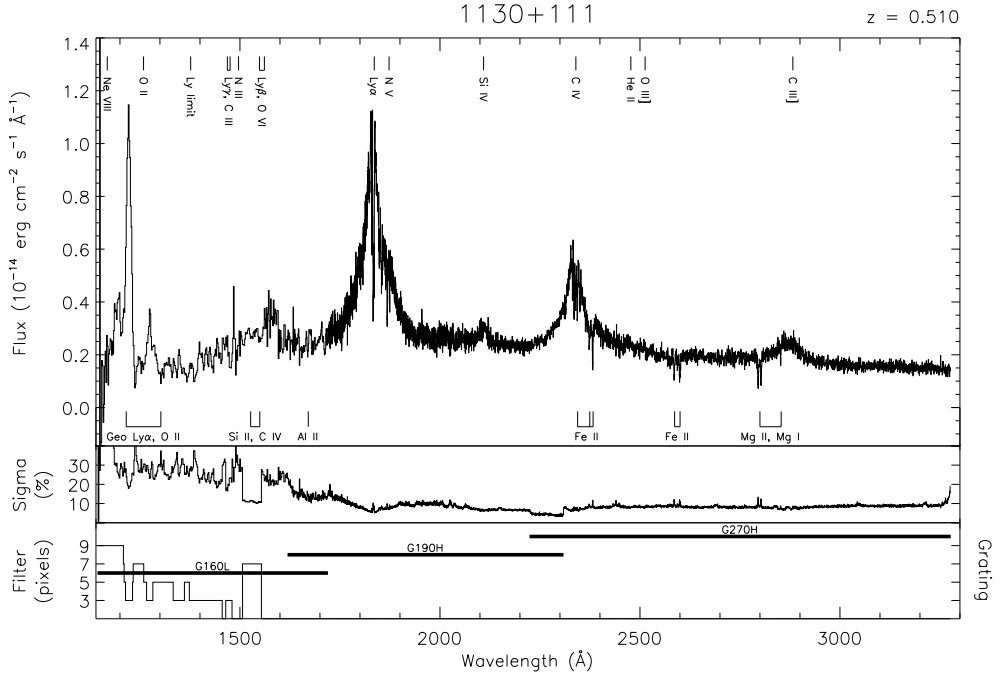
1130+111
z = 0.510
Flux (10^{-14} erg cm^{-2} s^{-1} Å^{-1})
Ne VIII
O II
Ly limit
N III
Lyγ, C III
Lyβ, O VI
Lyα
N V
Si IV
C IV
He II
O III]
C III]
Geo Lyα, O II
Si II, C IV
Al II
Fe II
Fe II
Mg II, Mg I
Sigma (%)
Filter (pixels)
G160L
G190H
G270H
Grating
Wavelength (Å)

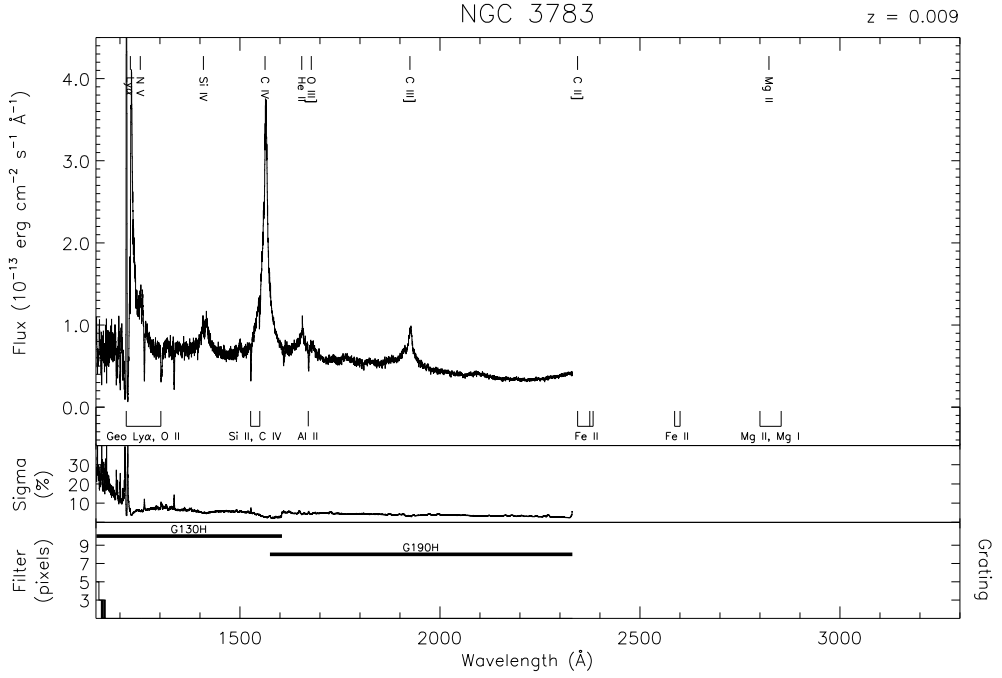
NGC 3783
z = 0.009
Flux (10^{-13} erg cm^{-2} s^{-1} Å^{-1})
Lyα
N V
Si IV
C IV
He II
O III]
C III]
C II]
Mg II
Geo Lyα, O II
Si II, C IV
Al II
Fe II
Fe II
Mg II, Mg I
Sigma (%)
Filter (pixels)
G130H
G190H
Grating
Wavelength (Å)

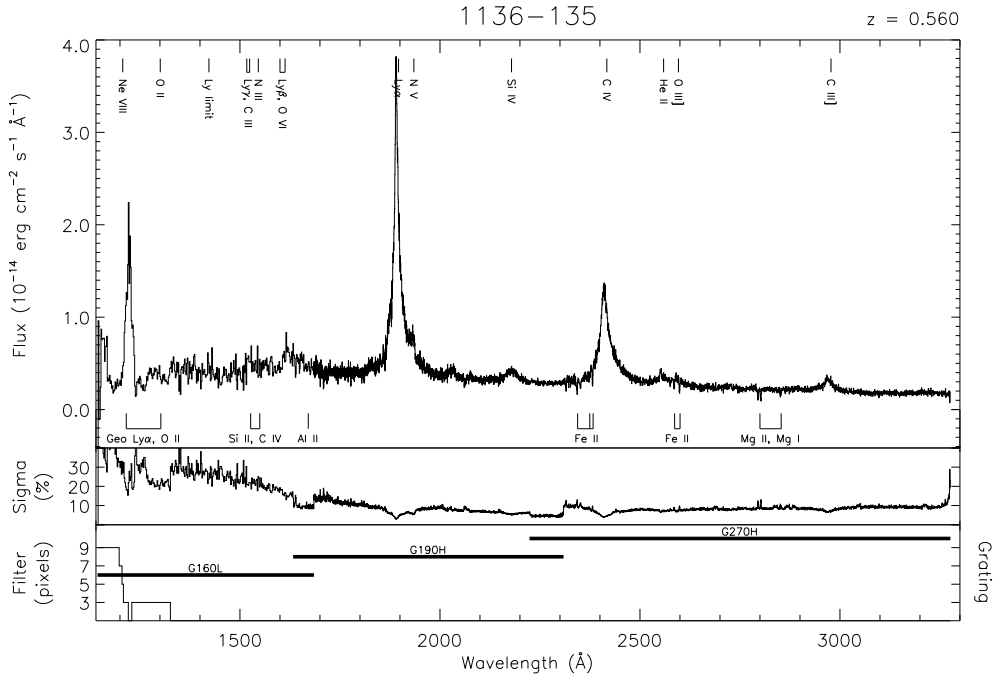
1136−135
z = 0.560
Flux (10^{-14} erg cm^{-2} s^{-1} Å^{-1})
Ne VIII
O II
Ly limit
N III
Lyγ, C III
Lyβ, O VI
Lyα
N V
Si IV
C IV
He II
O III]
C III]
Geo Lyα, O II
Si II, C IV
Al II
Fe II
Fe II
Mg II, Mg I
Sigma (%)
G270H
G190H
G160L
Filter (pixels)
Grating
Wavelength (Å)

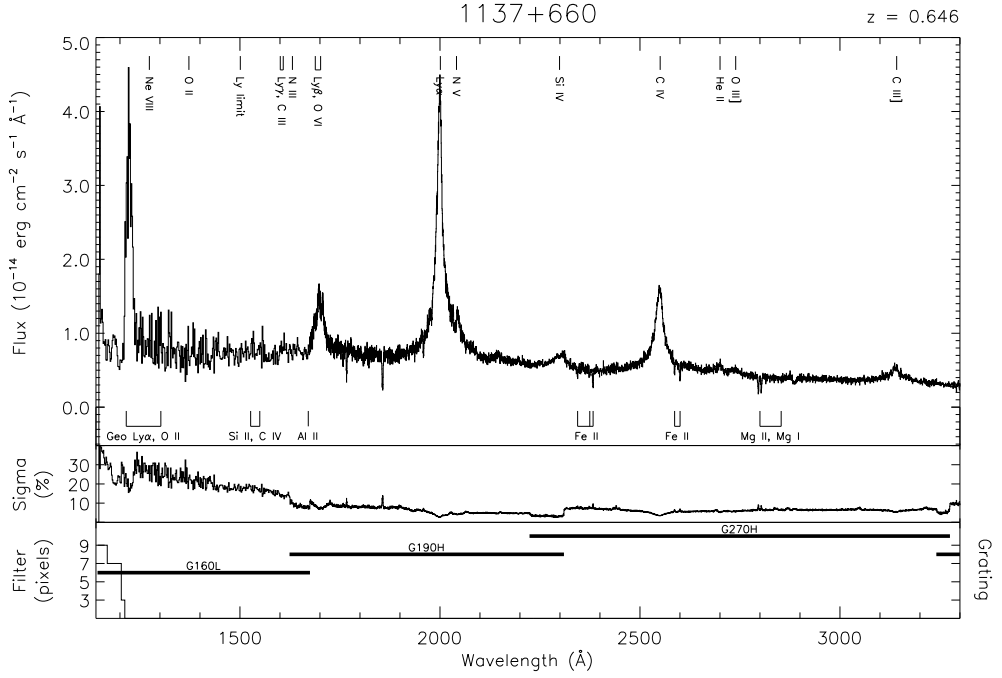
1137+660
z = 0.646
Flux (10^{-14} erg cm^{-2} s^{-1} Å^{-1})
Ne VIII
O II
Ly limit
N III
Lyγ, C III
Lyβ, O VI
Lyα
N V
Si IV
C IV
He II
O III]
C III]
Geo Lyα, O II
Si II, C IV
Al II
Fe II
Fe II
Mg II, Mg I
Sigma (%)
G270H
G190H
G160L
Filter (pixels)
Grating
Wavelength (Å)

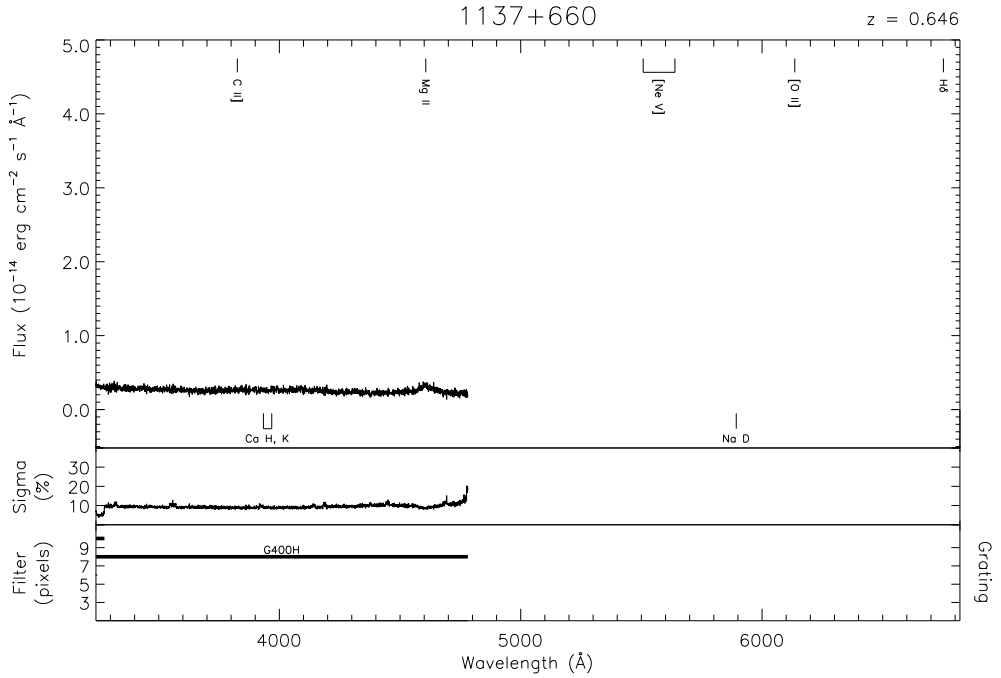
1137+660
z = 0.646
C II]
Mg II
[Ne V]
[O II]
Hδ
Ca H, K
Na D
G400H
Flux (10^-14 erg cm^-2 s^-1 Å^-1)
Sigma (%)
Filter (pixels)
Grating
Wavelength (Å)

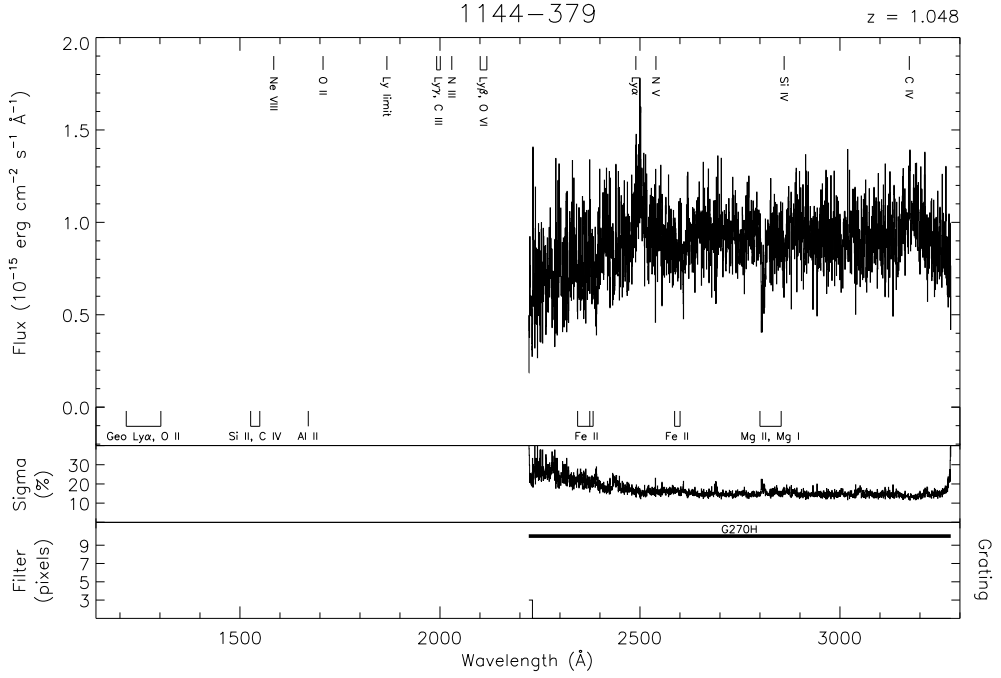
1144−379
z = 1.048
Ne VIII
O II
Ly limit
N III
Lyγ, C III
Lyβ, O VI
Lyα
N V
Si IV
C IV
Geo Lyα, O II
Si II, C IV
Al II
Fe II
Fe II
Mg II, Mg I
G270H
Flux (10^-15 erg cm^-2 s^-1 Å^-1)
Sigma (%)
Filter (pixels)
Grating
Wavelength (Å)

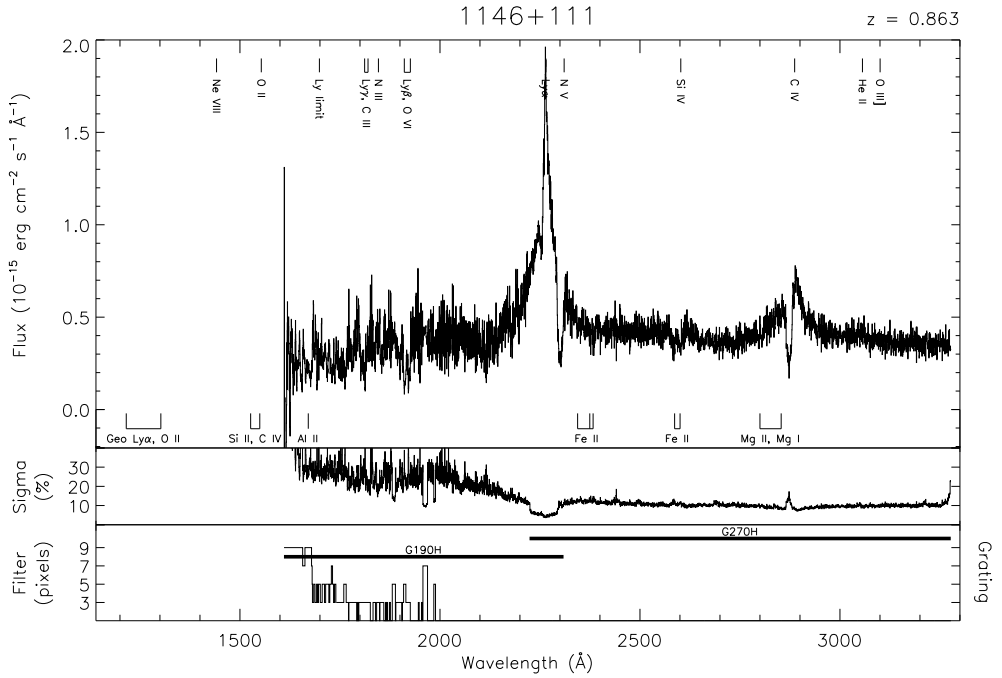
1146+111
z = 0.863
Flux (10^{-15} erg cm^{-2} s^{-1} Å^{-1})
Ne VIII
O II
Ly limit
N III
Lyγ, C III
Lyβ, O VI
Lyα
N V
Si IV
C IV
He II
O III]
Geo Lyα, O II
Si II, C IV
Al II
Fe II
Fe II
Mg II, Mg I
Sigma (%)
G270H
G190H
Filter (pixels)
Grating
Wavelength (Å)

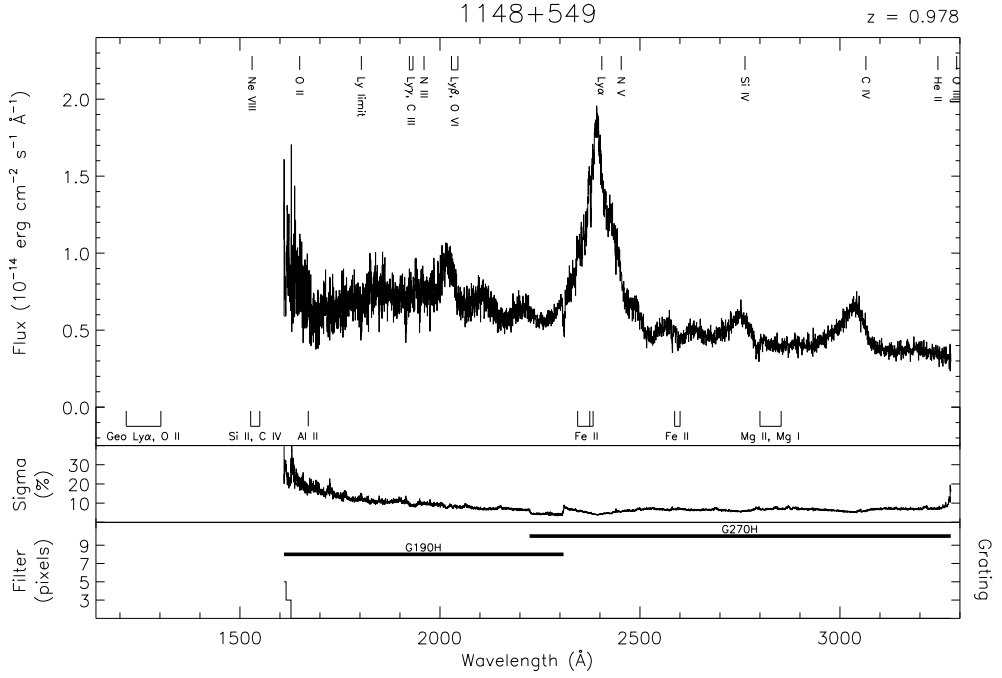
1148+549
z = 0.978
Flux (10^{-14} erg cm^{-2} s^{-1} Å^{-1})
Ne VIII
O II
Ly limit
N III
Lyγ, C III
Lyβ, O VI
Lyα
N V
Si IV
C IV
He II
O III]
Geo Lyα, O II
Si II, C IV
Al II
Fe II
Fe II
Mg II, Mg I
Sigma (%)
G270H
G190H
Filter (pixels)
Grating
Wavelength (Å)

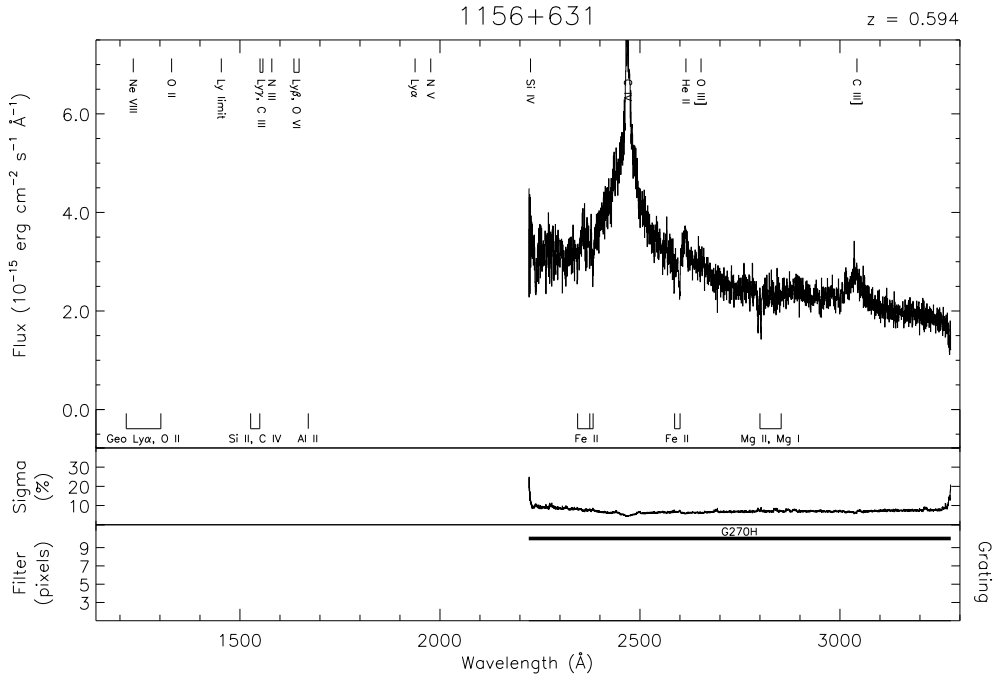
1156+631
z = 0.594
Flux (10^{-15} erg cm^{-2} s^{-1} Å^{-1})
Ne VIII
O II
Ly limit
N III
Lyγ, C III
Lyβ, O VI
Lyα
N V
Si IV
C IV
He II
O III]
C III]
Geo Lyα, O II
Si II, C IV
Al II
Fe II
Fe II
Mg II, Mg I
Sigma (%)
Filter (pixels)
G270H
Grating
Wavelength (Å)

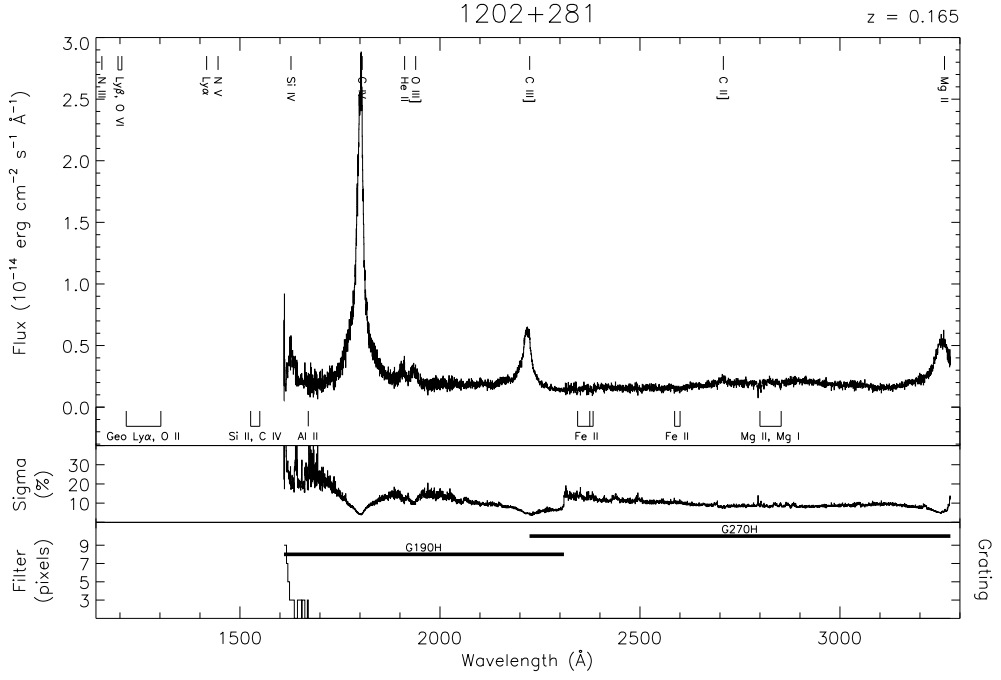
1202+281
z = 0.165
Flux (10^{-14} erg cm^{-2} s^{-1} Å^{-1})
N III]
Lyβ, O VI
Lyα
N V
Si IV
C IV
He II
O III]
C III]
C II]
Mg II
Geo Lyα, O II
Si II, C IV
Al II
Fe II
Fe II
Mg II, Mg I
Sigma (%)
Filter (pixels)
G190H
G270H
Grating
Wavelength (Å)

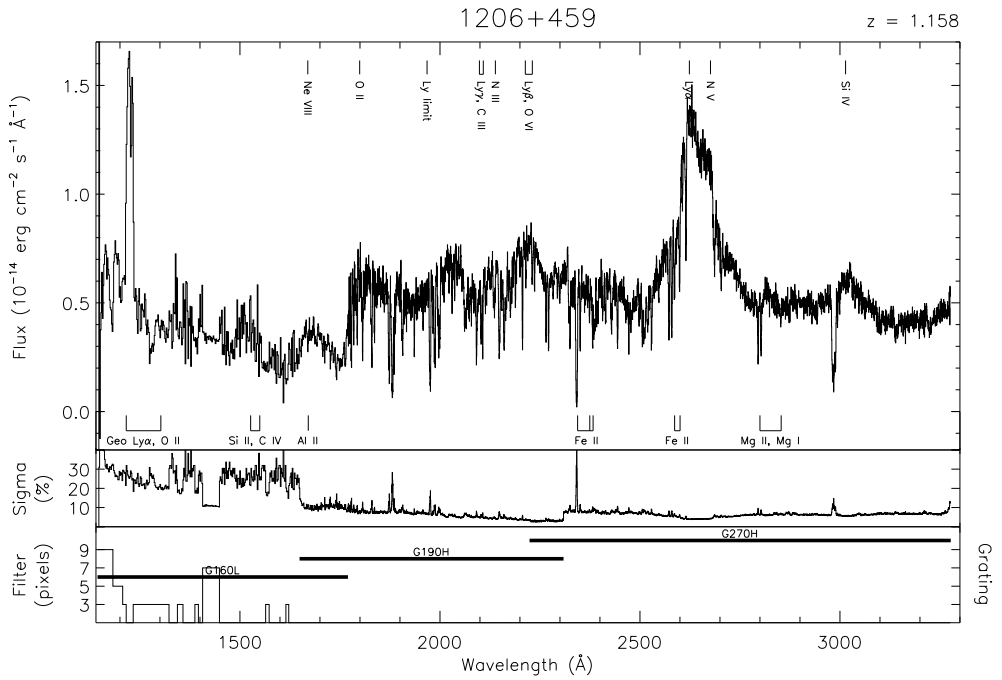
1206+459
z = 1.158
Flux (10^{-14} erg cm^{-2} s^{-1} Å^{-1})
Ne VIII
O II
Ly limit
Ly ε, C III
N III
Lyβ, O VI
Lyα
N V
Si IV
Geo Lyα, O II
Si II, C IV
Al II
Fe II
Fe II
Mg II, Mg I
Sigma (%)
G270H
G190H
G160L
Filter (pixels)
Grating
Wavelength (Å)

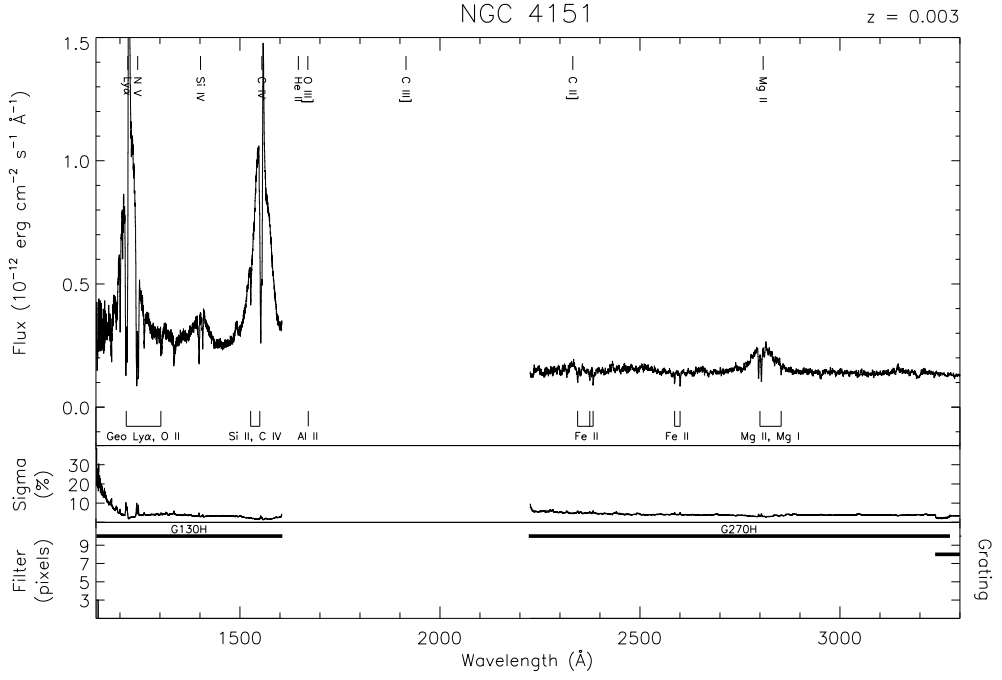
NGC 4151
z = 0.003
Flux (10^{-12} erg cm^{-2} s^{-1} Å^{-1})
Lyβ
N V
Si IV
C IV
He II
O III]
C III]
C II]
Mg II
Geo Lyα, O II
Si II, C IV
Al II
Fe II
Fe II
Mg II, Mg I
Sigma (%)
G130H
G270H
Filter (pixels)
Grating
Wavelength (Å)

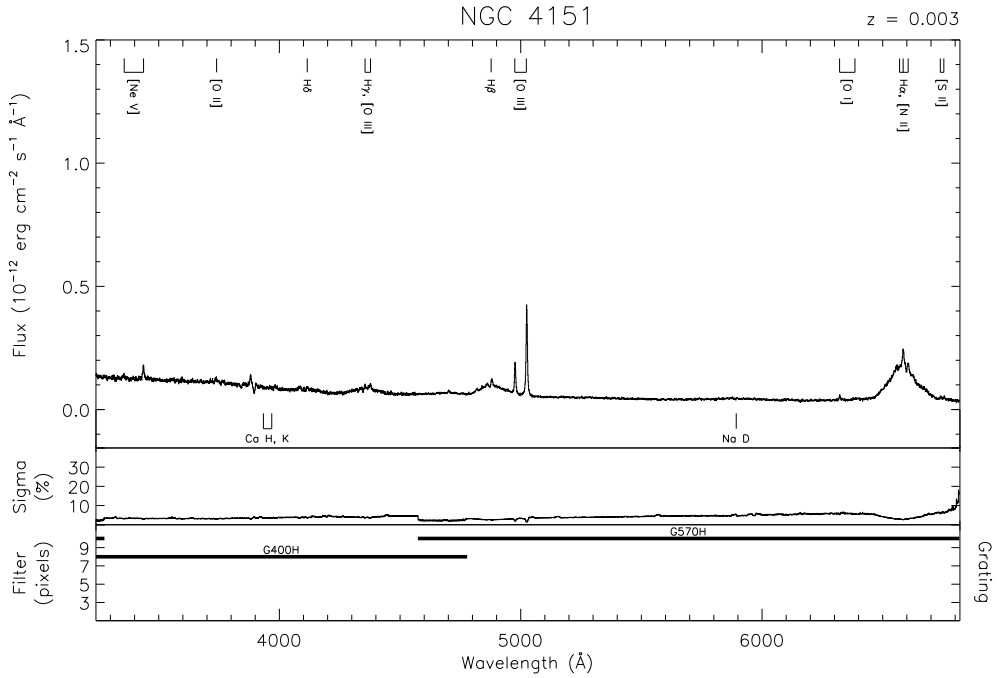
NGC 4151
z = 0.003
Flux (10^{-12} erg cm^{-2} s^{-1} Å^{-1})
[Ne V]
[O II]
Hδ
Hγ, [O III]
Hβ
[O III]
[O I]
[N II] Hα
[S II]
Ca H, K
Na D
Sigma (%)
Filter (pixels)
G400H
G570H
Grating
Wavelength (Å)

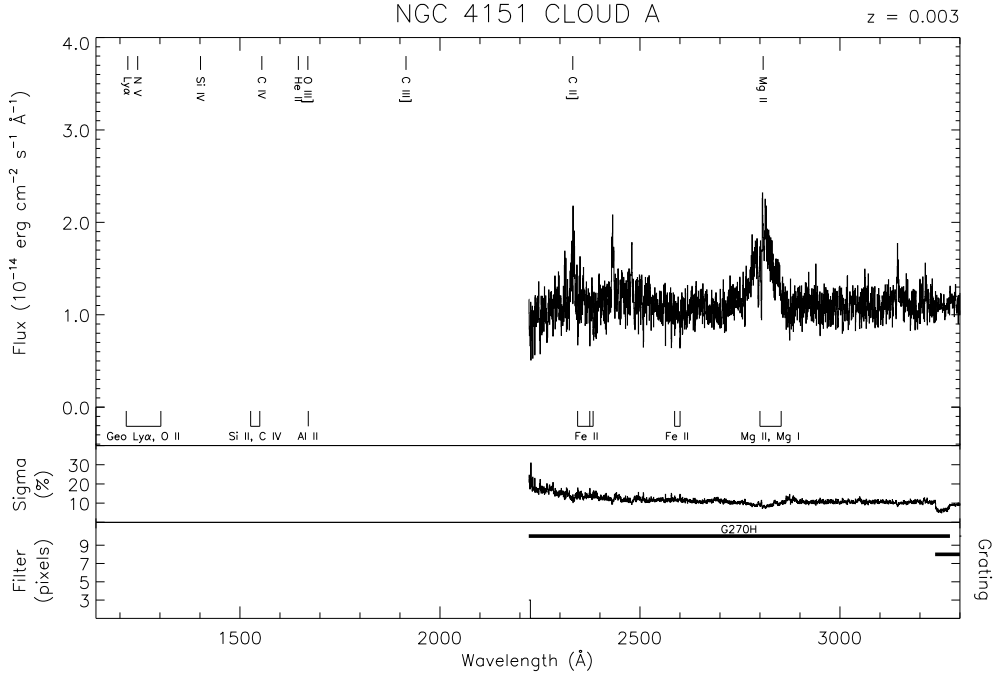
NGC 4151 CLOUD A
z = 0.003
Flux (10^{-14} erg cm^{-2} s^{-1} Å^{-1})
N V Lyα
Si IV
C IV
O III] He II
C III]
C II]
Mg II
Geo Lyα, O II
Si II, C IV
Al II
Fe II
Fe II
Mg II, Mg I
Sigma (%)
Filter (pixels)
G270H
Grating
Wavelength (Å)

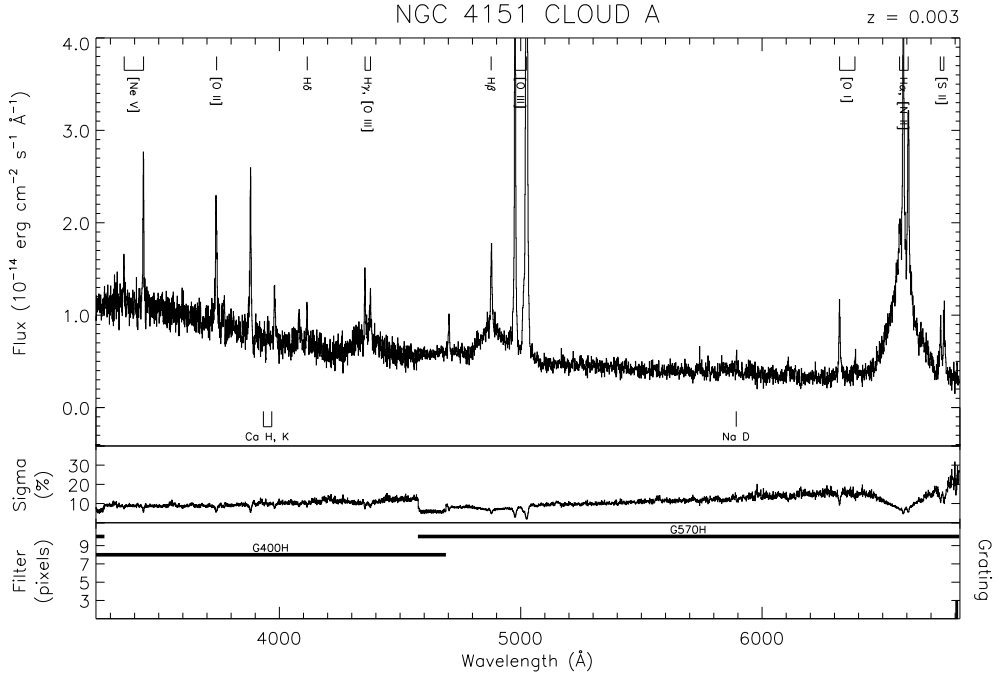
NGC 4151 CLOUD A
z = 0.003
Flux (10^{-14} erg cm^{-2} s^{-1} Å^{-1})
[Ne V]
[O II]
Hδ
[Ne III], O III]
Hβ
[O III]
[O I]
[Fe X], [S II]
[S II]
Ca H, K
Na D
Sigma (%)
Filter (pixels)
G400H
G570H
Grating
Wavelength (Å)

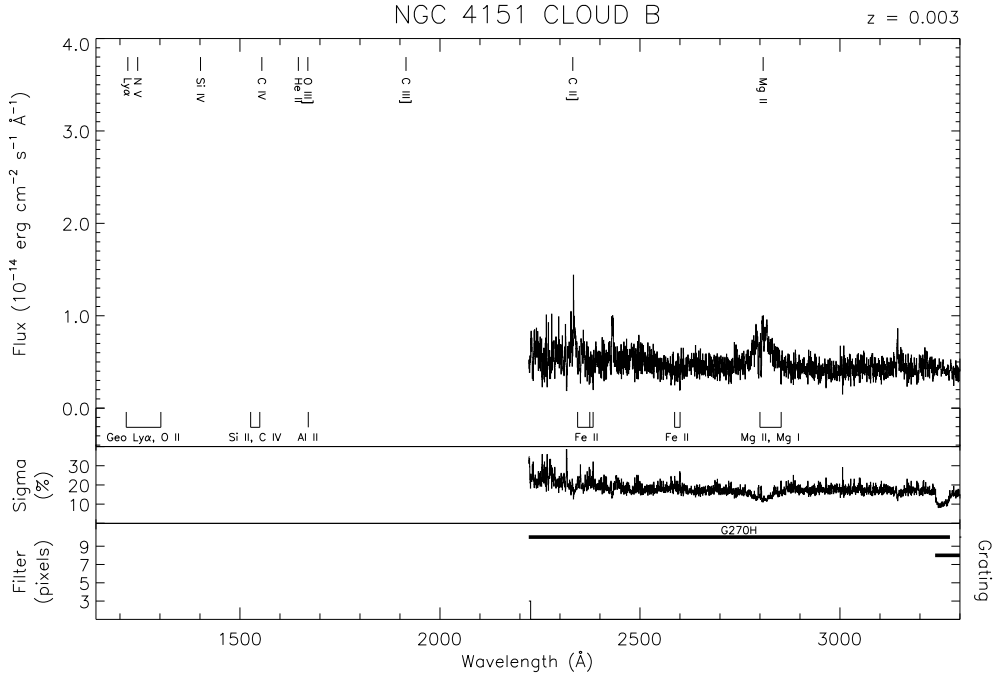
NGC 4151 CLOUD B
z = 0.003
Flux (10^{-14} erg cm^{-2} s^{-1} Å^{-1})
N V Lyα
Si IV
C IV
O III], He II
C III]
C II]
Mg II
Geo Lyα, O II
Si II, C IV
Al II
Fe II
Fe II
Mg II, Mg I
Sigma (%)
Filter (pixels)
G270H
Grating
Wavelength (Å)

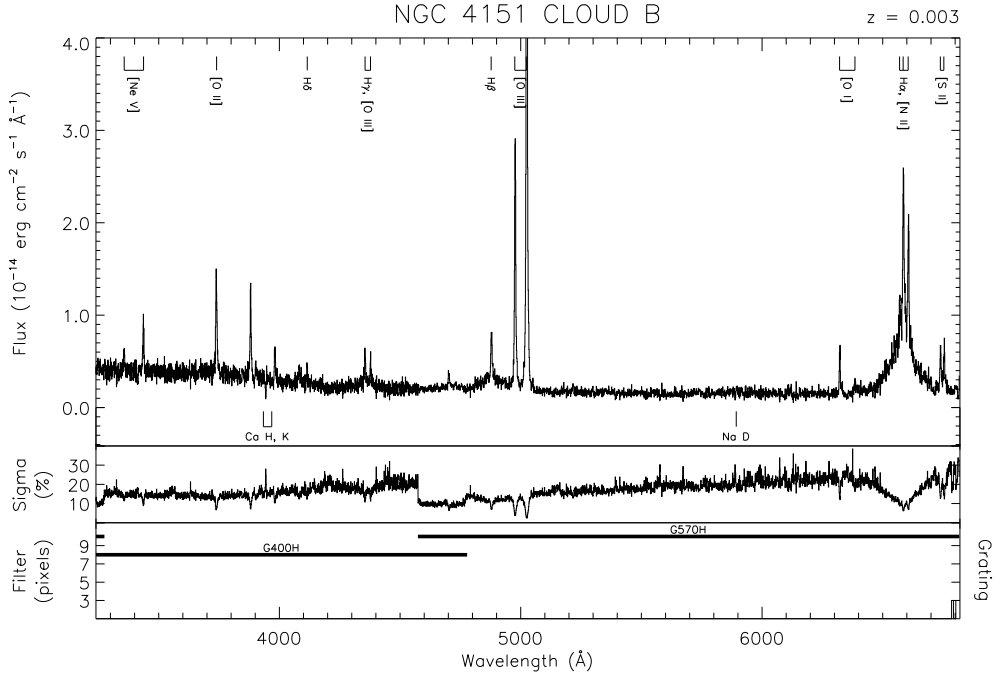
NGC 4151 CLOUD B
z = 0.003
Flux (10^{-14} erg cm^{-2} s^{-1} Å^{-1})
[Ne V]
[O II]
Hδ
[Ne III], Hε, [O III]
Hβ
[O III]
[O I]
Hα, [N II]
[S II]
Ca H, K
Na D
Sigma (%)
Filter (pixels)
G400H
G570H
Grating
Wavelength (Å)

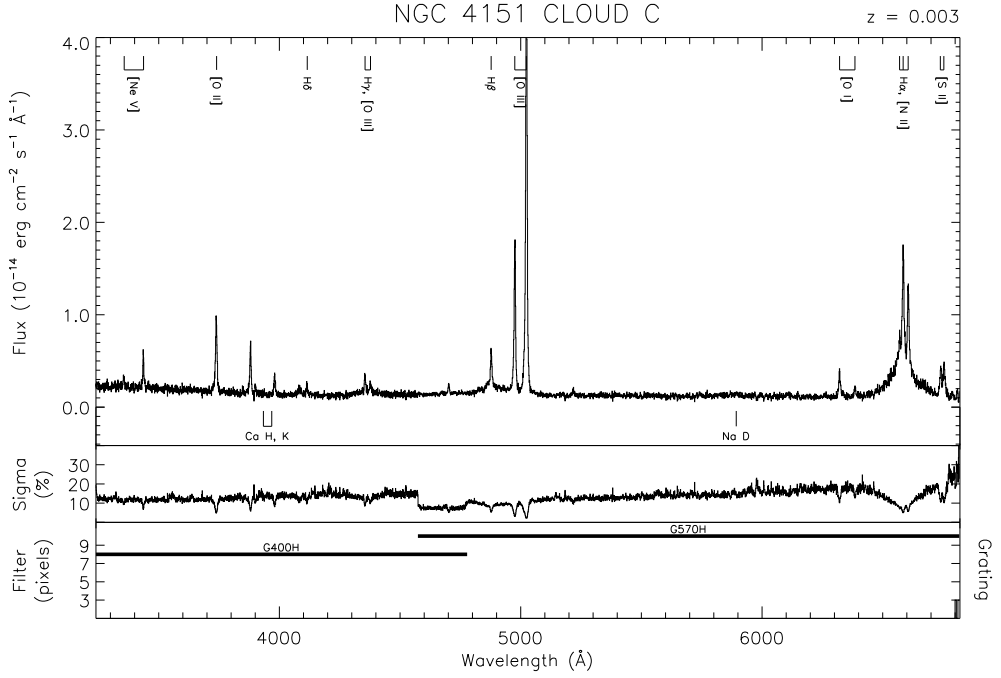
NGC 4151 CLOUD C
z = 0.003
Flux (10^{-14} erg cm^{-2} s^{-1} Å^{-1})
[Ne V]
[O II]
Hδ
[Ne III], Hε, [O III]
Hβ
[O III]
[O I]
Hα, [N II]
[S II]
Ca H, K
Na D
Sigma (%)
Filter (pixels)
G400H
G570H
Grating
Wavelength (Å)

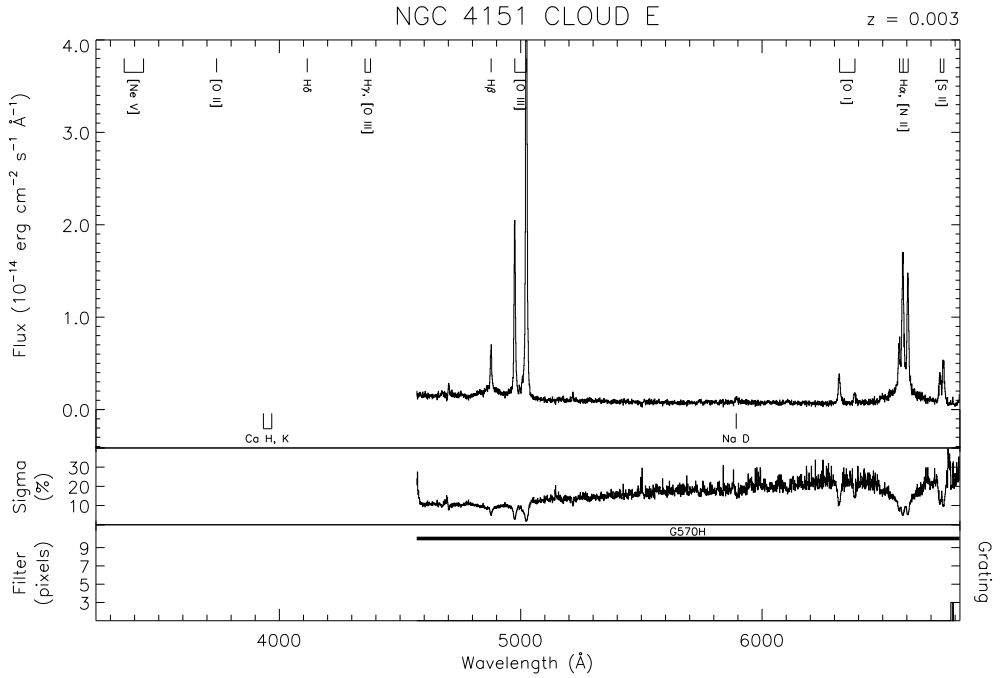
NGC 4151 CLOUD E
z = 0.003
Flux (10^{-14} erg cm^{-2} s^{-1} Å^{-1})
[Ne V]
[O II]
Hδ
[Ne III], Hε, [O III]
Hβ
[O III]
[O I]
Hα, [N II]
[S II]
Ca H, K
Na D
Sigma (%)
G570H
Filter (pixels)
Grating
Wavelength (Å)

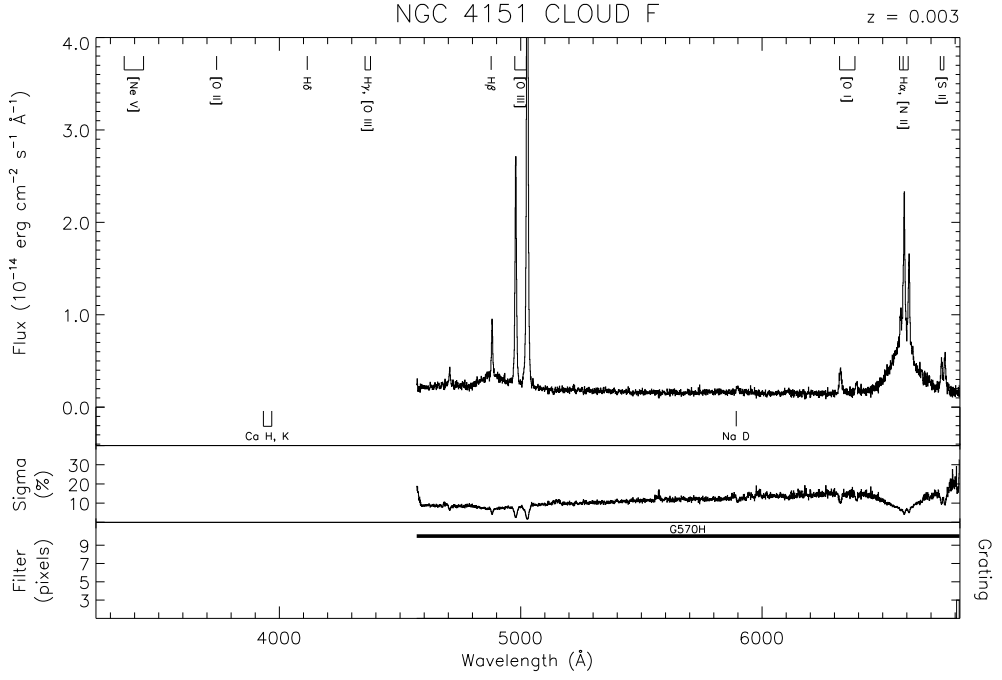
NGC 4151 CLOUD F
z = 0.003
Flux (10^{-14} erg cm^{-2} s^{-1} Å^{-1})
[Ne V]
[O II]
Hδ
[Ne III], Hε, [O III]
Hβ
[O III]
[O I]
Hα, [N II]
[S II]
Ca H, K
Na D
Sigma (%)
G570H
Filter (pixels)
Grating
Wavelength (Å)

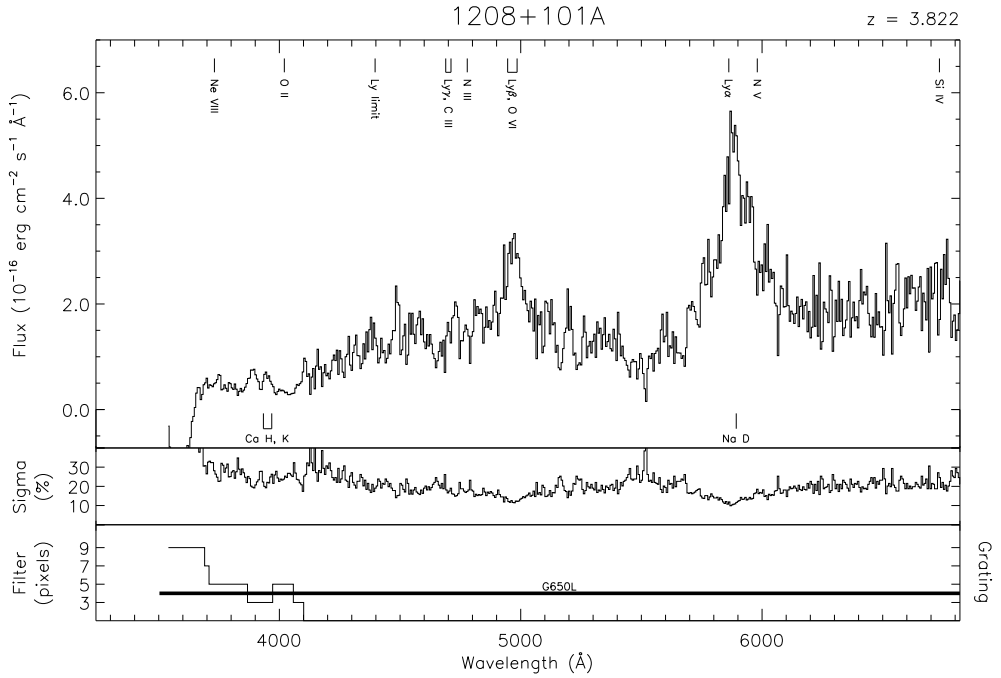
1208+101A
z = 3.822
Ne VIII
O II
Ly limit
Lyγ, C III
N III
Lyβ, O VI
Lyα
N V
Si IV
Ca H, K
Na D
Flux (10^{-16} erg cm^{-2} s^{-1} Å^{-1})
Sigma (%)
Filter (pixels)
G650L
Grating
Wavelength (Å)

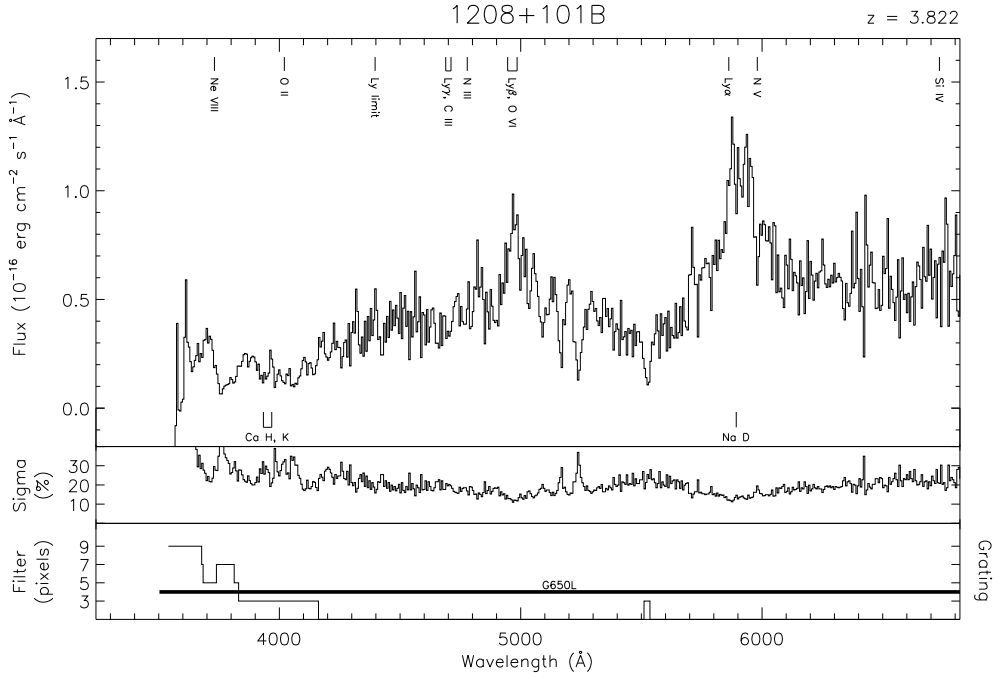
1208+101B
z = 3.822
Ne VIII
O II
Ly limit
Lyγ, C III
N III
Lyβ, O VI
Lyα
N V
Si IV
Ca H, K
Na D
Flux (10^{-16} erg cm^{-2} s^{-1} Å^{-1})
Sigma (%)
Filter (pixels)
G650L
Grating
Wavelength (Å)

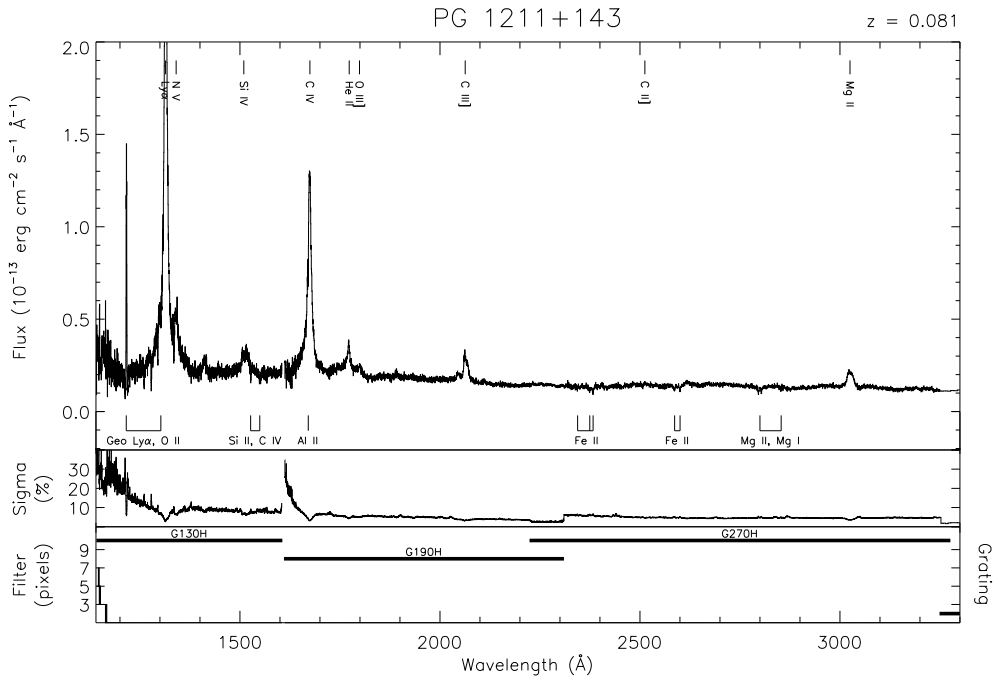
PG 1211+143
z = 0.081
Flux (10^{-13} erg cm^{-2} s^{-1} Å^{-1})
Geo Lyα
N V
Si IV
C IV
He II
O III]
C III]
C I
Mg II
Geo Lyα, O II
Si II, C IV
Al II
Fe II
Fe II
Mg II, Mg I
Sigma (%)
Filter (pixels)
G130H
G190H
G270H
Grating
Wavelength (Å)

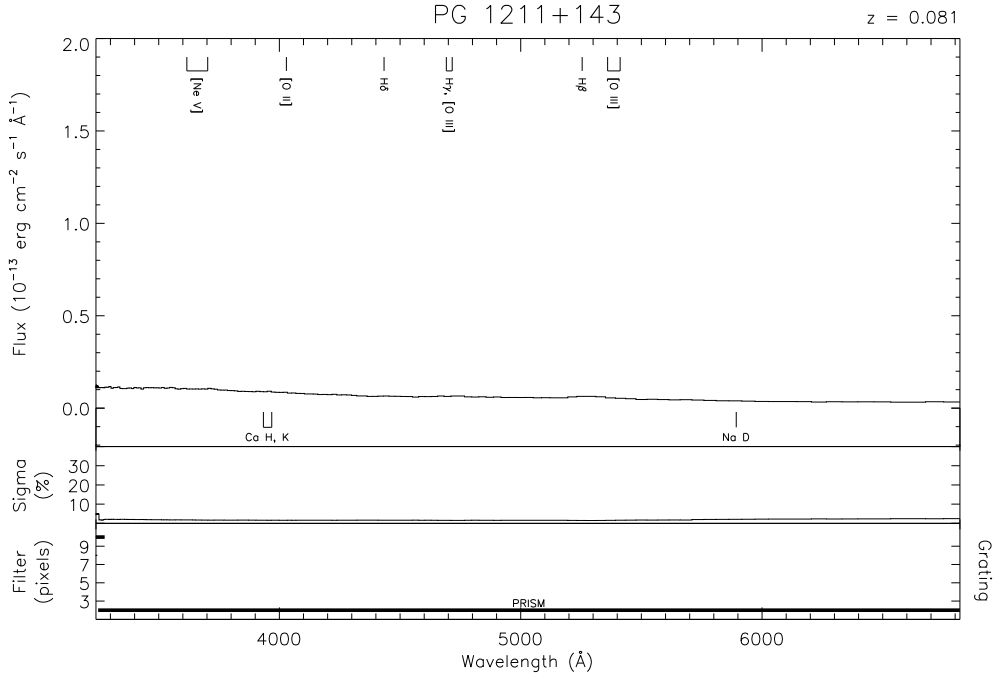
PG 1211+143
z = 0.081
Flux (10^{-13} erg cm^{-2} s^{-1} Å^{-1})
[Ne V]
[O II]
Hδ
[Ne III], Hε, [O II]
Hβ
[O III]
Ca H, K
Na D
Sigma (%)
Filter (pixels)
PRISM
Grating
Wavelength (Å)

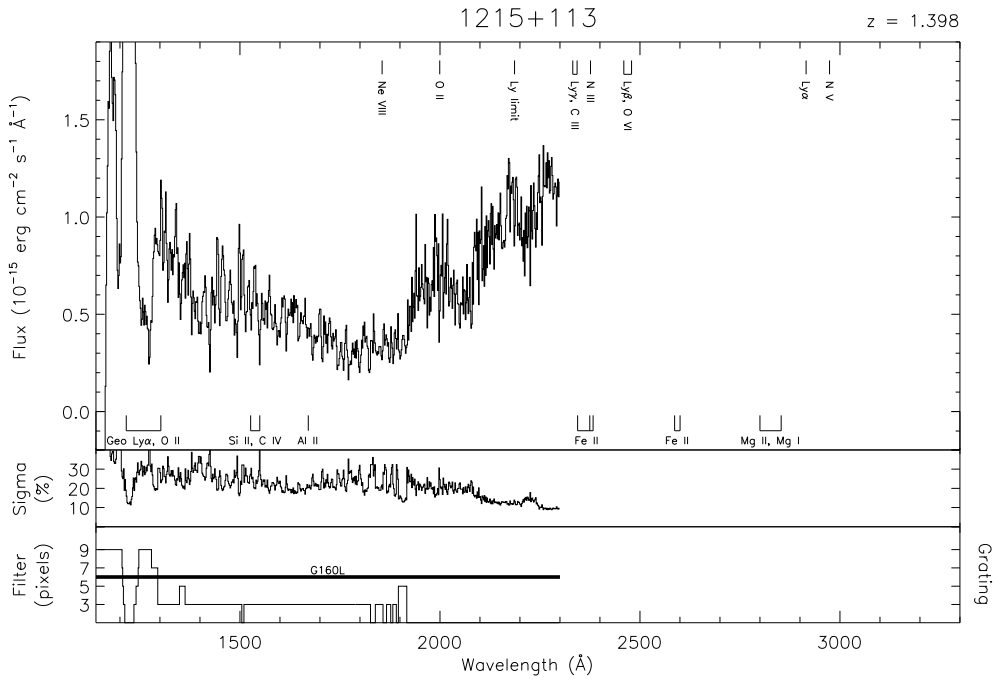
1215+113
z = 1.398
Flux (10^{-15} erg cm^{-2} s^{-1} Å^{-1})
Ne VIII
O II
Ly limit
Lyγ, C III
N III
Lyβ, O VI
Lyα
N V
Geo Lyα, O II
Si II, C IV
Al II
Fe II
Fe II
Mg II, Mg I
Sigma (%)
Filter (pixels)
G160L
Grating
Wavelength (Å)

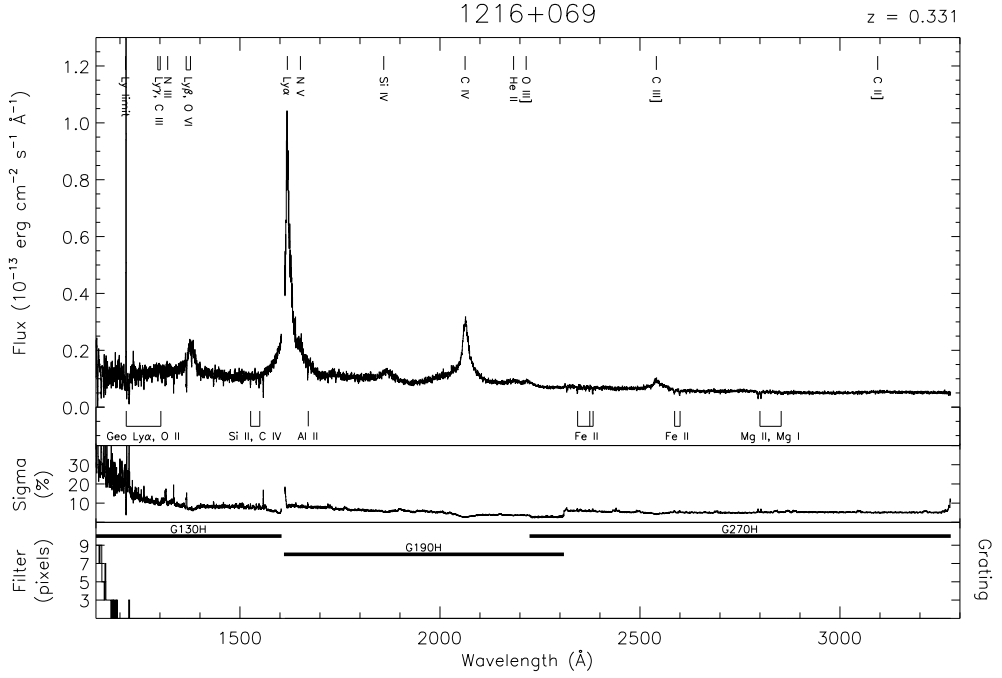
1216+069
z = 0.331
Flux (10^{-13} erg cm^{-2} s^{-1} Å^{-1})
Ly limit
Lyγ, C III
N III
Lyβ, O VI
Lyα
N V
Si IV
C IV
He II
O III]
C III]
C II]
Geo Lyα, O II
Si II, C IV
Al II
Fe II
Fe II
Mg II, Mg I
Sigma (%)
G130H
G190H
G270H
Filter (pixels)
Grating
Wavelength (Å)

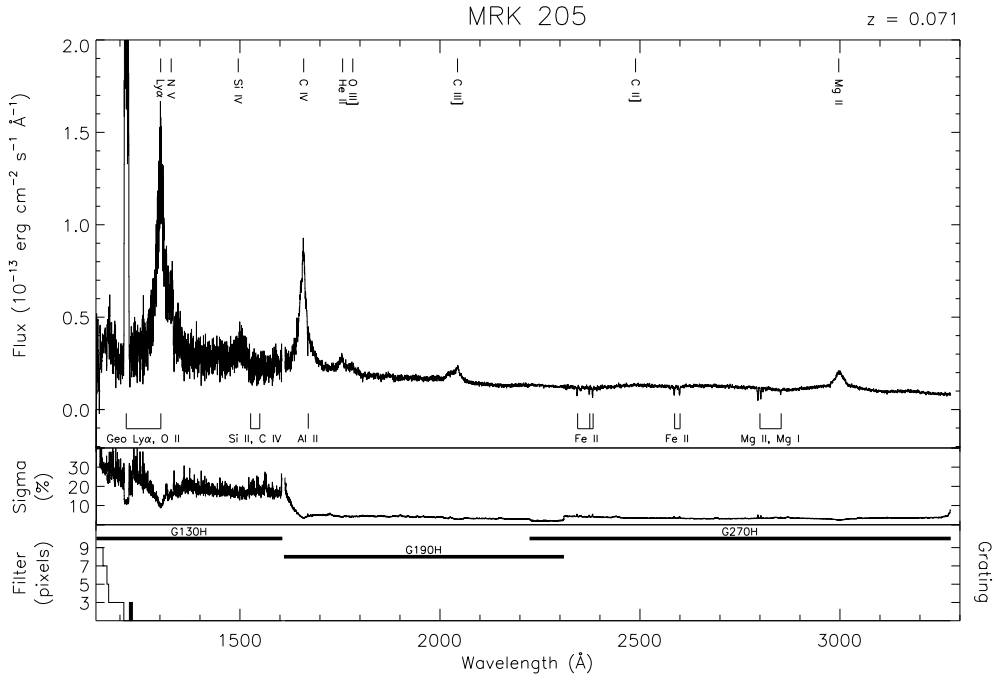
MRK 205
z = 0.071
Flux (10^{-13} erg cm^{-2} s^{-1} Å^{-1})
N V
Lyα
Si IV
C IV
O III]
He II
C III]
C II]
Mg II
Geo Lyα, O II
Si II, C IV
Al II
Fe II
Fe II
Mg II, Mg I
Sigma (%)
G130H
G270H
G190H
Filter (pixels)
Grating
Wavelength (Å)

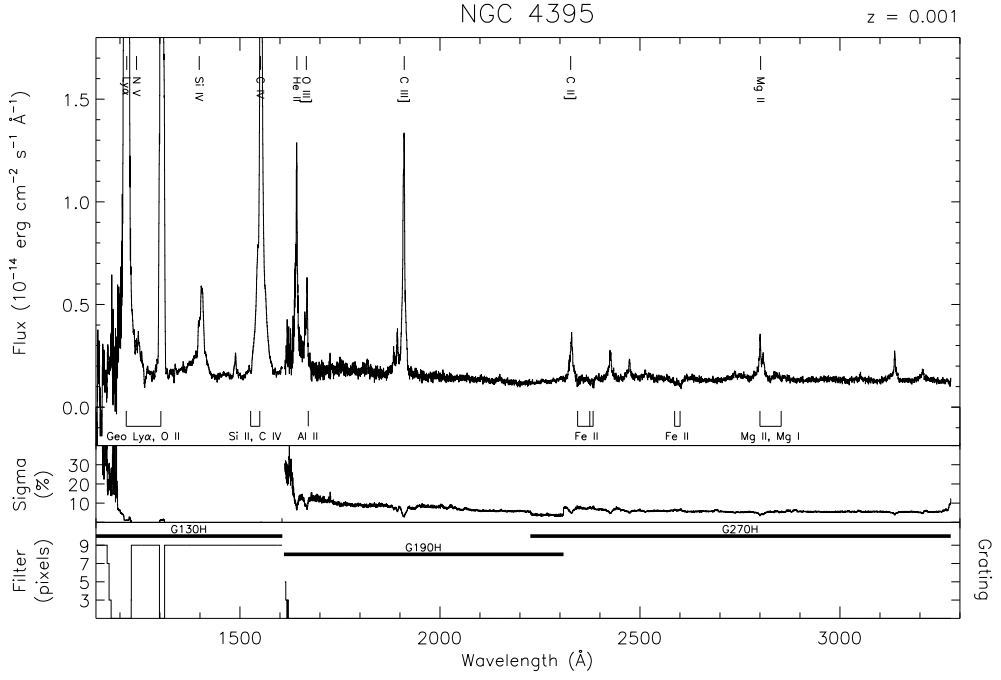
NGC 4395
z = 0.001
Flux (10^{-14} erg cm^{-2} s^{-1} Å^{-1})
N V
Lyα
Si IV
C IV
O III]
He II
C III]
C II]
Mg II
Geo Lyα, O II
Si II, C IV
Al II
Fe II
Fe II
Mg II, Mg I
Sigma (%)
G130H
G270H
G190H
Filter (pixels)
Grating
Wavelength (Å)

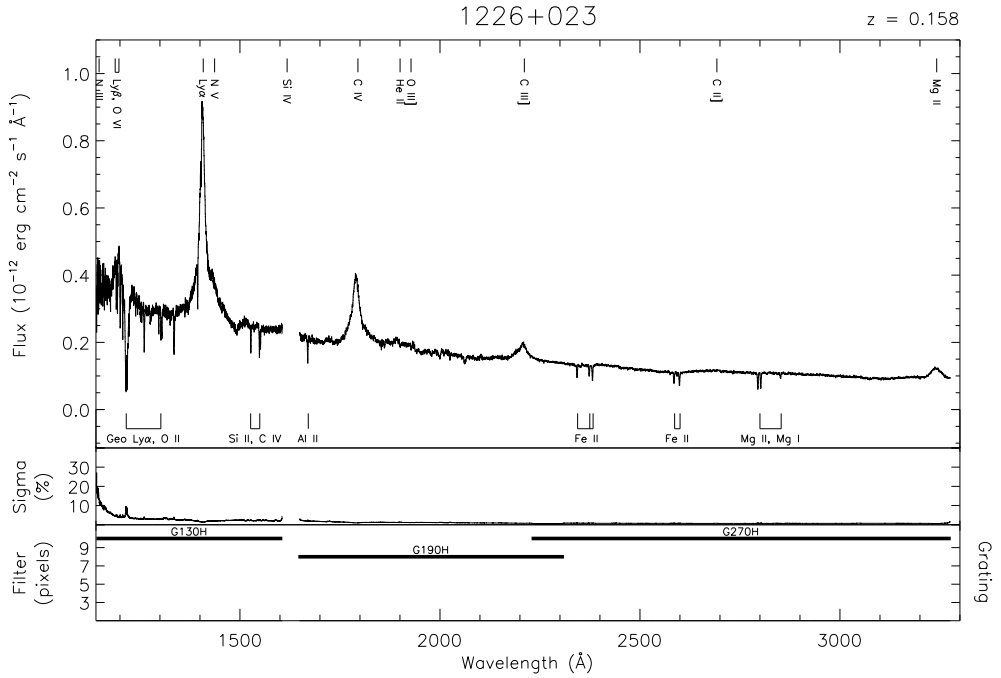
1226+023
z = 0.158
N III]
Lyβ, O VI
Lyα
N V
Si IV
C IV
He II
O III]
C III]
C II]
Mg II
Flux (10^{-12} erg cm^{-2} s^{-1} Å^{-1})
Geo Lyα, O II
Si II, C IV
Al II
Fe II
Fe II
Mg II, Mg I
Sigma (%)
G130H
G190H
G270H
Filter (pixels)
Grating
Wavelength (Å)

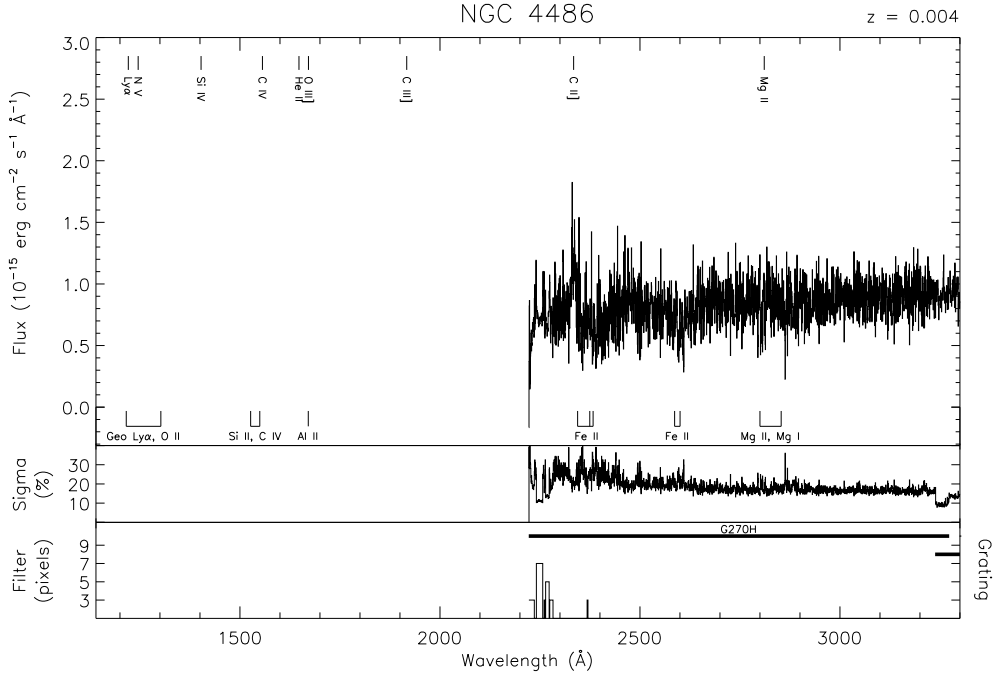
NGC 4486
z = 0.004
Lyα
N V
Si IV
C IV
He II
O III]
C III]
C II]
Mg II
Flux (10^{-15} erg cm^{-2} s^{-1} Å^{-1})
Geo Lyα, O II
Si II, C IV
Al II
Fe II
Fe II
Mg II, Mg I
Sigma (%)
G270H
Filter (pixels)
Grating
Wavelength (Å)

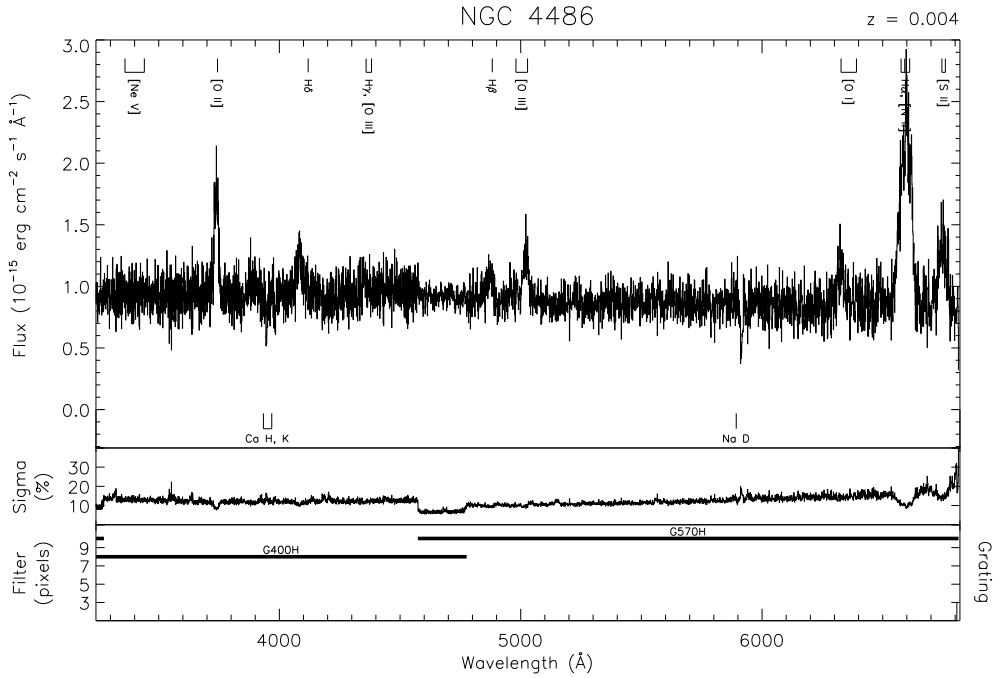
NGC 4486
z = 0.004
[Ne V]
[O II]
Hδ
Hγ, [O III]
Hβ
[O III]
[O I]
Mag. [Fe XIV]
[S II]
Ca H, K
Na D
Flux (10^-15 erg cm^-2 s^-1 Å^-1)
Sigma (%)
Filter (pixels)
G570H
G400H
Grating
Wavelength (Å)

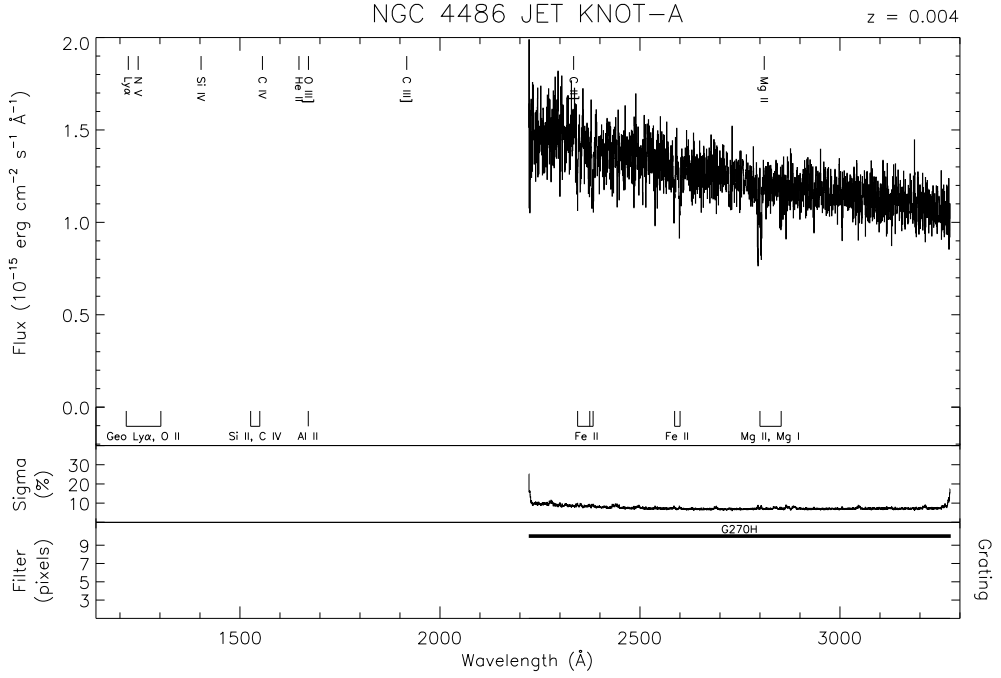
NGC 4486 JET KNOT−A
z = 0.004
N V Lyα
Si IV
C IV
[He II]
C III]
C II
Mg II
Geo Lyα, O II
Si II, C IV
Al II
Fe II
Fe II
Mg II, Mg I
Flux (10^-15 erg cm^-2 s^-1 Å^-1)
Sigma (%)
Filter (pixels)
G270H
Grating
Wavelength (Å)

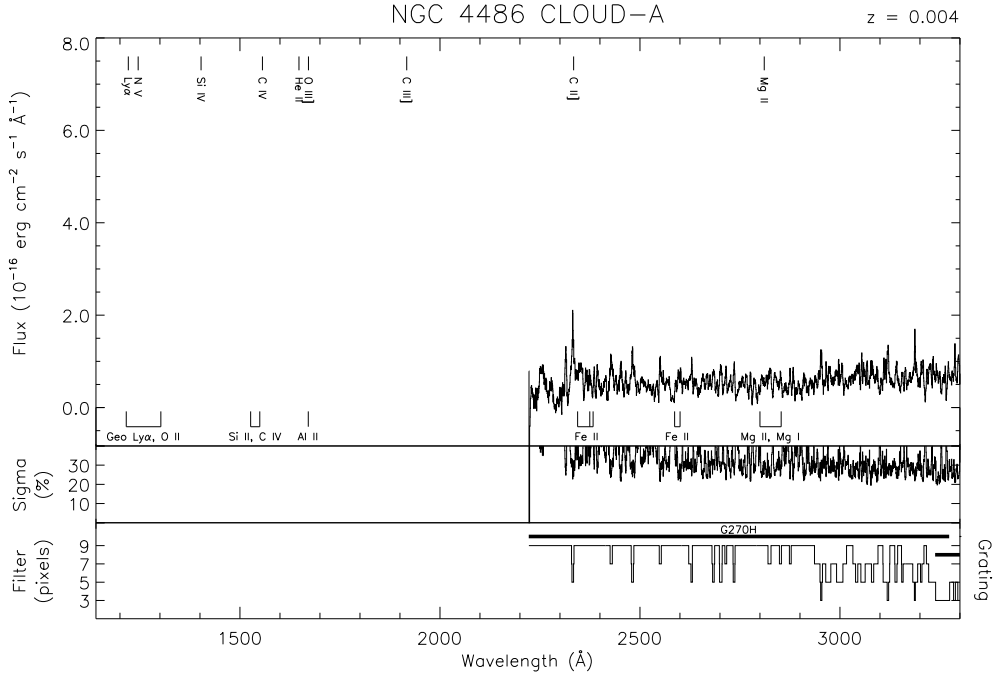
NGC 4486 CLOUD−A
z = 0.004
Flux (10^{-16} erg cm^{-2} s^{-1} Å^{-1})
N V Lyα
Si IV
C IV
He II
O III]
C III]
C I]
Mg II
Geo Lyα, O II
Si II, C IV
Al II
Fe II
Fe II
Mg II, Mg I
Sigma (%)
G270H
Filter (pixels)
Grating
Wavelength (Å)

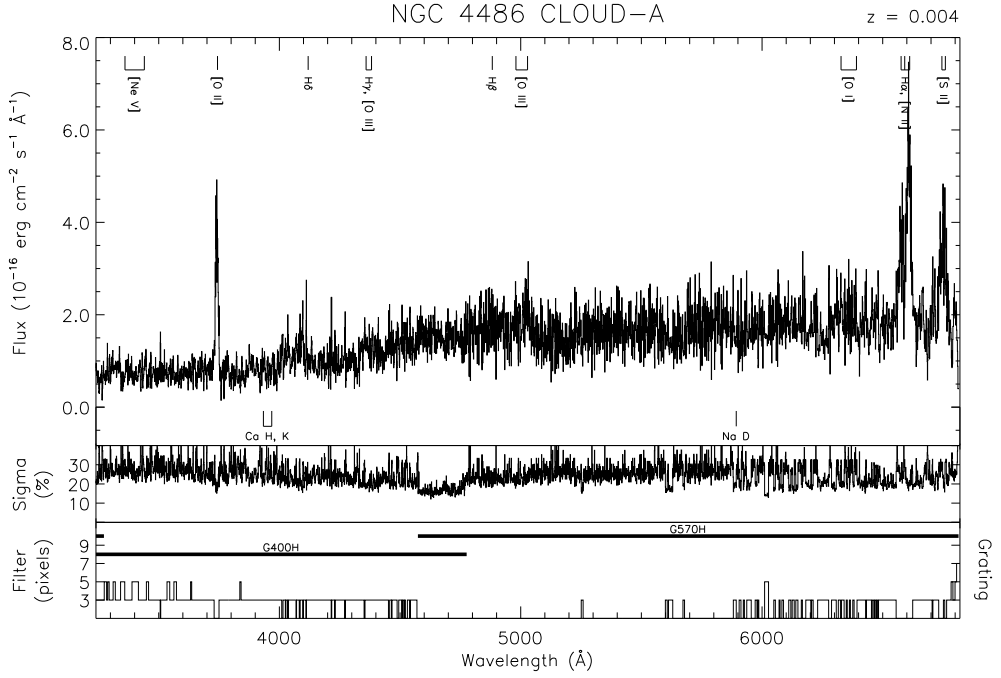
NGC 4486 CLOUD−A
z = 0.004
Flux (10^{-16} erg cm^{-2} s^{-1} Å^{-1})
[Ne V]
[O II]
Hδ
[Ne III], Hε, [O II]
Hβ
[O III]
[O I]
Hα, [N II]
[S II]
Ca H, K
Na D
Sigma (%)
G570H
G400H
Filter (pixels)
Grating
Wavelength (Å)

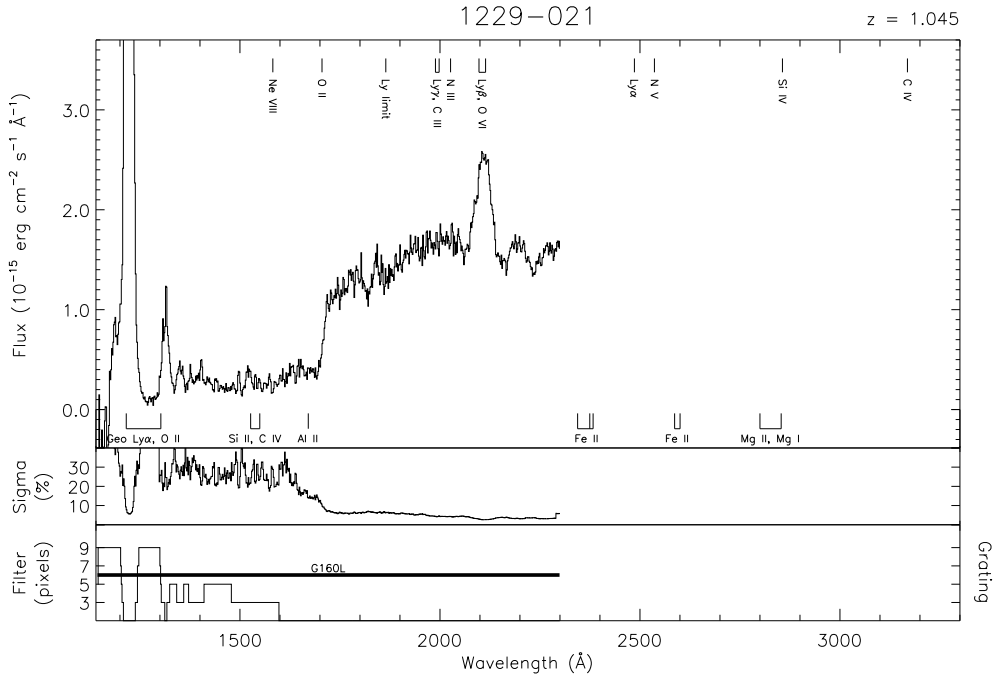
1229−021
z = 1.045
Ne VIII
O II
Ly limit
N III
Lyγ, C III
Lyβ, O VI
Lyα
N V
Si IV
C IV
Geo Lyα, O II
Si II, C IV
Al II
Fe II
Fe II
Mg II, Mg I
Flux (10−15 erg cm−2 s−1 Å−1)
Sigma (%)
Filter (pixels)
G160L
Grating
Wavelength (Å)

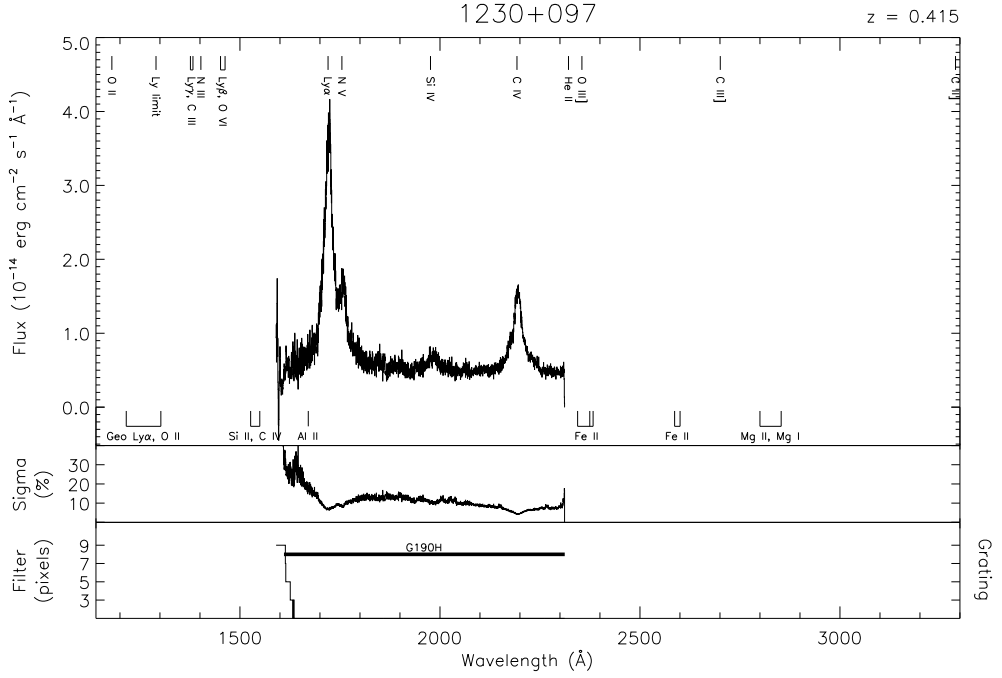
1230+097
z = 0.415
O II
Ly limit
N III
Lyγ, C III
Lyβ, O VI
N V
Lyα
Si IV
C IV
O III]
He II
C III]
Mg II
Geo Lyα, O II
Si II, C IV
Al II
Fe II
Fe II
Mg II, Mg I
Flux (10−14 erg cm−2 s−1 Å−1)
Sigma (%)
Filter (pixels)
G190H
Grating
Wavelength (Å)

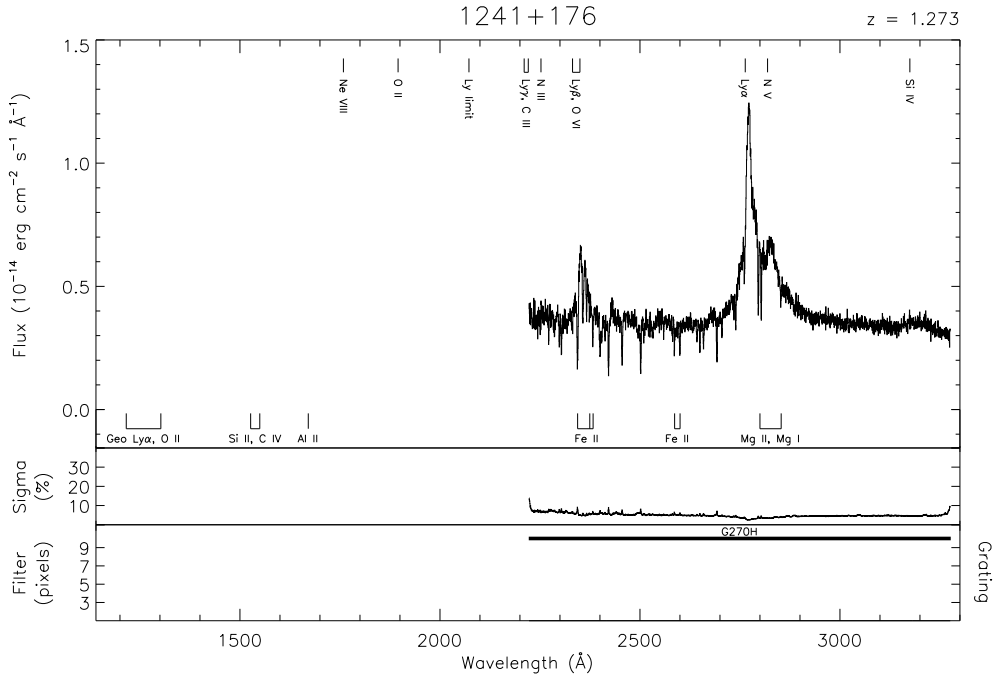
1241+176
z = 1.273
Flux (10^{-14} erg cm^{-2} s^{-1} Å^{-1})
Ne VIII
O II
Ly limit
N III
Lyγ, C III
Lyβ, O VI
Lyα
N V
Si IV
Geo Lyα, O II
Si II, C IV
Al II
Fe II
Fe II
Mg II, Mg I
Sigma (%)
G270H
Filter (pixels)
Grating
Wavelength (Å)

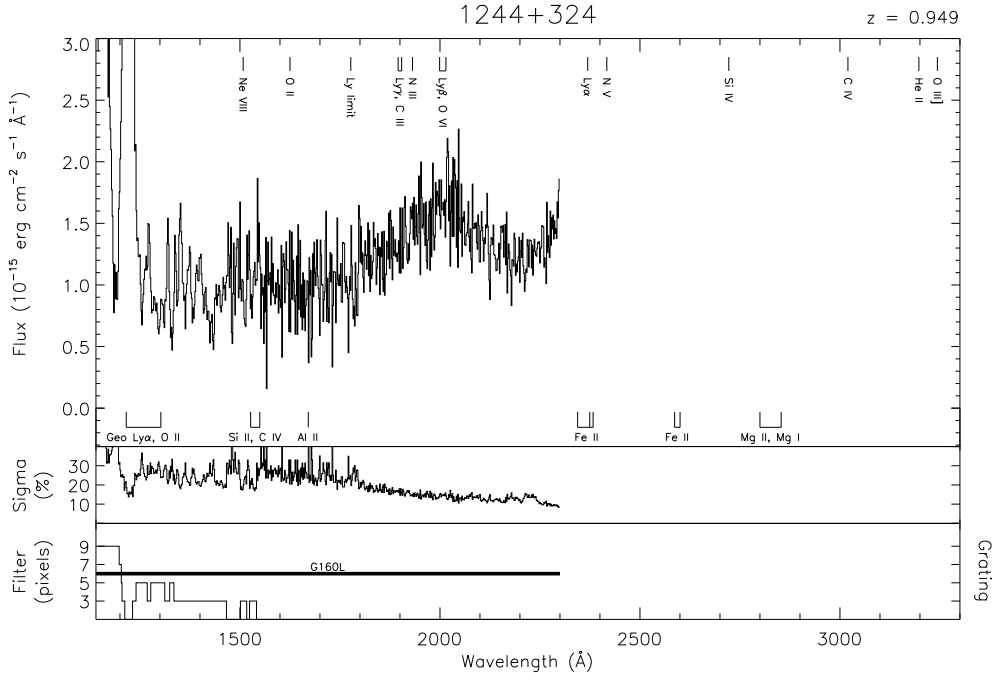
1244+324
z = 0.949
Flux (10^{-15} erg cm^{-2} s^{-1} Å^{-1})
Ne VIII
O II
Ly limit
N III
Lyγ, C III
Lyβ, O VI
Lyα
N V
Si IV
C IV
He II
O III]
Geo Lyα, O II
Si II, C IV
Al II
Fe II
Fe II
Mg II, Mg I
Sigma (%)
G160L
Filter (pixels)
Grating
Wavelength (Å)

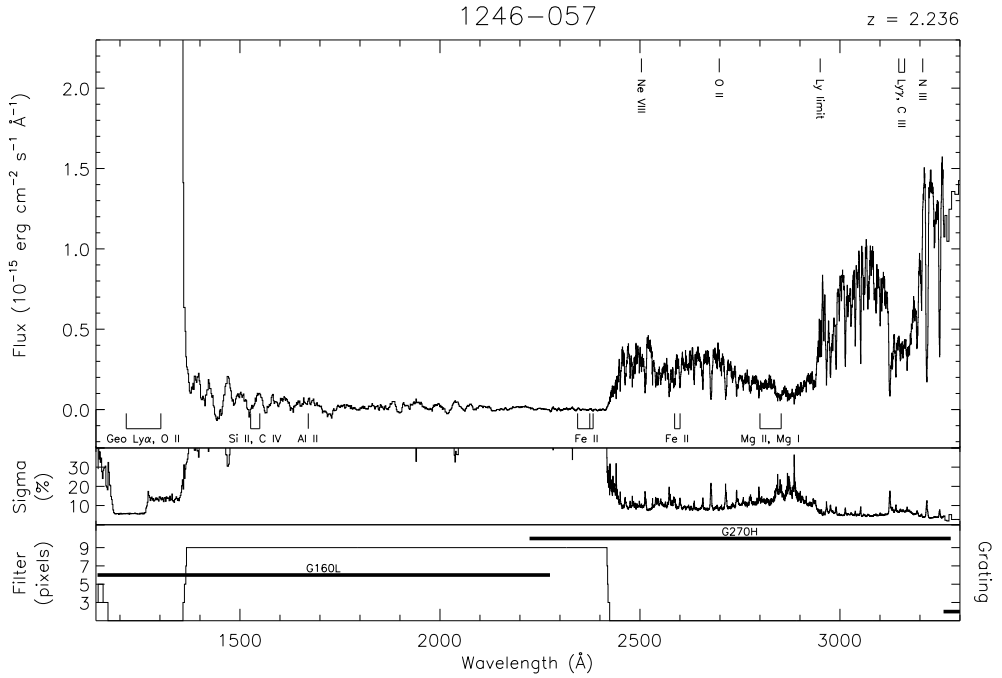
1246−057
z = 2.236
Flux (10^{-15} erg cm^{-2} s^{-1} Å^{-1})
Ne VIII
O II
Ly limit
Lyγ, C III
N III
Geo Lyα, O II
Si II, C IV
Al II
Fe II
Fe II
Mg II, Mg I
Sigma (%)
G270H
G160L
Filter (pixels)
Grating
Wavelength (Å)

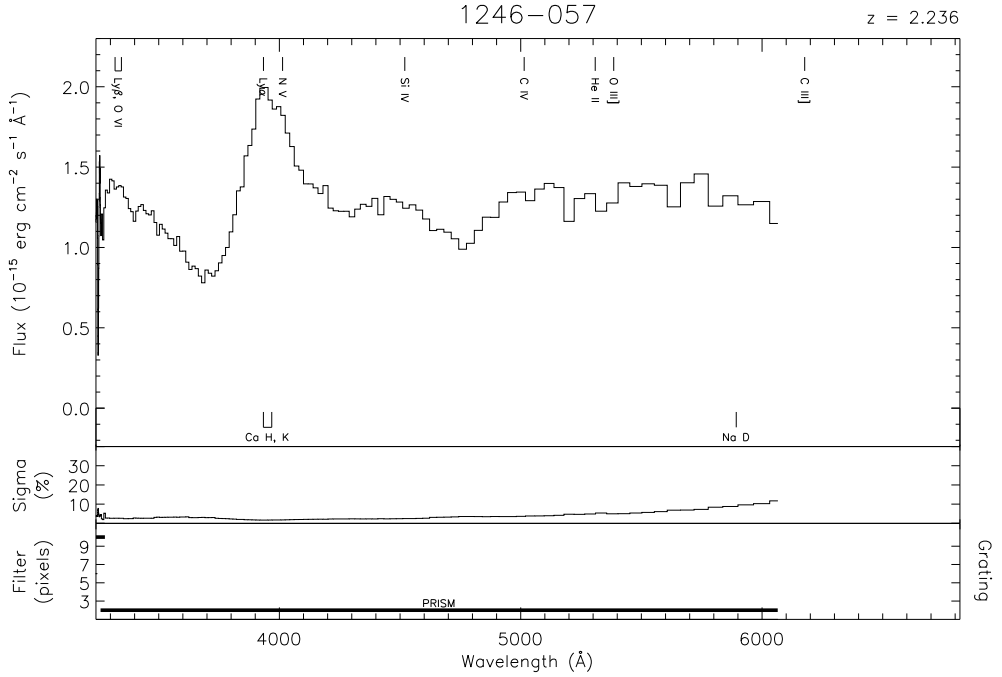
1246−057
z = 2.236
Flux (10^{-15} erg cm^{-2} s^{-1} Å^{-1})
Lyβ, O VI
Lyα
N V
Si IV
C IV
He II
O III]
C III]
Ca H, K
Na D
Sigma (%)
PRISM
Filter (pixels)
Grating
Wavelength (Å)

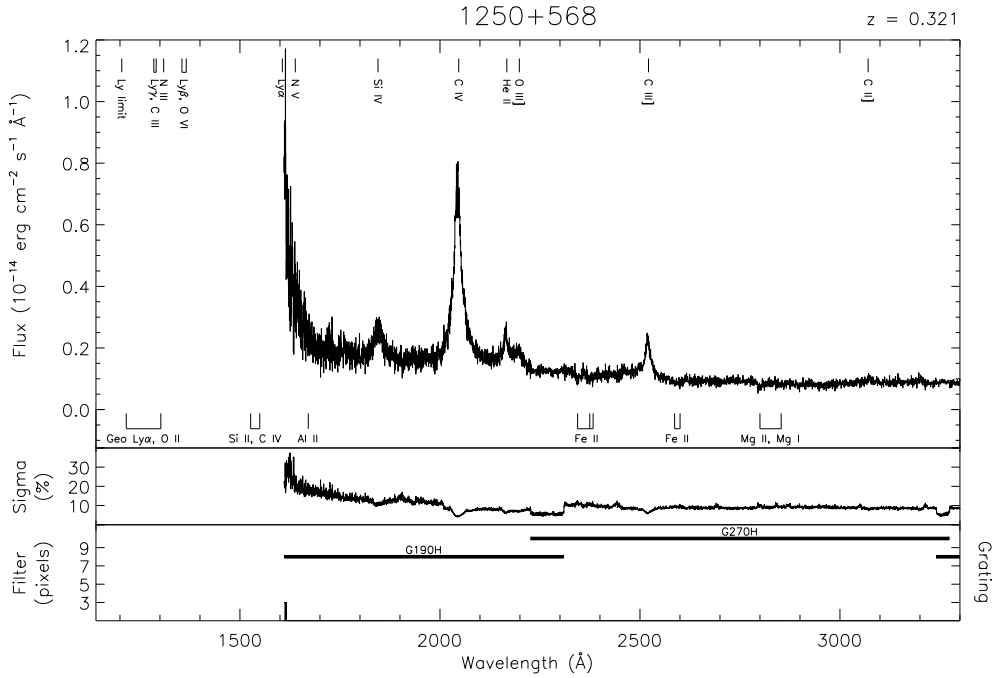
1250+568
z = 0.321
Flux (10^{-14} erg cm^{-2} s^{-1} Å^{-1})
Ly limit
N III
Ly7, C III
Ly8, O VI
Lyα
N V
Si IV
C IV
He II
O III]
C III]
C II]
Geo Lyα, O II
Si II, C IV
Al II
Fe II
Fe II
Mg II, Mg I
Sigma (%)
Filter (pixels)
G270H
G190H
Grating
Wavelength (Å)

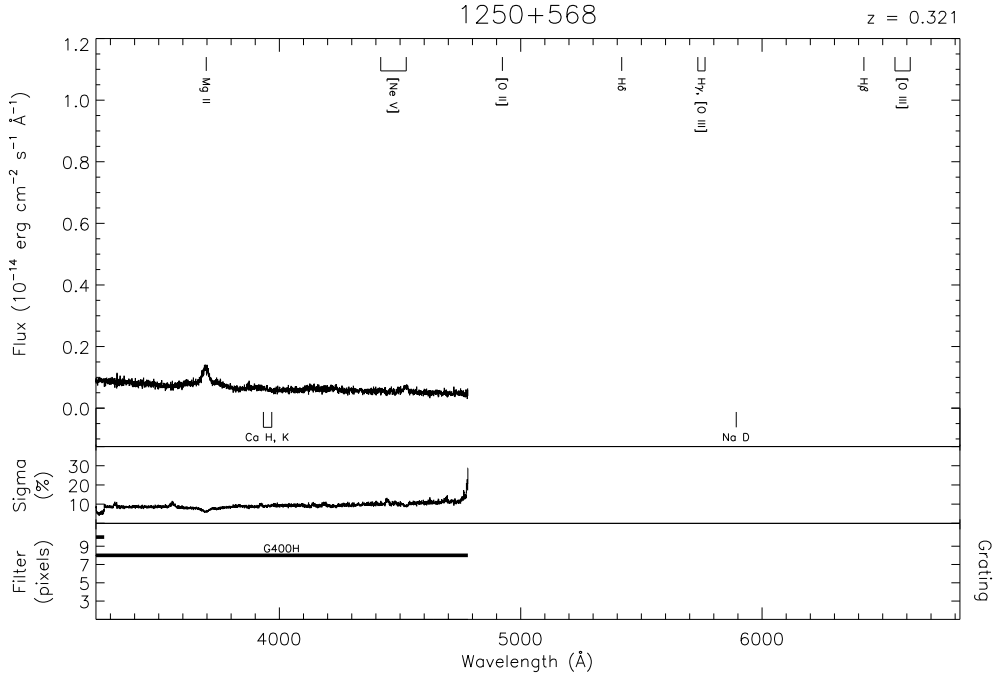
1250+568
z = 0.321
Flux (10^{-14} erg cm^{-2} s^{-1} Å^{-1})
Mg II
[Ne V]
[O II]
Hδ
H7, [O II]
Hβ
[O III]
Ca H, K
Na D
Sigma (%)
Filter (pixels)
G400H
Grating
Wavelength (Å)

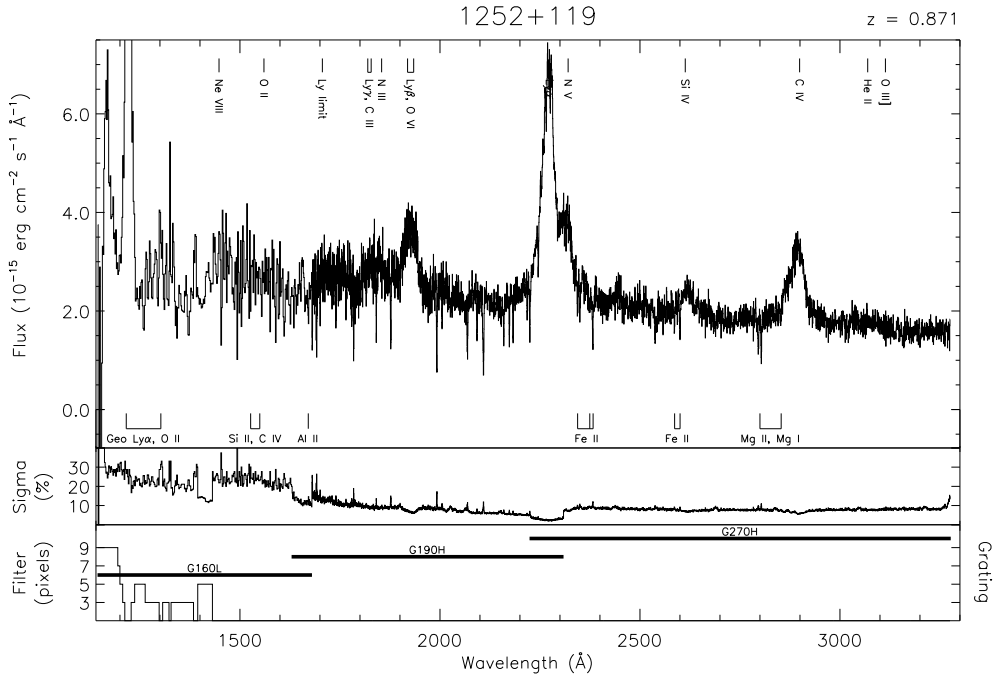
1252+119
z = 0.871
Flux (10^{-15} erg cm^{-2} s^{-1} Å^{-1})
Ne VIII
O II
Ly limit
N III
Lyγ, C III
Lyβ, O VI
N V
Si IV
C IV
He II
O III]
Geo Lyα, O II
Si II, C IV
Al II
Fe II
Fe II
Mg II, Mg I
Sigma (%)
Filter (pixels)
G160L
G190H
G270H
Grating
Wavelength (Å)

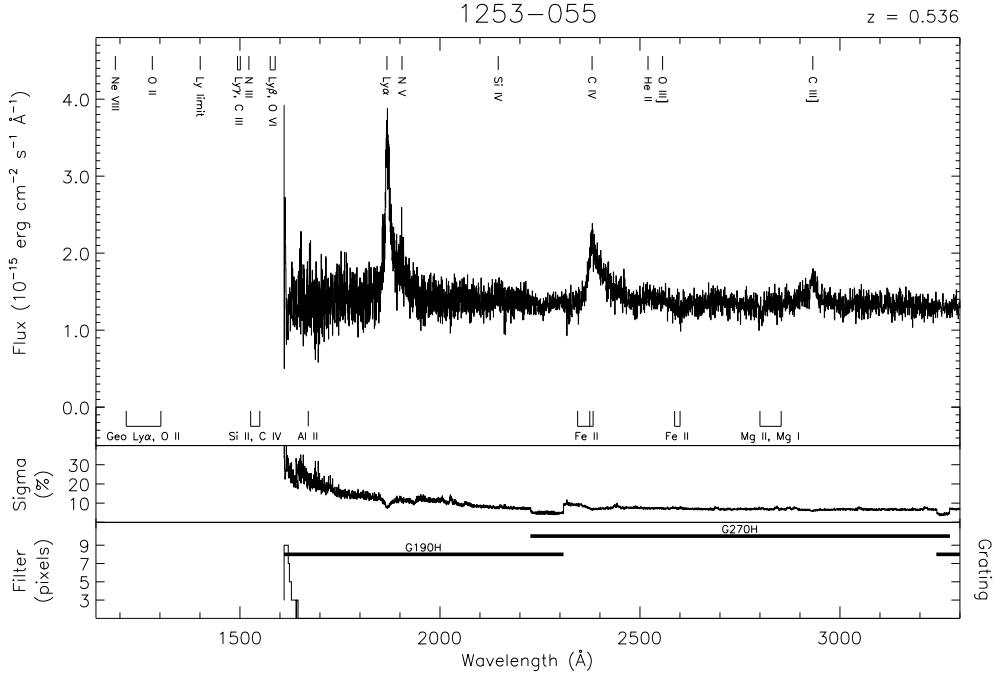
1253−055
z = 0.536
Flux (10^{-15} erg cm^{-2} s^{-1} Å^{-1})
Ne VIII
O II
Ly limit
N III
Lyγ, C III
Lyβ, O VI
Lyα
N V
Si IV
C IV
He II
O III]
C III]
Geo Lyα, O II
Si II, C IV
Al II
Fe II
Fe II
Mg II, Mg I
Sigma (%)
Filter (pixels)
G190H
G270H
Grating
Wavelength (Å)

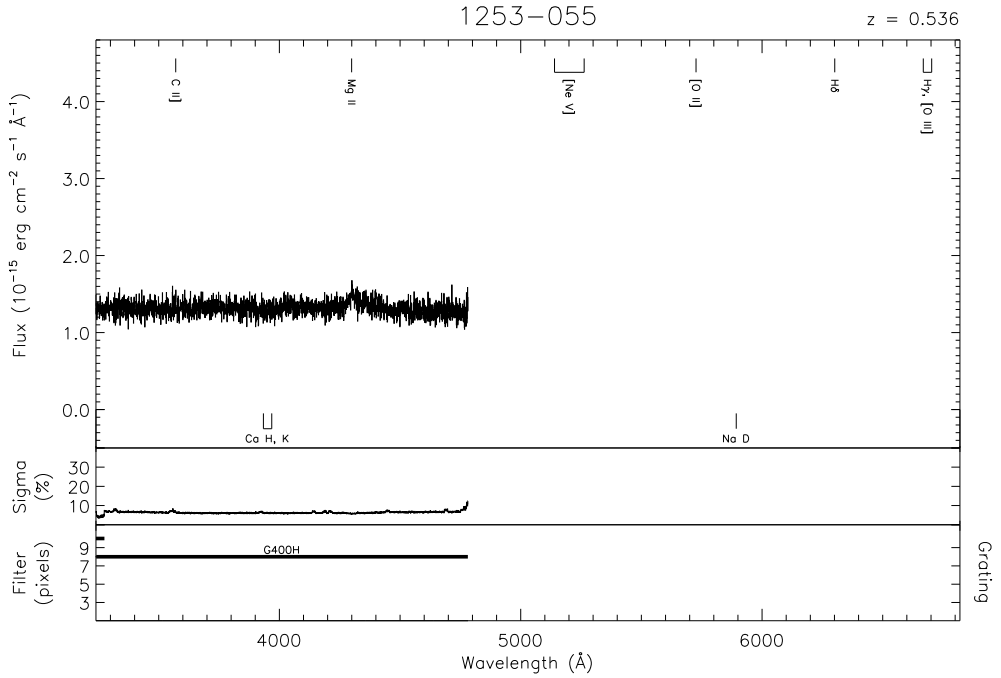
1253−055
z = 0.536
C II]
Mg II
[Ne V]
[O II]
Hδ
Hγ, [O III]
Ca H, K
Na D
G400H
Flux (10^-15 erg cm^-2 s^-1 Å^-1)
Sigma (%)
Filter (pixels)
Grating
Wavelength (Å)

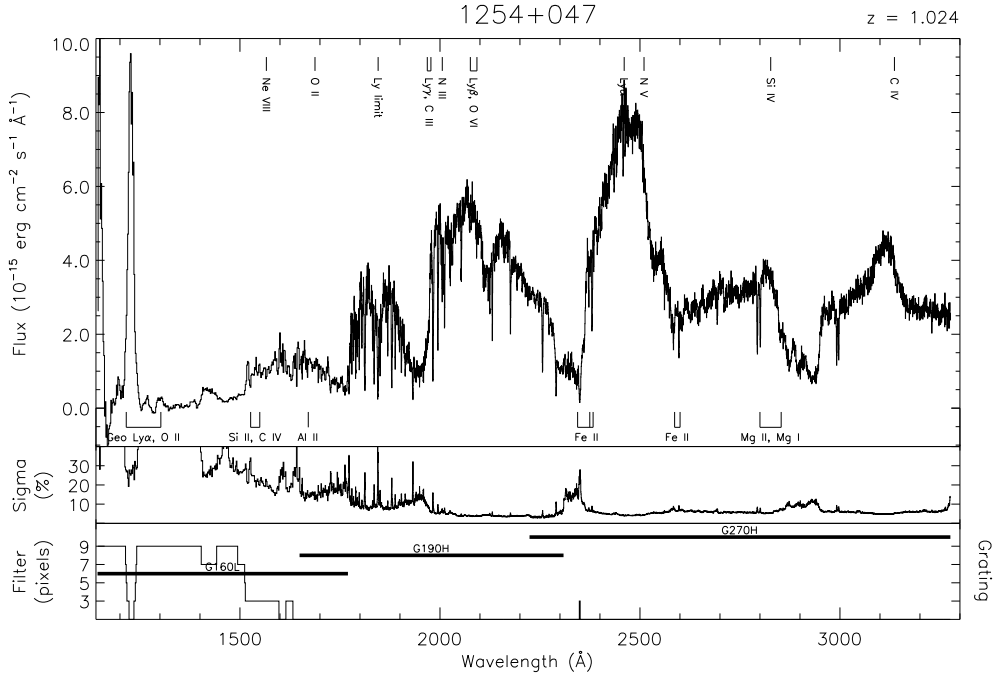
1254+047
z = 1.024
Ne VIII
O II
Ly limit
N III
Lyγ, C III
Lyδ, O VI
Lyβ
N V
Si IV
C IV
Geo Lyα, O II
Si II, C IV
Al II
Fe II
Fe II
Mg II, Mg I
G270H
G190H
G160L
Flux (10^-15 erg cm^-2 s^-1 Å^-1)
Sigma (%)
Filter (pixels)
Grating
Wavelength (Å)

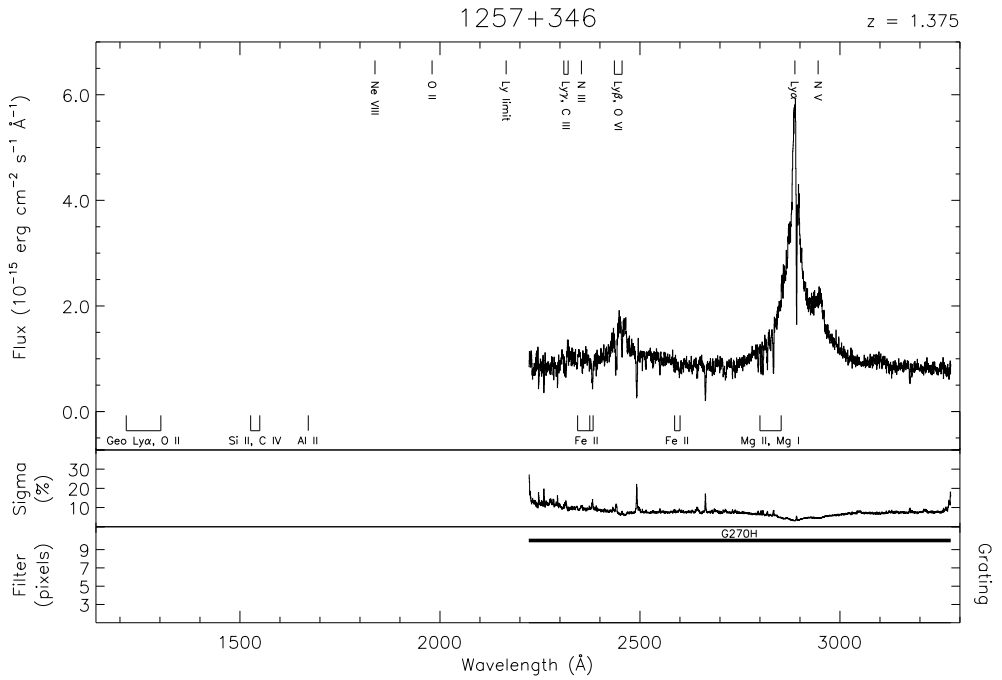
1257+346
z = 1.375
Ne VIII
O II
Ly limit
N III
Lyγ, C III
Lyβ, O VI
Lyα
N V
Flux (10^{-15} erg cm^{-2} s^{-1} Å^{-1})
Geo Lyα, O II
Si II, C IV
Al II
Fe II
Fe II
Mg II, Mg I
Sigma (%)
G270H
Filter (pixels)
Grating
Wavelength (Å)

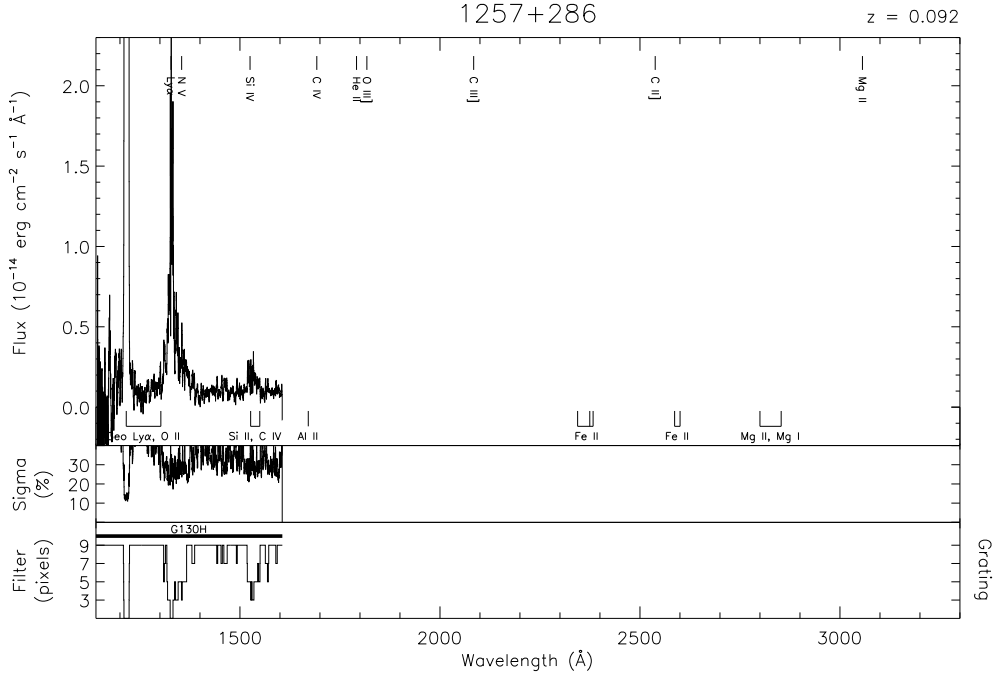
1257+286
z = 0.092
Lyα
N V
Si IV
C IV
O III]
He II
C III]
C II]
Mg II
Flux (10^{-14} erg cm^{-2} s^{-1} Å^{-1})
Geo Lyα, O II
Si II, C IV
Al II
Fe II
Fe II
Mg II, Mg I
Sigma (%)
G130H
Filter (pixels)
Grating
Wavelength (Å)

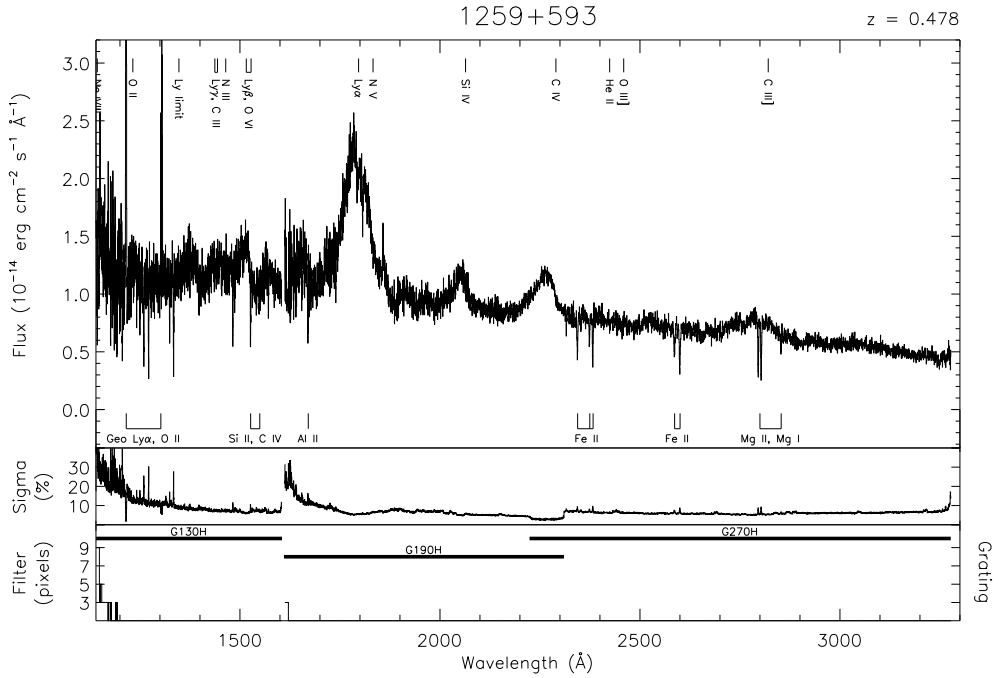
1259+593
z = 0.478
Flux (10^{-14} erg cm^{-2} s^{-1} Å^{-1})
O II
Ly limit
N III
Lyγ, C III
Lyβ, O VI
Lyα
N V
Si IV
C IV
He II
O III]
C III]
Geo Lyα, O II
Si II, C IV
Al II
Fe II
Fe II
Mg II, Mg I
Sigma (%)
G130H
G190H
G270H
Filter (pixels)
Grating
Wavelength (Å)

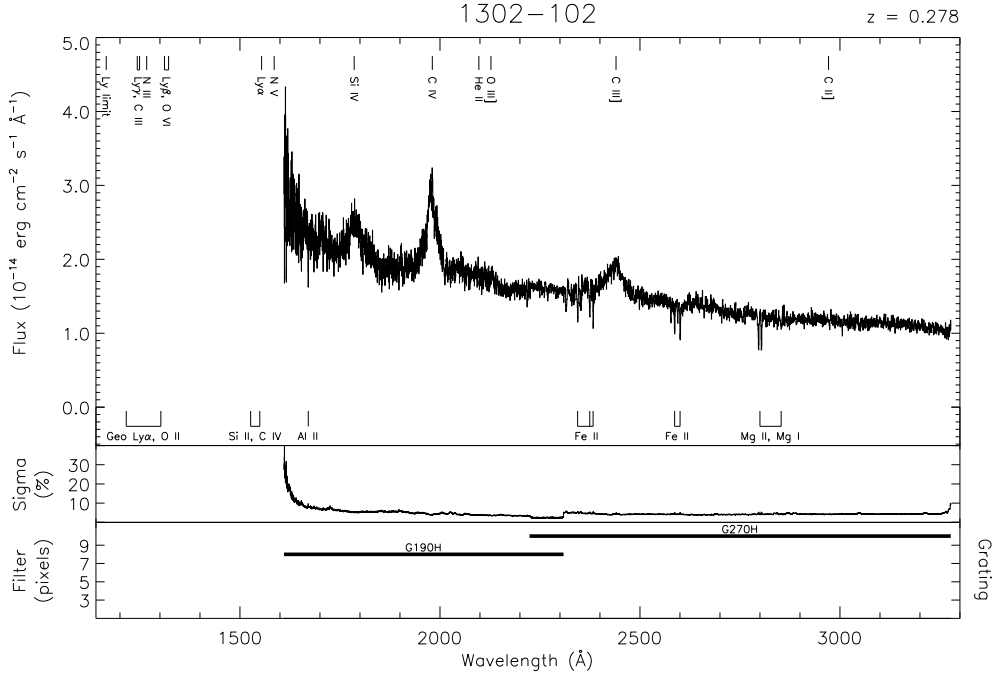
1302−102
z = 0.278
Flux (10^{-14} erg cm^{-2} s^{-1} Å^{-1})
Ly limit
N III
Lyγ, C III
Lyβ, O VI
N V
Lyα
Si IV
C IV
He II
O III]
C III]
C II]
Geo Lyα, O II
Si II, C IV
Al II
Fe II
Fe II
Mg II, Mg I
Sigma (%)
G190H
G270H
Filter (pixels)
Grating
Wavelength (Å)

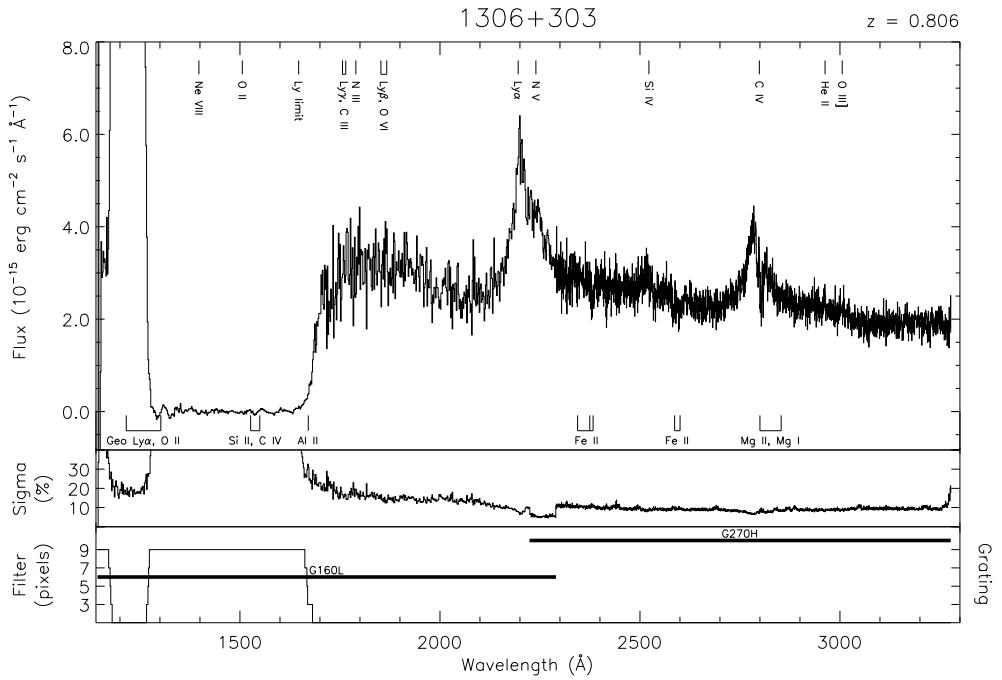
1306+303
z = 0.806
Flux (10^{-15} erg cm^{-2} s^{-1} Å^{-1})
Ne VIII
O II
Ly limit
N III
Lyγ, C III
Lyβ, O VI
Lyα
N V
Si IV
C IV
He II
O III]
Geo Lyα, O II
Si II, C IV
Al II
Fe II
Fe II
Mg II, Mg I
Sigma (%)
Filter (pixels)
G160L
G270H
Grating
Wavelength (Å)

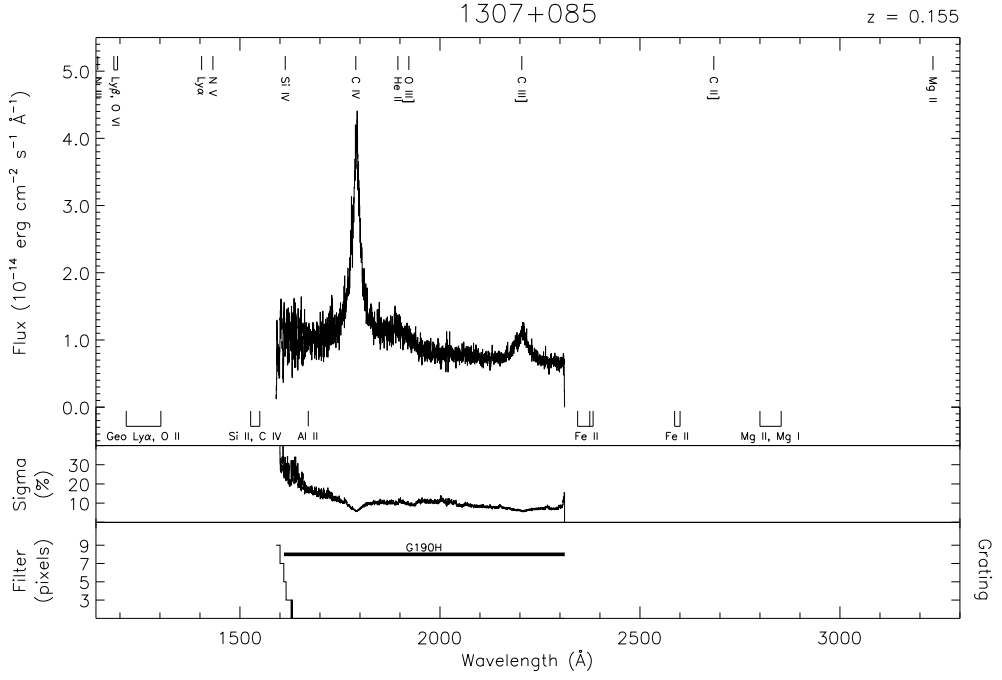
1307+085
z = 0.155
Flux (10^{-14} erg cm^{-2} s^{-1} Å^{-1})
Lyβ, O VI
N V
Lyα
Si IV
C IV
He II
O III]
C III]
C II]
Mg II
Geo Lyα, O II
Si II, C IV
Al II
Fe II
Fe II
Mg II, Mg I
Sigma (%)
Filter (pixels)
G190H
Grating
Wavelength (Å)

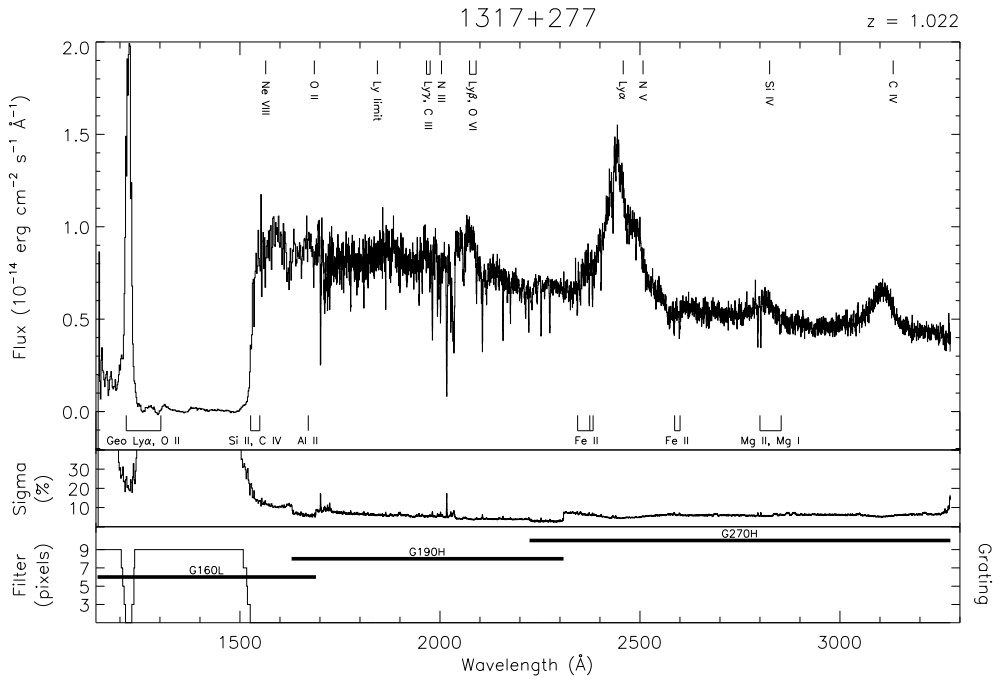
1317+277
z = 1.022
Flux (10^{-14} erg cm^{-2} s^{-1} Å^{-1})
Ne VIII
O II
Ly limit
N III
Lyγ, C III
Lyβ, O VI
Lyα
N V
Si IV
C IV
Geo Lyα, O II
Si II, C IV
Al II
Fe II
Fe II
Mg II, Mg I
Sigma (%)
G270H
G190H
G160L
Filter (pixels)
Grating
Wavelength (Å)

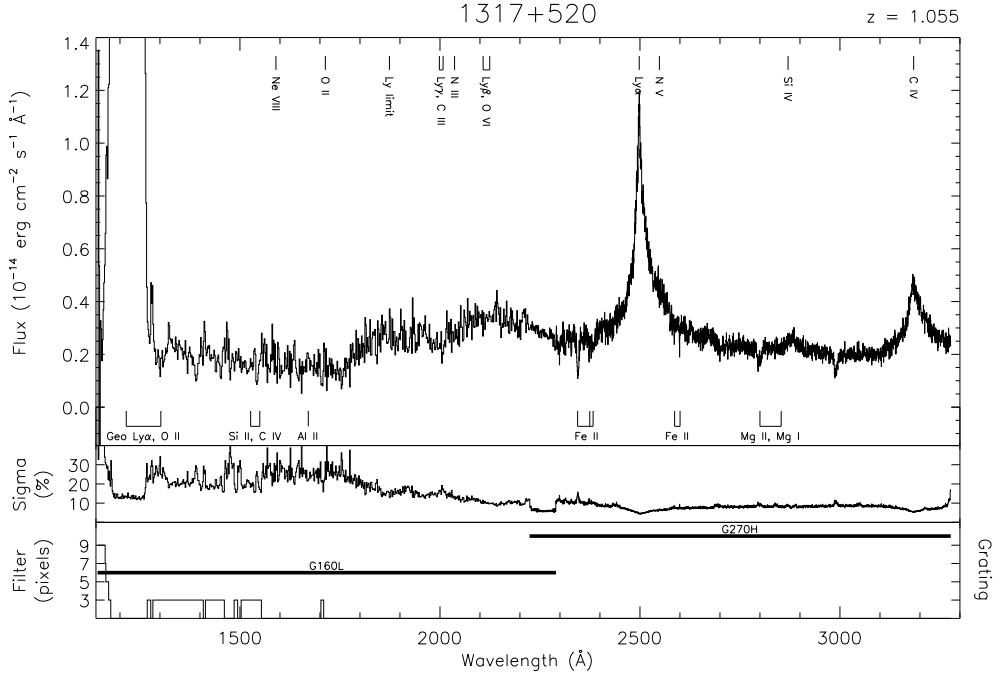
1317+520
z = 1.055
Flux (10^{-14} erg cm^{-2} s^{-1} Å^{-1})
Ne VIII
O II
Ly limit
N III
Lyγ, C III
Lyβ, O VI
Lyα
N V
Si IV
C IV
Geo Lyα, O II
Si II, C IV
Al II
Fe II
Fe II
Mg II, Mg I
Sigma (%)
G270H
G160L
Filter (pixels)
Grating
Wavelength (Å)

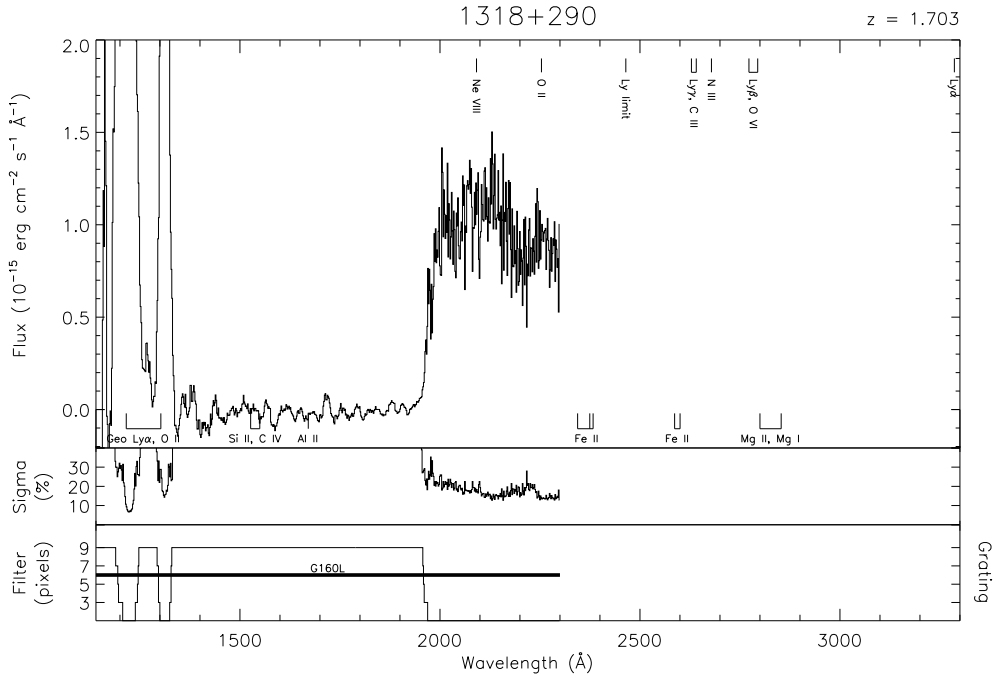
1318+290
z = 1.703
Flux (10^{-15} erg cm^{-2} s^{-1} Å^{-1})
Ne VIII
O II
Ly limit
N III
Lyγ, C III
Lyβ, O VI
Lyα
Geo Lyα, O II
Si II, C IV
Al II
Fe II
Fe II
Mg II, Mg I
Sigma (%)
Filter (pixels)
G160L
Grating
Wavelength (Å)

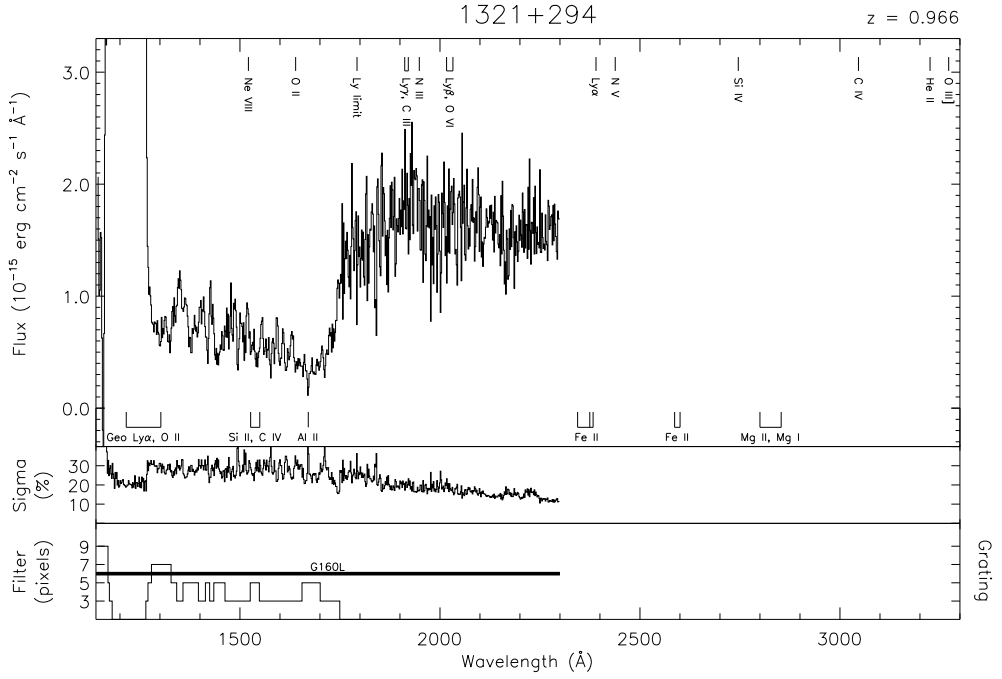
1321+294
z = 0.966
Flux (10^{-15} erg cm^{-2} s^{-1} Å^{-1})
Ne VIII
O II
Ly limit
N III
Lyγ, C III
Lyβ, O VI
N V
Lyα
Si IV
C IV
He II
O III]
Geo Lyα, O II
Si II, C IV
Al II
Fe II
Fe II
Mg II, Mg I
Sigma (%)
Filter (pixels)
G160L
Grating
Wavelength (Å)

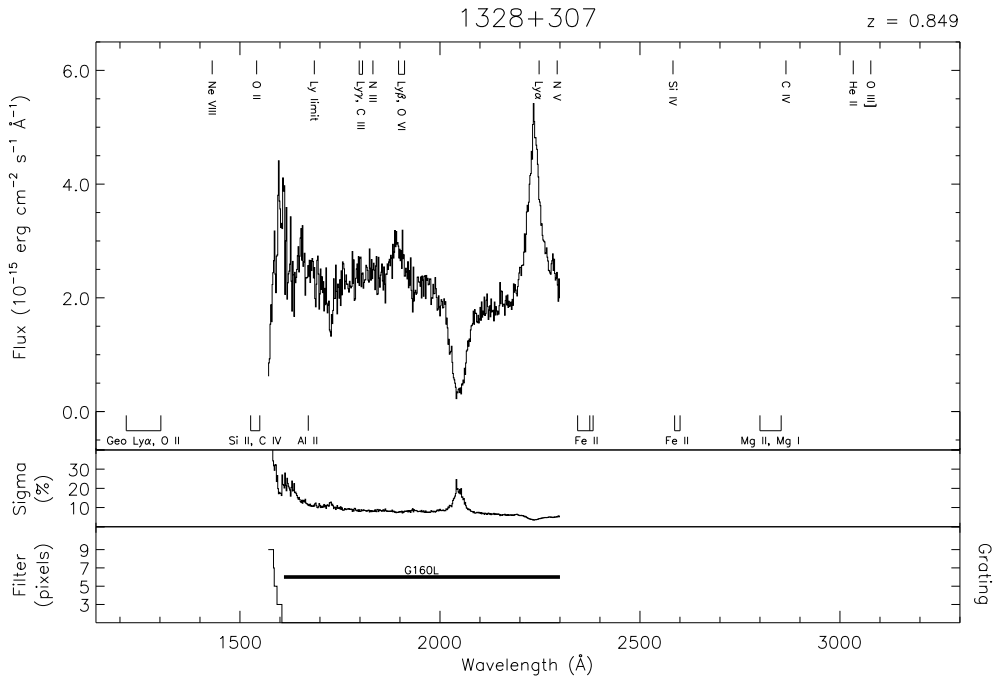
1328+307
z = 0.849
Flux (10^{-15} erg cm^{-2} s^{-1} Å^{-1})
Ne VIII
O II
Ly limit
N III
Lyγ, C III
Lyβ, O VI
Lyα
N V
Si IV
C IV
He II
O III]
Geo Lyα, O II
Si II, C IV
Al II
Fe II
Fe II
Mg II, Mg I
Sigma (%)
Filter (pixels)
G160L
Grating
Wavelength (Å)

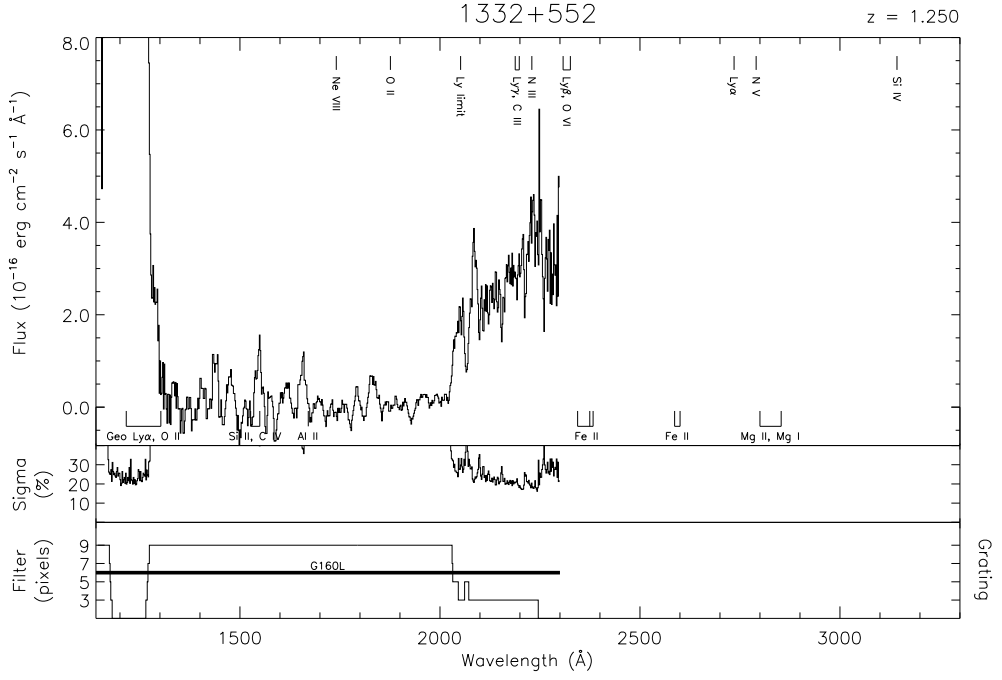
1332+552
z = 1.250
Flux (10^{-16} erg cm^{-2} s^{-1} Å^{-1})
Ne VIII
O II
Ly limit
N III
Lyγ, C III
Lyβ, O VI
Lyα
N V
Si IV
Geo Lyα, O II
Si II, C IV
Al II
Fe II
Fe II
Mg II, Mg I
Sigma (%)
Filter (pixels)
G160L
Grating
Wavelength (Å)

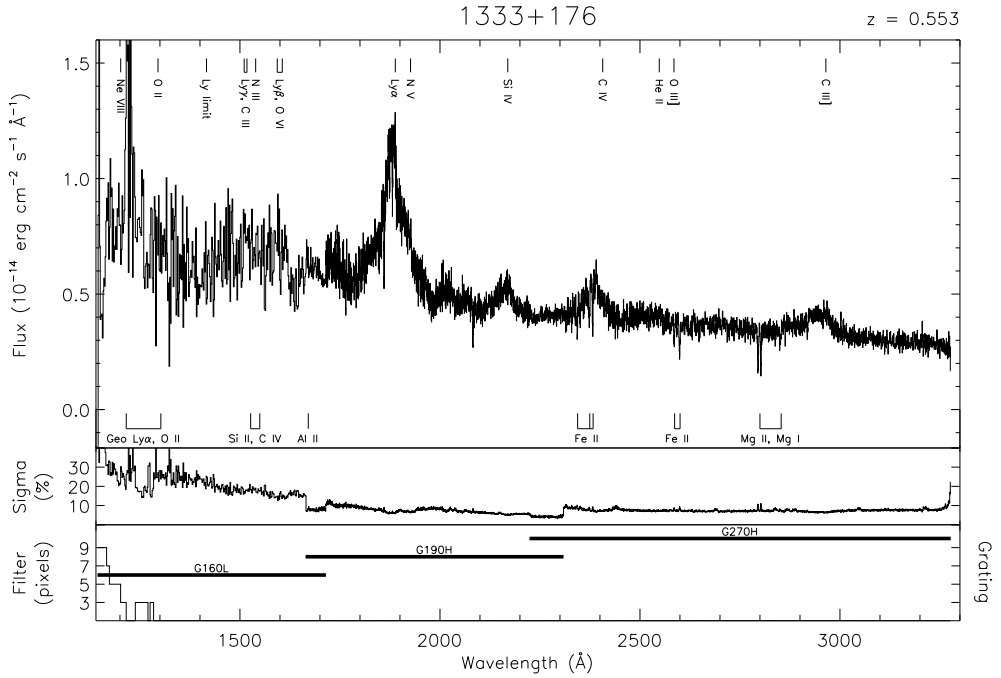
1333+176
z = 0.553
Flux (10^{-14} erg cm^{-2} s^{-1} Å^{-1})
Ne VIII
O II
Ly limit
C III, N III
Lyγ, O VI
Lyα
N V
Si IV
C IV
He II
O III]
C III]
Geo Lyα, O II
Si II, C IV
Al II
Fe II
Fe II
Mg II, Mg I
Sigma (%)
Filter (pixels)
G160L
G190H
G270H
Grating
Wavelength (Å)

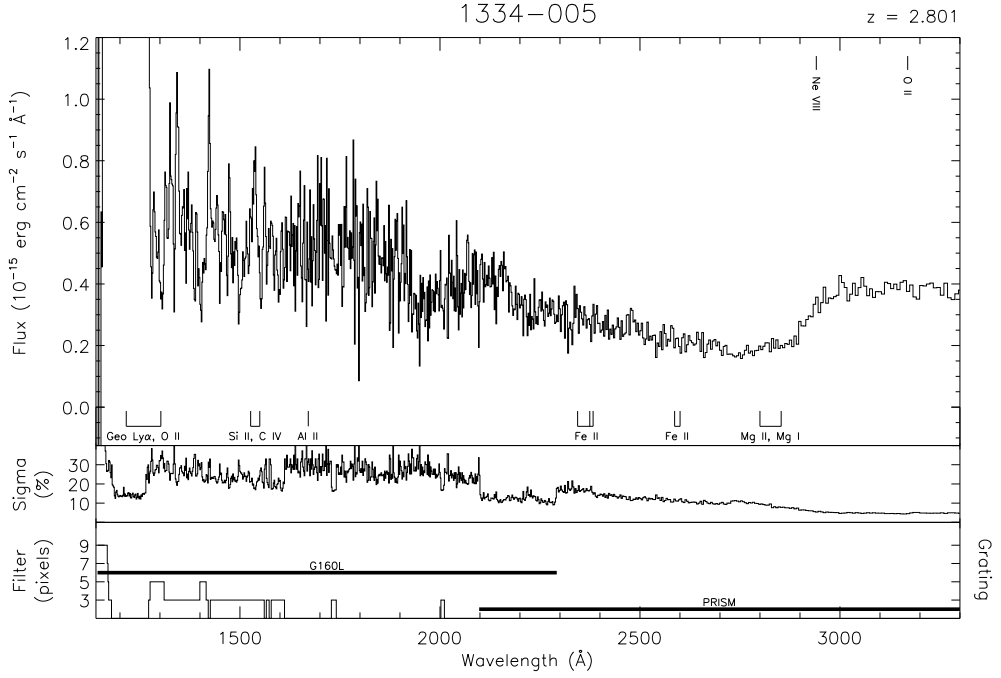
1334−005
z = 2.801
Flux (10^{-15} erg cm^{-2} s^{-1} Å^{-1})
Ne VIII
O II
Geo Lyα, O II
Si II, C IV
Al II
Fe II
Fe II
Mg II, Mg I
Sigma (%)
Filter (pixels)
G160L
PRISM
Grating
Wavelength (Å)

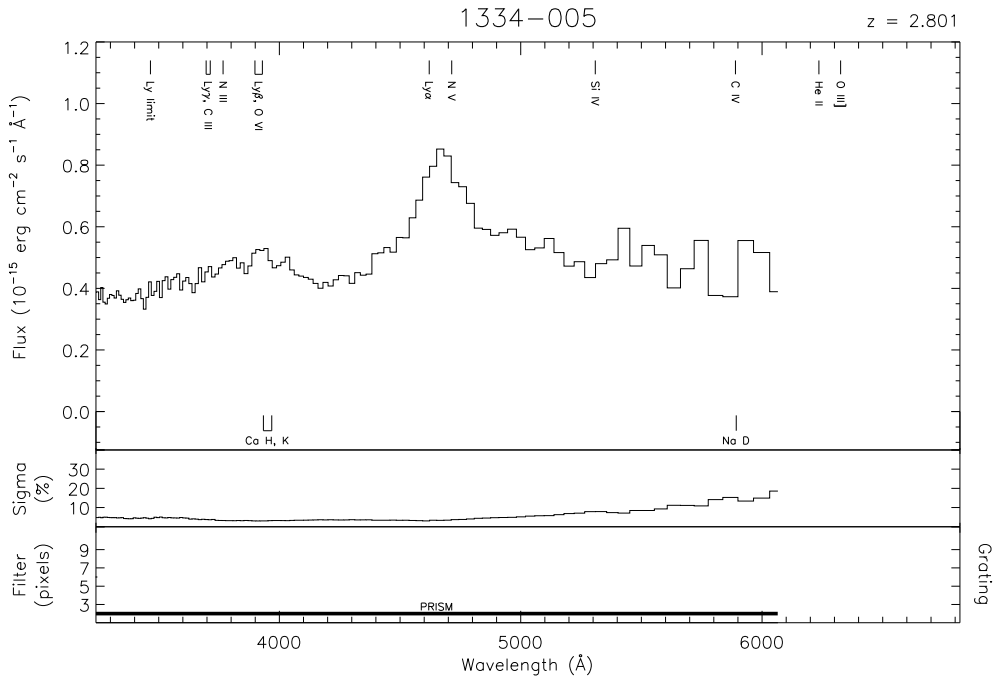
1334−005
z = 2.801
Flux (10^{-15} erg cm^{-2} s^{-1} Å^{-1})
Ly limit
N III
Lyγ, C III
Lyβ, O VI
Lyα
N V
Si IV
C IV
He II
O III]
Ca H, K
Na D
Sigma (%)
Filter (pixels)
PRISM
Grating
Wavelength (Å)

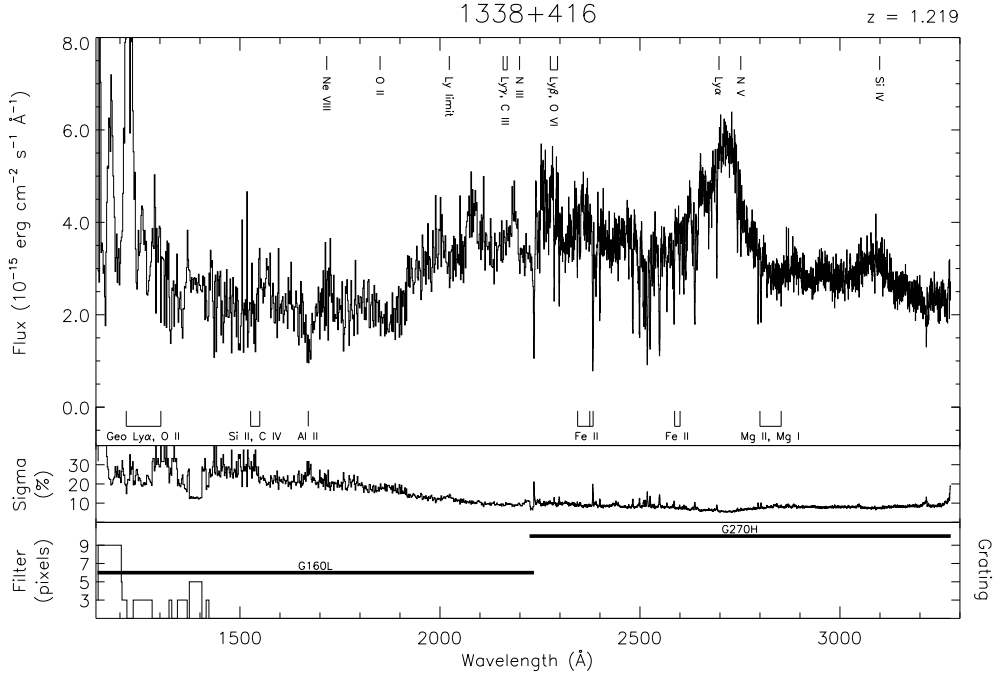
1338+416
z = 1.219
Flux (10^{-15} erg cm^{-2} s^{-1} Å^{-1})
Ne VIII
O II
Ly limit
N III
Lyγ, C III
Lyβ, O VI
Lyα
N V
Si IV
Geo Lyα, O II
Si II, C IV
Al II
Fe II
Fe II
Mg II, Mg I
Sigma (%)
G270H
G160L
Filter (pixels)
Grating
Wavelength (Å)

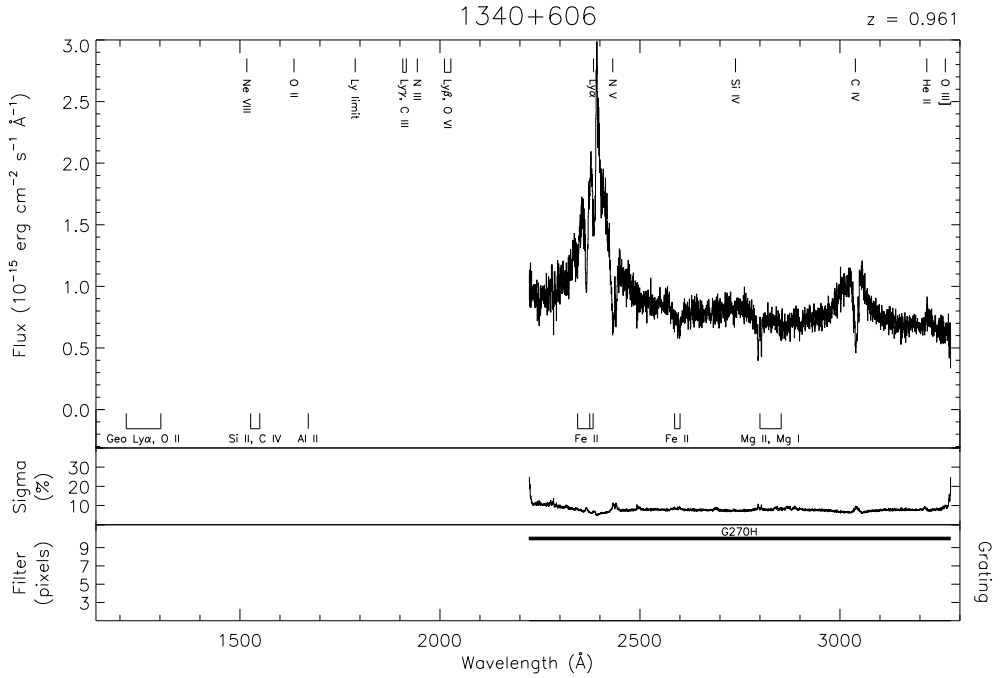
1340+606
z = 0.961
Flux (10^{-15} erg cm^{-2} s^{-1} Å^{-1})
Ne VIII
O II
Ly limit
N III
Lyγ, C III
Lyβ, O VI
Lyα
N V
Si IV
C IV
He II
O III]
Geo Lyα, O II
Si II, C IV
Al II
Fe II
Fe II
Mg II, Mg I
Sigma (%)
G270H
Filter (pixels)
Grating
Wavelength (Å)

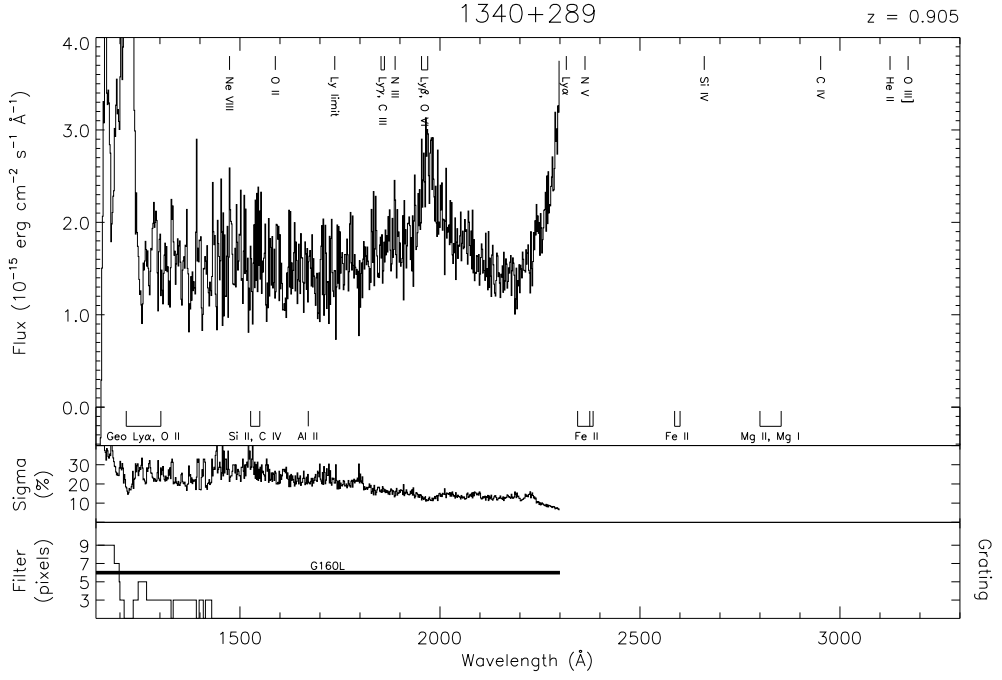
1340+289
z = 0.905
Flux (10^{-15} erg cm^{-2} s^{-1} Å^{-1})
Ne VIII
O II
Ly limit
N III
Lyγ, C III
Lyβ, O VI
Lyα
N V
Si IV
C IV
He II
O III]
Geo Lyα, O II
Si II, C IV
Al II
Fe II
Fe II
Mg II, Mg I
Sigma (%)
G160L
Filter (pixels)
Grating
Wavelength (Å)

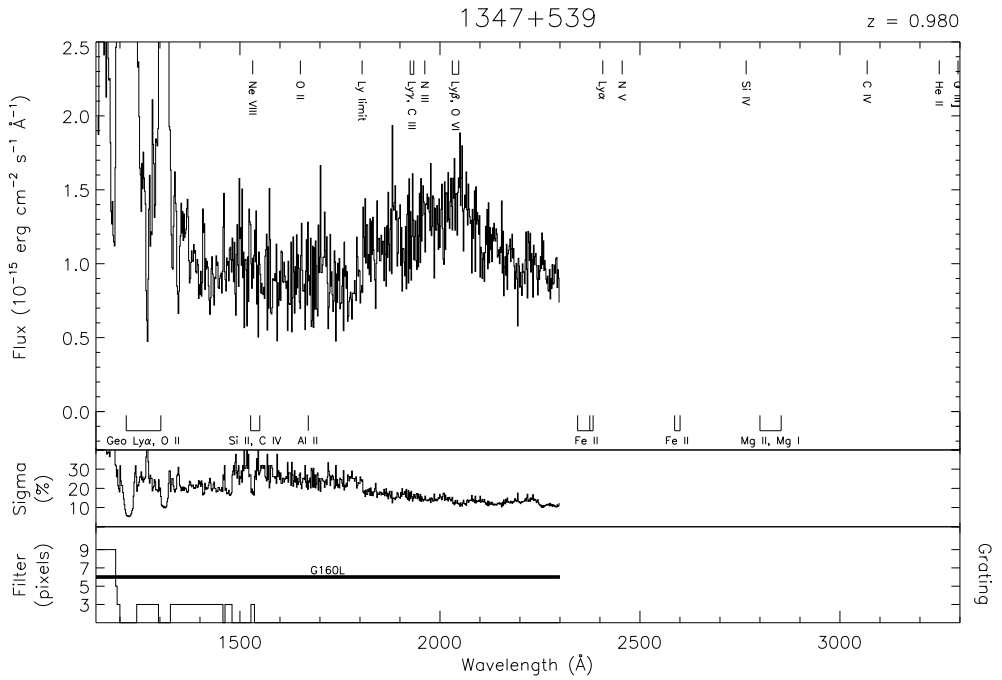
1347+539
z = 0.980
Flux (10^{-15} erg cm^{-2} s^{-1} Å^{-1})
Ne VIII
O II
Ly limit
N III
Lyγ, C III
Lyβ, O VI
Lyα
N V
Si IV
C IV
He II
Geo Lyα, O II
Si II, C IV
Al II
Fe II
Fe II
Mg II, Mg I
Sigma (%)
Filter (pixels)
G160L
Grating
Wavelength (Å)

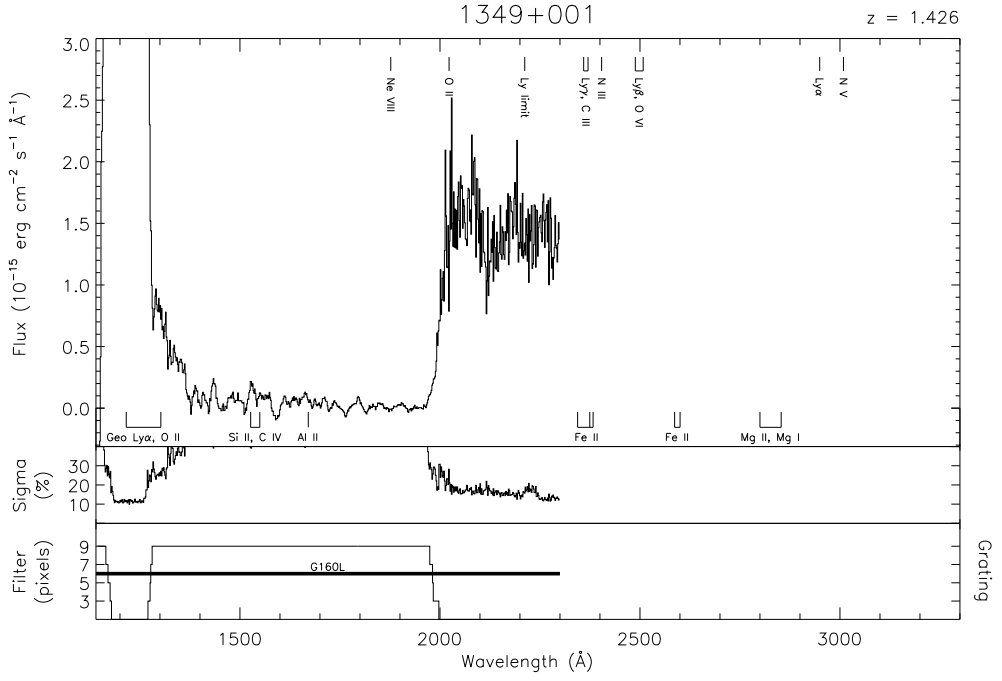
1349+001
z = 1.426
Flux (10^{-15} erg cm^{-2} s^{-1} Å^{-1})
Ne VIII
O II
Ly limit
N III
Lyγ, C III
Lyβ, O VI
Lyα
N V
Geo Lyα, O II
Si II, C IV
Al II
Fe II
Fe II
Mg II, Mg I
Sigma (%)
Filter (pixels)
G160L
Grating
Wavelength (Å)

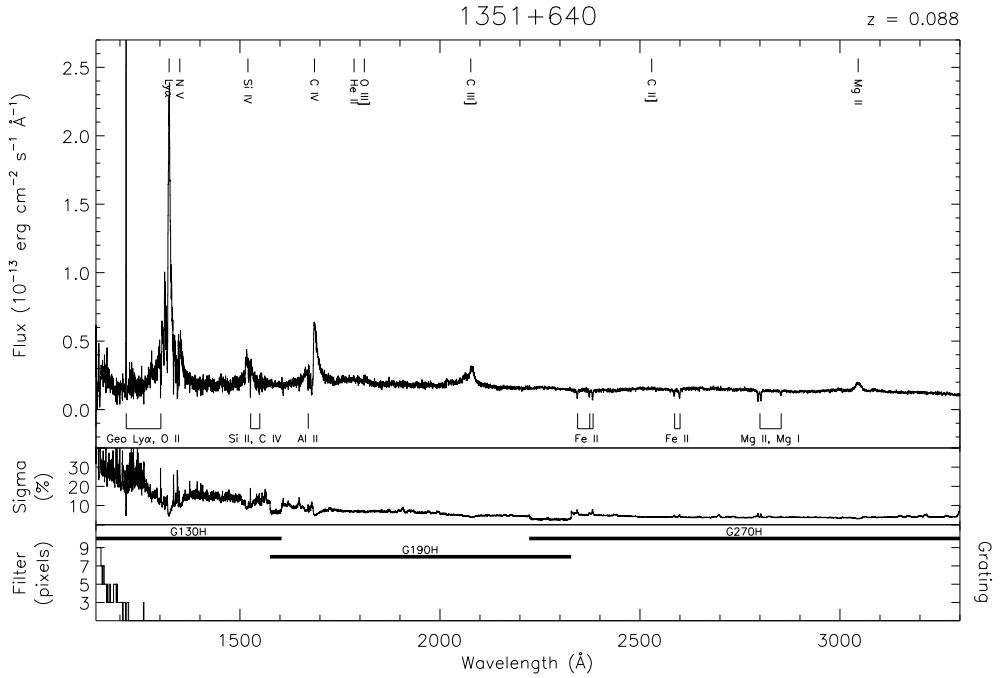
1351+640
z = 0.088
Flux (10^{-13} erg cm^{-2} s^{-1} Å^{-1})
Lyα
N V
Si IV
C IV
O III]
He II
C III]
C II]
Mg II
Geo Lyα, O II
Si II, C IV
Al II
Fe II
Fe II
Mg II, Mg I
Sigma (%)
G130H
G270H
G190H
Filter (pixels)
Grating
Wavelength (Å)

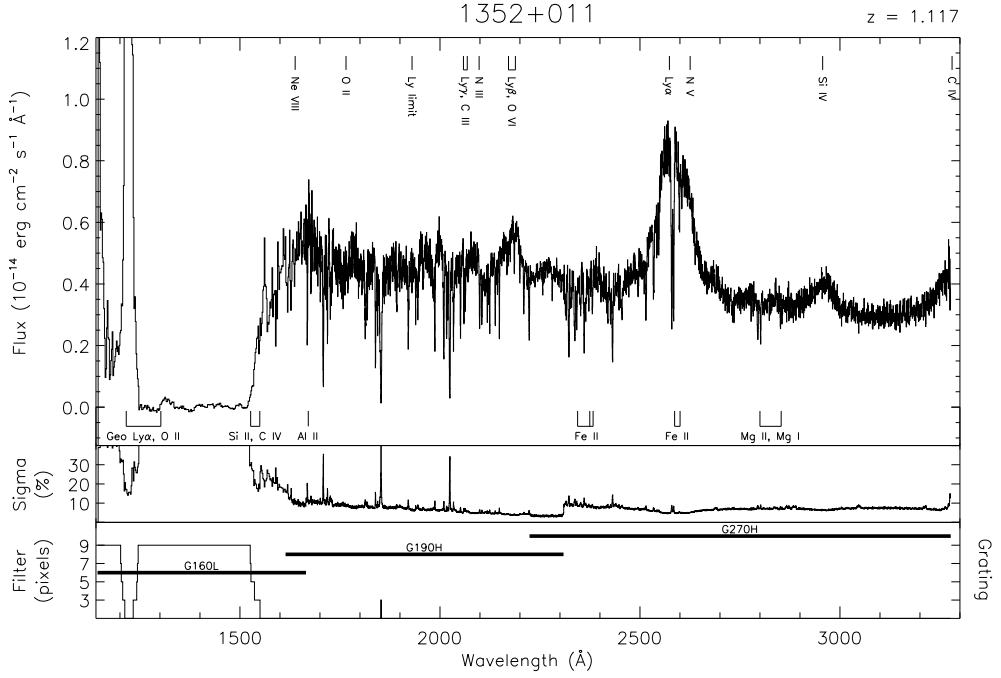
1352+011
z = 1.117
Flux (10^{-14} erg cm^{-2} s^{-1} Å^{-1})
Ne VIII
O II
Ly limit
Lyγ, C III
N III
Lyβ, O VI
Lyα
N V
Si IV
C IV
Geo Lyα, O II
Si II, C IV
Al II
Fe II
Fe II
Mg II, Mg I
Sigma (%)
G270H
G190H
G160L
Filter (pixels)
Grating
Wavelength (Å)

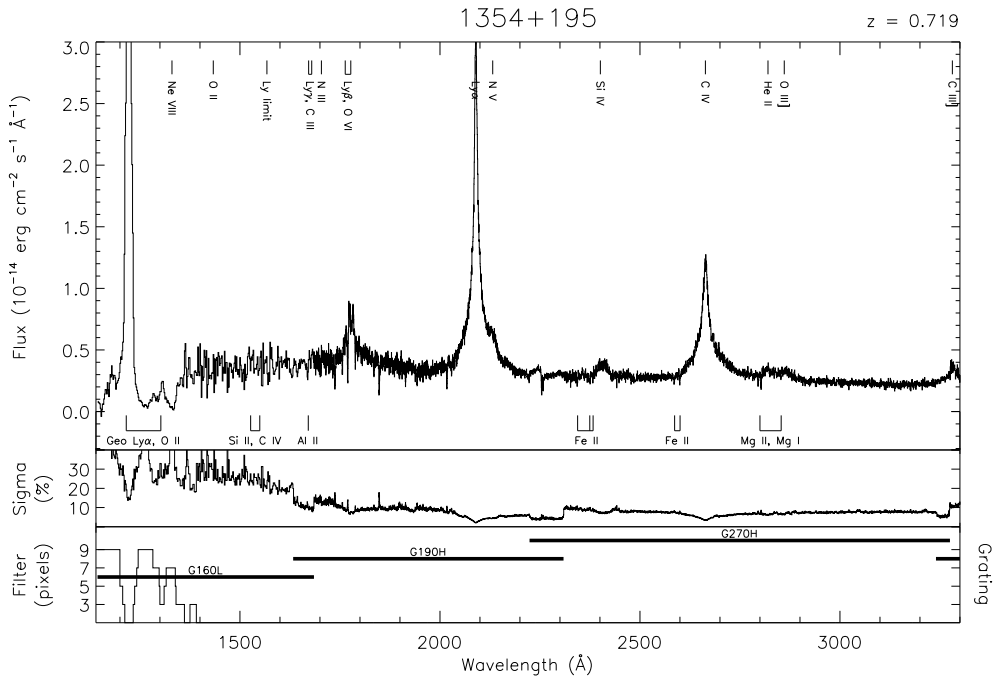
1354+195
z = 0.719
Flux (10^{-14} erg cm^{-2} s^{-1} Å^{-1})
Ne VIII
O II
Ly limit
N III
Lyγ, C III
Lyβ, O VI
Lyα
N V
Si IV
C IV
He II
O III]
C III]
Geo Lyα, O II
Si II, C IV
Al II
Fe II
Fe II
Mg II, Mg I
Sigma (%)
Filter (pixels)
G160L
G190H
G270H
Grating
Wavelength (Å)

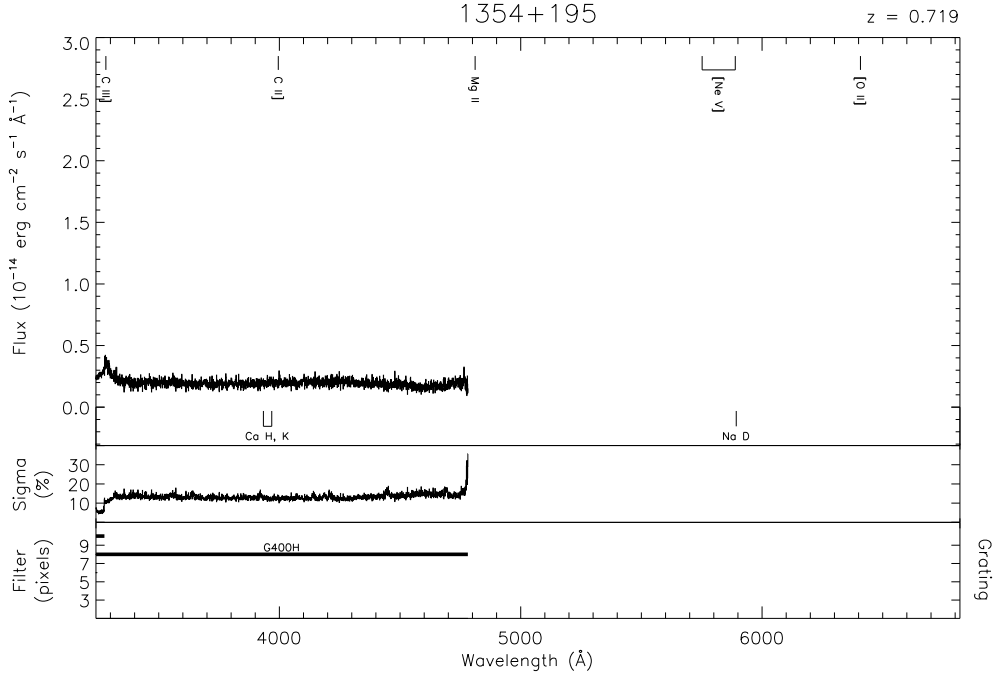
1354+195
z = 0.719
Flux (10^{-14} erg cm^{-2} s^{-1} Å^{-1})
[O III]
[O II]
Mg II
[Ne V]
[O II]
Ca H, K
Na D
Sigma (%)
Filter (pixels)
G400H
Grating
Wavelength (Å)

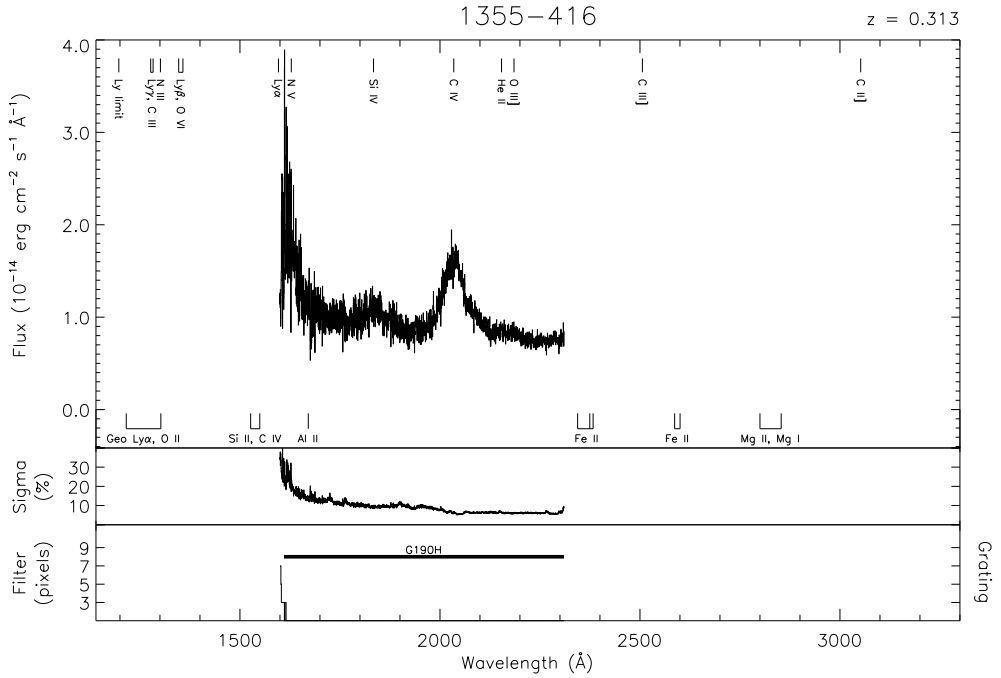
1355−416
z = 0.313
Flux (10^{-14} erg cm^{-2} s^{-1} Å^{-1})
Ly limit
N III, C III
Lyγ, O VI
Lyα
N V
Si IV
C IV
He II
O III]
C III]
C II]
Geo Lyα, O II
Si II, C IV
Al II
Fe II
Fe II
Mg II, Mg I
Sigma (%)
Filter (pixels)
G190H
Grating
Wavelength (Å)

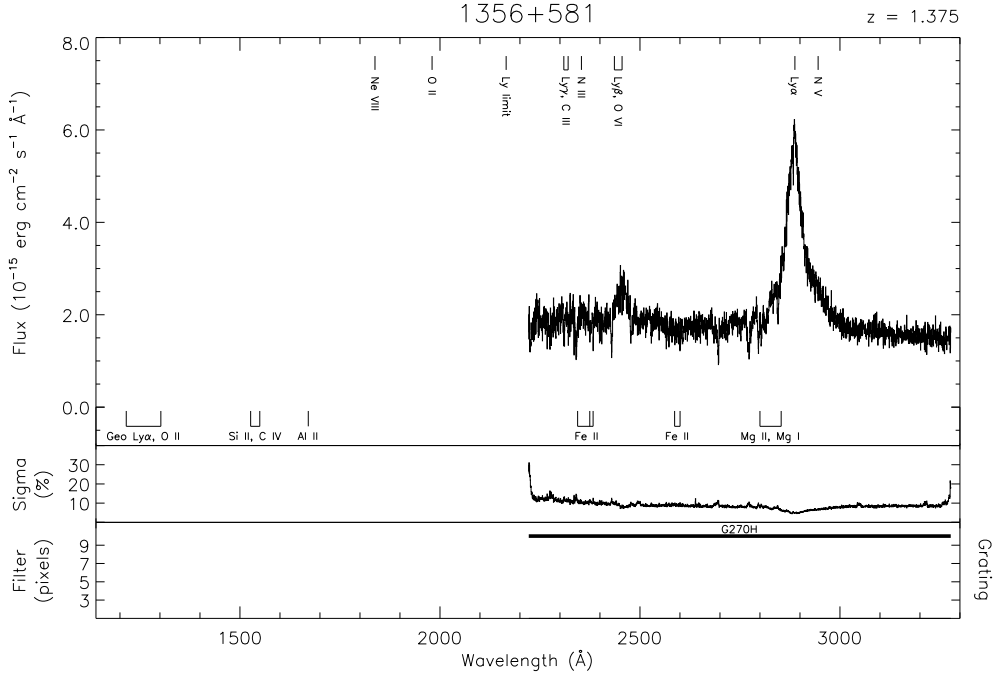
1356+581
z = 1.375
Flux (10^{-15} erg cm^{-2} s^{-1} Å^{-1})
Ne VIII
O II
Ly limit
N III
Lyγ, C III
Lyβ, O VI
Lyα
N V
Geo Lyα, O II
Si II, C IV
Al II
Fe II
Fe II
Mg II, Mg I
Sigma (%)
Filter (pixels)
G270H
Grating
Wavelength (Å)

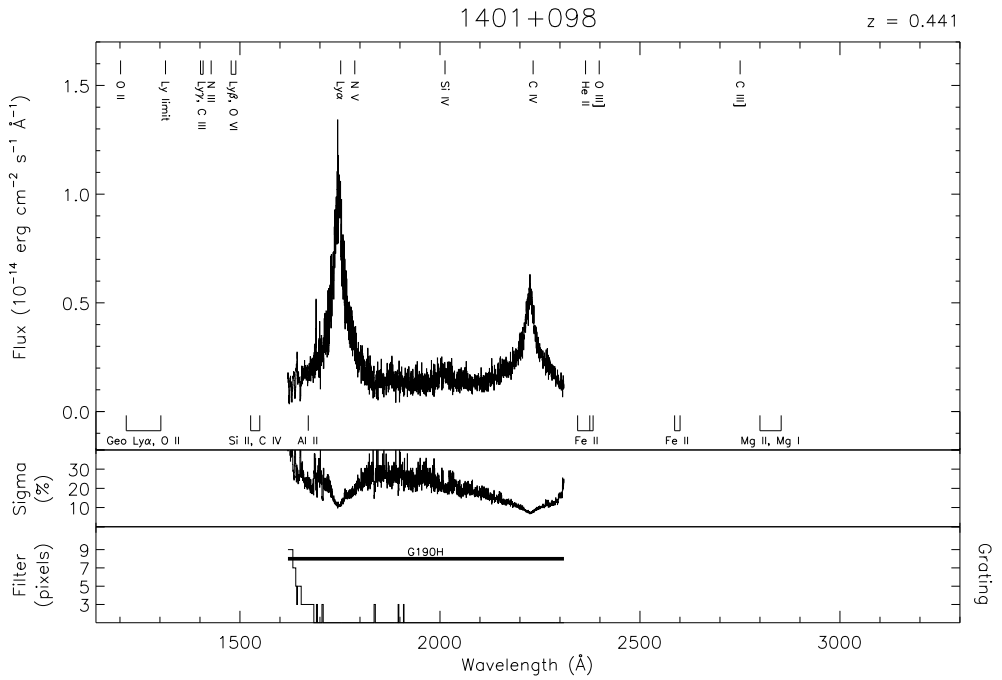
1401+098
z = 0.441
Flux (10^{-14} erg cm^{-2} s^{-1} Å^{-1})
O II
Ly limit
C III
N III
Lyβ, O VI
Lyα
N V
Si IV
C IV
He II
O III]
C III]
Geo Lyα, O II
Si II, C IV
Al II
Fe II
Fe II
Mg II, Mg I
Sigma (%)
Filter (pixels)
G190H
Grating
Wavelength (Å)

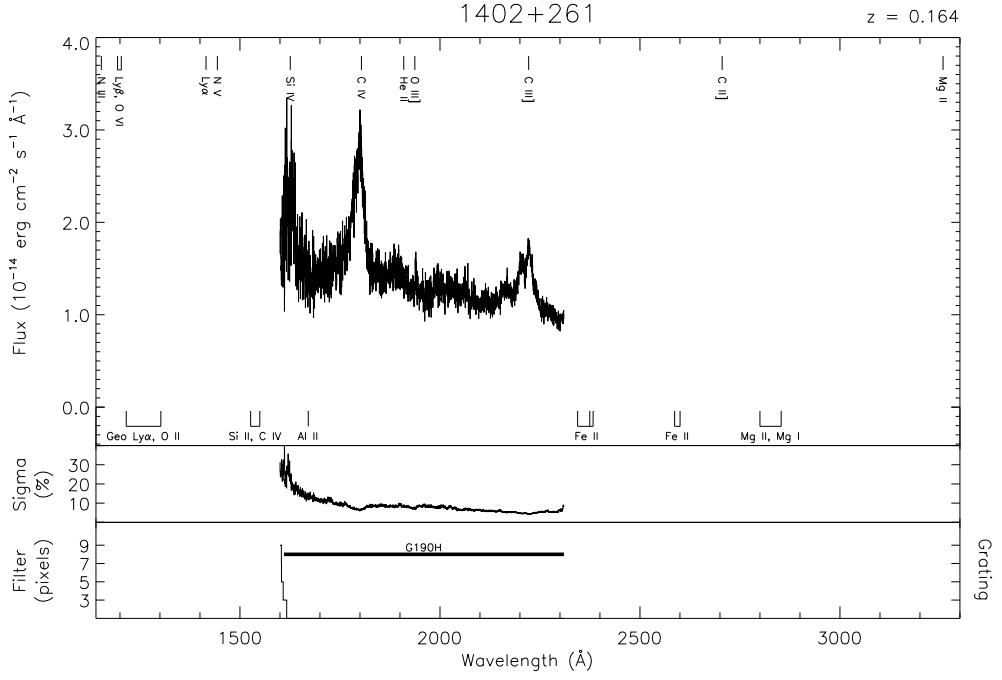
1402+261
z = 0.164
Flux (10^{-14} erg cm^{-2} s^{-1} Å^{-1})
N III
Lyβ, O VI
Lyα
N V
Si IV
C IV
He II
O III]
C III]
C II]
Mg II
Geo Lyα, O II
Si II, C IV
Al II
Fe II
Fe II
Mg II, Mg I
Sigma (%)
Filter (pixels)
G190H
Grating
Wavelength (Å)

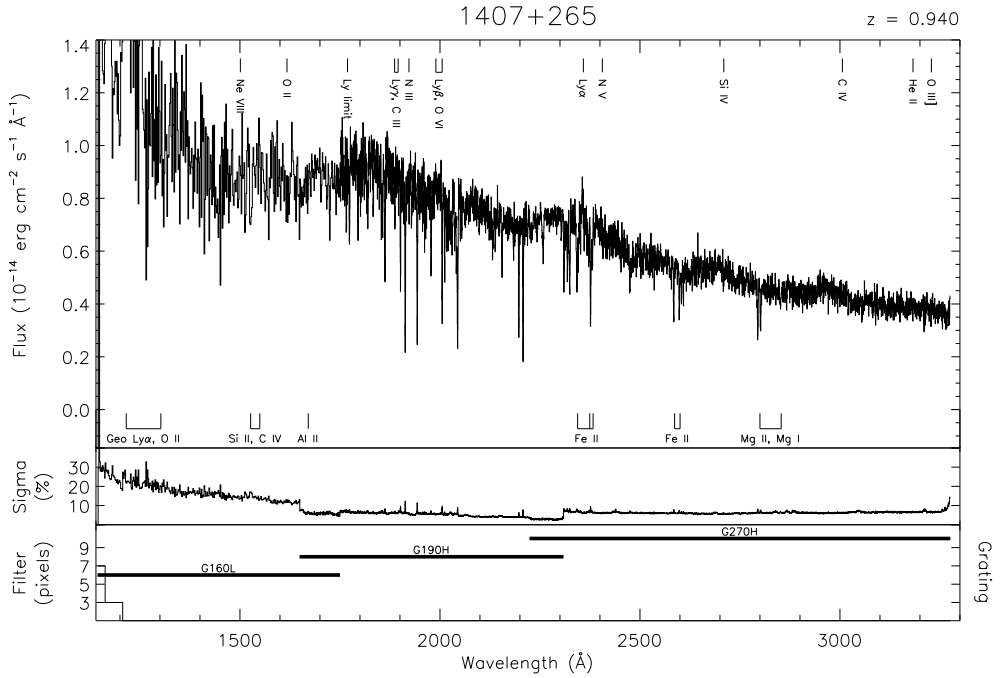
1407+265
z = 0.940
Flux (10^{-14} erg cm^{-2} s^{-1} Å^{-1})
Ne VIII
O II
Ly limit
N III
Lyγ, C III
Lyβ, O VI
Lyα
N V
Si IV
C IV
He II
O III]
Geo Lyα, O II
Si II, C IV
Al II
Fe II
Fe II
Mg II, Mg I
Sigma (%)
Filter (pixels)
G270H
G190H
G160L
Grating
Wavelength (Å)

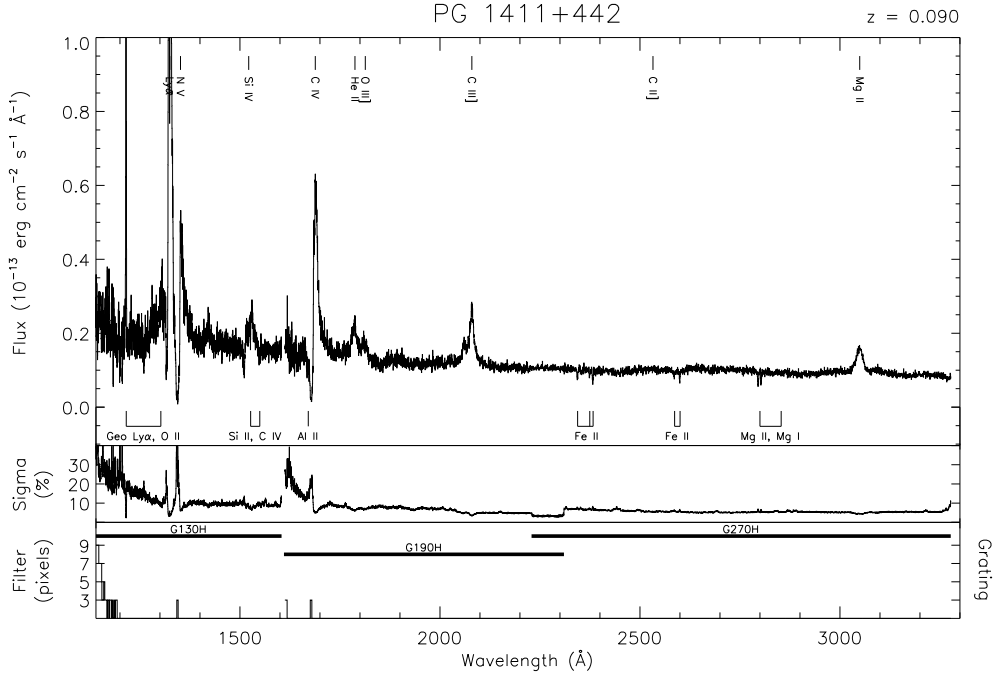
PG 1411+442
z = 0.090
Flux (10^{-13} erg cm^{-2} s^{-1} Å^{-1})
Lyβ
N V
Si IV
C IV
O III]
He II
C III]
C II]
Mg II
Geo Lyα, O II
Si II, C IV
Al II
Fe II
Fe II
Mg II, Mg I
Sigma (%)
Filter (pixels)
G130H
G190H
G270H
Grating
Wavelength (Å)

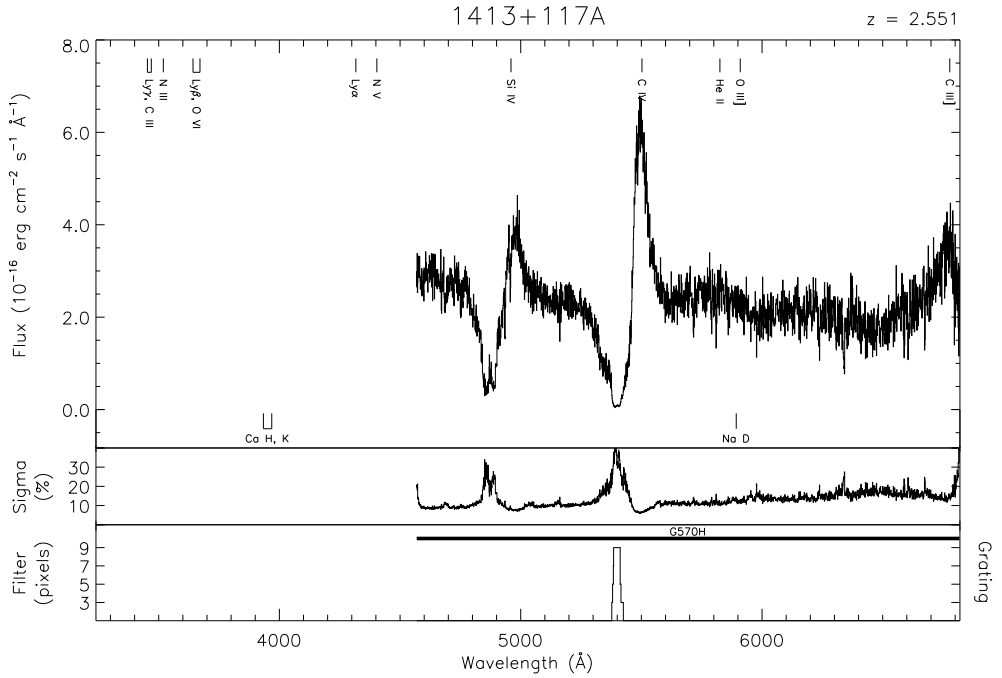
1413+117A
z = 2.551
Flux (10^{-16} erg cm^{-2} s^{-1} Å^{-1})
Lyδ, O VI
C III, N III
Lyα
N V
Si IV
C IV
He II
O III]
C III]
Ca H, K
Na D
Sigma (%)
G570H
Filter (pixels)
Grating
Wavelength (Å)

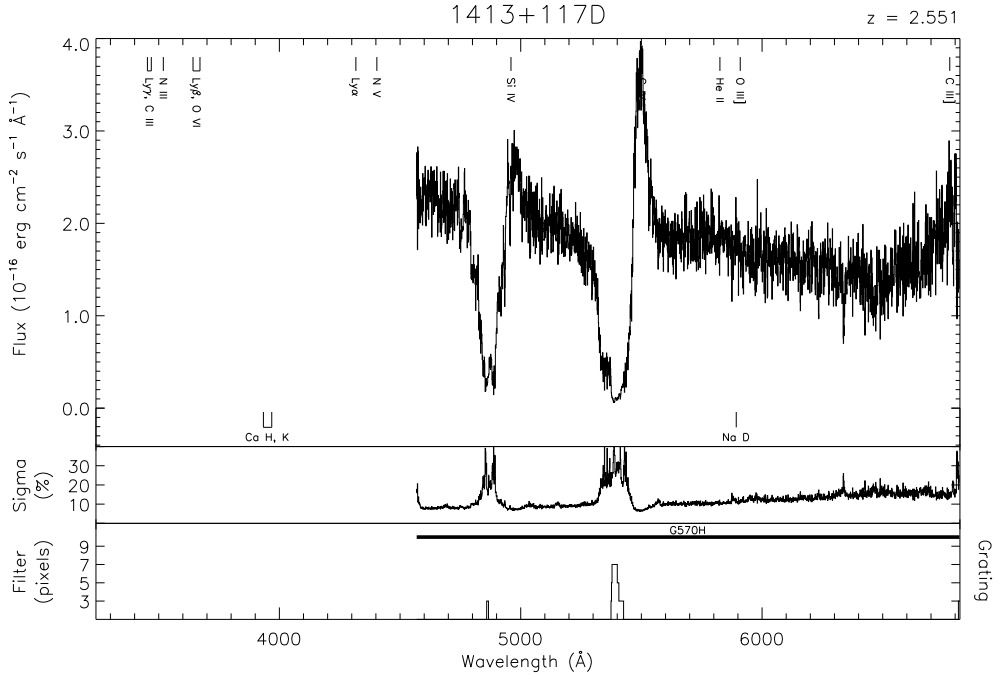
1413+117D
z = 2.551
Flux (10^{-16} erg cm^{-2} s^{-1} Å^{-1})
Lyδ, O VI
C III, N III
Lyα
N V
Si IV
C IV
He II
O III]
C III]
Ca H, K
Na D
Sigma (%)
G570H
Filter (pixels)
Grating
Wavelength (Å)

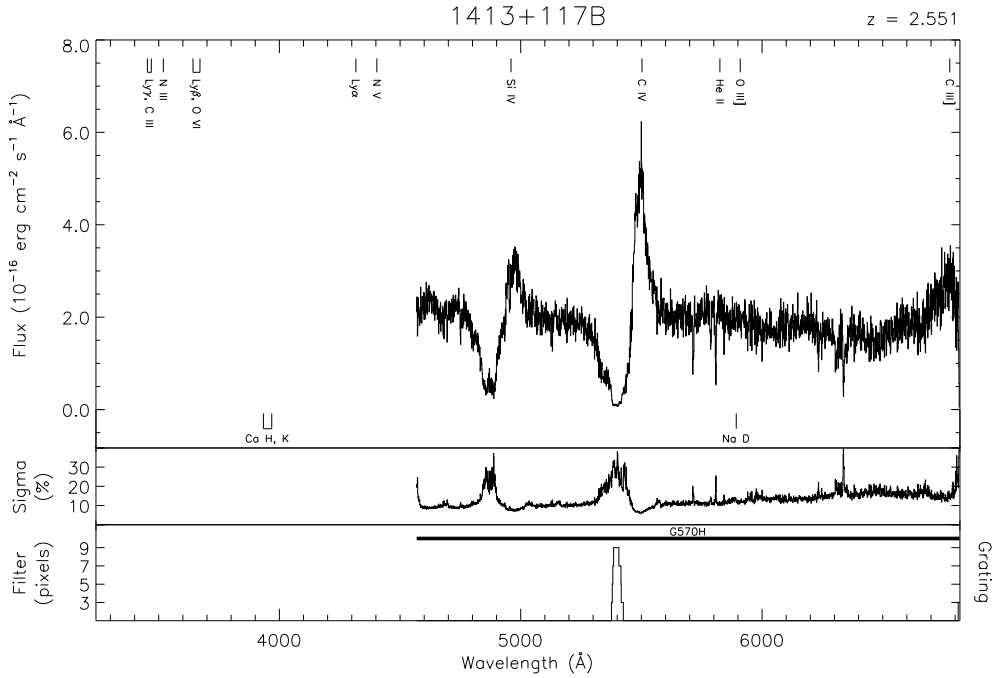
1413+117B
z = 2.551
Flux (10^{-16} erg cm^{-2} s^{-1} Å^{-1})
Lyβ, O VI
C III, Lyγ
N III
Lyα
N V
Si IV
C IV
He II
O III]
C III]
Ca H, K
Na D
Sigma (%)
G570H
Filter (pixels)
Grating
Wavelength (Å)

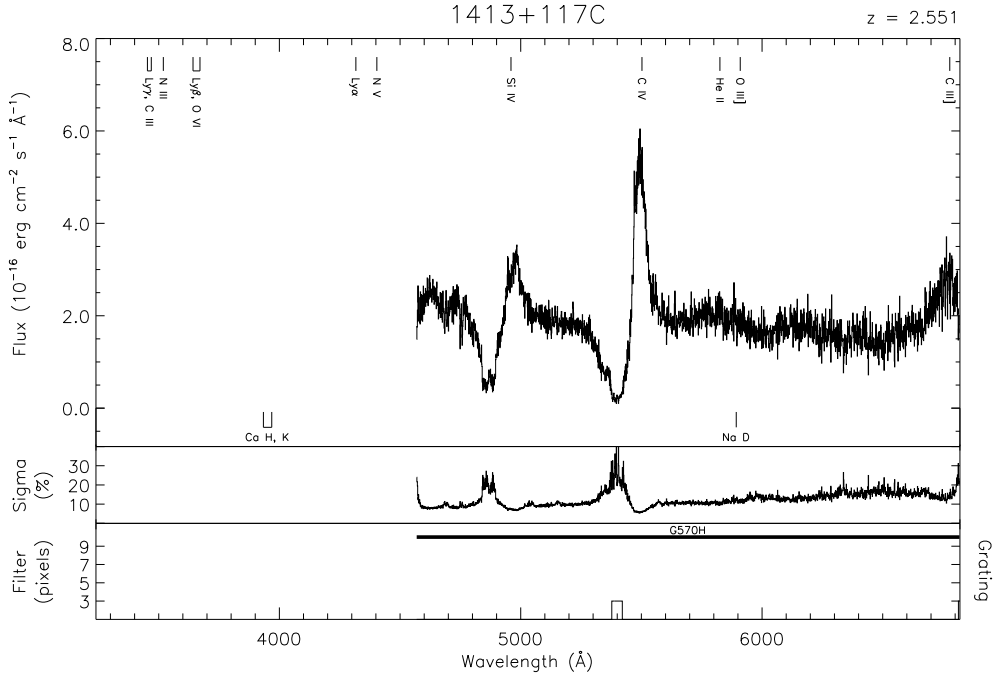
1413+117C
z = 2.551
Flux (10^{-16} erg cm^{-2} s^{-1} Å^{-1})
Lyβ, O VI
C III, Lyγ
N III
Lyα
N V
Si IV
C IV
He II
O III]
C III]
Ca H, K
Na D
Sigma (%)
G570H
Filter (pixels)
Grating
Wavelength (Å)

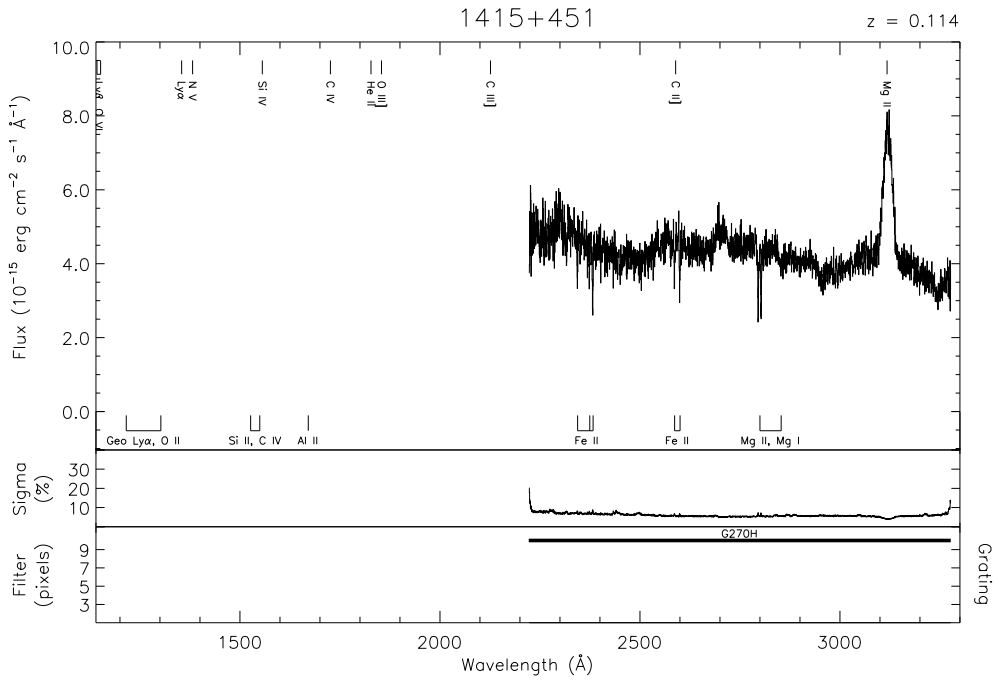
1415+451
z = 0.114
Flux (10^{-15} erg cm^{-2} s^{-1} Å^{-1})
Mg II
C I]
C III]
C IV
Si IV
N V
Lyα
O III]
He II
Geo Lyα, O II
Si II, C IV
Al II
Fe II
Fe II
Mg II, Mg I
Sigma (%)
Filter (pixels)
G270H
Grating
Wavelength (Å)

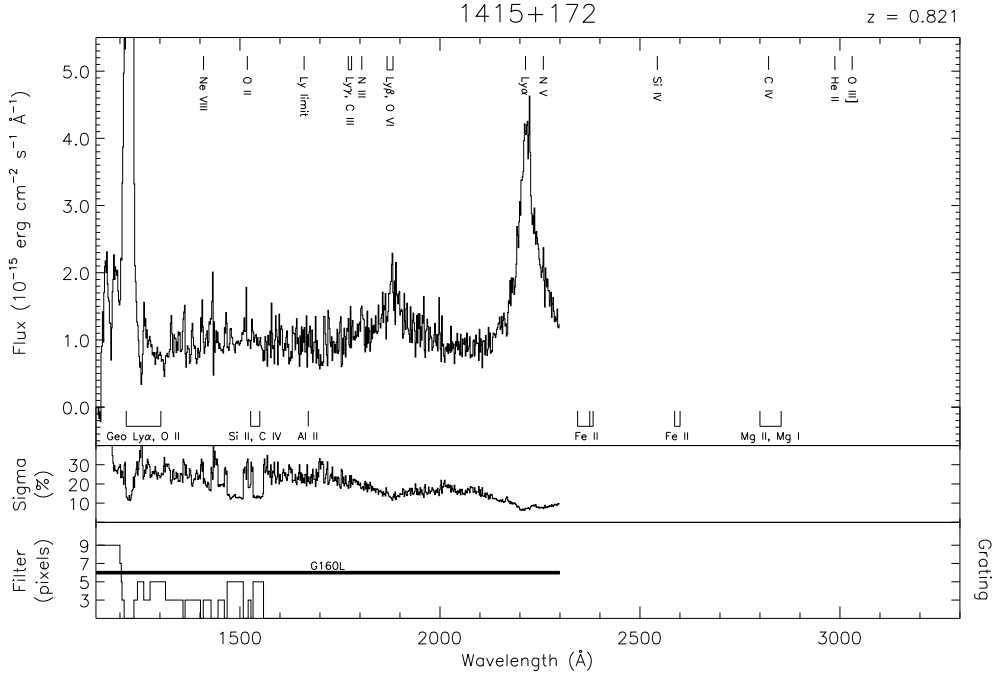
1415+172
z = 0.821
Flux (10^{-15} erg cm^{-2} s^{-1} Å^{-1})
Ne VIII
O II
Ly limit
N III
Lyγ, C III
Lyδ, O VI
N V
Lyα
Si IV
C IV
He II
O III]
Geo Lyα, O II
Si II, C IV
Al II
Fe II
Fe II
Mg II, Mg I
Sigma (%)
Filter (pixels)
G160L
Grating
Wavelength (Å)

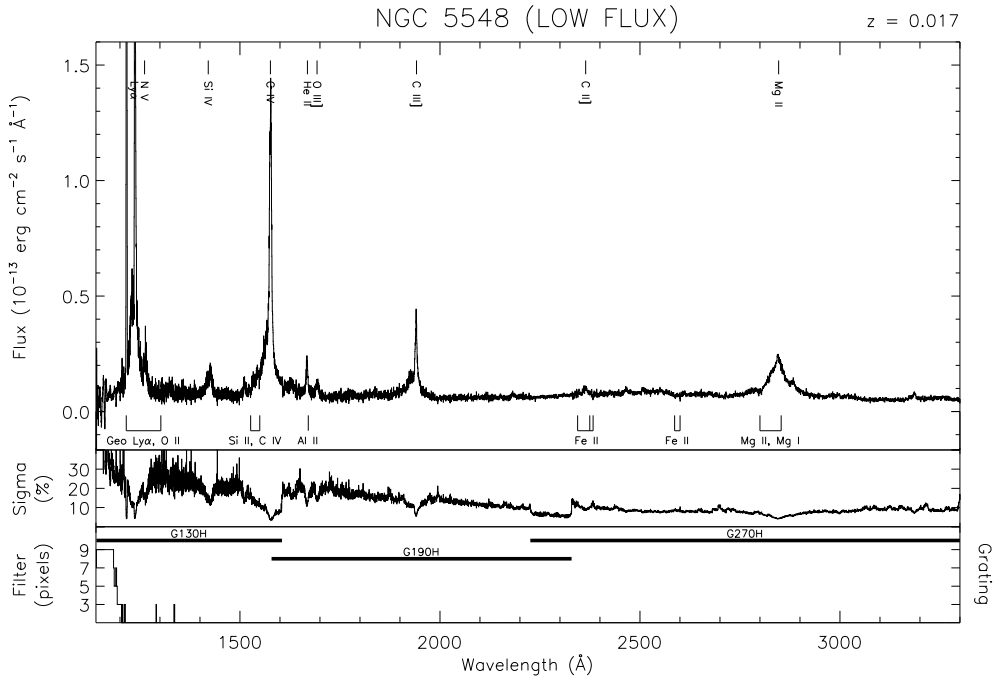
NGC 5548 (LOW FLUX)
z = 0.017
Flux (10^{-13} erg cm^{-2} s^{-1} Å^{-1})
Lyα
N V
Si IV
C IV
He II
O III]
C III]
C II]
Mg II
Geo Lyα, O II
Si II, C IV
Al II
Fe II
Fe II
Mg II, Mg I
Sigma (%)
G130H
G270H
G190H
Filter (pixels)
Grating
Wavelength (Å)

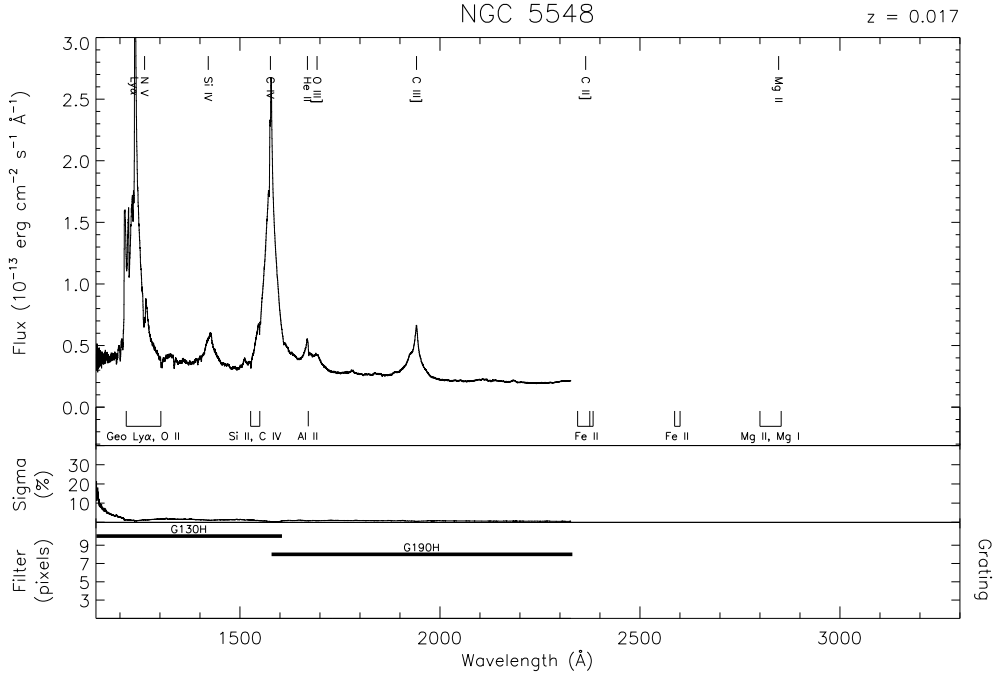
NGC 5548
z = 0.017
Flux (10^{-13} erg cm^{-2} s^{-1} Å^{-1})
Lyα
N V
Si IV
C IV
He II
O III]
C III]
C II]
Mg II
Geo Lyα, O II
Si II, C IV
Al II
Fe II
Fe II
Mg II, Mg I
Sigma (%)
G130H
G190H
Filter (pixels)
Grating
Wavelength (Å)

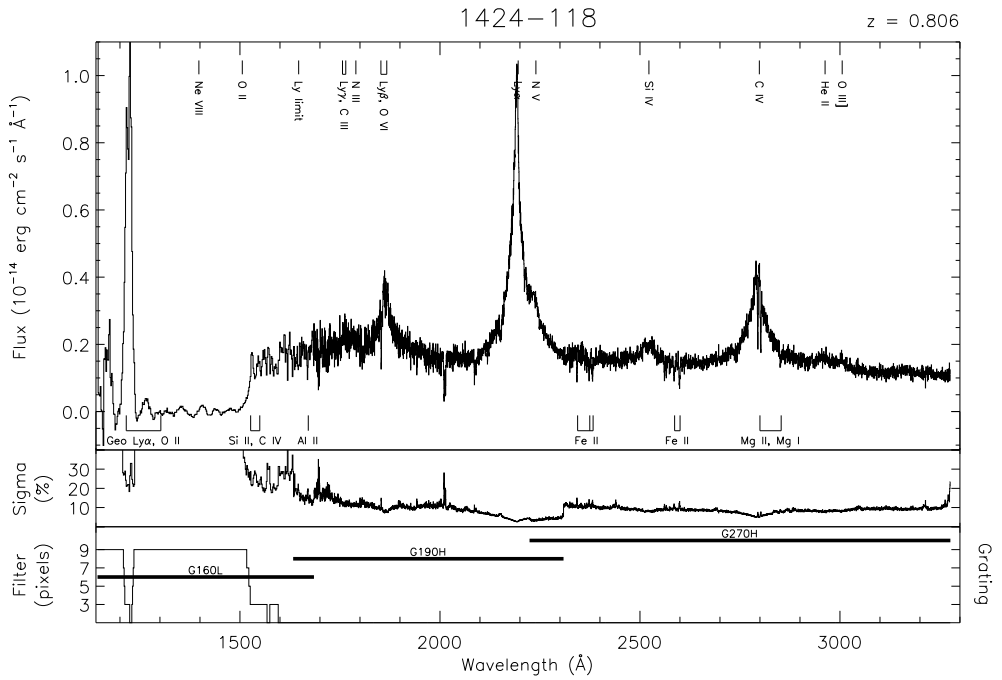
1424−118
z = 0.806
Flux (10^{-14} erg cm^{-2} s^{-1} Å^{-1})
Ne VIII
O II
Ly limit
N III
Lyγ, C III
Lyβ, O VI
Lyα
N V
Si IV
C IV
He II
O III]
Geo Lyα, O II
Si II, C IV
Al II
Fe II
Fe II
Mg II, Mg I
Sigma (%)
Filter (pixels)
G160L
G190H
G270H
Grating
Wavelength (Å)

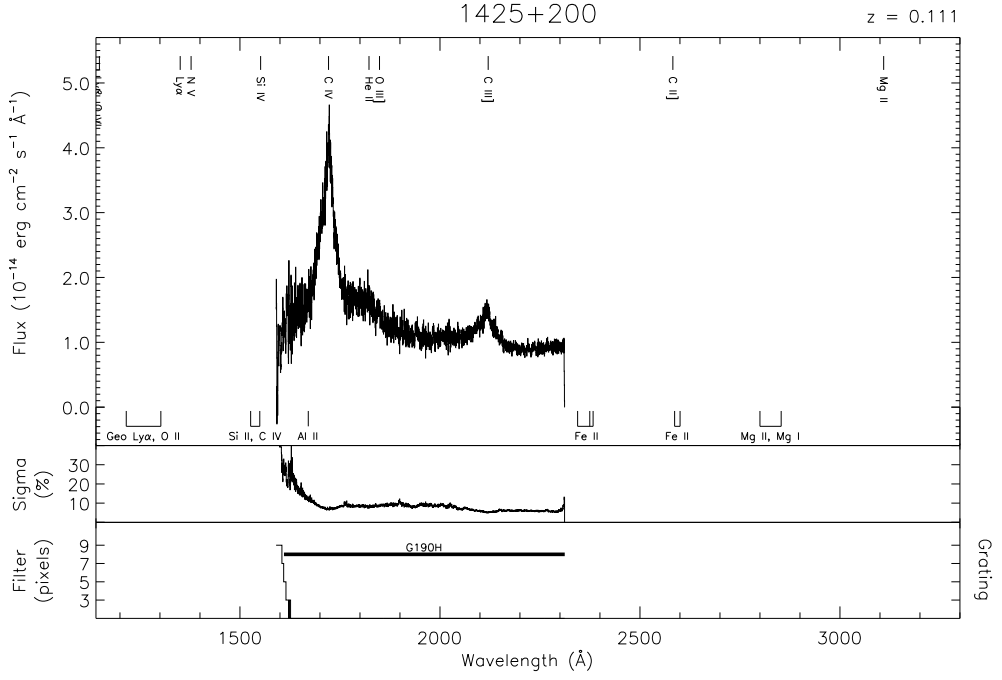
1425+200
z = 0.111
Flux (10^{-14} erg cm^{-2} s^{-1} Å^{-1})
Geo Lyα
N V
Lyα
Si IV
C IV
O III]
He II
C III]
C II]
Mg II
Geo Lyα, O II
Si II, C IV
Al II
Fe II
Fe II
Mg II, Mg I
Sigma (%)
Filter (pixels)
G190H
Grating
Wavelength (Å)

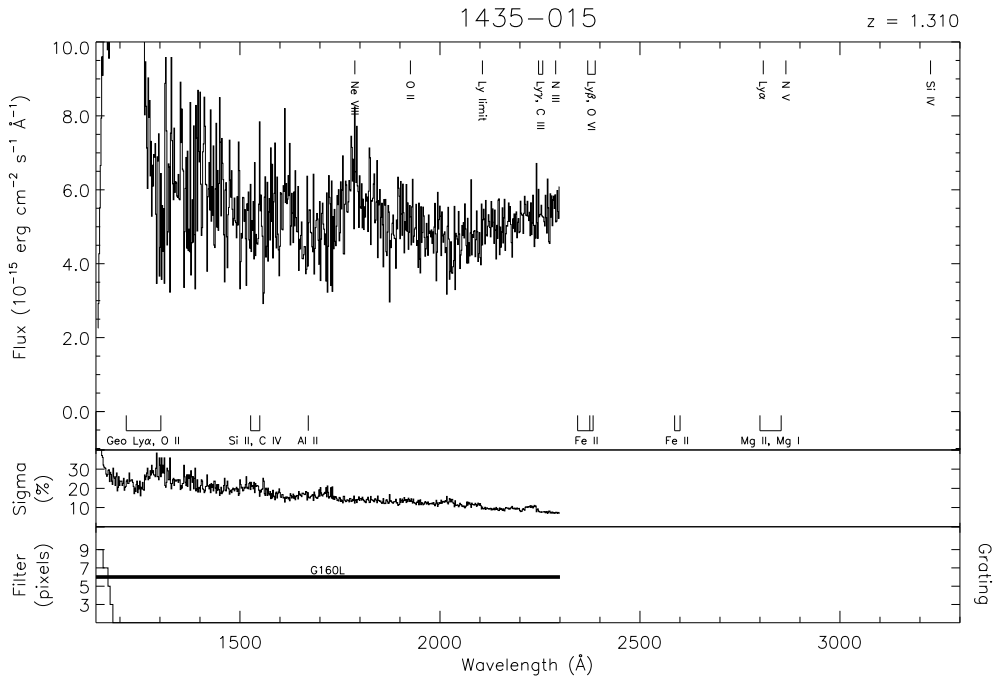
1435−015
z = 1.310
Flux (10^{-15} erg cm^{-2} s^{-1} Å^{-1})
Ne VIII
O II
Ly limit
N III
Lyγ, C III
Lyβ, O VI
Lyα
N V
Si IV
Geo Lyα, O II
Si II, C IV
Al II
Fe II
Fe II
Mg II, Mg I
Sigma (%)
Filter (pixels)
G160L
Grating
Wavelength (Å)

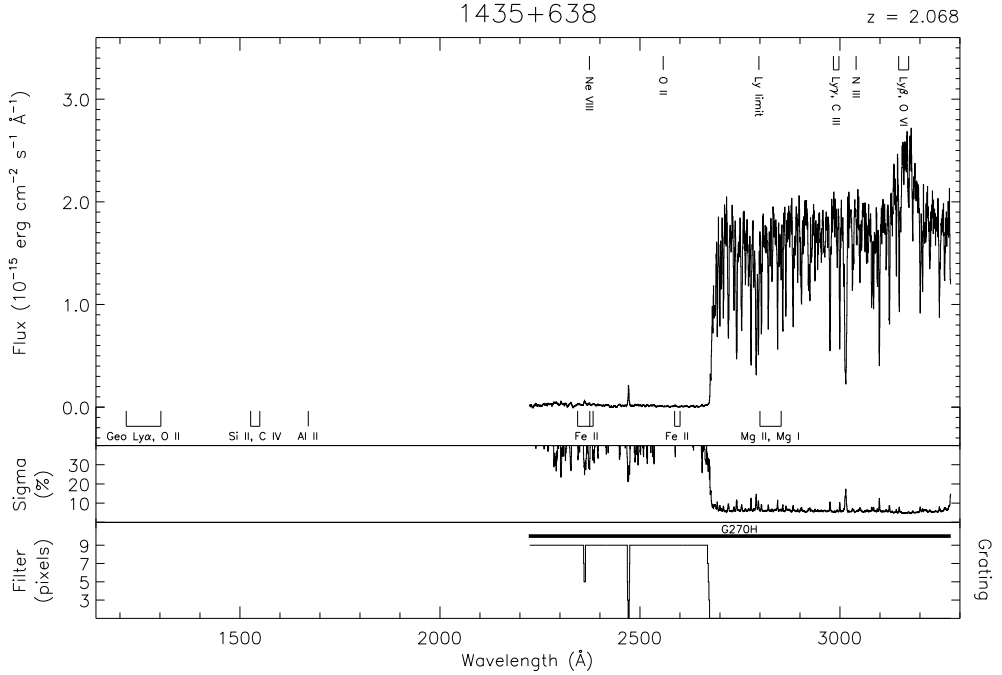
1435+638
z = 2.068
Flux (10^{-15} erg cm^{-2} s^{-1} Å^{-1})
Ne VIII
O II
Ly limit
N III
Lyγ, C III
Lyβ, O VI
Geo Lyα, O II
Si II, C IV
Al II
Fe II
Fe II
Mg II, Mg I
Sigma (%)
G270H
Filter (pixels)
Grating
Wavelength (Å)

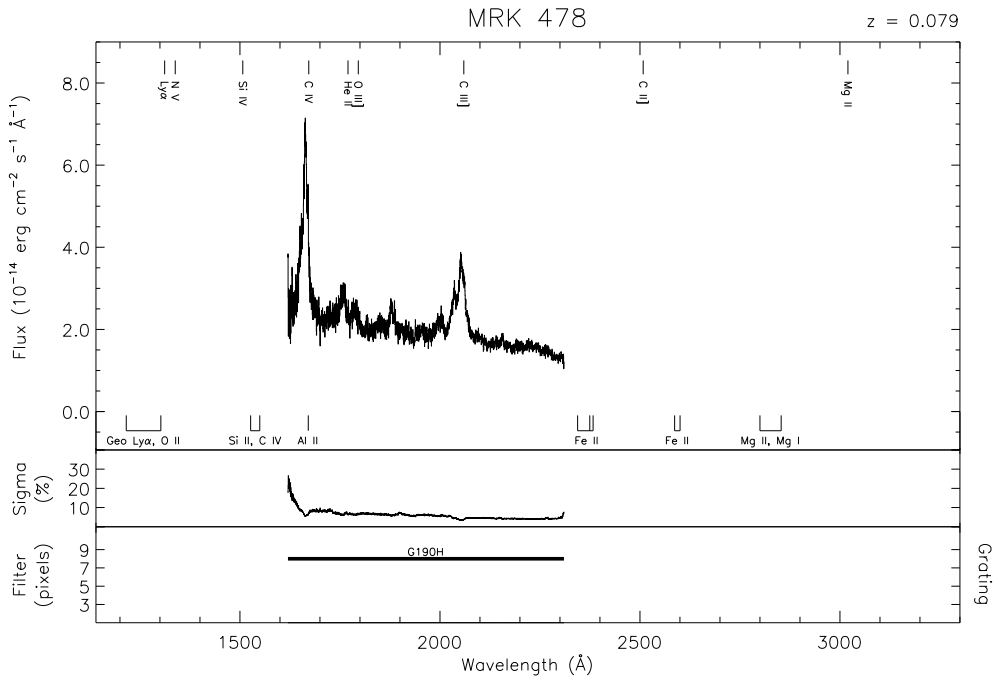
MRK 478
z = 0.079
Flux (10^{-14} erg cm^{-2} s^{-1} Å^{-1})
N V Lyα
Si IV
C IV
He II
O III]
C III]
C II]
Mg II
Geo Lyα, O II
Si II, C IV
Al II
Fe II
Fe II
Mg II, Mg I
Sigma (%)
Filter (pixels)
G190H
Grating
Wavelength (Å)

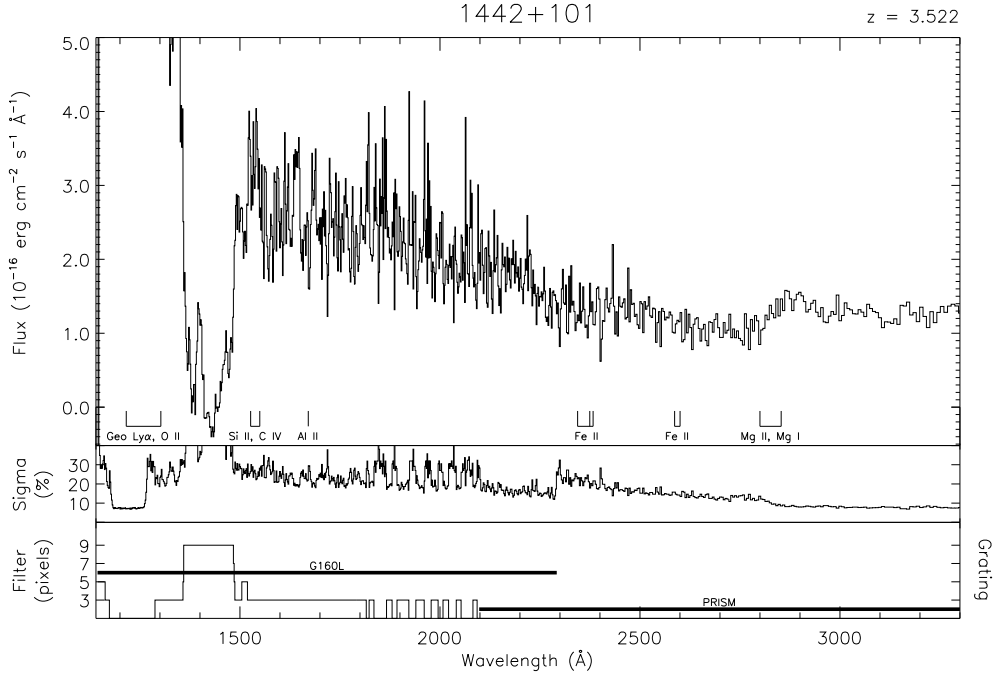
1442+101
z = 3.522
Flux (10^{-16} erg cm^{-2} s^{-1} Å^{-1})
Geo Lyα, O II
Si II, C IV
Al II
Fe II
Fe II
Mg II, Mg I
Sigma (%)
Filter (pixels)
G160L
PRISM
Grating
Wavelength (Å)

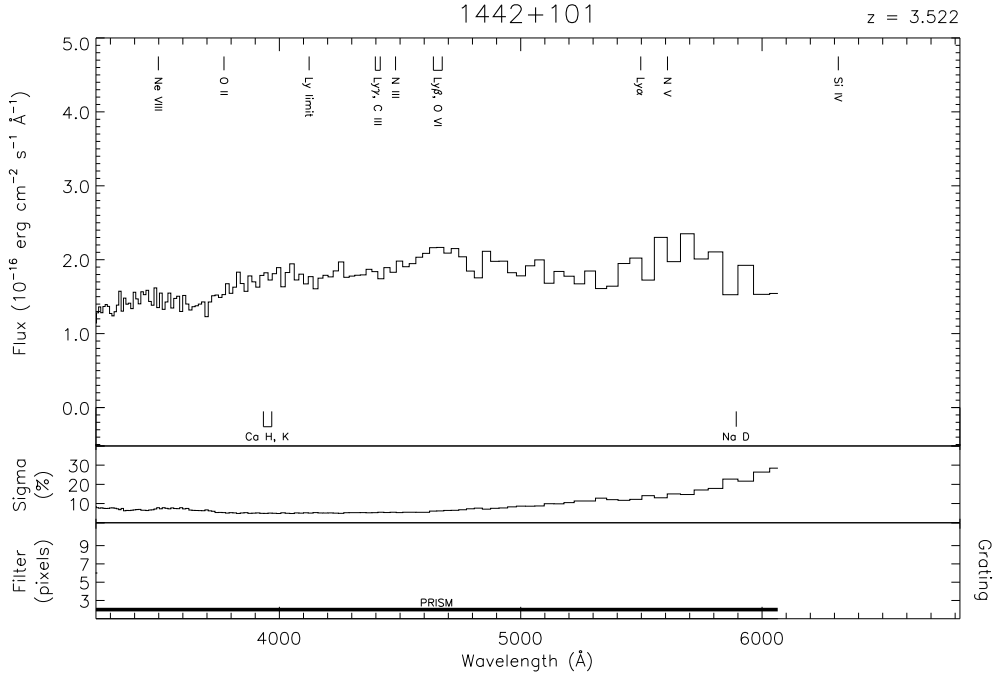
1442+101
z = 3.522
Flux (10^{-16} erg cm^{-2} s^{-1} Å^{-1})
Ne VIII
O II
Ly limit
N III
Lyγ, C III
Lyβ, O VI
Lyα
N V
Si IV
Ca H, K
Na D
Sigma (%)
Filter (pixels)
PRISM
Grating
Wavelength (Å)

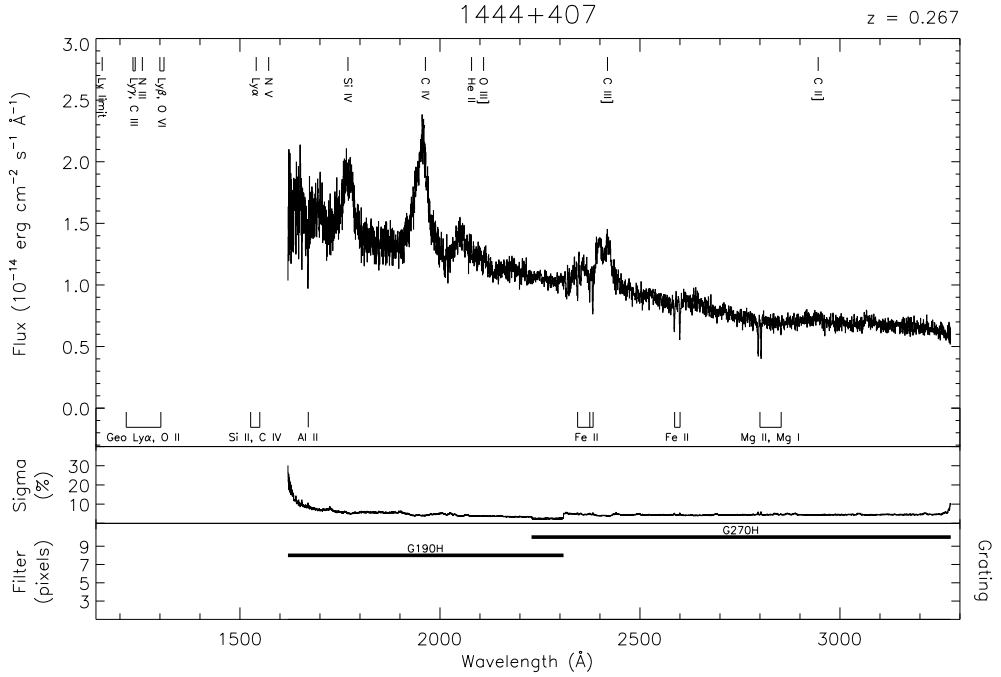
1444+407
z = 0.267
Flux (10^{-14} erg cm^{-2} s^{-1} Å^{-1})
Ly limit
N III
Lyγ, C III
Lyβ, O VI
N V
Lyα
Si IV
C IV
O III]
He II
C III]
C II]
Geo Lyα, O II
Si II, C IV
Al II
Fe II
Fe II
Mg II, Mg I
Sigma (%)
G270H
G190H
Filter (pixels)
Grating
Wavelength (Å)

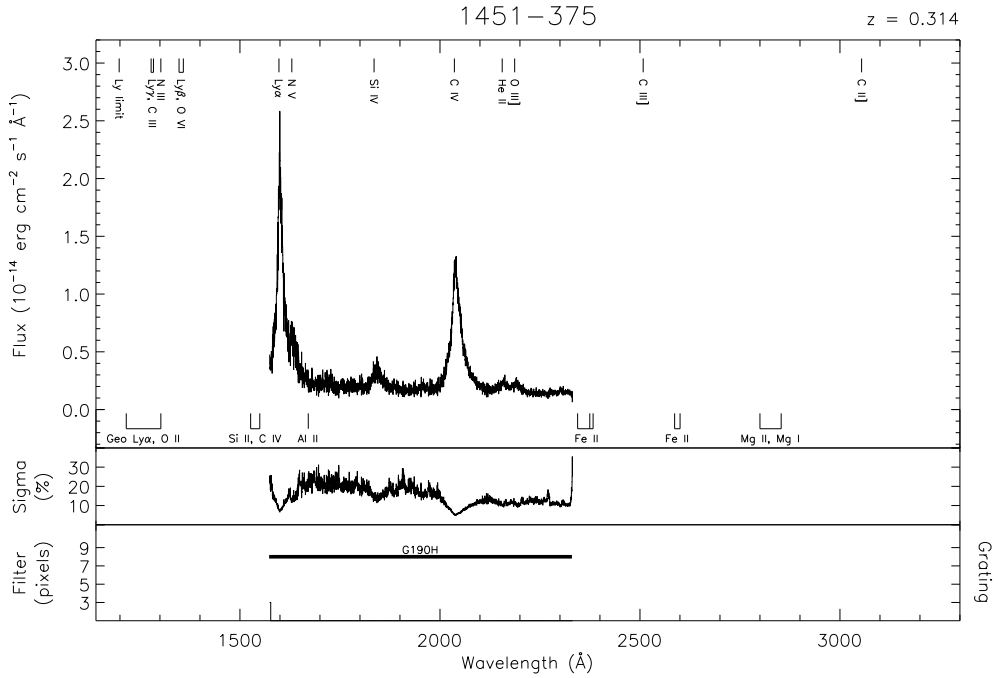
1451−375
z = 0.314
Ly limit
N III, C III
Lyβ, O VI
N V
Lyα
Si IV
C IV
O III]
He II
C III]
C II]
Geo Lyα, O II
Si II, C IV
Al II
Fe II
Fe II
Mg II, Mg I
Flux (10^-14 erg cm^-2 s^-1 Å^-1)
Sigma (%)
Filter (pixels)
G190H
Grating
Wavelength (Å)

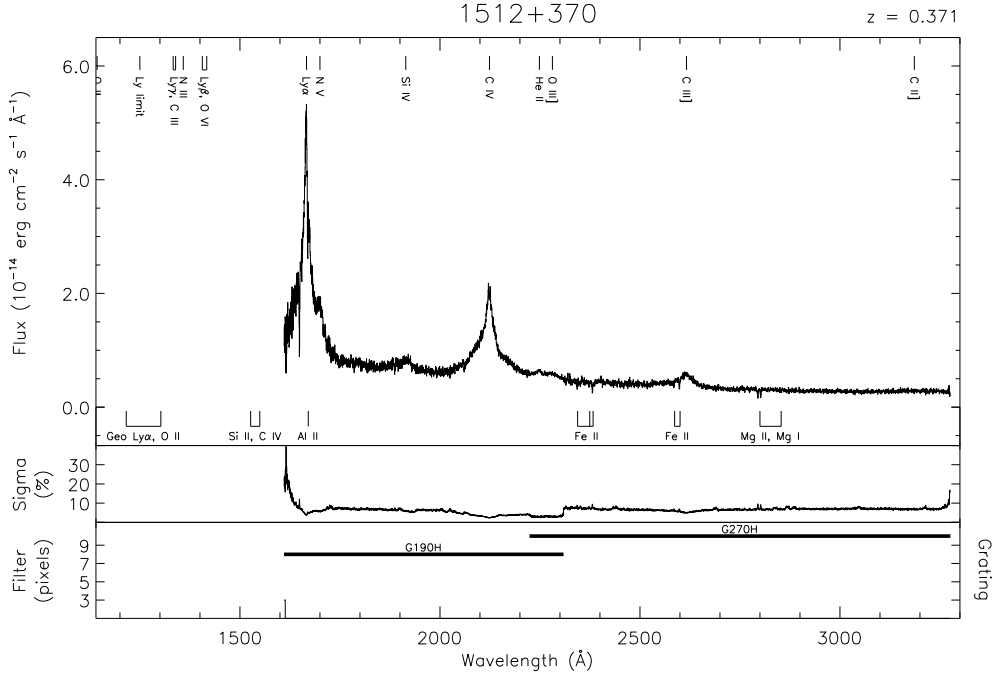
1512+370
z = 0.371
Ly limit
N III, C III
Lyβ, O VI
N V
Lyα
Si IV
C IV
O III]
He II
C III]
C II]
Geo Lyα, O II
Si II, C IV
Al II
Fe II
Fe II
Mg II, Mg I
Flux (10^-14 erg cm^-2 s^-1 Å^-1)
Sigma (%)
Filter (pixels)
G270H
G190H
Grating
Wavelength (Å)

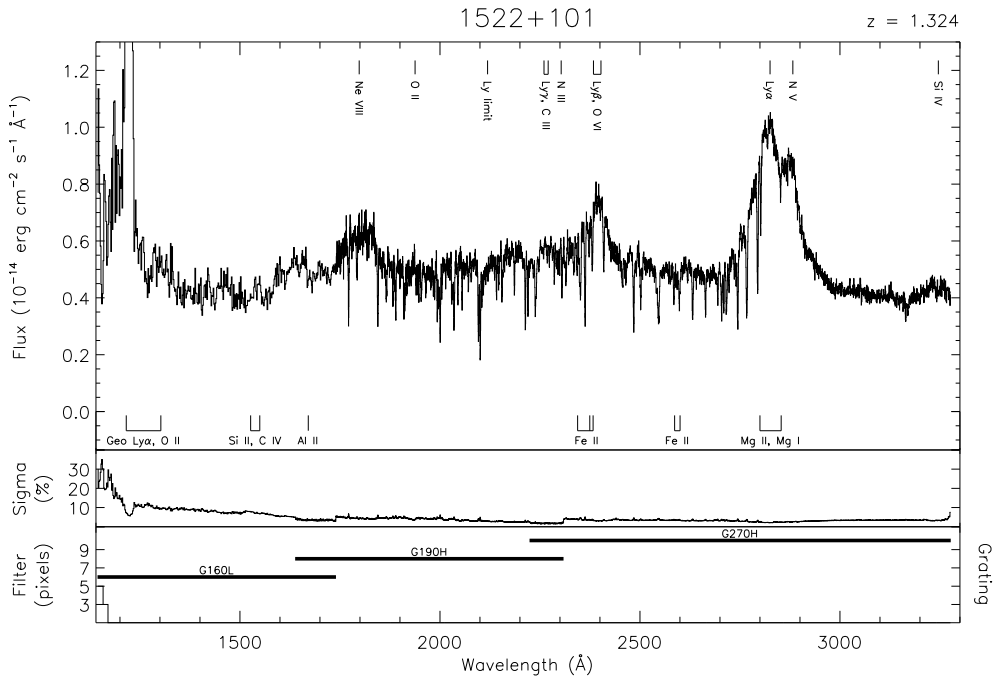
1522+101
z = 1.324
Flux (10^{-14} erg cm^{-2} s^{-1} Å^{-1})
Ne VIII
O II
Ly limit
N III
Lyγ, C III
Lyβ, O VI
Lyα
N V
Si IV
Geo Lyα, O II
Si II, C IV
Al II
Fe II
Fe II
Mg II, Mg I
Sigma (%)
Filter (pixels)
G160L
G190H
G270H
Grating
Wavelength (Å)

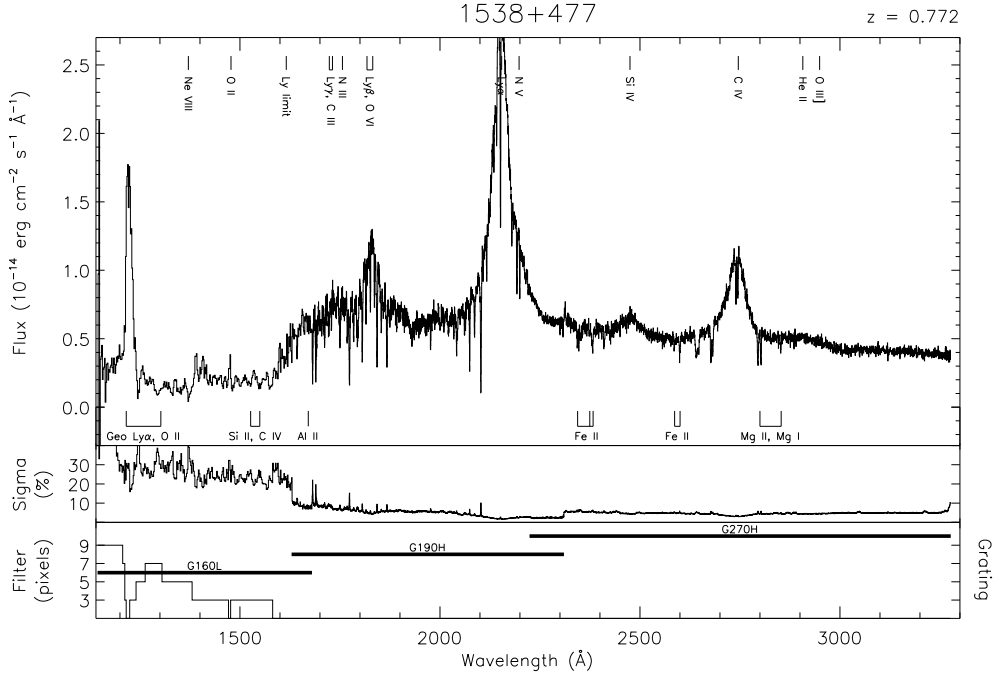
1538+477
z = 0.772
Flux (10^{-14} erg cm^{-2} s^{-1} Å^{-1})
Ne VIII
O II
Ly limit
N III
Lyγ, C III
Lyβ, O VI
Lyα
N V
Si IV
C IV
He II
O III]
Geo Lyα, O II
Si II, C IV
Al II
Fe II
Fe II
Mg II, Mg I
Sigma (%)
Filter (pixels)
G160L
G190H
G270H
Grating
Wavelength (Å)

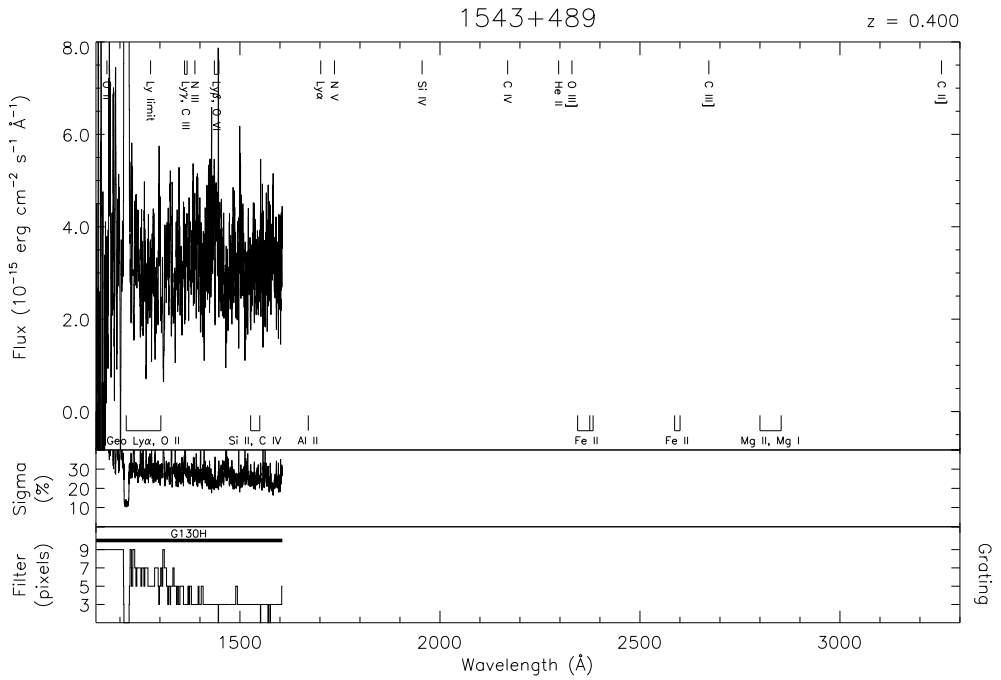
1543+489
z = 0.400
Flux (10^{-15} erg cm^{-2} s^{-1} Å^{-1})
Ly limit
N III, C III
Lyβ, O VI
N V
Lyα
Si IV
C IV
O III] He II
C III]
C II]
Geo Lyα, O II
Si II, C IV
Al II
Fe II
Fe II
Mg II, Mg I
Sigma (%)
G130H
Filter (pixels)
Grating
Wavelength (Å)

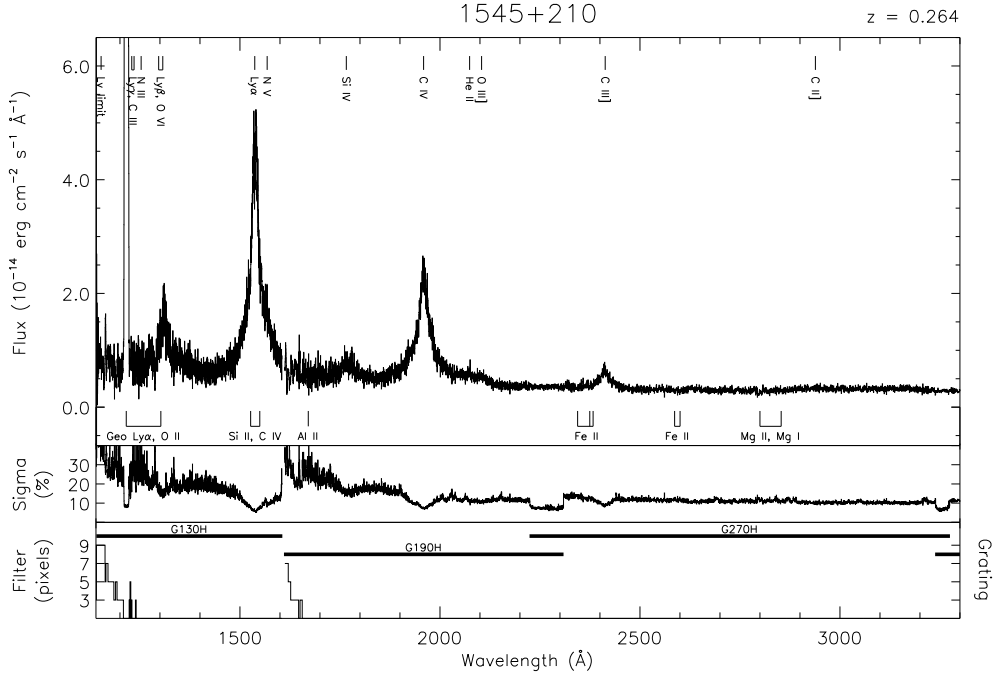
1545+210
z = 0.264
Flux (10^{-14} erg cm^{-2} s^{-1} Å^{-1})
Ly limit
N III, C III
Lyβ, O VI
N V
Lyα
Si IV
C IV
O III] He II
C III]
C II]
Geo Lyα, O II
Si II, C IV
Al II
Fe II
Fe II
Mg II, Mg I
Sigma (%)
G130H
G190H
G270H
Filter (pixels)
Grating
Wavelength (Å)

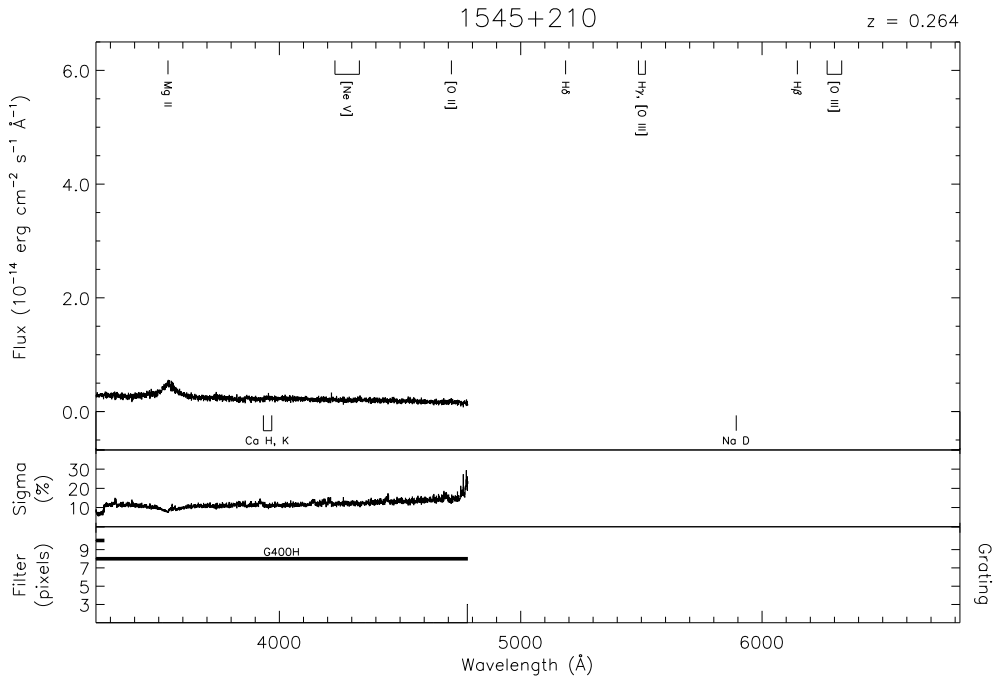
1545+210
z = 0.264
Mg II
[Ne V]
[O II]
Hδ
[O III], He I
Hε
[O III]
Ca H, K
Na D
G400H
Flux (10^-14 erg cm^-2 s^-1 Å^-1)
Sigma (%)
Filter (pixels)
Grating
Wavelength (Å)

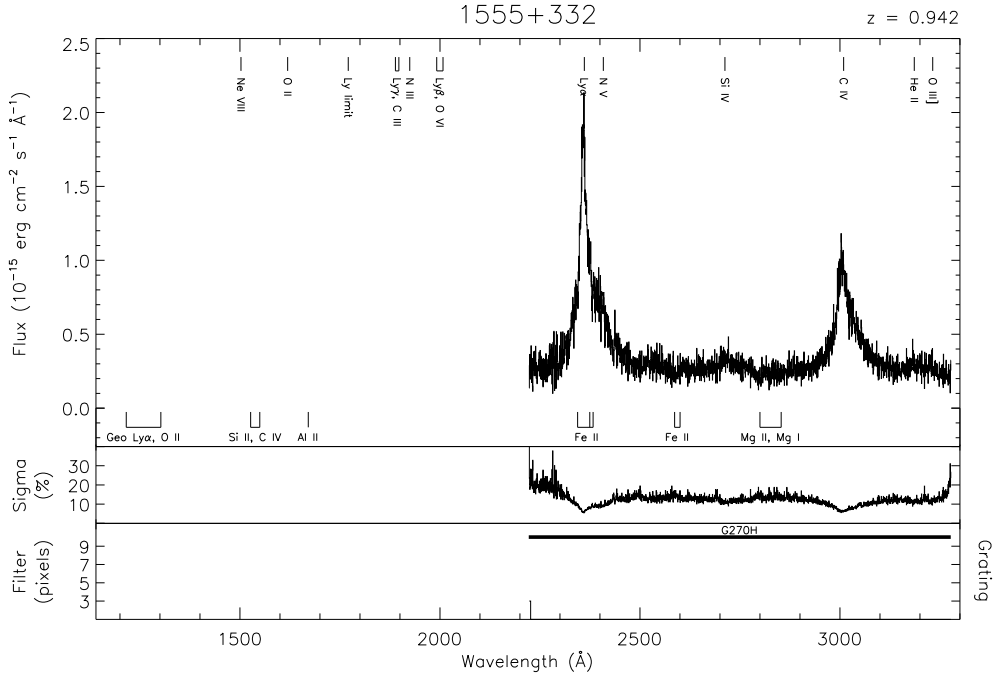
1555+332
z = 0.942
Ne VIII
O II
Ly limit
N III, Ly7, C III
Ly6, O VI
Ly α
N V
Si IV
C IV
He II
O III]
Geo Lyα, O II
Si II, C IV
Al II
Fe II
Fe II
Mg II, Mg I
G270H
Flux (10^-15 erg cm^-2 s^-1 Å^-1)
Sigma (%)
Filter (pixels)
Grating
Wavelength (Å)

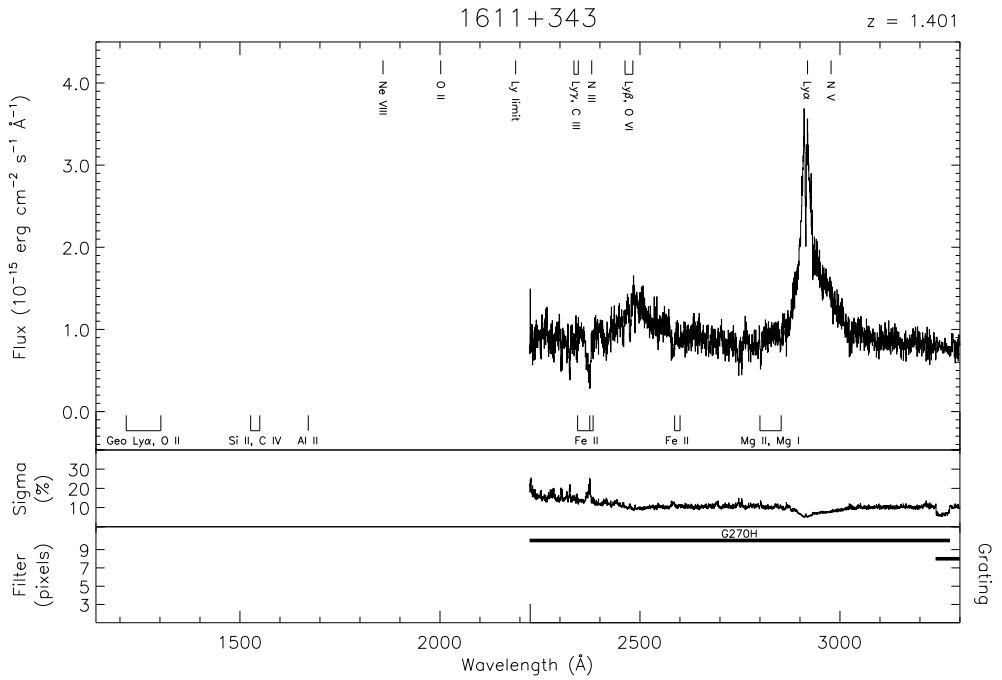
1611+343
z = 1.401
Ne VIII
O II
Ly limit
Lyγ, C III
N III
Lyβ, O VI
Lyα
N V
Geo Lyα, O II
Si II, C IV
Al II
Fe II
Fe II
Mg II, Mg I
Flux (10^-15 erg cm^-2 s^-1 Å^-1)
Sigma (%)
Filter (pixels)
G270H
Grating
Wavelength (Å)

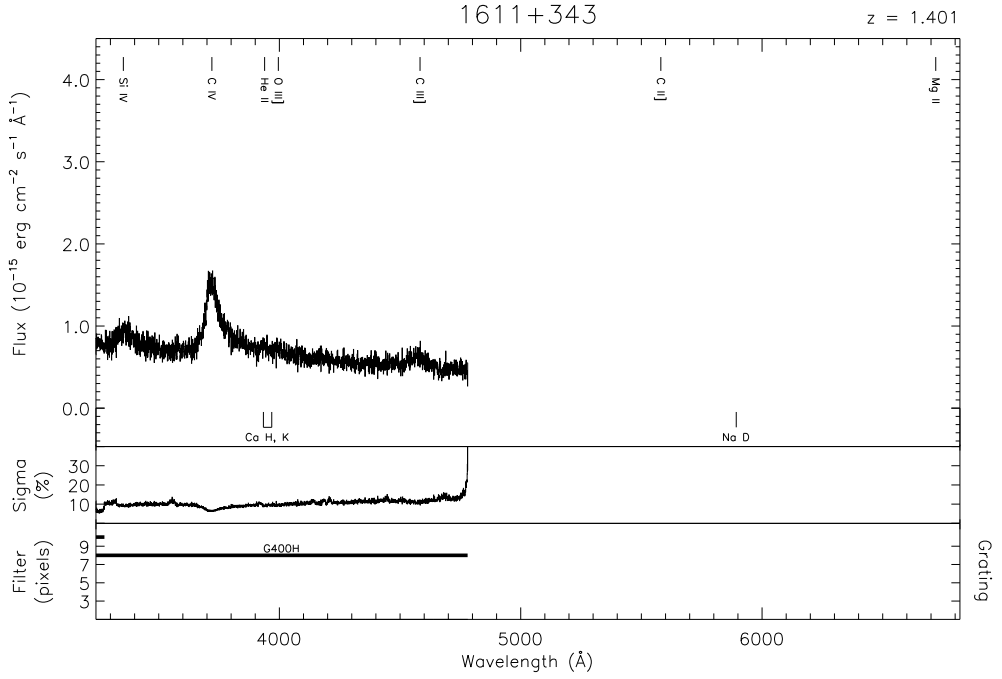
1611+343
z = 1.401
Si IV
C IV
He II
O III]
C III]
C II]
Mg II
Ca H, K
Na D
Flux (10^-15 erg cm^-2 s^-1 Å^-1)
Sigma (%)
Filter (pixels)
G400H
Grating
Wavelength (Å)

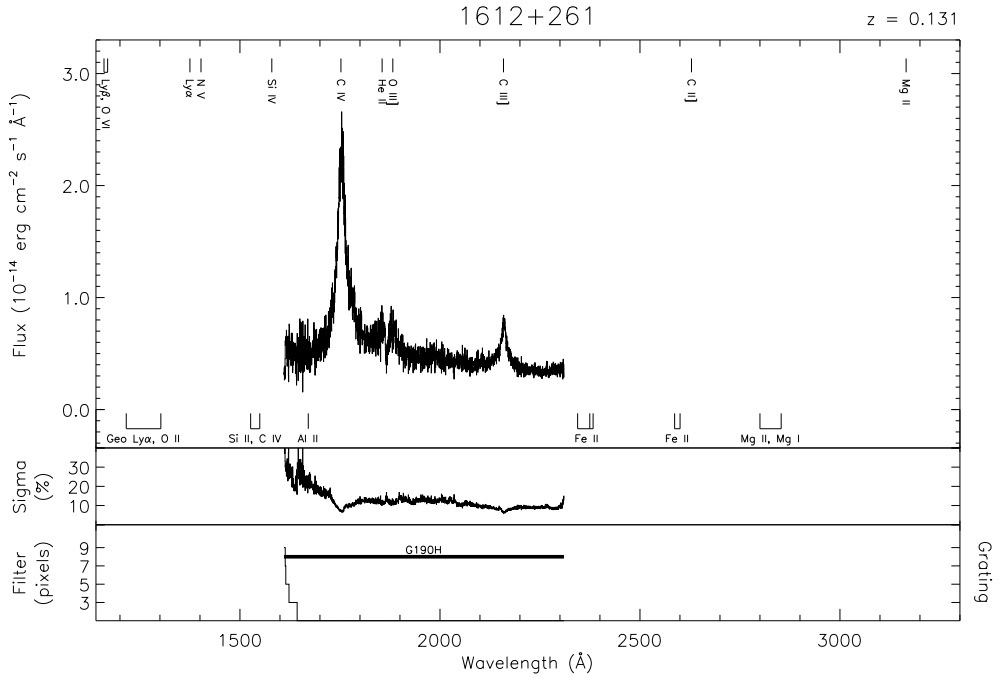
1612+261
z = 0.131
Lyβ, O VI
N V
Lyα
Si IV
C IV
O III]
He II
C III]
C II]
Mg II
Flux (10^-14 erg cm^-2 s^-1 Å^-1)
Geo Lyα, O II
Si II, C IV
Al II
Fe II
Fe II
Mg II, Mg I
Sigma (%)
Filter (pixels)
G190H
Grating
Wavelength (Å)

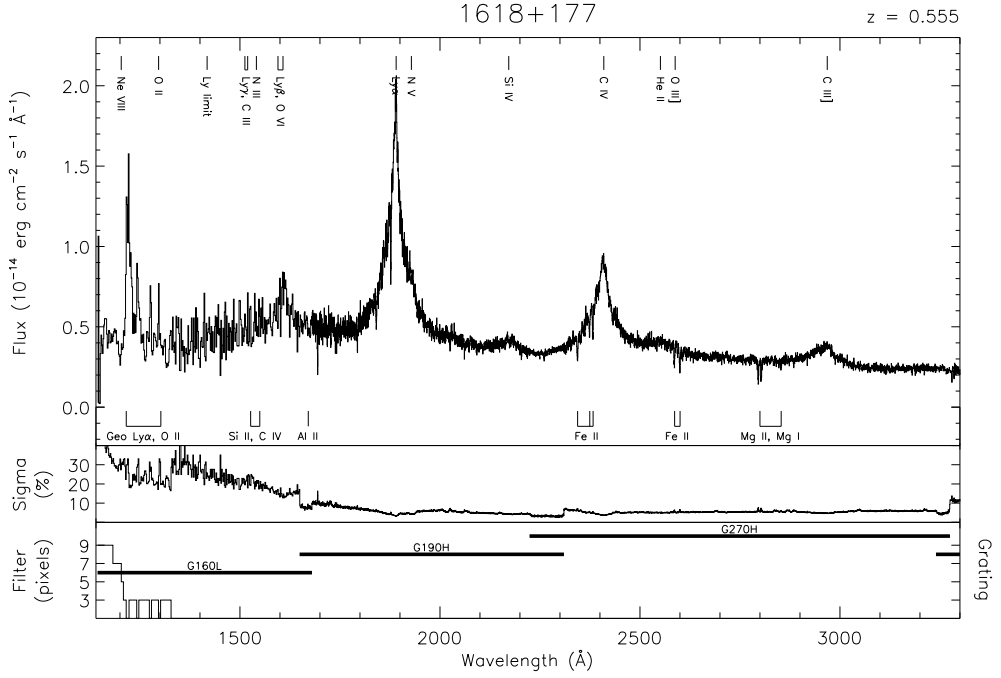
1618+177
z = 0.555
Ne VIII
O II
Ly limit
N III
Lyγ, C III
Lyβ, O VI
Lyα
N V
Si IV
C IV
He II
O III]
C III]
Flux (10^-14 erg cm^-2 s^-1 Å^-1)
Geo Lyα, O II
Si II, C IV
Al II
Fe II
Fe II
Mg II, Mg I
Sigma (%)
G270H
G190H
G160L
Filter (pixels)
Grating
Wavelength (Å)

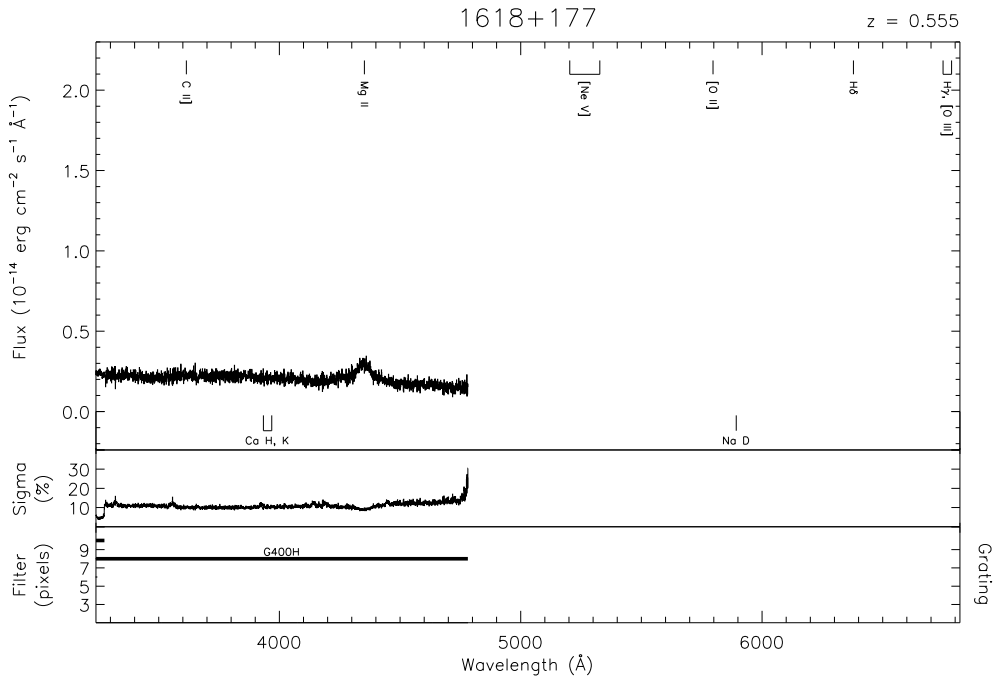
1618+177
z = 0.555
C II
Mg II
[Ne V]
[O II]
Hδ
Hγ, [O III]
Flux (10^{-14} erg cm^{-2} s^{-1} Å^{-1})
Ca H, K
Na D
Sigma (%)
Filter (pixels)
G400H
Grating
Wavelength (Å)

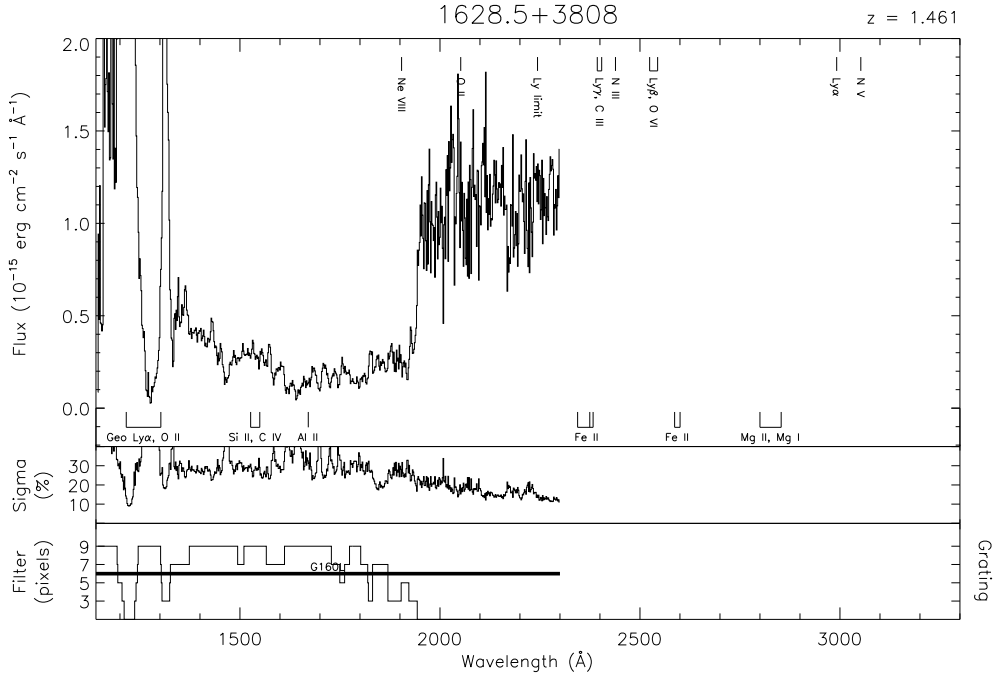
1628.5+3808
z = 1.461
Ne VIII
O VI
Ly limit
Lyγ, C III
N III
Lyβ, O VI
Lyα
N V
Flux (10^{-15} erg cm^{-2} s^{-1} Å^{-1})
Geo Lyα, O II
Si II, C IV
Al II
Fe II
Fe II
Mg II, Mg I
Sigma (%)
Filter (pixels)
G160L
Grating
Wavelength (Å)

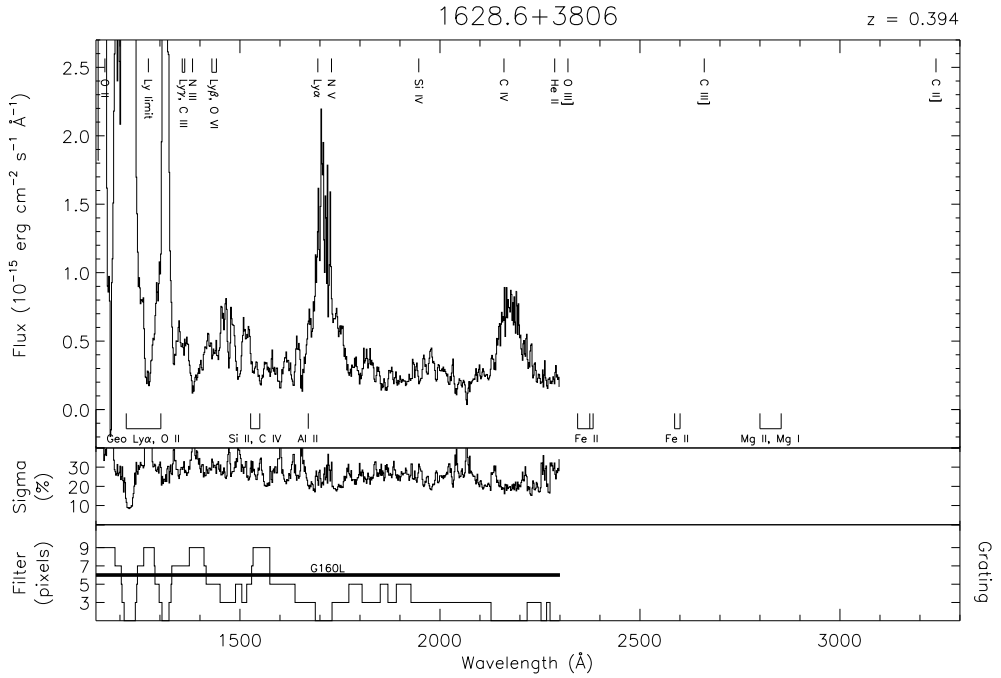
1628.6+3806
z = 0.394
Flux (10^{-15} erg cm^{-2} s^{-1} Å^{-1})
O I
Ly limit
N III
Lyγ, C III
Lyβ, O VI
N V
Lyα
Si IV
C IV
O III]
He II
C III]
C II]
Geo Lyα, O II
Si II, C IV
Al II
Fe II
Fe II
Mg II, Mg I
Sigma (%)
Filter (pixels)
G160L
Grating
Wavelength (Å)

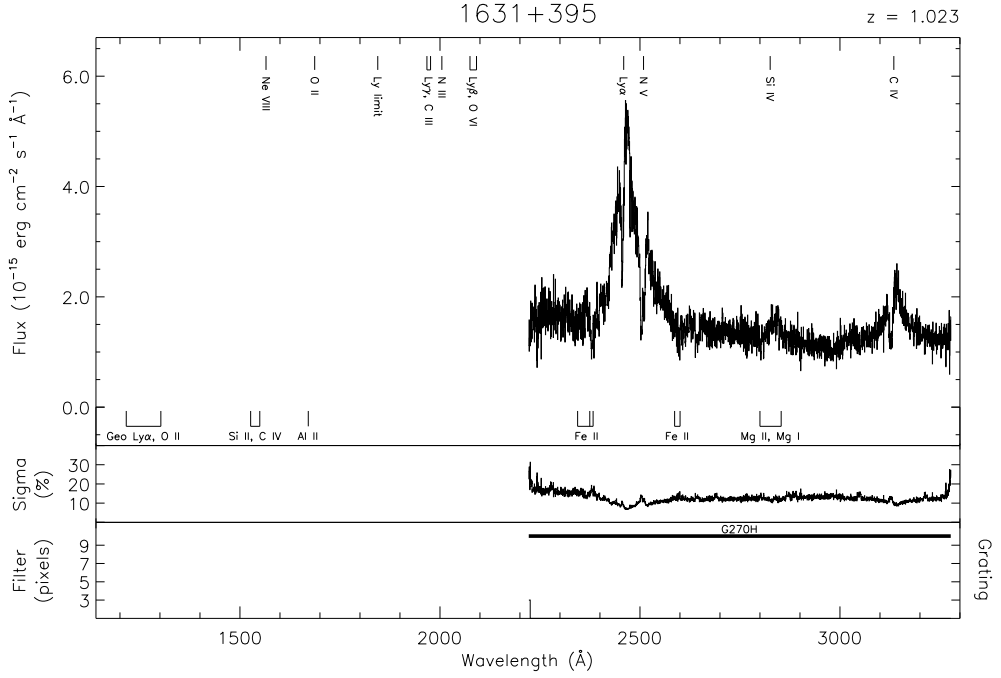
1631+395
z = 1.023
Flux (10^{-15} erg cm^{-2} s^{-1} Å^{-1})
Ne VIII
O II
Ly limit
N III
Lyγ, C III
Lyβ, O VI
N V
Lyα
Si IV
C IV
Geo Lyα, O II
Si II, C IV
Al II
Fe II
Fe II
Mg II, Mg I
Sigma (%)
Filter (pixels)
G270H
Grating
Wavelength (Å)

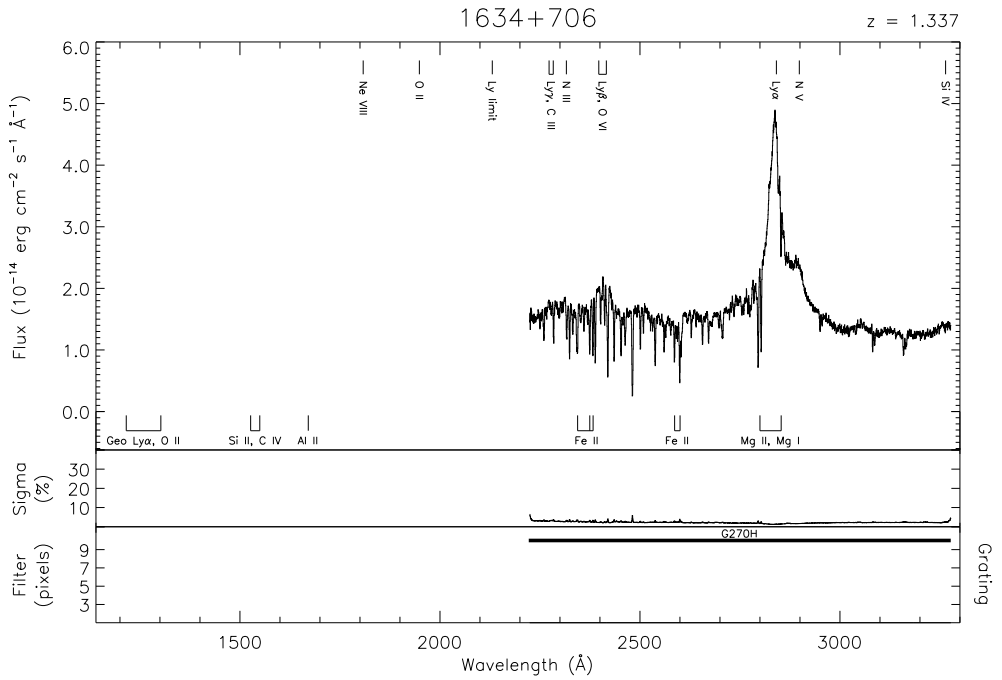
1634+706
z = 1.337
Flux (10^{-14} erg cm^{-2} s^{-1} Å^{-1})
Ne VIII
O II
Ly limit
Lyγ, C III
N III
Lyβ, O VI
Lyα
N V
Si IV
Geo Lyα, O II
Si II, C IV
Al II
Fe II
Fe II
Mg II, Mg I
Sigma (%)
G270H
Filter (pixels)
Grating
Wavelength (Å)

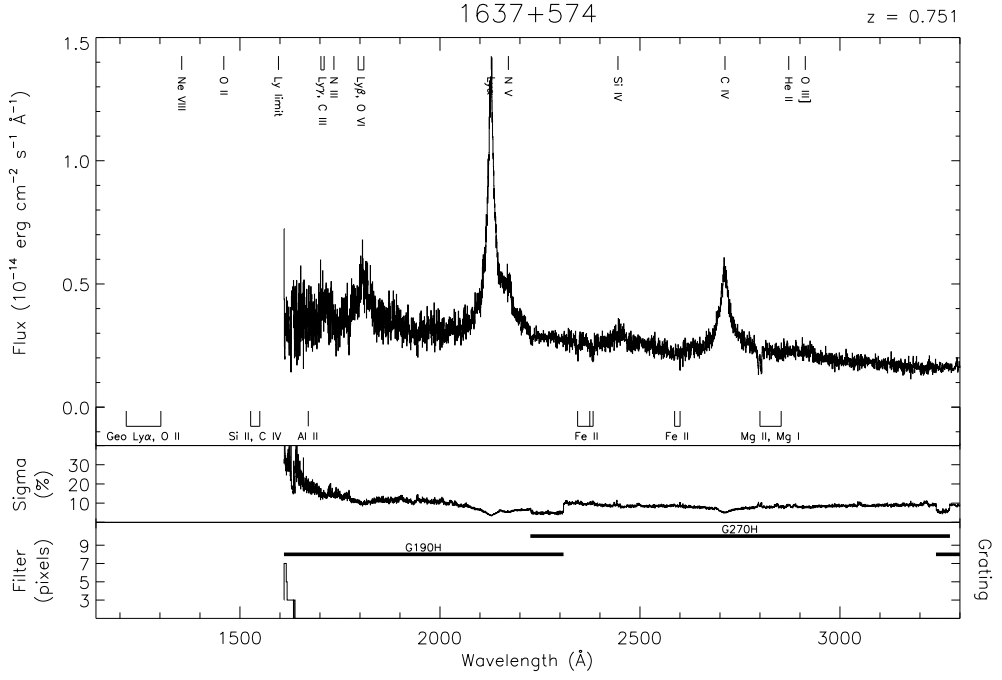
1637+574
z = 0.751
Flux (10^{-14} erg cm^{-2} s^{-1} Å^{-1})
Ne VIII
O II
Ly limit
Lyγ, C III
N III
Lyβ, O VI
Lyα
N V
Si IV
C IV
He II
O III]
Geo Lyα, O II
Si II, C IV
Al II
Fe II
Fe II
Mg II, Mg I
Sigma (%)
G190H
G270H
Filter (pixels)
Grating
Wavelength (Å)

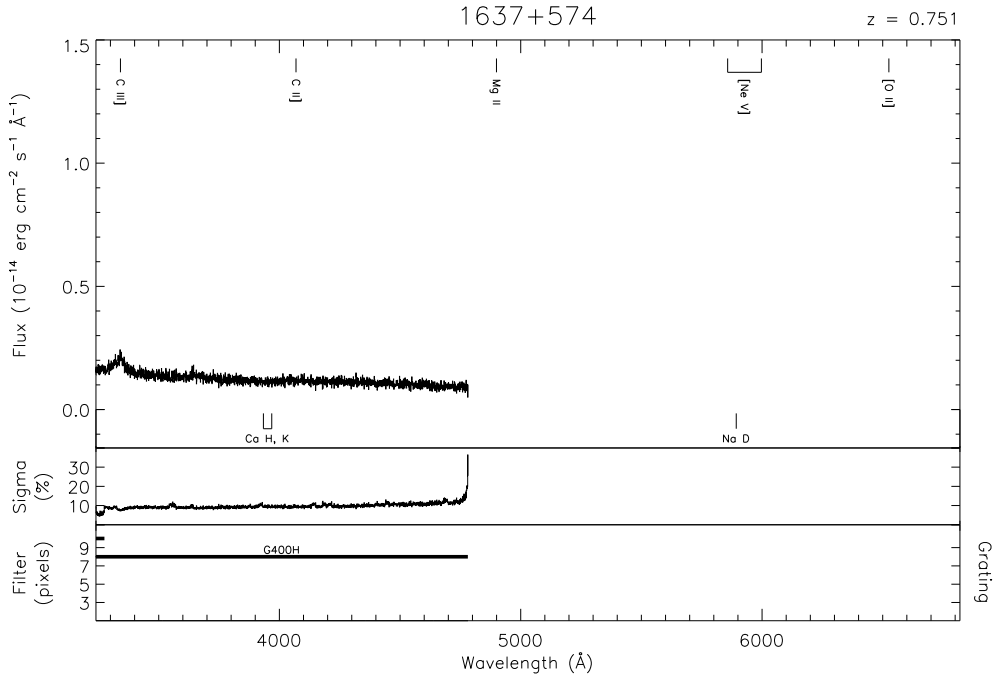
1637+574
z = 0.751
[O III]
C II]
Mg II
[Ne V]
[O II]
Flux (10^{-14} erg cm^{-2} s^{-1} Å^{-1})
Ca H, K
Na D
Sigma (%)
Filter (pixels)
G400H
Grating
Wavelength (Å)

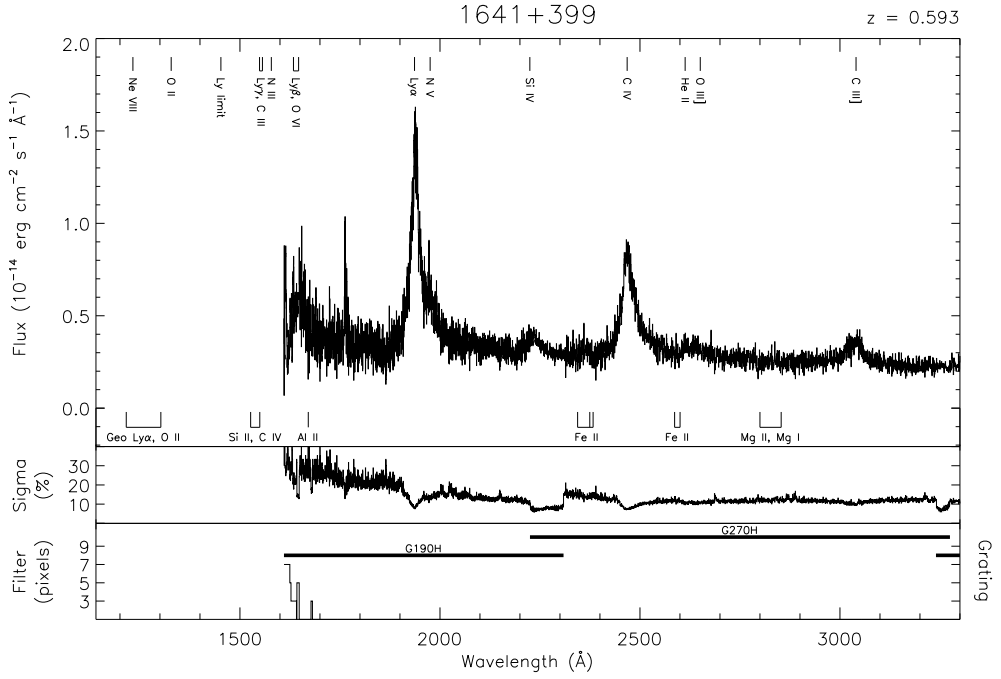
1641+399
z = 0.593
Ne VIII
O II
Ly limit
N III
Lyδ, O VI
Lyα
N V
Si IV
C IV
He II
O III]
C III]
Flux (10^{-14} erg cm^{-2} s^{-1} Å^{-1})
Geo Lyα, O II
Si II, C IV
Al II
Fe II
Fe II
Mg II, Mg I
Sigma (%)
Filter (pixels)
G190H
G270H
Grating
Wavelength (Å)

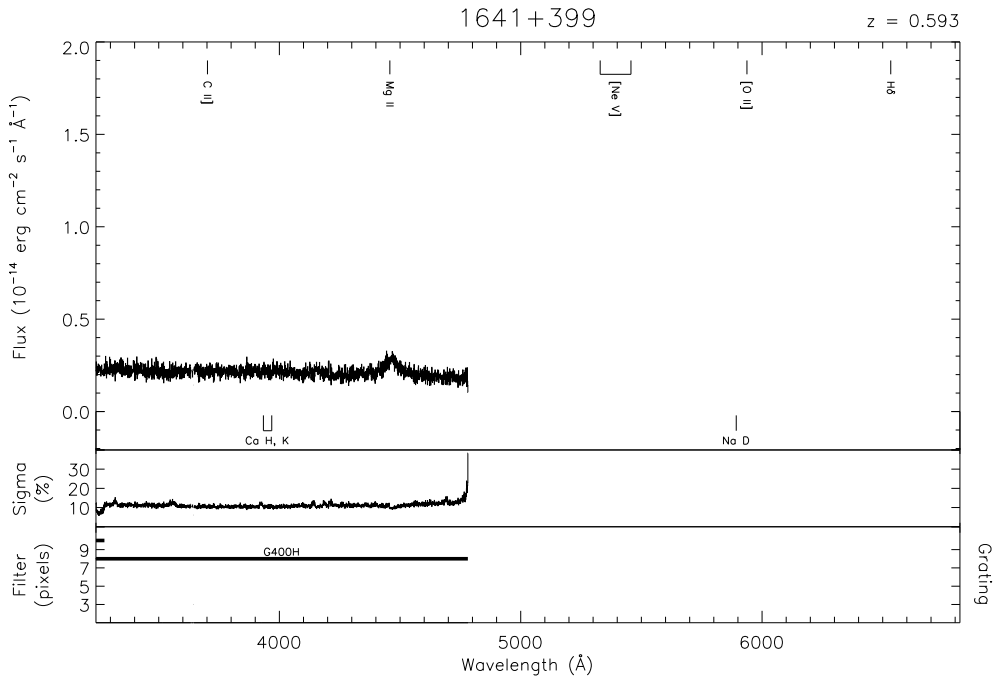
1641+399
z = 0.593
C II]
Mg II
[Ne V]
[O II]
H6
Ca H, K
Na D
G400H
Flux (10^{-14} erg cm^{-2} s^{-1} Å^{-1})
Sigma (%)
Filter (pixels)
Grating
Wavelength (Å)

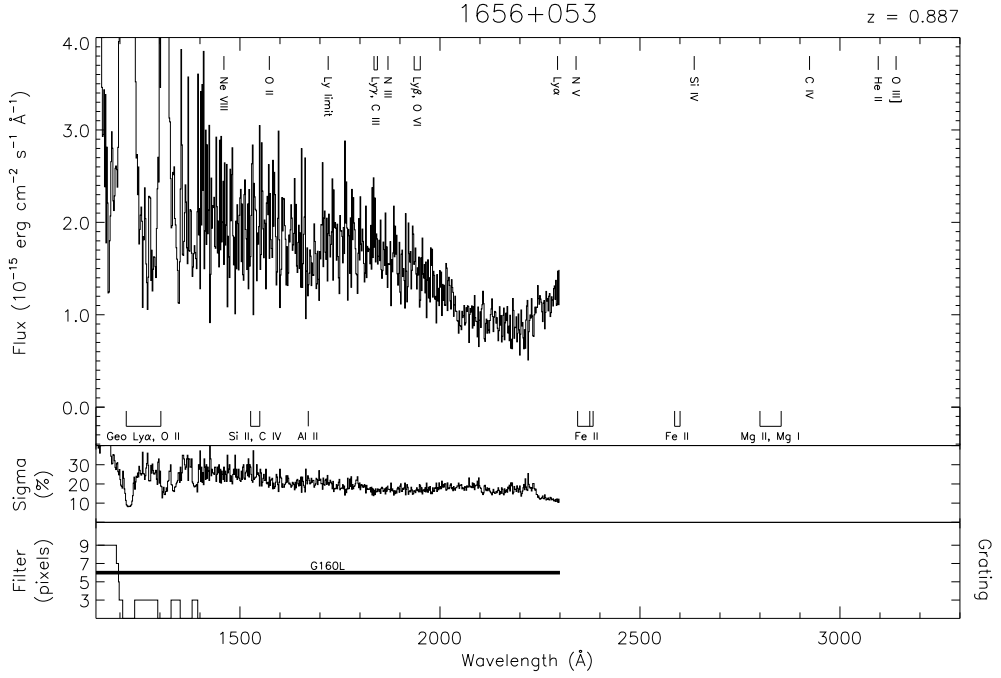
1656+053
z = 0.887
Ne VIII
O II
Ly limit
N III
Lyγ, C III
Lyβ, O VI
Lyα
N V
Si IV
C IV
He II
O III]
Geo Lyα, O II
Si II, C IV
Al II
Fe II
Fe II
Mg II, Mg I
G160L
Flux (10^{-15} erg cm^{-2} s^{-1} Å^{-1})
Sigma (%)
Filter (pixels)
Grating
Wavelength (Å)

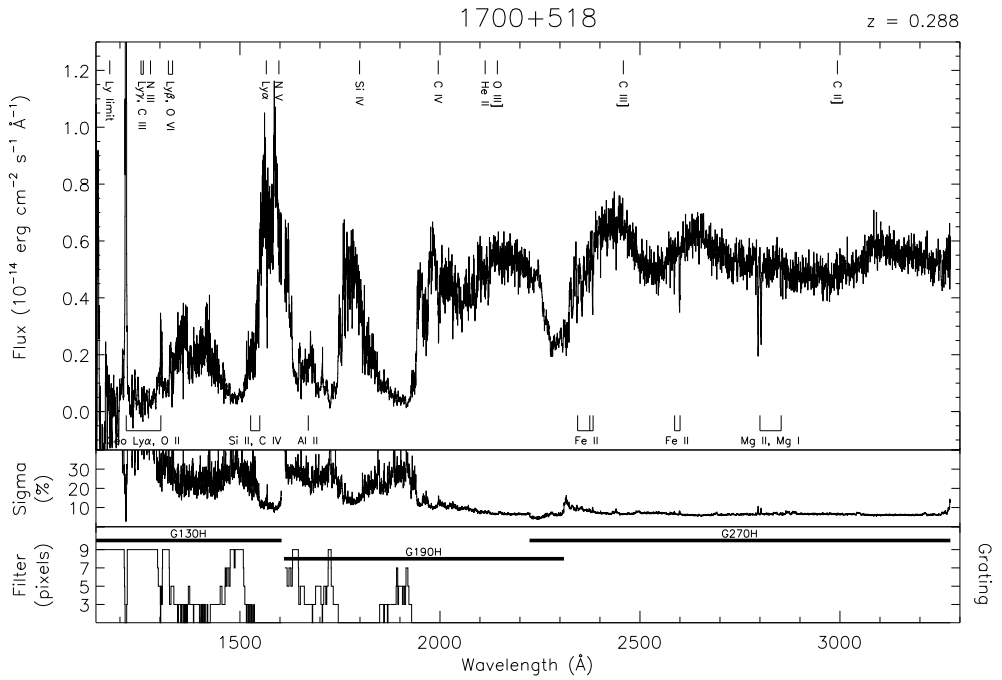
1700+518
z = 0.288
Flux (10^{-14} erg cm^{-2} s^{-1} Å^{-1})
Ly limit
N III, C III
Lyγ, O VI
Lyβ, O VI
Lyα
N V
Si IV
C IV
He II
O III]
C III]
C II]
Geo Lyα, O II
Si II, C IV
Al II
Fe II
Fe II
Mg II, Mg I
Sigma (%)
G130H
G190H
G270H
Filter (pixels)
Grating
Wavelength (Å)

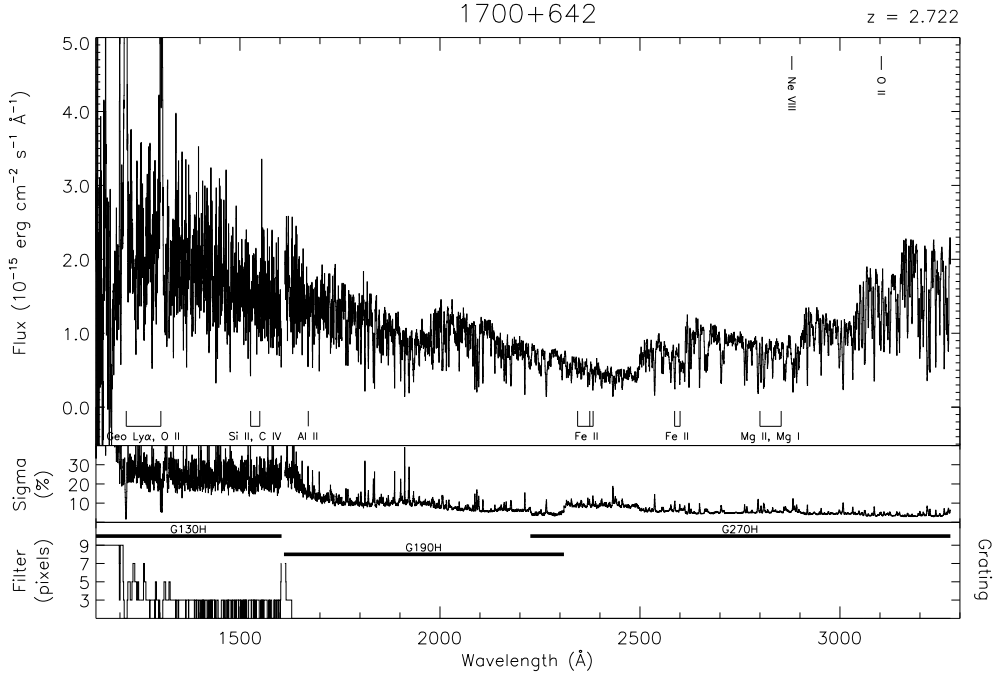
1700+642
z = 2.722
Flux (10^{-15} erg cm^{-2} s^{-1} Å^{-1})
Ne VIII
O II
Geo Lyα, O II
Si II, C IV
Al II
Fe II
Fe II
Mg II, Mg I
Sigma (%)
G130H
G190H
G270H
Filter (pixels)
Grating
Wavelength (Å)

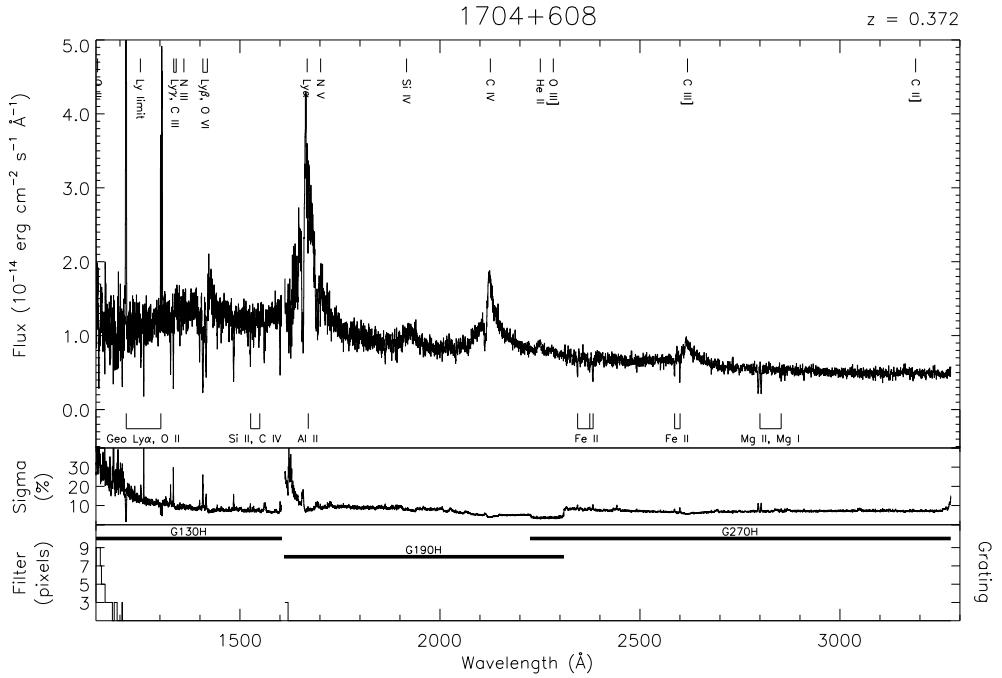
1704+608
z = 0.372
Flux (10^{-14} erg cm^{-2} s^{-1} Å^{-1})
Ly limit
N III, C III
Lyβ, O VI
N V
Lyα
Si IV
C IV
O III]
He II
C III]
C II]
Geo Lyα, O II
Si II, C IV
Al II
Fe II
Fe II
Mg II, Mg I
Sigma (%)
G130H
G190H
G270H
Filter (pixels)
Grating
Wavelength (Å)

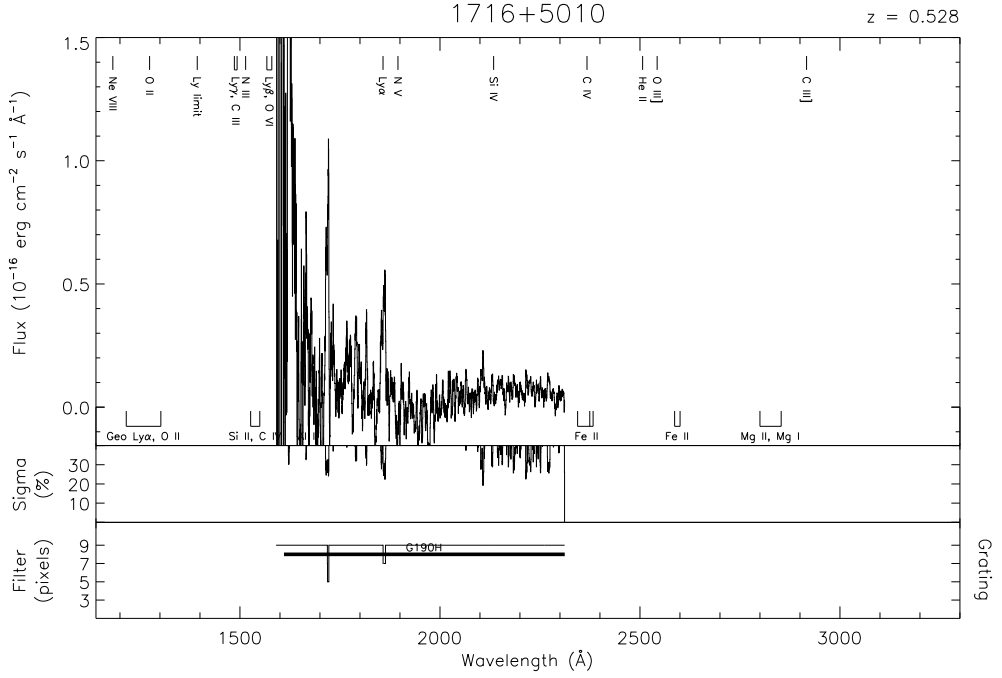
1716+5010
z = 0.528
Flux (10^{-16} erg cm^{-2} s^{-1} Å^{-1})
Ne VIII
O II
Ly limit
N III, C III
Lyβ, O VI
N V
Lyα
Si IV
C IV
O III]
He II
C III]
Geo Lyα, O II
Si II, C II
Fe II
Fe II
Mg II, Mg I
Sigma (%)
G190H
Filter (pixels)
Grating
Wavelength (Å)

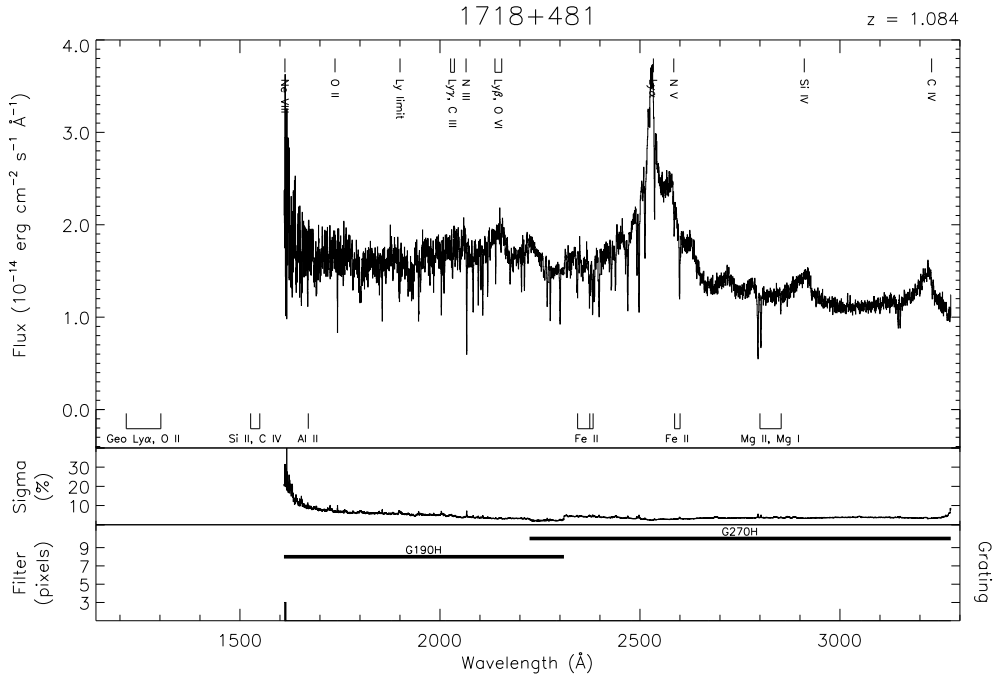
1718+481
z = 1.084
Flux (10^{-14} erg cm^{-2} s^{-1} Å^{-1})
Ne VIII
O II
Ly limit
N III
Lyγ, C III
Lyβ, O VI
Lyα
N V
Si IV
C IV
Geo Lyα, O II
Si II, C IV
Al II
Fe II
Fe II
Mg II, Mg I
Sigma (%)
G270H
G190H
Filter (pixels)
Grating
Wavelength (Å)

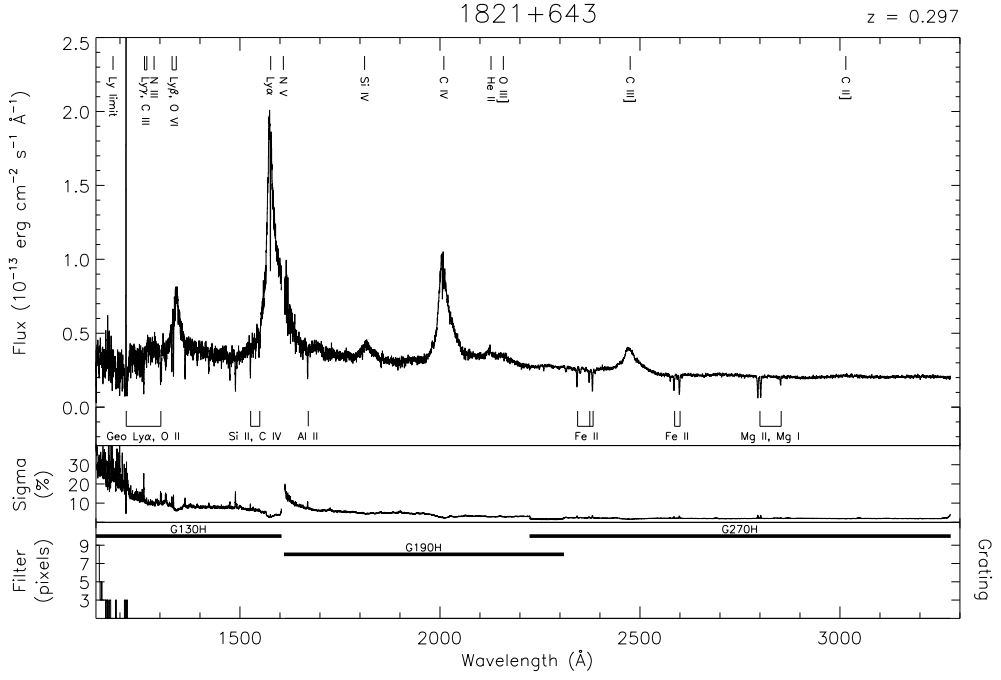
1821+643
z = 0.297
Flux (10^{-13} erg cm^{-2} s^{-1} Å^{-1})
Ly limit
N III
Lyγ, C III
Lyβ, O VI
N V
Lyα
Si IV
C IV
O III]
He II
C III]
C II]
Geo Lyα, O II
Si II, C IV
Al II
Fe II
Fe II
Mg II, Mg I
Sigma (%)
G130H
G270H
G190H
Filter (pixels)
Grating
Wavelength (Å)

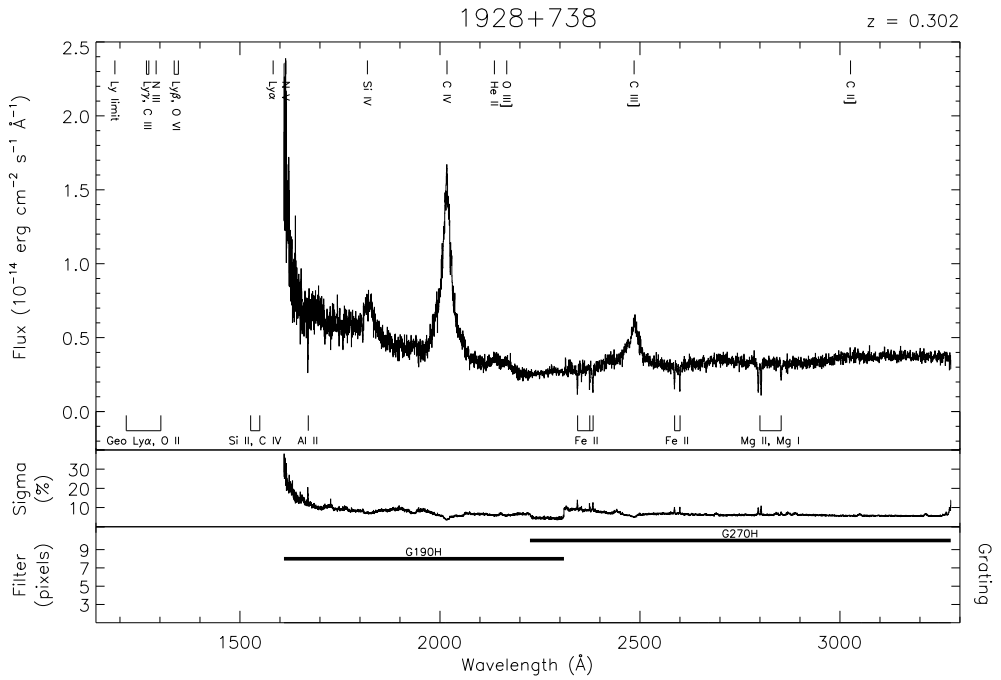
1928+738
z = 0.302
Flux (10^{-14} erg cm^{-2} s^{-1} Å^{-1})
Ly limit
N III, C III, Lyγ
Lyβ, O VI
N V, Lyα
Si IV
C IV
He II, O III]
C III]
C II]
Geo Lyα, O II
Si II, C IV
Al II
Fe II
Fe II
Mg II, Mg I
Sigma (%)
Filter (pixels)
G270H
G190H
Grating
Wavelength (Å)

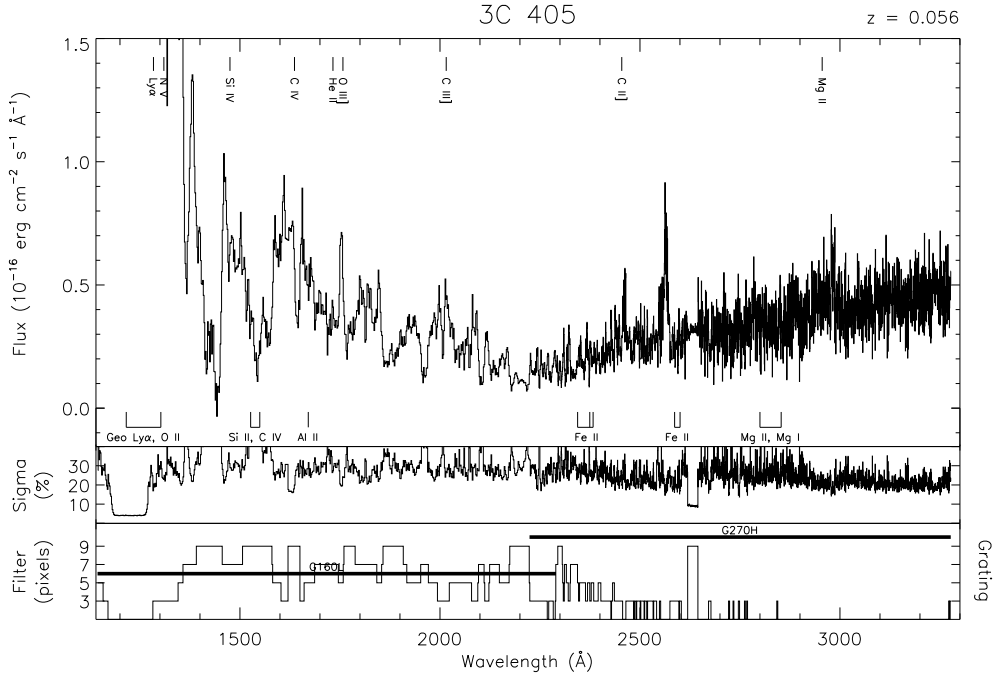
3C 405
z = 0.056
Flux (10^{-16} erg cm^{-2} s^{-1} Å^{-1})
N V, Lyα
Si IV
C IV
He II, O III]
C III]
C II]
Mg II
Geo Lyα, O II
Si II, C IV
Al II
Fe II
Fe II
Mg II, Mg I
Sigma (%)
Filter (pixels)
G270H
G160L
Grating
Wavelength (Å)

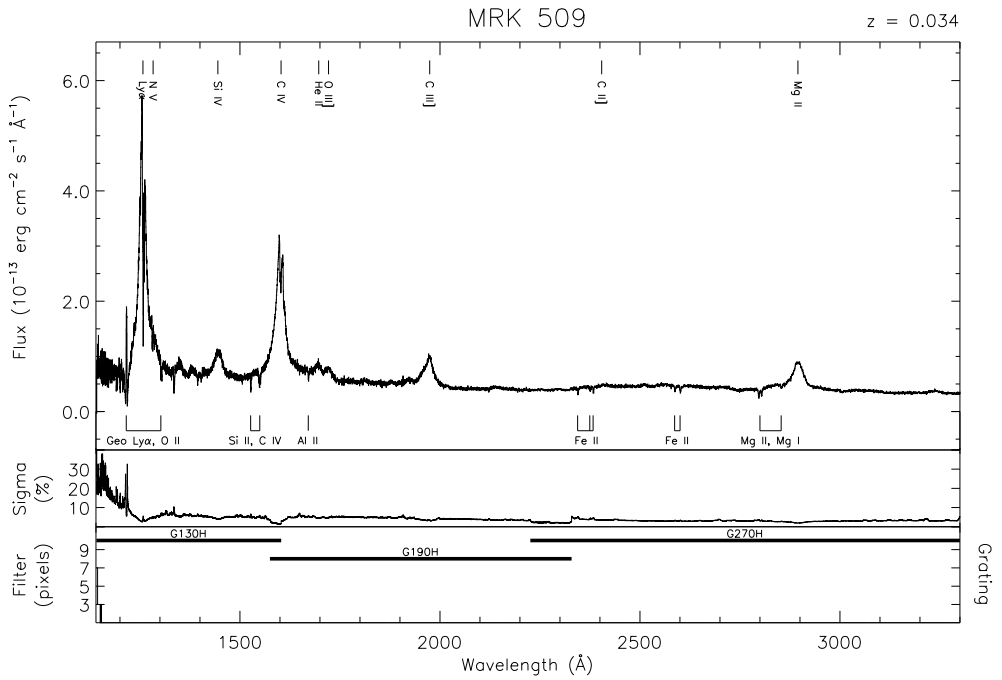
MRK 509
z = 0.034
Flux (10^{-13} erg cm^{-2} s^{-1} Å^{-1})
N V Lyα
Si IV
C IV
O III] He II
C III]
C II]
Mg II
Geo Lyα, O II
Si II, C IV
Al II
Fe II
Fe II
Mg II, Mg I
Sigma (%)
G130H
G270H
G190H
Filter (pixels)
Grating
Wavelength (Å)

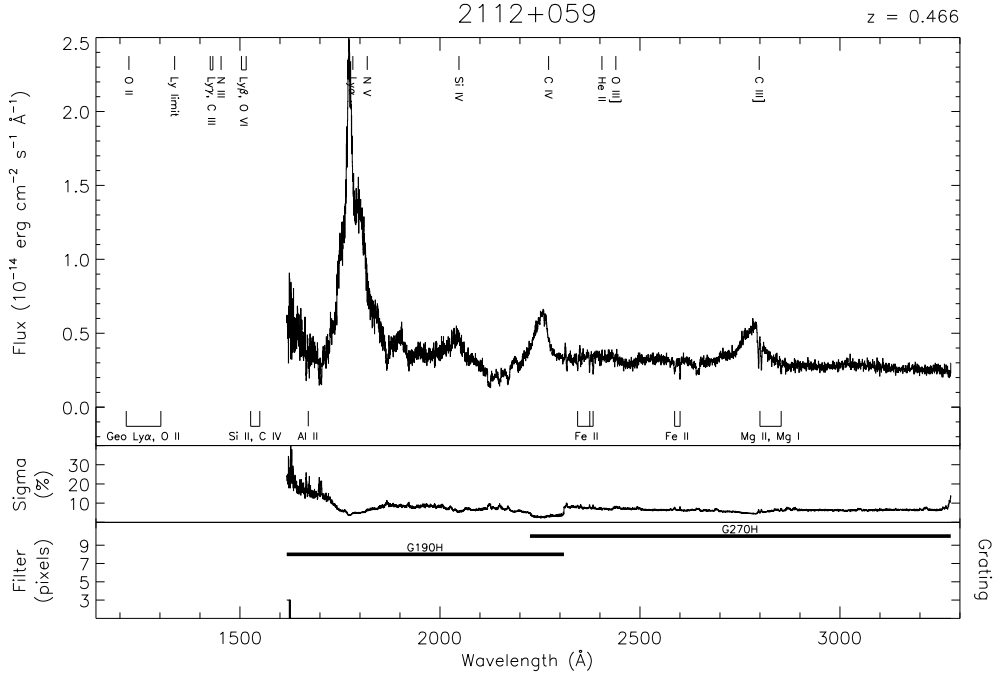
2112+059
z = 0.466
Flux (10^{-14} erg cm^{-2} s^{-1} Å^{-1})
O II
Ly limit
N III Lyγ, C III
Lyβ, O VI
N V Lyα
Si IV
C IV
O III] He II
C III]
Geo Lyα, O II
Si II, C IV
Al II
Fe II
Fe II
Mg II, Mg I
Sigma (%)
G270H
G190H
Filter (pixels)
Grating
Wavelength (Å)

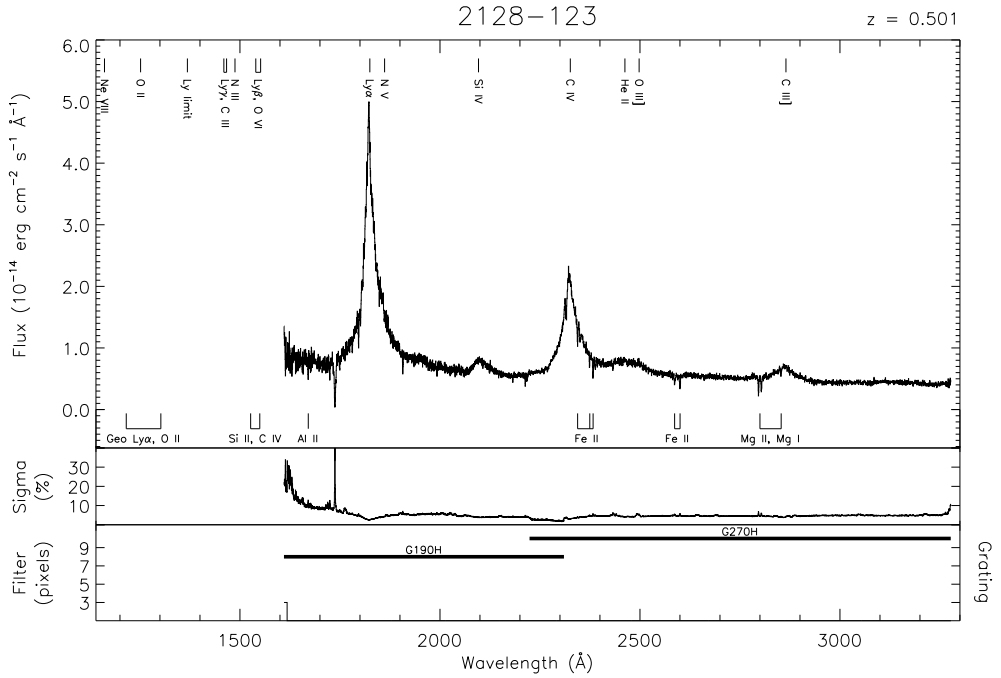
2128−123
z = 0.501
Flux (10^{-14} erg cm^{-2} s^{-1} Å^{-1})
Ne VIII
O II
Ly limit
N III
Lyγ, C III
Lyβ, O VI
Lyα
N V
Si IV
C IV
He II
O III]
C III]
Geo Lyα, O II
Si II, C IV
Al II
Fe II
Fe II
Mg II, Mg I
Sigma (%)
G270H
G190H
Filter (pixels)
Grating
Wavelength (Å)

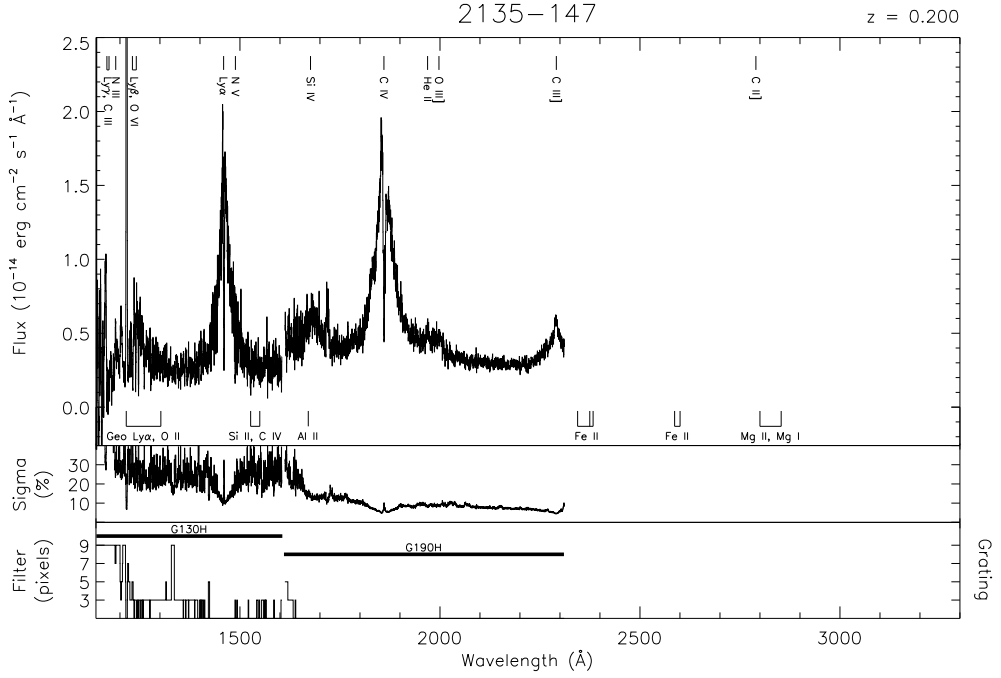
2135−147
z = 0.200
Flux (10^{-14} erg cm^{-2} s^{-1} Å^{-1})
N III
Lyγ, C III
Lyβ, O VI
N V
Lyα
Si IV
C IV
He II
O III]
C III]
C II]
Geo Lyα, O II
Si II, C IV
Al II
Fe II
Fe II
Mg II, Mg I
Sigma (%)
G130H
G190H
Filter (pixels)
Grating
Wavelength (Å)

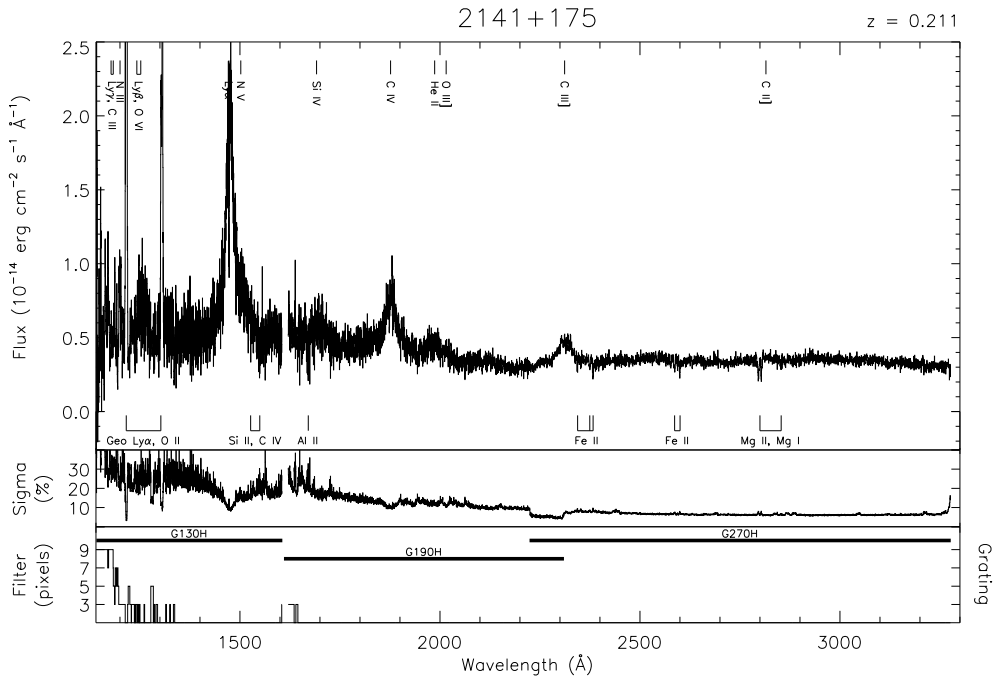
2141+175
z = 0.211
Flux (10^{-14} erg cm^{-2} s^{-1} Å^{-1})
Lyγ, C III
N III
Lyβ, O VI
Lyα
N V
Si IV
C IV
He II
O III]
C III]
C II]
Geo Lyα, O II
Si II, C IV
Al II
Fe II
Fe II
Mg II, Mg I
Sigma (%)
G130H
G190H
G270H
Filter (pixels)
Grating
Wavelength (Å)

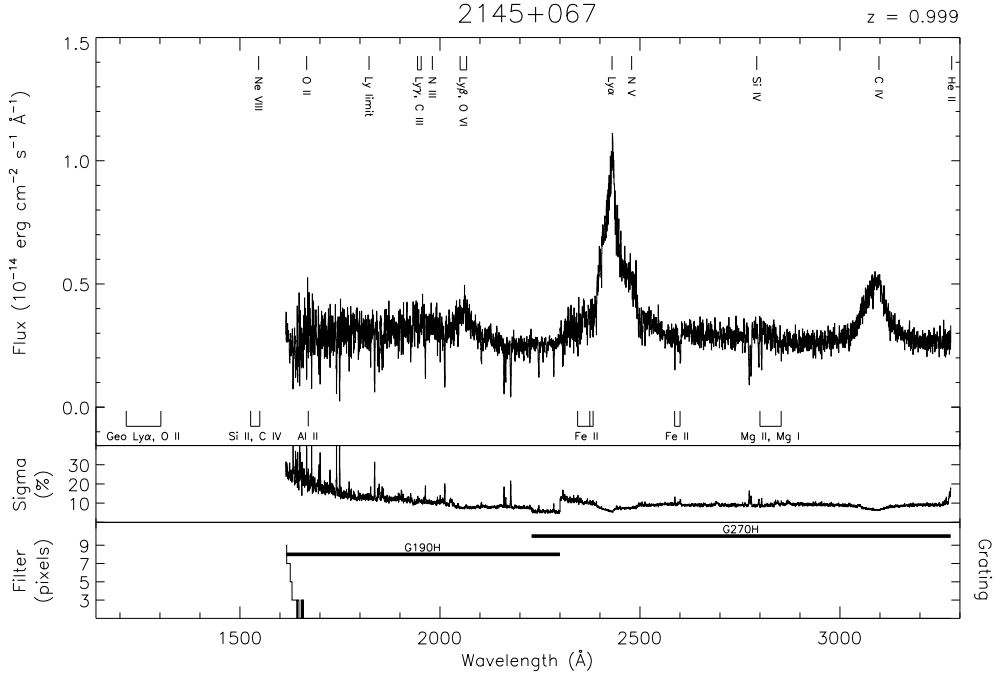
2145+067
z = 0.999
Flux (10^{-14} erg cm^{-2} s^{-1} Å^{-1})
Ne VIII
O II
Ly limit
N III
Lyγ, C III
Lyβ, O VI
Lyα
N V
Si IV
C IV
He II
Geo Lyα, O II
Si II, C IV
Al II
Fe II
Fe II
Mg II, Mg I
Sigma (%)
G190H
G270H
Filter (pixels)
Grating
Wavelength (Å)

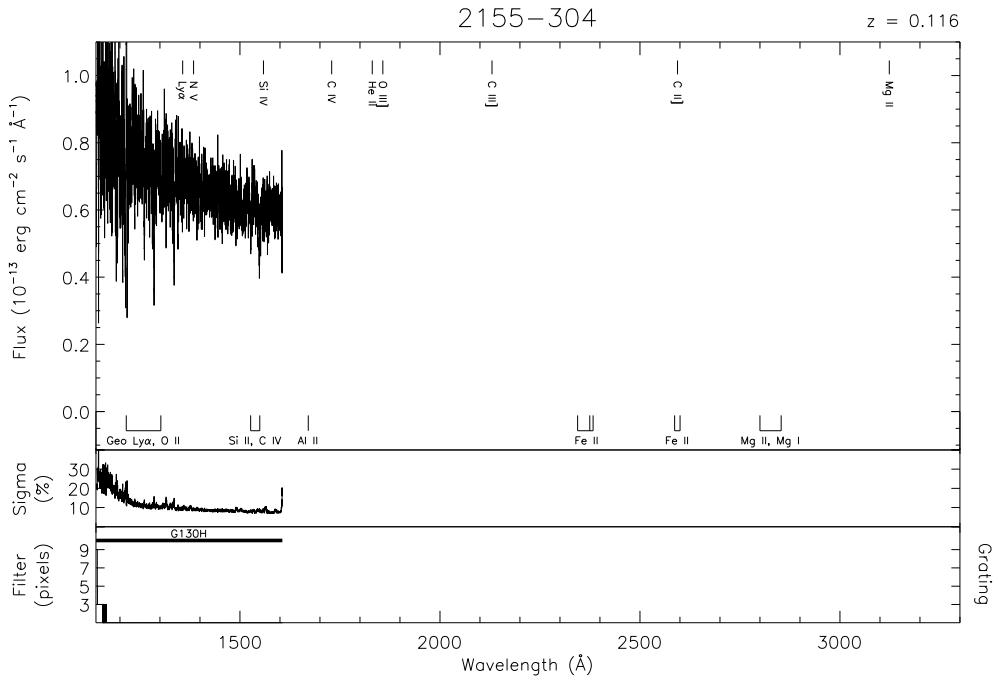
2155−304
z = 0.116
Flux (10^{-13} erg cm^{-2} s^{-1} Å^{-1})
N V Lyα
Si IV
C IV
O III] He II
C III]
C II]
Mg II
Geo Lyα, O II
Si II, C IV
Al II
Fe II
Fe II
Mg II, Mg I
Sigma (%)
G130H
Filter (pixels)
Grating
Wavelength (Å)

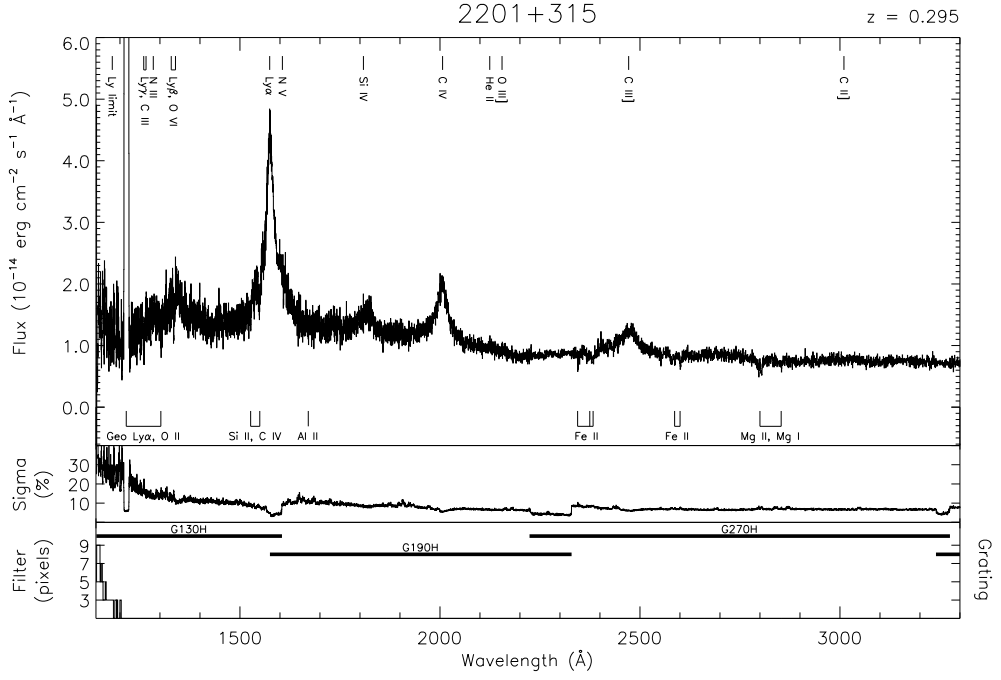
2201+315
z = 0.295
Flux (10^{-14} erg cm^{-2} s^{-1} Å^{-1})
Ly limit
N III Lyγ, C III
Lyβ, O VI
N V Lyα
Si IV
C IV
O III] He II
C III]
C II]
Geo Lyα, O II
Si II, C IV
Al II
Fe II
Fe II
Mg II, Mg I
Sigma (%)
G130H
G190H
G270H
Filter (pixels)
Grating
Wavelength (Å)

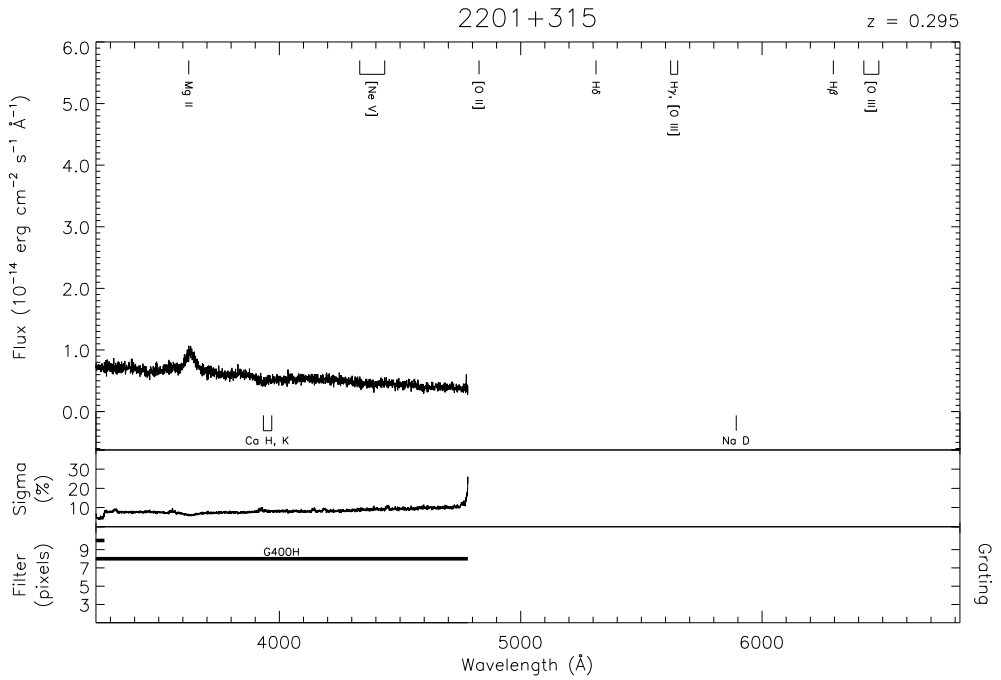
2201+315
z = 0.295
Mg II
[Ne V]
[O II]
Hδ
Hγ, [O III]
Hβ
[O III]
Ca H, K
Na D
G400H
Flux (10^{-14} erg cm^{-2} s^{-1} Å^{-1})
Sigma (%)
Filter (pixels)
Grating
Wavelength (Å)

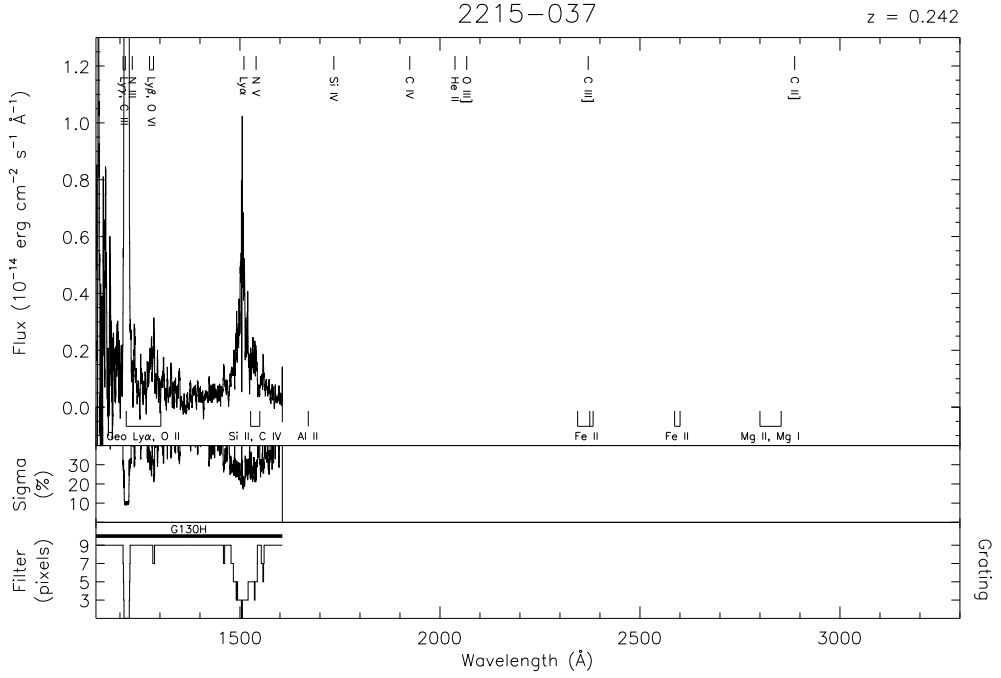
2215−037
z = 0.242
Lyβ, O VI
Lyα
N V
Si IV
C IV
He II
O III]
C III]
C II]
Geo Lyα, O II
Si II, C IV
Al II
Fe II
Fe II
Mg II, Mg I
G130H
Flux (10^{-14} erg cm^{-2} s^{-1} Å^{-1})
Sigma (%)
Filter (pixels)
Grating
Wavelength (Å)

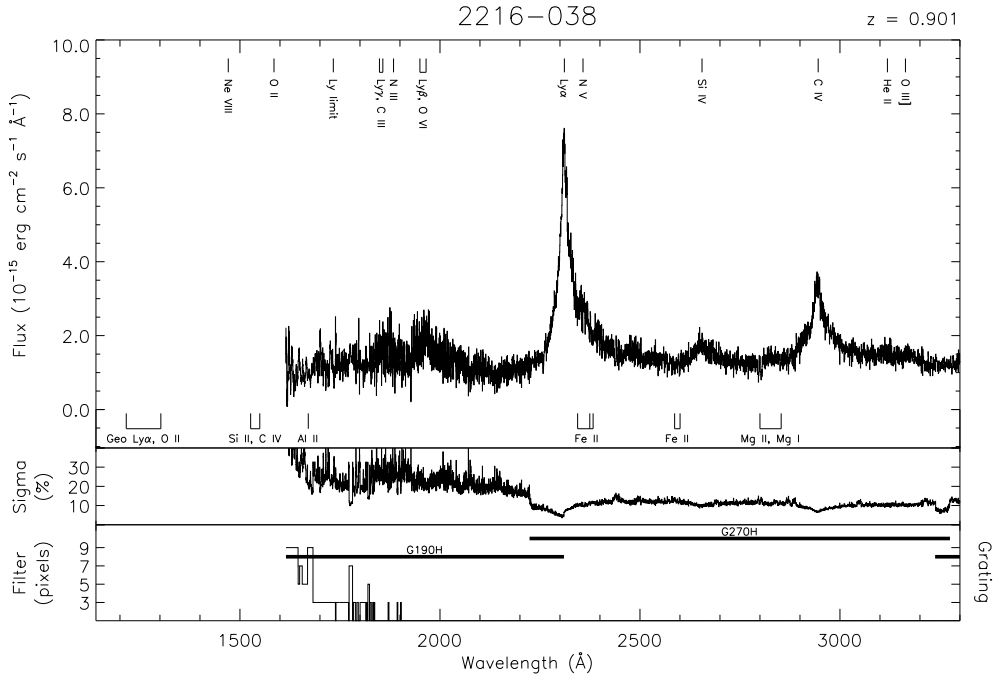
2216−038
z = 0.901
Flux (10^{-15} erg cm^{-2} s^{-1} Å^{-1})
Ne VIII
O II
Ly limit
N III
Lyγ, C III
Lyβ, O VI
Lyα
N V
Si IV
C IV
He II
O III]
Geo Lyα, O II
Si II, C IV
Al II
Fe II
Fe II
Mg II, Mg I
Sigma (%)
G270H
G190H
Filter (pixels)
Grating
Wavelength (Å)

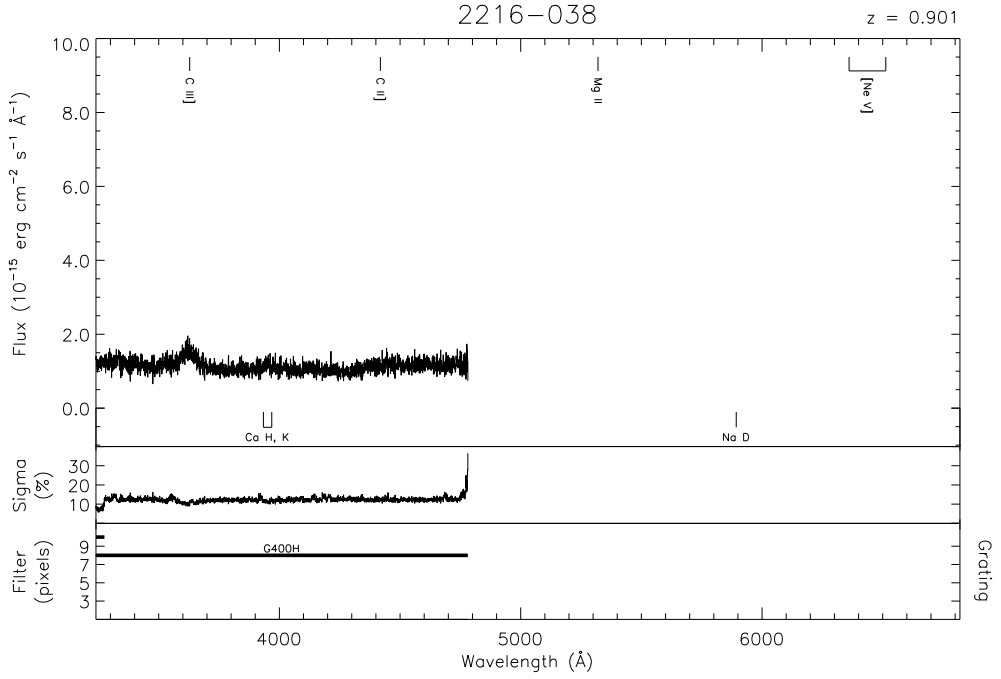
2216−038
z = 0.901
Flux (10^{-15} erg cm^{-2} s^{-1} Å^{-1})
[III] C
C II]
Mg II
[Ne V]
Ca H, K
Na D
Sigma (%)
G400H
Filter (pixels)
Grating
Wavelength (Å)

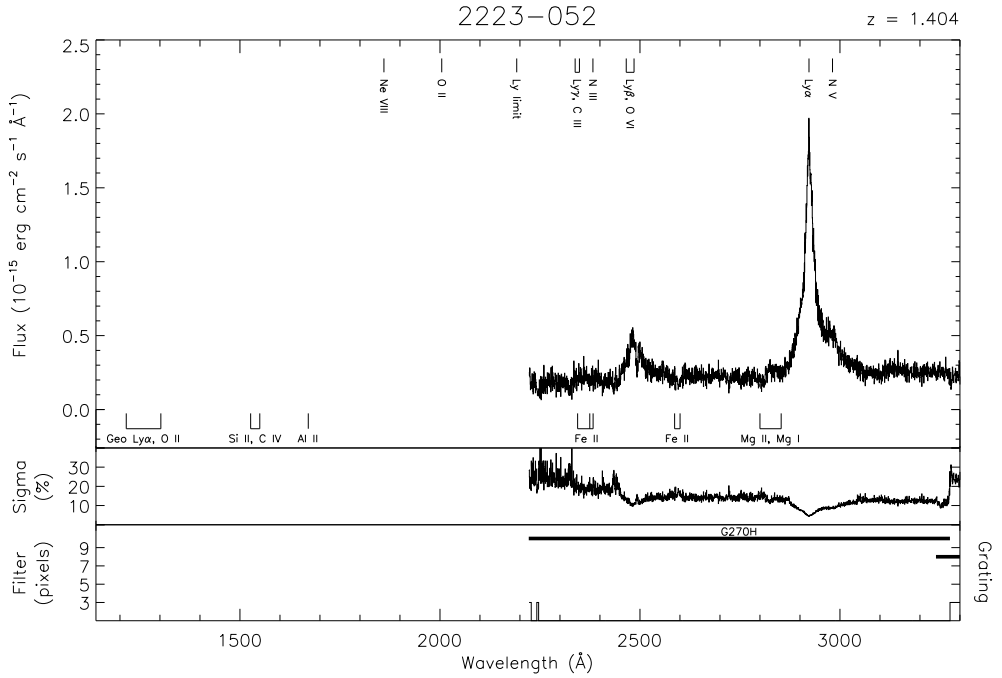
2223−052
z = 1.404
Flux (10^{-15} erg cm^{-2} s^{-1} Å^{-1})
Ne VIII
O II
Ly limit
Lyε, C III
N III
Lyδ, O VI
Lyα
N V
Geo Lyα, O II
Si II, C IV
Al II
Fe II
Fe II
Mg II, Mg I
Sigma (%)
G270H
Filter (pixels)
Grating
Wavelength (Å)

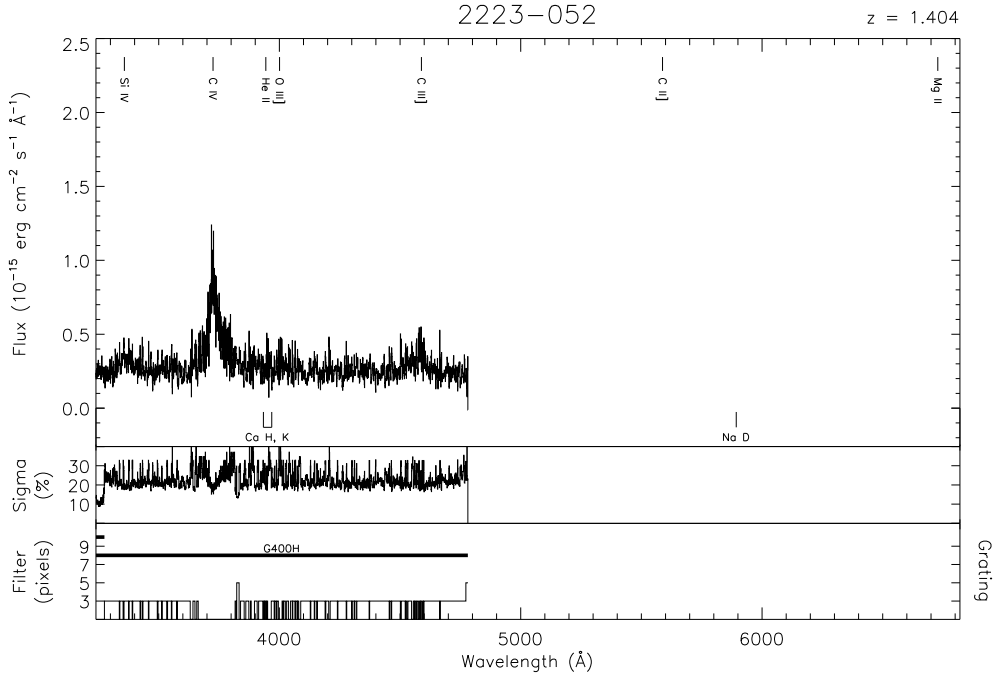
2223−052
z = 1.404
Flux (10^{-15} erg cm^{-2} s^{-1} Å^{-1})
Si IV
C IV
He II
O III]
C III]
C II]
Mg II
Ca H, K
Na D
Sigma (%)
G400H
Filter (pixels)
Grating
Wavelength (Å)

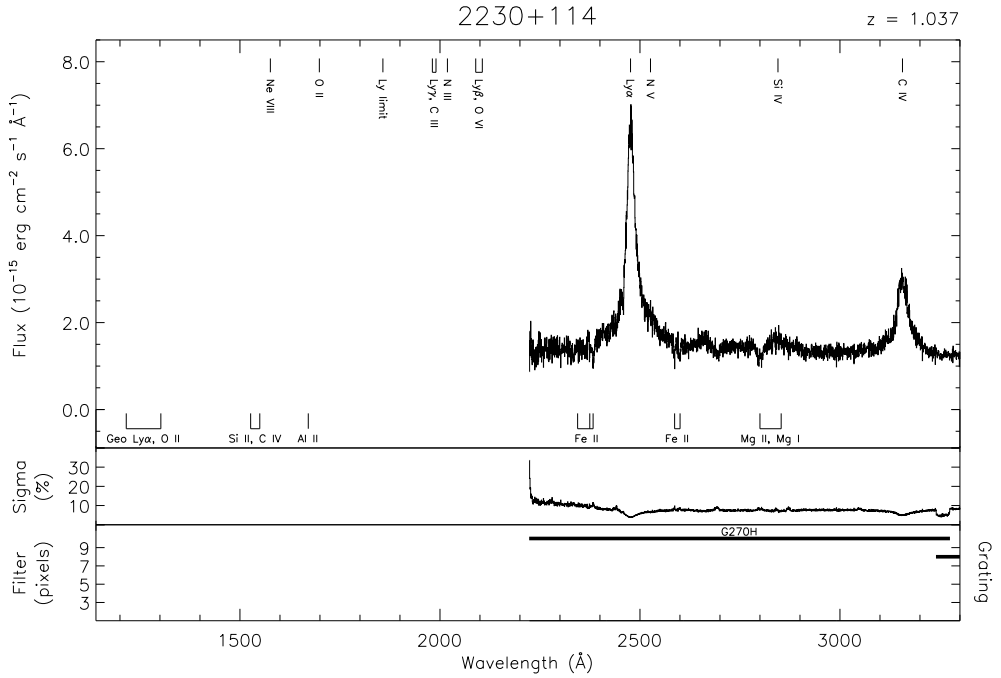
2230+114
z = 1.037
Flux (10^{-15} erg cm^{-2} s^{-1} Å^{-1})
Ne VIII
O II
Ly limit
N III
Lyγ, C III
Lyβ, O VI
Lyα
N V
Si IV
C IV
Geo Lyα, O II
Si II, C IV
Al II
Fe II
Fe II
Mg II, Mg I
Sigma (%)
G270H
Filter (pixels)
Grating
Wavelength (Å)

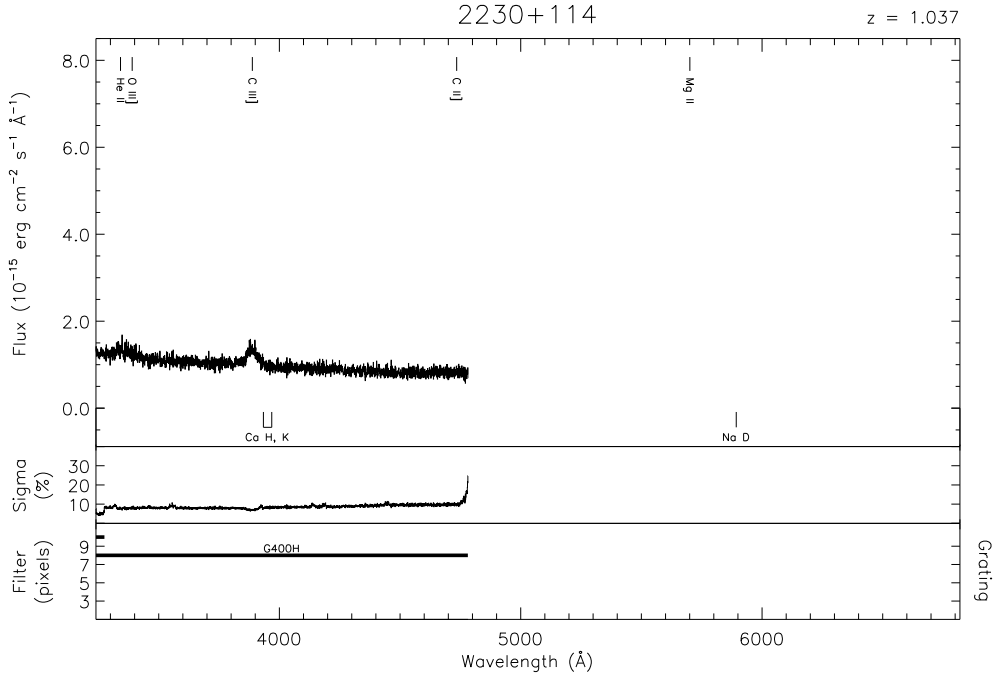
2230+114
z = 1.037
Flux (10^{-15} erg cm^{-2} s^{-1} Å^{-1})
He II
O III]
C III]
C II]
Mg II
Ca H, K
Na D
Sigma (%)
G400H
Filter (pixels)
Grating
Wavelength (Å)

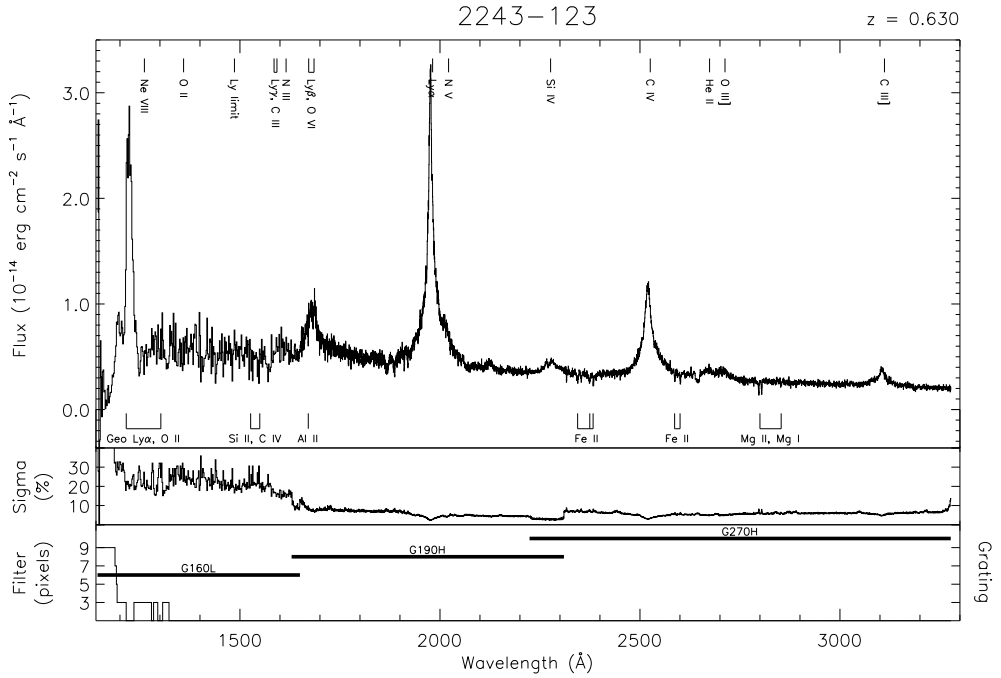
2243−123
z = 0.630
Flux (10^{-14} erg cm^{-2} s^{-1} Å^{-1})
Ne VIII
O II
Ly limit
N III
Lyγ, C III
Lyβ, O VI
Lyα
N V
Si IV
C IV
He II
O III]
C III]
Geo Lyα, O II
Si II, C IV
Al II
Fe II
Fe II
Mg II, Mg I
Sigma (%)
Filter (pixels)
G160L
G190H
G270H
Grating
Wavelength (Å)

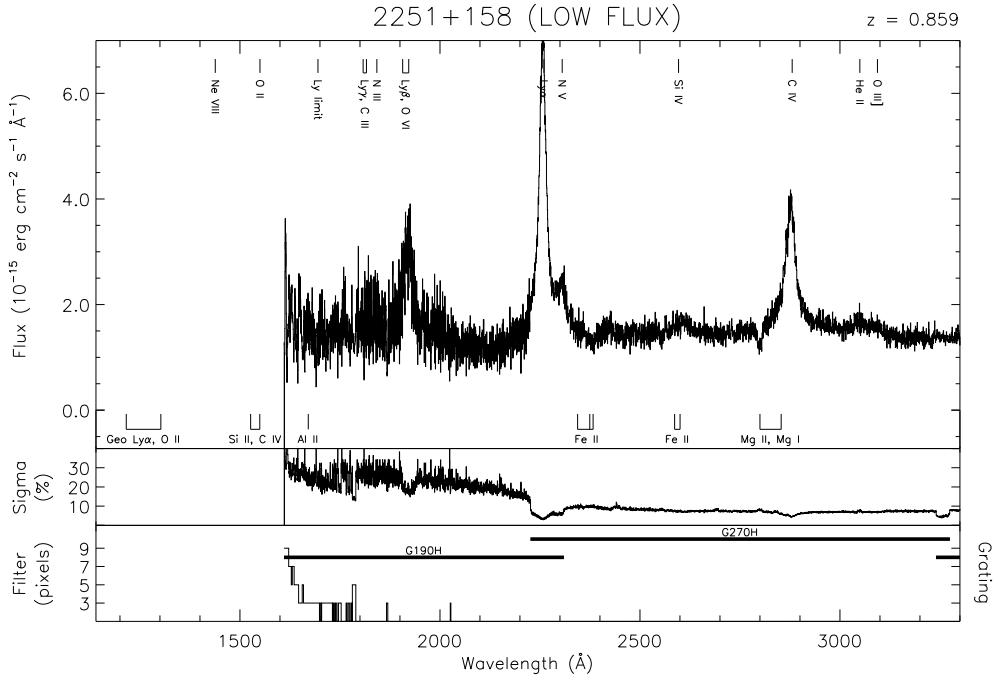
2251+158 (LOW FLUX)
z = 0.859
Flux (10^{-15} erg cm^{-2} s^{-1} Å^{-1})
Ne VIII
O II
Ly limit
N III
Lyγ, C III
Lyβ, O VI
Lyα
N V
Si IV
C IV
He II
O III]
Geo Lyα, O II
Si II, C IV
Al II
Fe II
Fe II
Mg II, Mg I
Sigma (%)
Filter (pixels)
G190H
G270H
Grating
Wavelength (Å)

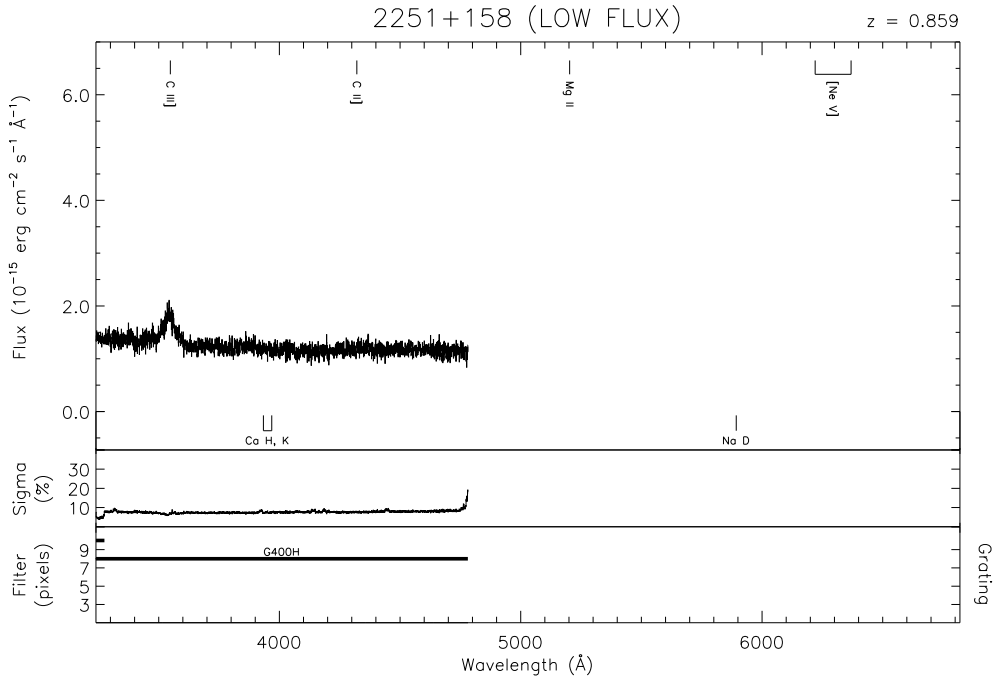
2251+158 (LOW FLUX)
z = 0.859
C III]
C I]
Mg II
[Ne V]
Ca H, K
Na D
G400H
Flux (10^-15 erg cm^-2 s^-1 Å^-1)
Sigma (%)
Filter (pixels)
Grating
Wavelength (Å)

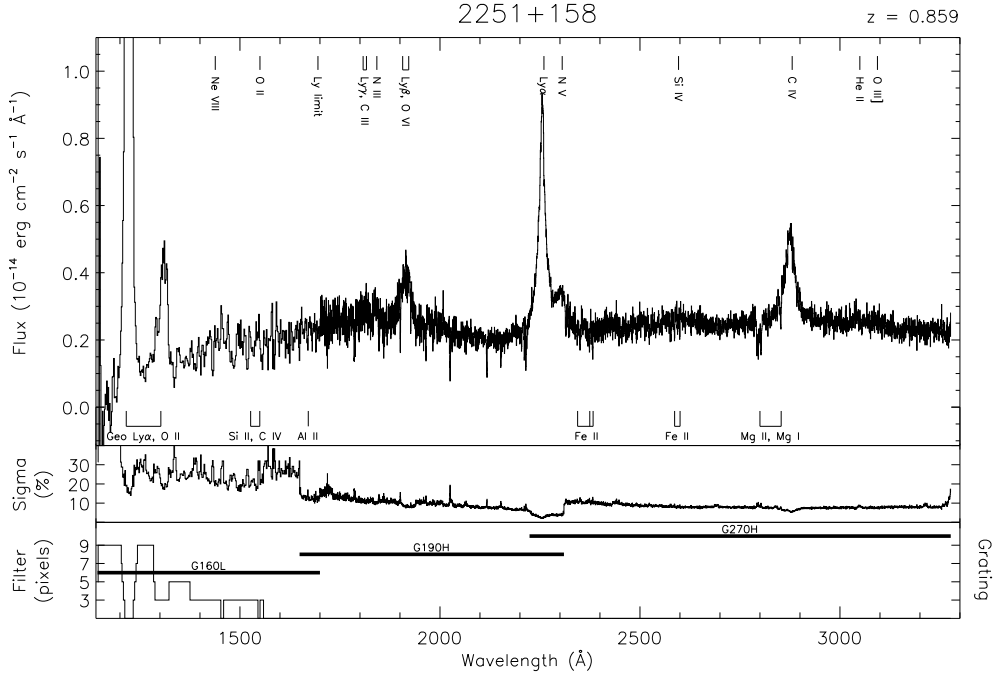
2251+158
z = 0.859
Ne VIII
O II
Ly limit
N III
Lyγ, C III
Lyβ, O VI
Lyα
N V
Si IV
C IV
He II
O III]
Geo Lyα, O II
Si II, C IV
Al II
Fe II
Fe II
Mg II, Mg I
G160L
G190H
G270H
Flux (10^-14 erg cm^-2 s^-1 Å^-1)
Sigma (%)
Filter (pixels)
Grating
Wavelength (Å)

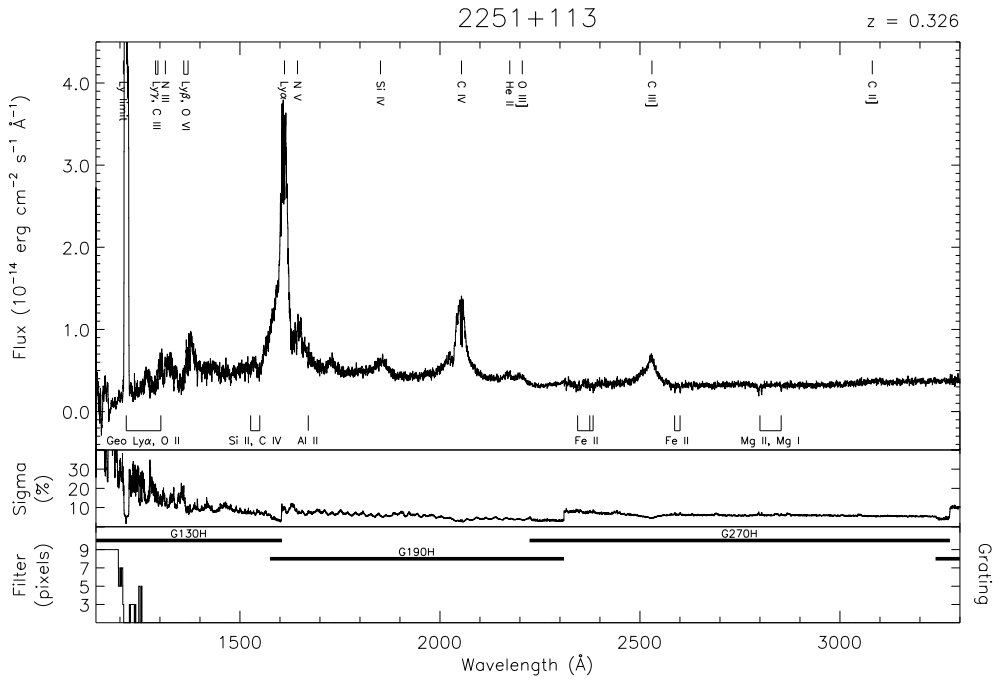
2251+113
z = 0.326
Flux (10^{-14} erg cm^{-2} s^{-1} Å^{-1})
Ly limit
N III
Ly7, C III
Lyβ, O VI
Lyα
N V
Si IV
C IV
He II
O III]
C III]
C II]
Geo Lyα, O II
Si II, C IV
Al II
Fe II
Fe II
Mg II, Mg I
Sigma (%)
G130H
G190H
G270H
Filter (pixels)
Grating
Wavelength (Å)

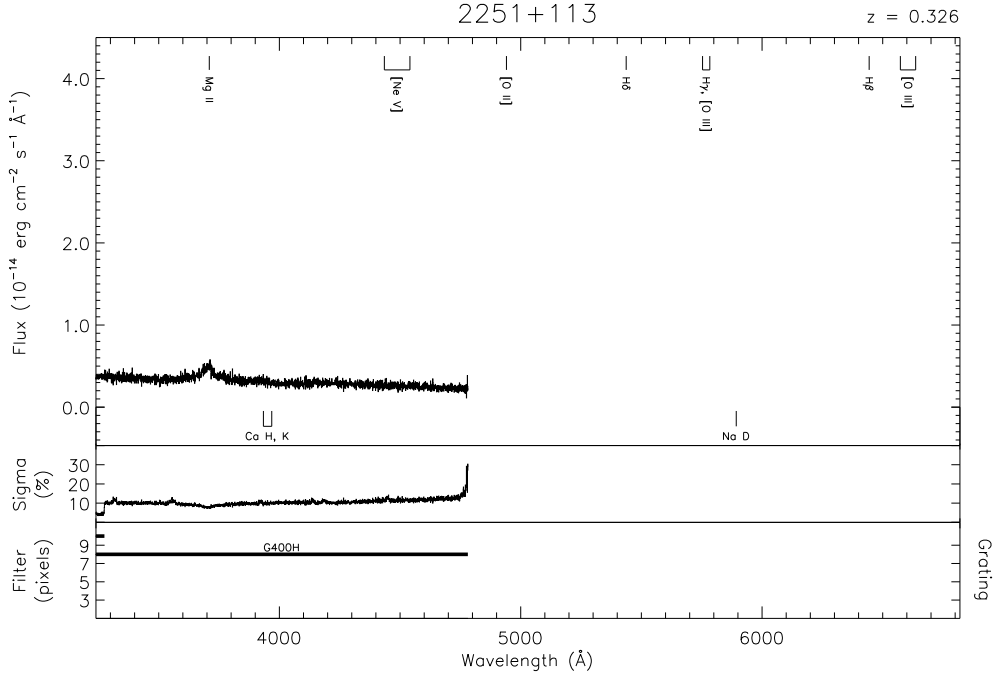
2251+113
z = 0.326
Flux (10^{-14} erg cm^{-2} s^{-1} Å^{-1})
Mg II
[Ne V]
[O I]
Hδ
[III O III]
Hβ
[O III]
Ca H, K
Na D
Sigma (%)
G400H
Filter (pixels)
Grating
Wavelength (Å)

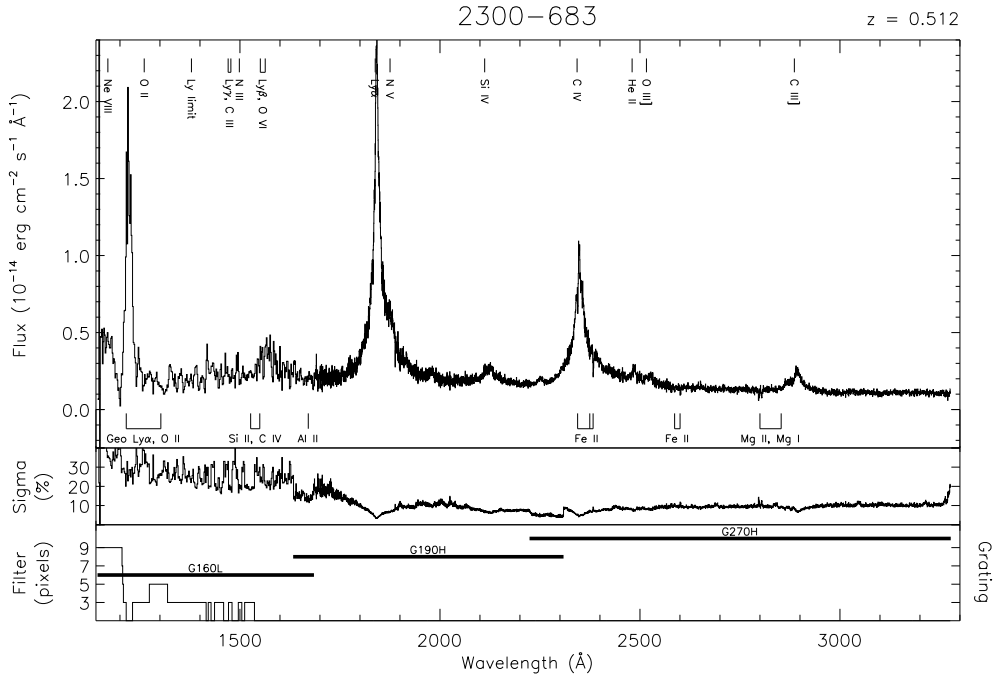
2300−683
z = 0.512
Ne VIII
O II
Ly limit
N III
Lyγ, C III
Lyβ, O VI
Lyα
N V
Si IV
C IV
He II
O III]
C III]
Flux (10^-14 erg cm^-2 s^-1 Å^-1)
Geo Lyα, O II
Si II, C IV
Al II
Fe II
Fe II
Mg II, Mg I
Sigma (%)
G270H
G190H
G160L
Filter (pixels)
Grating
Wavelength (Å)

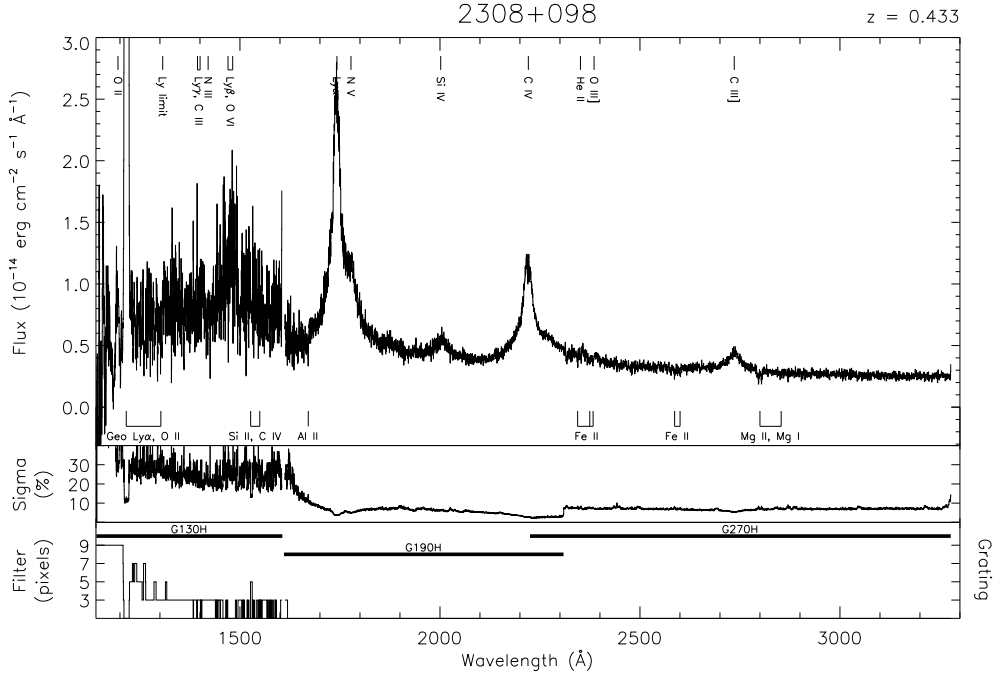
2308+098
z = 0.433
O II
Ly limit
N III
Lyγ, C III
Lyβ, O VI
Lyα
N V
Si IV
C IV
He II
O III]
C III]
Flux (10^-14 erg cm^-2 s^-1 Å^-1)
Geo Lyα, O II
Si II, C IV
Al II
Fe II
Fe II
Mg II, Mg I
Sigma (%)
G130H
G270H
G190H
Filter (pixels)
Grating
Wavelength (Å)

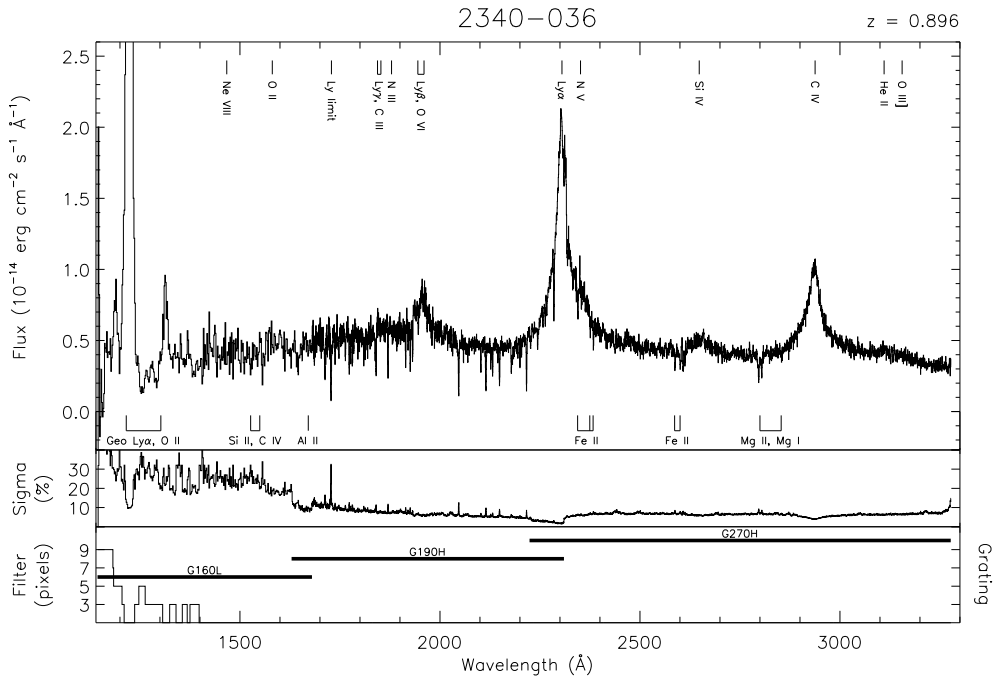
2340−036
z = 0.896
Ne VIII
O II
Ly limit
N III
Lyγ, C III
Lyβ, O VI
Lyα
N V
Si IV
C IV
He II
O III]
Geo Lyα, O II
Si II, C IV
Al II
Fe II
Fe II
Mg II, Mg I
Flux (10^-14 erg cm^-2 s^-1 Å^-1)
Sigma (%)
Filter (pixels)
G160L
G190H
G270H
Grating
Wavelength (Å)

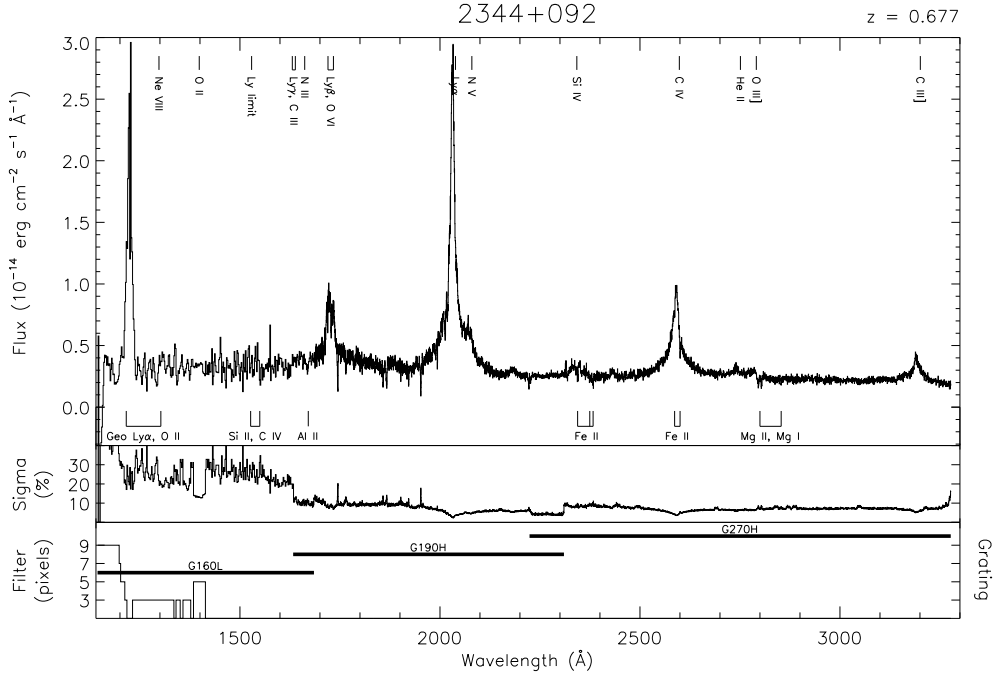
2344+092
z = 0.677
Ne VIII
O II
Ly limit
N III
Lyγ, C III
Lyβ, O VI
Lyα
N V
Si IV
C IV
He II
O III]
C III]
Geo Lyα, O II
Si II, C IV
Al II
Fe II
Fe II
Mg II, Mg I
Flux (10^-14 erg cm^-2 s^-1 Å^-1)
Sigma (%)
Filter (pixels)
G160L
G190H
G270H
Grating
Wavelength (Å)

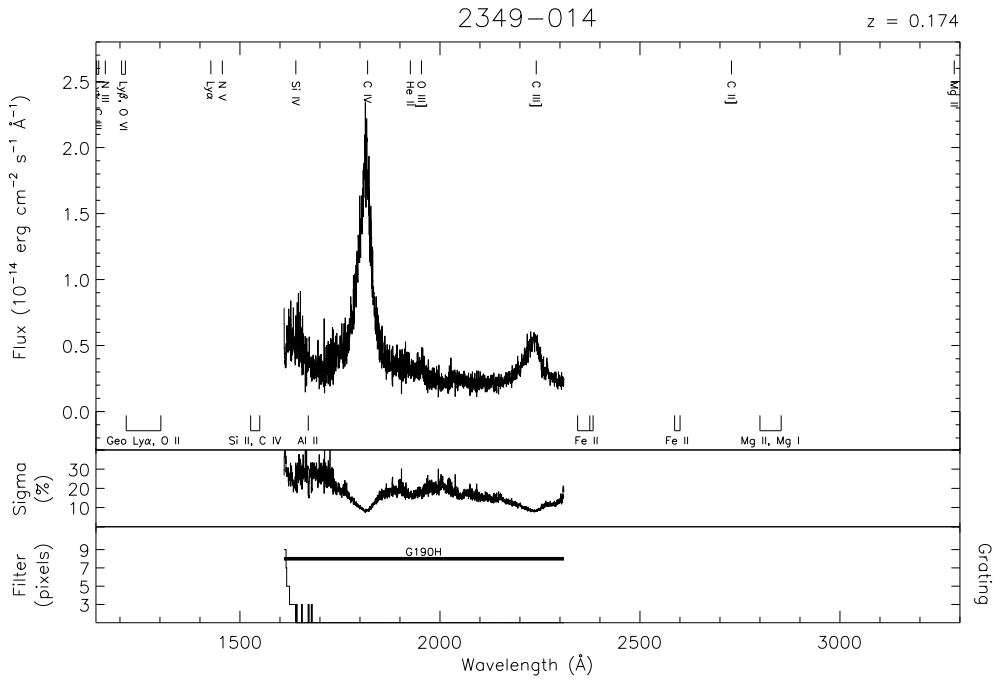
2349−014
z = 0.174
Flux (10^{-14} erg cm^{-2} s^{-1} Å^{-1})
N III, C III
Lyβ, O VI
N V
Lyα
Si IV
C IV
O III]
He II
C III]
C II
Mg II
Geo Lyα, O II
Si II, C IV
Al II
Fe II
Fe II
Mg II, Mg I
Sigma (%)
Filter (pixels)
G190H
Grating
Wavelength (Å)

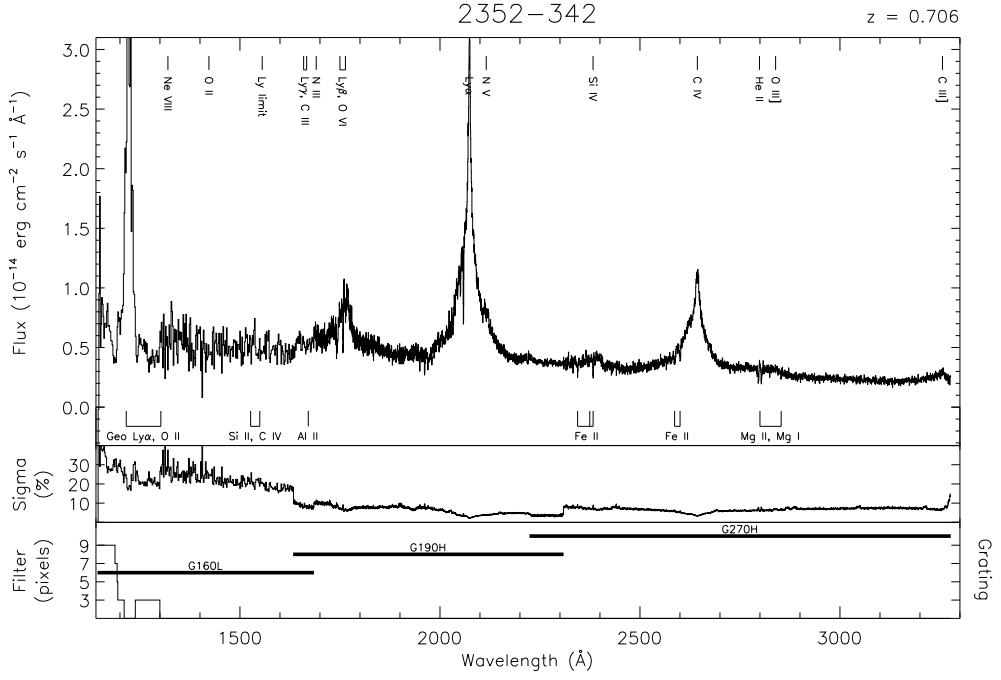
2352−342
z = 0.706
Flux (10^{-14} erg cm^{-2} s^{-1} Å^{-1})
Ne VIII
O II
Ly limit
N III
Lyγ, C III
Lyβ, O VI
Lyα
N V
Si IV
C IV
O III]
He II
C III]
Geo Lyα, O II
Si II, C IV
Al II
Fe II
Fe II
Mg II, Mg I
Sigma (%)
Filter (pixels)
G160L
G190H
G270H
Grating
Wavelength (Å)

Table 1. FOS Dataset Information

Target	Rootname	Scale Factor[a]	Observation Date	Exp. Time (s)	FOS Configuration[b]	Targ. Acq. Strategy[c]	Targ. Acq. Uncert.[d] (″)
0002+051	Y1HE0103T		1993 Nov 04	864	R/A/G270H/0.25X2.0	BIN+PK	0.034
	Y1HE0104T		1993 Nov 04	2366	R/A/G270H/0.25X2.0		
	Y1HE0105T		1993 Nov 04	976	R/A/G270H/0.25X2.0		
0003+158	Y1450B03T		1993 Nov 07	1863	R/A/G190H/0.25X2.0	BIN+PK	0.034
	Y1450B04T		1993 Nov 07	1863	R/A/G190H/0.25X2.0		
	Y1450B05T		1993 Nov 07	1194	R/A/G270H/0.25X2.0		
	Y1450C03T		1993 Nov 05	2453	R/B/G130H/0.25X2.0	BIN+PK	0.034
	Y1450C04T		1993 Nov 05	2453	R/B/G130H/0.25X2.0		
	Y1450C05T		1993 Nov 05	2453	R/B/G130H/0.25X2.0		
	Y1450C06T		1993 Nov 05	2453	R/B/G130H/0.25X2.0		
	Y1450C07T		1993 Nov 05	2453	R/B/G130H/0.25X2.0		
	Y1450C08T		1993 Nov 05	2453	R/B/G130H/0.25X2.0		
	Y1450C09T		1993 Nov 05	2453	R/B/G130H/0.25X2.0		
III ZW2	Y0P80203T		1992 Jan 18	1459	S/B/G130H/0.25X2.0	BIN+PK	0.025
	Y0P80204T		1992 Jan 18	1469	S/B/G130H/0.25X2.0		
	Y0P80205T		1992 Jan 18	1469	S/B/G130H/0.25X2.0		
	Y0P80206T		1992 Jan 18	1599	S/B/G270H/0.25X2.0		
0014+813	Y0LF0103T		1991 Jun 06	25	S/B/G160L/4.3	BIN	0.12
	Y0LF0104T		1991 Jun 06	600	S/B/G160L/4.3		
	Y0LF0105T		1991 Jun 06	25	S/B/G160L/4.3		
	Y0LF0106T		1991 Jun 06	300	S/B/PRISM/4.3		
0024+224	Y0RV1802T		1991 Nov 05	1331	R/B/G160L/1.0	BIN	0.12
	Y1010103T		1992 Jul 22	1765	R/A/G270H/0.25X2.0	BIN+PK	0.025
	Y1010104T		1992 Jul 22	2593	R/A/G190H/0.25X2.0		
	Y1010105T		1992 Jul 22	2592	R/A/G190H/0.25X2.0		
	Y1010106T		1992 Jul 22	2592	R/A/G190H/0.25X2.0		
0031-707	Y0RV0103T		1991 Oct 29	2121	R/A/G190H/0.25X2.0	BIN+PK	0.034

Table 1—Continued

Target	Rootname	Scale Factor[a]	Observation Date	Exp. Time (s)	FOS Configuration[b]	Targ. Acq. Strategy[c]	Targ. Acq. Uncert.[d] (″)
	Y0RV0104T		1991 Oct 29	930	R/A/G270H/0.25X2.0		
0043+039	Y0RV0203T		1991 Oct 28	1314	R/A/G190H/0.25X2.0	BIN+PK	0.034
	Y0RV0204T		1991 Oct 28	1314	R/A/G190H/0.25X2.0		
	Y0RV0205T		1991 Oct 28	930	R/A/G270H/0.25X2.0		
0044+030	Y0RV0N03T		1991 Nov 03	1651	R/A/G190H/0.25X2.0	BIN+PK	0.034
	Y0RV0N04T		1991 Nov 03	1651	R/A/G190H/0.25X2.0		
	Y0RV0N05T		1991 Nov 03	904	R/A/G270H/0.25X2.0		
	Y0RV0O01T		1991 Nov 03	530	R/B/G160L/1.0	BLIND	
I ZW1	Y0ZV0102T		1992 Jul 29	1427	R/A/G270H/1.0	BIN	0.12
0052+251	Y1HH0202T		1993 Jul 22	600	S/A/G190H/4.3	PK	0.4
0055-269	Y0UR0102T		1992 Sep 10	1200	S/B/G160L/4.3	BIN	0.12
	Y0UR0103T		1992 Sep 10	600	S/B/PRISM/4.3		
0100+020	Y1HH0302T		1993 Jul 09	639	S/A/G190H/4.3	PK	0.4
0110+297	Y12B0102T		1992 Sep 06	935	S/A/G190H/4.3	BIN	0.12
	Y12B0103T		1992 Sep 06	437	S/A/G270H/4.3		
0112-017	Y0PE0102T		1991 Sep 06	917	S/A/G270H/4.3	BIN	0.12
	Y0PE0103T		1991 Sep 06	731	S/A/G400H/4.3		
0114-089	Y1290202T	1.429	1992 Nov 23	1126	R/B/G160L/4.3	BIN	0.12
	Y1290203T	1.326	1992 Nov 23	563	R/B/PRISM/4.3		
	Y1MG0102T		1993 Nov 29	345	S/B/G160L/1.0	BIN	0.12
	Y1MG0103T		1993 Nov 29	1142	S/B/G160L/1.0		
	Y1MG0104T		1993 Nov 29	1142	S/B/G160L/1.0		
	Y1MG0105T		1993 Nov 29	1142	S/B/G160L/1.0		
	Y1MG0106T		1993 Nov 29	1142	S/B/G160L/1.0		
	Y1MG0107T		1993 Nov 29	430	S/B/G400H/4.3		
	Y1MG0108T		1993 Nov 29	470	S/B/G400H/4.3		
0115+027	Y1F90803T		1993 Aug 16	1331	S/A/G190H/4.3	PK2	0.35

Table 1—Continued

Target	Rootname	Scale Factor[a]	Observation Date	Exp. Time (s)	FOS Configuration[b]	Targ. Acq. Strategy[c]	Targ. Acq. Uncert.[d] (″)
	Y1F90804T		1993 Aug 16	581	S/A/G270H/4.3		
0117+213	Y1HH0502T		1993 Jul 09	420	S/B/G160L/4.3	PK	0.4
FAIRALL 9	Y0YA0102T		1993 Jan 21	2400	S/B/G130H/1.0	BIN	0.12
	Y0YA0103T		1993 Jan 22	900	S/B/G190H/1.0		
	Y0YA0104T		1993 Jan 22	360	S/B/G270H/1.0		
0122-003	Y0RV1903T		1991 Nov 09	1504	R/A/G190H/0.25X2.0	BIN+PK	0.034
	Y0RV1904T		1991 Nov 09	1504	R/A/G190H/0.25X2.0		
	Y0RV1905T		1991 Nov 09	728	R/A/G270H/0.25X2.0		
0133+207	Y12B0202T		1992 Aug 30	1883	S/A/G190H/4.3	BIN	0.12
	Y12B0203T		1992 Aug 30	911	S/A/G270H/4.3		
0143-015	Y0LF0203T		1991 Jun 21	50	S/B/G160L/4.3	BIN	0.12
	Y0LF0204T		1991 Jun 21	1200	S/B/G160L/4.3		
	Y0LF0205T		1991 Jun 21	50	S/B/G160L/4.3		
	Y0LF0206T		1991 Jun 21	600	S/B/PRISM/4.3		
0145+386	Y1HH0702T		1993 Jul 23	420	S/B/G160L/4.3	PK	0.4
0150-202	Y0DK0104R		1990 Oct 28	2000	S/A/G160L/1.0	BIN	0.12
	Y0DK0105R		1990 Oct 28	2000	S/A/G160L/1.0		
	Y0DK0106T		1990 Oct 28	2000	S/A/G160L/1.0		
	Y0UR0302T		1992 Feb 03	1599	S/A/G270H/4.3	BIN	0.12
	Y0UR0303T		1992 Feb 03	1599	S/A/G270H/4.3		
0151+045	Y1HH0802T		1993 Jul 18	759	S/B/G130H/4.3	PK	0.4
0153+045	Y0UR0202T		1992 Sep 30	1200	S/B/G160L/4.3	BIN	0.12
	Y0UR0203T		1992 Sep 30	600	S/B/PRISM/4.3		
0200-089	Y1HH0902T		1993 Jul 30	759	S/B/G130H/4.3	PK	0.4
0219+428	Y10D0103T		1992 Oct 02	720	S/B/G270H/0.25X2.0	BIN+PK	0.034
	Y10D0104T		1992 Oct 02	1200	S/B/G190H/0.25X2.0		
	Y10D0105T		1992 Oct 02	2145	S/B/G130H/0.25X2.0		

Table 1—Continued

Target	Rootname	Scale Factor[a]	Observation Date	Exp. Time (s)	FOS Configuration[b]	Targ. Acq. Strategy[c]	Targ. Acq. Uncert.[d] (″)
	Y10D0106T		1992 Oct 02	2139	S/B/G130H/0.25X2.0		
	Y10D0107T		1992 Oct 02	2139	S/B/G130H/0.25X2.0		
	Y10D0108T		1992 Oct 02	2149	S/B/G130H/0.25X2.0		
	Y10D0109T		1992 Oct 02	2149	S/B/G130H/0.25X2.0		
0226-1024	Y0LS0102T		1991 Jun 13	999	S/A/G270H/1.0	BIN	0.12
	Y0LS0103T		1991 Jun 13	999	S/A/G270H/1.0		
	Y0ZX0102T		1992 Jul 25	1499	S/A/G190H/1.0	BIN	0.12
	Y0ZX0103T		1992 Jul 25	1499	S/A/G190H/1.0		
0232-042	Y1AC0102T		1993 Mar 07	1803	R/B/G160L/1.0	BIN	0.12
NGC 1068	Y0GQ0106T		1991 Jan 27	1000	S/B/G190H/0.3	PK4	0.030
	Y0GQ0107T		1991 Jan 27	1500	S/B/G130H/0.3		
	Y0GQ0108T		1991 Jan 27	700	S/B/G270H/0.3		
	Y0MW0706T		1991 Jun 25	1000	S/B/G190H/0.3	PK4	0.030
	Y0MW0707T		1991 Jun 25	1500	S/B/G130H/0.3		
	Y0MW0806T	1.067	1991 Jun 25	700	S/A/G270H/0.3	PK4	0.030
	Y0MW0807T		1991 Jun 25	600	S/A/G570H/0.3		
	Y0MW0809T		1991 Jun 25	600	S/A/G400H/0.3		
NGC 1068 CLOUD A	Y0MW0709T	1.115	1991 Jun 25	1000	S/B/G190H/0.3	PK4+OFF	0.030
	Y0MW070AT	1.115	1991 Jun 25	1500	S/B/G130H/0.3		
	Y0MW080BT		1991 Jun 25	700	S/A/G270H/0.3	PK4+OFF	0.030
	Y0MW080CT		1991 Jun 26	600	S/A/G570H/0.3		
	Y0MW080ET		1991 Jun 26	600	S/A/G400H/0.3		
NGC 1068 CLOUD B	Y0MW070CT		1991 Jun 25	1000	S/B/G190H/0.3	PK4+OFF	0.030
	Y0MW070DT		1991 Jun 25	1500	S/B/G130H/0.3		
	Y0MW080GT		1991 Jun 26	700	S/A/G270H/0.3	PK4+OFF	0.030
	Y0MW080HT		1991 Jun 26	600	S/A/G570H/0.3		
	Y0MW080JT		1991 Jun 26	600	S/A/G400H/0.3		

Table 1—Continued

Target	Rootname	Scale Factor[a]	Observation Date	Exp. Time (s)	FOS Configuration[b]	Targ. Acq. Strategy[c]	Targ. Acq. Uncert.[d] (″)
NGC 1068 CLOUD C	Y19G0105T		1993 Mar 01	849	S/A/G570H/0.3	PK3	0.030
	Y19G0106T		1993 Mar 01	849	S/A/G400H/0.3		
	Y19G0107T		1993 Mar 01	999	S/A/G270H/0.3		
	Y19G0205T		1993 Mar 03	1350	S/B/G190H/0.3	PK3	0.030
	Y19G0206T		1993 Mar 04	2000	S/B/G130H/0.3		
NGC 1068 CLOUD D	Y19G0108T		1993 Mar 01	1139	S/A/G570H/0.5	PK3+OFF	0.030
	Y19G0109T	1.046	1993 Mar 01	1139	S/A/G400H/0.5		
0253-0139	Y1HH0D02T	1.122	1993 Sep 26	360	S/B/G160L/4.3	PK	0.4
	Y1HH0E02T		1993 Jul 30	480	S/A/G270H/4.3	PK	0.4
NGC 1275	Y1050103T		1993 Feb 03	2269	S/B/G130H/0.25X2.0	BIN+PK+OFF	0.034
	Y1050104T		1993 Feb 03	2269	S/B/G130H/0.25X2.0		
	Y1050105T		1993 Feb 03	2279	S/B/G130H/0.25X2.0		
	Y1050106T		1993 Feb 03	2279	S/B/G130H/0.25X2.0		
RXJ03233-4931	Y1FI0104T		1993 Aug 18	1359	S/B/G160L/1.0	PK3	0.18
	Y1FI0105T		1993 Aug 18	1359	S/B/G160L/1.0		
MS 0334.2-3617	Y1HH0K02T		1993 Aug 15	420	S/B/G160L/4.3	PK	0.4
	Y1HH0L02T		1993 Oct 06	639	S/A/G270H/4.3	PK	0.4
NGC 1399	Y15I0102T		1993 Jan 17	1764	S/A/G190H/1.0	PK	0.35
	Y15I0103T		1993 Jan 17	1759	S/A/G190H/1.0		
	Y15I0104T		1993 Jan 17	1759	S/A/G190H/1.0		
	Y15I0105T		1993 Jan 17	1772	S/A/G270H/1.0		
	Y15I0106T		1993 Jan 17	1769	S/A/G270H/1.0		
	Y15I0202T		1993 Jan 17	2093	S/B/G130H/1.0	PK	0.35
	Y15I0203T		1993 Jan 17	2089	S/B/G130H/1.0		
	Y15I0204T		1993 Jan 17	2089	S/B/G130H/1.0		
	Y15I0205T		1993 Jan 17	2089	S/B/G130H/1.0		
	Y15I0206T		1993 Jan 17	2089	S/B/G130H/1.0		

Table 1—Continued

Target	Rootname	Scale Factor[a]	Observation Date	Exp. Time (s)	FOS Configuration[b]	Targ. Acq. Strategy[c]	Targ. Acq. Uncert.[d] (″)
0349-146	Y0RV0P03T		1991 Dec 21	1485	R/A/G190H/0.25X2.0	BIN+PK	0.034
	Y0RV0P04T		1991 Dec 21	1485	R/A/G190H/0.25X2.0		
	Y0RV0P05T		1991 Dec 21	954	R/A/G270H/0.25X2.0		
	Y0RV0P06T		1991 Dec 21	530	R/B/G160L/1.0		
0350-073	Y1HH0N02T		1993 Sep 26	560	S/A/G270H/4.3	PK	0.4
0355-483	Y1HH0O02T		1993 Aug 22	420	S/B/G160L/4.3	PK	0.4
	Y1HH0P02T	1.154	1993 Aug 03	520	S/A/G270H/4.3	PK	0.4
0403-132	Y0PE0202T		1991 Oct 11	1409	S/A/G190H/4.3	BIN	0.12
	Y0PE0203T		1991 Oct 11	756	S/A/G270H/4.3		
	Y0PE0204T		1991 Oct 11	533	S/A/G400H/4.3		
0405-123	Y0NT0103T		1991 Jul 04	1750	S/B/G130H/0.25X2.0	BIN+PK	0.025
	Y0NT0104T		1991 Jul 04	1750	S/B/G130H/0.25X2.0		
	Y0NT0105T		1991 Jul 04	1750	S/B/G130H/0.25X2.0		
	Y0NT0106T		1991 Jul 04	1750	S/B/G130H/0.25X2.0		
	Y0NT0108T		1991 Jul 04	1799	S/B/G190H/0.25X2.0		
	Y0NT0109T		1991 Jul 04	1799	S/B/G190H/0.25X2.0		
	Y0NT0203T		1991 Jul 01	1060	R/A/G270H/0.25X2.0	BIN+PK	0.034
	Y0NT0204T		1991 Jul 01	1060	R/A/G270H/0.25X2.0		
0414-060	Y1030102T		1992 Oct 18	939	R/A/G270H/1.0	BIN	0.12
	Y1030103T		1992 Oct 18	2030	R/A/G190H/1.0		
NGC 1566	Y0H70207T	1.176	1991 Feb 08	2000	S/A/G270H/0.3	PK+BIN+PK3	0.030
	Y0H70208T	1.176	1991 Feb 08	2000	S/A/G570H/0.3		
	Y0H7020AT	1.176	1991 Feb 08	2000	S/A/G400H/0.3		
	Y0H75107T		1991 Feb 11	2000	S/B/G190H/0.3	PK+BIN+PK3	0.030
	Y0H75108T		1991 Feb 11	2000	S/B/G190H/0.3		
	Y0H75109T		1991 Feb 11	2000	S/B/G130H/0.3		
	Y0H7510AT		1991 Feb 11	2000	S/B/G130H/0.3		

Table 1—Continued

Target	Rootname	Scale Factor[a]	Observation Date	Exp. Time (s)	FOS Configuration[b]	Targ. Acq. Strategy[c]	Targ. Acq. Uncert.[d] (″)
0439-433	Y1HE0503T		1993 Oct 23	1089	R/A/G190H/0.25X2.0	BIN+PK	0.034
	Y1HE0504T		1993 Oct 23	2629	R/A/G190H/0.25X2.0		
	Y1HE0505T		1993 Oct 23	2629	R/A/G190H/0.25X2.0		
	Y1HE0506T		1993 Oct 23	1540	R/A/G190H/0.25X2.0		
	Y1HE0507T		1993 Oct 23	788	R/A/G270H/0.25X2.0		
	Y1HE0508T		1993 Oct 23	1728	R/A/G270H/0.25X2.0		
0446-208	Y1HH0Q02T		1993 Aug 14	480	S/B/G160L/4.3	PK	0.4
0448-392	Y1HH0R02T		1993 Jul 09	420	S/B/G160L/4.3	PK	0.4
0454-220	Y0IZ0103T		1991 Apr 15	50	S/B/G130H/4.3	BIN	0.12
	Y0IZ0104T		1991 Apr 16	1620	S/B/G130H/1.0		
	Y0IZ0105T		1991 Apr 16	1620	S/B/G130H/1.0		
	Y0IZ0106T		1991 Apr 16	1629	S/B/G130H/1.0		
	Y0IZ0107T		1991 Apr 16	1629	S/B/G130H/1.0		
	Y0IZ0203T	1.075	1991 Apr 19	50	S/A/G270H/4.3	BIN	0.12
	Y0IZ0204T	1.075	1991 Apr 19	1999	S/A/G270H/1.0		
	Y0IZ0205T		1991 Apr 20	50	S/A/G190H/4.3		
	Y0IZ0206T		1991 Apr 20	1959	S/A/G190H/1.0		
	Y0IZ0207T		1991 Apr 20	1969	S/A/G190H/1.0		
	Y0IZ0208T		1991 Apr 20	1969	S/A/G190H/1.0		
	Y0IZ0209T	1.064	1991 Apr 20	50	S/A/PRISM/4.3		
0506-612	Y1HH0T02T		1993 Jul 07	639	S/A/G270H/4.3	PK	0.4
0537-441	Y1HH0U02T		1993 Jul 12	480	S/B/G130H/4.3	PK	0.4
	Y1HH0V02T		1993 Sep 16	600	S/A/G270H/4.3	PK	0.4
MRK 3 CLOUD E1	Y1GG0106T		1993 Sep 23	2250	S/B/G190H/0.3	BIN+PK+OFF+PK	0.034
	Y1GG0107T		1993 Sep 23	2250	S/B/G190H/0.3		
	Y1HV0204T		1993 Sep 23	1269	S/A/G570H/0.3	BIN+PK+OFF+PK	0.034
	Y1HV0205T		1993 Sep 24	3060	S/A/G570H/0.3		

Table 1—Continued

Target	Rootname	Scale Factor[a]	Observation Date	Exp. Time (s)	FOS Configuration[b]	Targ. Acq. Strategy[c]	Targ. Acq. Uncert.[d] (″)
	Y1HV0206T		1993 Sep 24	3060	S/A/G400H/0.3		
	Y1HV0207T		1993 Sep 24	1040	S/A/G400H/0.3		
	Y1HV0208T		1993 Sep 24	1759	S/A/G270H/0.3		
0624+691	Y10G0103T		1993 Feb 04	2817	R/B/G130H/0.25X2.0	BIN+PK	0.025
	Y10G0104T		1993 Feb 04	2817	R/B/G130H/0.25X2.0		
	Y10G0105T		1993 Feb 04	2817	R/B/G130H/0.25X2.0		
0710+118	Y0PE0302T		1991 Dec 03	1691	S/A/G190H/4.3	BIN	0.12
	Y0PE0303T		1991 Dec 03	720	S/A/G270H/4.3		
	Y0PE0304T		1991 Dec 03	486	S/A/G400H/4.3		
0740+380	Y0PE0402T		1991 Dec 03	1080	S/A/G270H/4.3	BIN	0.12
	Y0PE0403T		1991 Dec 03	845	S/A/G400H/4.3		
0742+318	Y1450403T		1992 Dec 09	2241	R/A/G190H/0.25X2.0	BIN+PK	0.034
	Y1450404T		1992 Dec 09	2241	R/A/G190H/0.25X2.0		
	Y1450405T		1992 Dec 09	1598	R/A/G270H/0.25X2.0		
	Y1450406T		1992 Dec 09	563	R/B/G160L/1.0		
0743-673	Y1L00103T		1993 Oct 15	1577	R/A/G270H/0.25X2.0	BIN+PK	0.034
	Y1L00104T		1993 Oct 15	3230	R/A/G270H/0.25X2.0		
	Y1L00105T		1993 Oct 15	1051	R/A/G270H/0.25X2.0		
0752+258	Y0XW0102T		1992 May 21	1819	S/A/G190H/4.3	BIN	0.12
	Y0XW0103T		1992 May 21	1829	S/A/G190H/4.3		
0809+483	Y0PL0303T	1.070	1991 Dec 04	1200	S/A/G160L/4.3	BIN	0.12
	Y0ZW0202T		1992 Sep 26	2173	R/A/G160L/1.0	BIN	0.12
	Y0ZW0203T		1992 Sep 26	2171	R/A/G160L/1.0		
	Y0ZW0204T		1992 Sep 26	2171	R/A/G160L/1.0		
	Y0ZW0205T		1992 Sep 26	2171	R/A/G160L/1.0		
0834+4501	Y1460302T		1993 Jan 20	1400	S/B/G160L/4.3	BIN	0.12
	Y1460303T		1993 Jan 20	1400	S/B/G160L/4.3		

Table 1—Continued

Target	Rootname	Scale Factor[a]	Observation Date	Exp. Time (s)	FOS Configuration[b]	Targ. Acq. Strategy[c]	Targ. Acq. Uncert.[d] (″)
	Y1460304T		1993 Jan 20	1400	S/B/G160L/4.3		
	Y1460305T		1993 Jan 20	1400	S/B/G160L/4.3		
0838+133	Y0PE0502T		1991 Dec 04	1254	S/A/G190H/4.3	BIN	0.12
	Y0PE0503T		1991 Dec 04	1260	S/A/G190H/4.3		
	Y0PE0504T		1991 Dec 04	747	S/A/G270H/4.3		
	Y0PE0505T		1991 Dec 04	739	S/A/G270H/4.3		
	Y0PE0506T		1991 Dec 04	1230	S/A/G400H/4.3		
PG 0844+349	Y0P80103T		1992 Jan 10	1250	S/B/G130H/0.25X2.0	BIN+PK	0.025
	Y0P80104T		1992 Jan 10	1250	S/B/G130H/0.25X2.0		
	Y0P80105T		1992 Jan 10	1500	S/B/G270H/0.25X2.0		
0850+440	Y0RV0303T		1991 Nov 07	1520	R/A/G190H/0.25X2.0	BIN+PK	0.034
	Y0RV0304T		1991 Nov 07	1520	R/A/G190H/0.25X2.0		
	Y0RV0305T		1991 Nov 07	1520	R/A/G190H/0.25X2.0		
	Y0RV0306T	1.124	1991 Nov 07	1564	R/A/G270H/0.25X2.0		
	Y0RV0401T		1991 Nov 07	530	R/B/G160L/1.0	OFF	
0851+202	Y1C30105T	1.141	1993 Nov 15	1650	R/A/G190H/0.25X2.0	PK4	0.034
	Y1C30106T	1.141	1993 Nov 15	1650	R/A/G190H/0.25X2.0		
	Y1C30107T		1993 Nov 15	1239	R/A/G270H/0.25X2.0		
0856+468	Y1HI0202T		1993 Nov 23	480	S/B/G160L/4.3	PK	0.4
0859-140	Y12B0302T		1993 Mar 05	450	S/A/G270H/4.3	BIN	0.12
0903+169	Y0PE0602T		1992 May 01	1829	S/A/G190H/4.3	BIN	0.12
	Y0PE0603T		1992 May 01	1829	S/A/G190H/4.3		
	Y0PE0604T		1992 May 01	1829	S/A/G190H/4.3		
	Y0PE0605T		1992 May 01	725	S/A/G270H/4.3		
	Y0PE0606T		1992 May 01	720	S/A/G270H/4.3		
	Y0PE0607T		1992 May 01	1134	S/A/G400H/4.3		
0906+430	Y12B0402T		1992 Dec 28	1687	S/A/G190H/4.3	BIN	0.12

Table 1—Continued

Target	Rootname	Scale Factor[a]	Observation Date	Exp. Time (s)	FOS Configuration[b]	Targ. Acq. Strategy[c]	Targ. Acq. Uncert.[d] (″)
	Y12B0403T		1992 Dec 28	1689	S/A/G190H/4.3		
	Y12B0404T		1992 Dec 28	817	S/A/G270H/4.3		
	Y12B0405T		1992 Dec 29	819	S/A/G270H/4.3		
0916+513	Y0RV1E03T		1992 Apr 03	1992	R/A/G190H/0.25X2.0	BIN+PK	0.034
	Y0RV1E04T		1992 Apr 03	1992	R/A/G190H/0.25X2.0		
	Y0RV1E05T		1992 Apr 03	1327	R/A/G270H/0.25X2.0		
	Y0RV1E06T		1992 Apr 03	563	R/B/G160L/1.0	OFF	
0923+392	Y1170102T		1993 Jan 24	2185	S/A/G190H/4.3	BIN	0.12
	Y1170103T		1993 Jan 24	1206	S/A/G270H/4.3		
	Y1170104T		1993 Jan 24	1002	S/A/G400H/4.3		
0932+501	Y1AL0102T		1993 Apr 21	1617	S/A/G270H/1.0	BIN	0.12
	Y1AL0103T		1993 Apr 21	1609	S/A/G270H/1.0		
0946+301	Y0UW0202T		1992 Feb 16	100	S/A/G270H/4.3	BIN	0.12
	Y0UW0203T		1992 Feb 16	1331	R/A/G270H/1.0		
	Y0UW0204T		1992 Feb 16	1331	R/A/G270H/1.0		
	Y0UW0205T		1992 Feb 16	2220	R/A/G190H/1.0		
	Y0UW0206T		1992 Feb 16	2220	R/A/G190H/1.0		
	Y0UW0207T		1992 Feb 16	1768	R/B/G160L/1.0		
	Y0UW0208T		1992 Feb 16	100	S/B/G160L/4.3		
0953+414	Y0ML0103T		1991 Jun 18	1591	R/A/G190H/0.25X2.0	BIN+PK	0.025
	Y0ML0105T	1.071	1991 Jun 18	884	R/A/G270H/0.25X2.0		
	Y0R40103T		1991 Nov 05	2000	S/B/G130H/0.25X2.0	BIN+PK	0.025
	Y0R40104T		1991 Nov 05	2000	S/B/G130H/0.25X2.0		
	Y0R40105T		1991 Nov 06	2000	S/B/G130H/0.25X2.0		
	Y0R40106T		1991 Nov 06	2000	S/B/G130H/0.25X2.0		
0954+556	Y1170302T		1993 Jan 20	1927	S/A/G190H/4.3	BIN	0.12
	Y1170303T		1993 Jan 20	1929	S/A/G190H/4.3		

Table 1—Continued

Target	Rootname	Scale Factor[a]	Observation Date	Exp. Time (s)	FOS Configuration[b]	Targ. Acq. Strategy[c]	Targ. Acq. Uncert.[d] (″)
	Y1170304T		1993 Jan 20	1649	S/A/G270H/4.3		
0955+326	Y10Q0103T		1992 Dec 25	1690	R/A/G270H/0.25X2.0	BIN+PK	0.025
	Y10Q0104T		1992 Dec 26	2066	R/A/G190H/0.25X2.0		
	Y10Q0105T		1992 Dec 26	2066	R/A/G190H/0.25X2.0		
	Y1HI0802T		1993 Nov 26	759	S/B/G130H/4.3	PK	0.4
NGC 3031	Y1AU0103T	3.043	1993 Apr 14	1499	S/A/G570H/0.3	BIN+PK	0.05
	Y1AU0104T		1993 Apr 14	1499	S/A/G400H/0.3		
	Y1AU0105T		1993 Apr 14	1999	S/A/G270H/0.3		
	Y1AU0204T		1993 Apr 05	1500	S/B/G130H/0.3	BIN+PK2	0.05
	Y1AU0205T		1993 Apr 05	1500	S/B/G130H/0.3		
0959+6827	Y1450703T		1992 Dec 11	2780	R/A/G190H/0.25X2.0	BIN+PK	0.034
	Y1450704T		1992 Dec 11	2780	R/A/G190H/0.25X2.0		
	Y1450705T		1992 Dec 11	1690	R/A/G270H/0.25X2.0		
	Y1450706T		1992 Dec 11	563	R/B/G160L/1.0	OFF	
1001+291	Y0VM0203T		1992 Mar 19	2498	R/B/G130H/0.25X2.0	BIN+PK	0.034
	Y0VM0204T		1992 Mar 19	2424	R/B/G130H/0.25X2.0		
	Y0VM0205T		1992 Mar 19	2214	R/B/G130H/0.25X2.0		
	Y0VM0206T		1992 Mar 19	2163	R/B/G130H/0.25X2.0		
	Y0VM0207T		1992 Mar 19	2148	R/B/G130H/0.25X2.0		
	Y0VM0208T		1992 Mar 20	2550	R/B/G130H/0.25X2.0		
	Y0VM0209T		1992 Mar 20	2577	R/B/G130H/0.25X2.0		
	Y0XX0103T		1992 May 21	1352	R/A/G190H/0.25X2.0	BIN+PK	0.034
	Y0XX0104T		1992 May 21	1352	R/A/G190H/0.25X2.0		
	Y0XX0105T		1992 May 21	1014	R/A/G270H/0.25X2.0		
1007+417	Y1450803T		1992 Dec 09	2703	R/A/G190H/0.25X2.0	BIN+PK	0.034
	Y1450804T		1992 Dec 09	2703	R/A/G190H/0.25X2.0		
	Y1450805T		1992 Dec 10	1803	R/A/G270H/0.25X2.0		

Table 1—Continued

Target	Rootname	Scale Factor[a]	Observation Date	Exp. Time (s)	FOS Configuration[b]	Targ. Acq. Strategy[c]	Targ. Acq. Uncert.[d] (″)
	Y1450806T	1.107	1992 Dec 10	563	R/B/G160L/1.0	OFF	
1008+133	Y1HE0803T		1993 Nov 22	864	R/A/G270H/0.25X2.0	BIN+PK	0.034
	Y1HE0804T		1993 Nov 23	1389	R/A/G270H/0.25X2.0		
	Y1HI0C02T		1993 Nov 03	420	S/B/G160L/4.3	PK	0.4
CSO 251	Y0DT0104T		1991 Jan 07	100	S/B/G130H/4.3	PK+BIN	0.12
	Y0DT0105T		1991 Jan 07	1680	S/B/G130H/1.0		
	Y0DT0106T		1991 Jan 07	1680	S/B/G130H/1.0		
	Y0DT0107T		1991 Jan 07	1680	S/B/G130H/1.0		
	Y0DT0108T		1991 Jan 07	1680	S/B/G130H/1.0		
1022+194	Y0RV1U02T		1992 Feb 17	1463	R/B/G160L/1.0	BIN	0.12
1038+064	Y0RV1V02T		1992 Jan 31	1331	R/B/G160L/1.0	BIN	0.12
1040+123	Y0RV1W02T		1992 Jan 31	1544	R/B/G160L/1.0	BIN	0.12
NGC 3393 KNOT	Y1DB0103T		1993 Nov 16	2010	S/B/G130H/1.0	BIN+OFF	0.12
	Y1DB0104T		1993 Nov 16	2010	S/B/G130H/1.0		
	Y1DB0105T		1993 Nov 16	2010	S/B/G130H/1.0		
	Y1DB0106T		1993 Nov 16	2010	S/B/G130H/1.0		
	Y1DB0107T		1993 Nov 16	1799	S/B/G190H/1.0		
	Y1DB0108T		1993 Nov 16	1799	S/B/G190H/1.0		
	Y1DB0203T		1993 Nov 16	539	S/A/G270H/1.0	BIN+OFF	0.12
	Y1DB0204T		1993 Nov 16	180	S/A/G400H/1.0		
	Y1DB0205T		1993 Nov 16	1080	S/A/G570H/1.0		
1049-005	Y0RV1G03T		1992 Apr 01	1625	R/A/G190H/0.25X2.0	BIN+PK	0.034
	Y0RV1G04T		1992 Apr 01	1625	R/A/G190H/0.25X2.0		
	Y0RV1G05T		1992 Apr 01	1142	R/A/G270H/0.25X2.0		
1055+201	Y0RV0J02T		1992 Jan 26	1060	R/B/G160L/1.0	BIN	0.12
1100+772	Y0RV0V03T	1.384	1993 Feb 02	1911	R/A/G190H/0.25X2.0	BIN+PK	0.034
	Y0RV0V04T	1.384	1993 Feb 02	1911	R/A/G190H/0.25X2.0		

Table 1—Continued

Target	Rootname	Scale Factor[a]	Observation Date	Exp. Time (s)	FOS Configuration[b]	Targ. Acq. Strategy[c]	Targ. Acq. Uncert.[d] (″)
	Y0RV0V05T	1.384	1993 Feb 03	1911	R/A/G190H/0.25X2.0		
	Y0RV0V06T	1.464	1993 Feb 03	2020	R/A/G270H/0.25X2.0		
	Y1DC0103T		1993 Sep 13	2742	R/B/G130H/0.25X2.0	BIN+PK	0.034
	Y1DC0104T		1993 Sep 13	2742	R/B/G130H/0.25X2.0		
	Y1DC0105T		1993 Sep 13	2742	R/B/G130H/0.25X2.0		
	Y1DC0106T		1993 Sep 13	2742	R/B/G130H/0.25X2.0		
	Y1DC0107T		1993 Sep 14	2742	R/B/G130H/0.25X2.0		
	Y1DC0108T		1993 Sep 14	2742	R/B/G130H/0.25X2.0		
	Y1DC0109T		1993 Sep 14	2704	R/B/G130H/0.25X2.0		
1103-006	Y12B0502T		1992 Dec 29	498	S/A/G190H/4.3	BIN	0.12
	Y12B0503T		1992 Dec 29	240	S/A/G270H/4.3		
1104+167	Y1450903T		1992 Oct 30	1921	R/A/G190H/0.25X2.0	BIN+PK	0.034
	Y1450904T		1992 Oct 30	1921	R/A/G190H/0.25X2.0		
	Y1450905T		1992 Oct 30	1222	R/A/G270H/0.25X2.0		
	Y1450906T	1.094	1992 Oct 30	563	R/B/G160L/1.0	OFF	
1111+408	Y0PE0802T		1992 Apr 15	1109	S/A/G190H/4.3	BIN	0.12
	Y0PE0803T		1992 Apr 15	1109	S/A/G190H/4.3		
	Y0PE0804T		1992 Apr 15	1373	S/A/G270H/4.3		
	Y0PE0805T		1992 Apr 15	1151	S/A/G400H/4.3		
1115+080	Y0J30K08T		1991 Apr 15	487	S/B/PRISM/1.0	BIN	0.12
	Y0J30O06T		1991 May 31	487	S/B/PRISM/1.0	BIN	0.12
1116+215	Y17J0103T		1993 Feb 19	1878	R/A/G190H/0.25X2.0	BIN+PK	0.034
	Y17J0104T	1.054	1993 Feb 19	751	R/A/G270H/0.25X2.0		
	Y17J0106T		1993 Feb 19	2181	R/B/G130H/0.25X2.0		
	Y17J0107T		1993 Feb 20	2181	R/B/G130H/0.25X2.0		
	Y17J0108T		1993 Feb 20	2181	R/B/G130H/0.25X2.0		
	Y17J0109T		1993 Feb 20	2181	R/B/G130H/0.25X2.0		

Table 1—Continued

Target	Rootname	Scale Factor[a]	Observation Date	Exp. Time (s)	FOS Configuration[b]	Targ. Acq. Strategy[c]	Targ. Acq. Uncert.[d] (″)
1123+594	Y1HI0L02T		1993 Jul 07	360	S/B/G160L/4.3	PK	0.4
B3 1123+395	Y1HI0N02T		1993 Jul 06	360	S/B/G160L/4.3	PK	0.4
1127-145	Y12B0602T		1993 Jan 01	533	S/A/G270H/4.3	BIN	0.12
1130+111	Y0RV0603T		1992 Mar 07	1574	R/A/G190H/0.25X2.0	BIN+PK	0.034
	Y0RV0604T		1992 Mar 07	1574	R/A/G190H/0.25X2.0		
	Y0RV0605T		1992 Mar 07	1574	R/A/G190H/0.25X2.0		
	Y0RV0606T		1992 Mar 07	1610	R/A/G270H/0.25X2.0		
	Y0RV0607T		1992 Mar 07	563	R/B/G160L/1.0	OFF	
NGC 3783	Y10Z0103M		1992 Jul 27	2099	S/B/G190H/1.0	BIN	0.12
	Y10Z0104M		1992 Jul 27	1799	S/B/G130H/1.0		
	Y10Z0105M		1992 Jul 27	1799	S/B/G130H/1.0		
1136-135	Y0RV0T03T		1992 Jan 30	1870	R/A/G190H/0.25X2.0	BIN+PK	0.034
	Y0RV0T04T		1992 Jan 30	1870	R/A/G190H/0.25X2.0		
	Y0RV0T05T		1992 Jan 30	1250	R/A/G270H/0.25X2.0		
	Y0RV0T06T		1992 Jan 30	530	R/B/G160L/1.0	OFF	
1137+660	Y0PE0902T		1991 Nov 06	533	S/A/G190H/4.3	BIN	0.12
	Y0PE0903T		1991 Nov 06	275	S/A/G270H/4.3		
	Y0PE0904T		1991 Nov 06	204	S/A/G400H/4.3		
	Y0RV1H03T		1991 Dec 12	2447	R/A/G190H/0.25X2.0	BIN+PK	0.034
	Y0RV1H04T		1991 Dec 12	703	R/A/G270H/0.25X2.0		
	Y0XX0602T		1992 May 19	516	R/B/G160L/1.0	BIN	0.12
1144-379	Y1HI0P02T		1993 Jul 15	399	S/A/G270H/4.3	PK	0.4
1146+111	Y1F90303T		1993 Jun 17	2142	S/A/G190H/4.3	PK2	0.35
	Y1F90304T		1993 Jun 17	2142	S/A/G270H/4.3		
1148+549	Y1HI0R02T		1993 Jul 08	679	S/A/G190H/4.3	PK	0.4
	Y1HI0S02T		1993 Jul 08	399	S/A/G270H/4.3	PK	0.4
1156+631	Y1HI0U02T		1993 Jul 08	679	S/A/G270H/4.3	PK	0.4

Table 1—Continued

Target	Rootname	Scale Factor[a]	Observation Date	Exp. Time (s)	FOS Configuration[b]	Targ. Acq. Strategy[c]	Targ. Acq. Uncert.[d] (″)
1202+281	Y17J0203T		1992 Dec 14	1690	R/A/G190H/0.25X2.0	BIN+PK	0.034
	Y17J0204T		1992 Dec 14	1690	R/A/G190H/0.25X2.0		
	Y17J0205T		1992 Dec 14	1314	R/A/G270H/0.25X2.0		
1206+459	Y0RV0803T		1992 Jan 28	1509	R/A/G190H/0.25X2.0	BIN+PK	0.034
	Y0RV0804T		1992 Jan 28	1509	R/A/G190H/0.25X2.0		
	Y0RV0805T		1992 Jan 28	1509	R/A/G190H/0.25X2.0		
	Y0RV0806T	1.061	1992 Jan 28	1030	R/A/G270H/0.25X2.0		
	Y0RV0807T		1992 Jan 28	530	R/B/G160L/1.0	OFF	
NGC 4151	Y0YC0102T		1992 Jun 22	360	S/B/G130H/1.0	BIN	0.12
	Y0YC0103T		1992 Jun 22	360	S/B/G130H/1.0		
	Y0YC0104T		1992 Jun 22	360	S/B/G130H/1.0		
	Y0YC0202T		1992 Jun 23	360	S/B/G130H/1.0		
	Y0YC0203T		1992 Jun 23	360	S/B/G130H/1.0		
	Y0YC0204T		1992 Jun 23	360	S/B/G130H/1.0		
	Y0YC0402T	3.720	1992 Jun 25	360	S/B/G130H/1.0	BIN	0.12
	Y0YC0403T	3.720	1992 Jun 25	360	S/B/G130H/1.0		
	Y0YC0404T	3.720	1992 Jun 25	360	S/B/G130H/1.0		
	Y0YC0602T		1992 Jun 27	360	S/B/G130H/1.0	BIN	0.12
	Y0YC0603T		1992 Jun 27	360	S/B/G130H/1.0		
	Y0YC0604T		1992 Jun 27	360	S/B/G130H/1.0		
	Y19G0303T		1993 Apr 22	150	S/A/G570H/0.3	BIN+PK	0.05
	Y19G0304T		1993 Apr 22	120	S/A/G400H/0.3		
	Y19G0305T		1993 Apr 22	120	S/A/G270H/0.3		
NGC 4151 CLOUD A	Y19G0306T		1993 Apr 22	249	S/A/G570H/0.3	BIN+PK+OFF	0.05
	Y19G0307T	1.050	1993 Apr 22	200	S/A/G400H/0.3		
	Y19G0308T		1993 Apr 22	200	S/A/G270H/0.3		
NGC 4151 CLOUD B	Y19G0309T		1993 Apr 22	249	S/A/G570H/0.3	BIN+PK+OFF	0.05

Table 1—Continued

Target	Rootname	Scale Factor[a]	Observation Date	Exp. Time (s)	FOS Configuration[b]	Targ. Acq. Strategy[c]	Targ. Acq. Uncert.[d] (″)
	Y19G030AT		1993 Apr 22	200	S/A/G400H/0.3		
	Y19G030BT		1993 Apr 22	200	S/A/G270H/0.3		
NGC 4151 CLOUD C	Y19G030CT		1993 Apr 22	569	S/A/G570H/0.3	BIN+PK+OFF	0.05
	Y19G030DT		1993 Apr 22	569	S/A/G400H/0.3		
NGC 4151 CLOUD E	Y19G030ET		1993 Apr 22	600	S/A/G570H/0.3	BIN+PK+OFF	0.05
NGC 4151 CLOUD F	Y19G030FT		1993 Apr 22	600	S/A/G570H/0.3	BIN+PK+OFF	0.05
1208+101A	Y0UV0103T		1992 Mar 21	563	R/A/G650L/0.3	BIN+PK	0.03
1208+101B	Y0UV0104T		1992 Mar 22	2141	R/A/G650L/0.3	BIN+PK+OFF	0.03
PG 1211+143	Y0IZ0303T		1991 Apr 13	50	S/B/G130H/4.3	BIN	0.12
	Y0IZ0304T		1991 Apr 13	2000	S/B/G130H/1.0		
	Y0IZ0305T		1991 Apr 13	2000	S/B/G130H/1.0		
	Y0IZ0403T		1991 Apr 16	50	S/A/G270H/4.3	BIN	0.12
	Y0IZ0404T		1991 Apr 16	349	S/A/G270H/1.0		
	Y0IZ0405T		1991 Apr 16	50	S/A/G190H/4.3		
	Y0IZ0406T		1991 Apr 16	1339	S/A/G190H/1.0		
	Y0IZ0407T		1991 Apr 16	50	S/A/PRISM/4.3		
1215+113	Y0RV1C02T		1992 Jan 26	1677	R/B/G160L/1.0	BIN	0.12
1216+069	Y10G0503T		1993 Mar 15	1314	R/A/G270H/0.25X2.0	BIN+PK	0.025
	Y10G0504T		1993 Mar 15	1878	R/A/G190H/0.25X2.0		
	Y10G0505T		1993 Mar 15	1878	R/A/G190H/0.25X2.0		
	Y1450D03T		1993 Mar 16	2413	R/B/G130H/0.25X2.0	BIN+PK	0.034
	Y1450D04T		1993 Mar 16	2412	R/B/G130H/0.25X2.0		
	Y1450D05T		1993 Mar 16	2412	R/B/G130H/0.25X2.0		
	Y1450D06T		1993 Mar 16	2412	R/B/G130H/0.25X2.0		
	Y1450D07T		1993 Mar 16	2412	R/B/G130H/0.25X2.0		
	Y1450D08T		1993 Mar 16	2412	R/B/G130H/0.25X2.0		
	Y1450D09T		1993 Mar 16	2412	R/B/G130H/0.25X2.0		

Table 1—Continued

Target	Rootname	Scale Factor[a]	Observation Date	Exp. Time (s)	FOS Configuration[b]	Targ. Acq. Strategy[c]	Targ. Acq. Uncert.[d] (″)
MRK 205	Y0NA0103T		1991 Jul 11	1414	R/A/G270H/0.25X2.0	BIN+PK	0.025
	Y0NA0105T		1991 Jul 11	1945	R/A/G190H/0.25X2.0		
	Y0NA0106T		1991 Jul 11	1591	R/A/G190H/0.25X2.0		
	Y1HI0X02T	1.500	1993 Jul 18	759	S/B/G130H/4.3	PK	0.4
NGC 4395	Y0ZQ0102T		1992 Jul 15	2219	S/B/G130H/4.3	BIN	0.12
	Y0ZQ0103T		1992 Jul 15	2229	S/B/G130H/4.3		
	Y0ZQ0104T		1992 Jul 15	2229	S/B/G130H/4.3		
	Y0ZQ0105T		1992 Jul 15	2229	S/B/G130H/4.3		
	Y0ZQ0106T		1992 Jul 15	2229	S/B/G130H/4.3		
	Y0ZQ0107T		1992 Jul 15	2229	S/B/G130H/4.3		
	Y0ZQ0108T		1992 Jul 15	2229	S/B/G130H/4.3		
	Y0ZQ0202T	1.170	1992 Jul 19	1939	S/A/G190H/4.3	BIN	0.12
	Y0ZQ0203T	1.170	1992 Jul 19	1939	S/A/G190H/4.3		
	Y0ZQ0204T	1.170	1992 Jul 19	1939	S/A/G190H/4.3		
	Y0ZQ0205T		1992 Jul 19	1932	S/A/G270H/4.3		
1226+023	Y0G40106T		1991 Jan 16	500	S/B/G130H/4.3	PK+BIN+PK	0.030
	Y0G40107T		1991 Jan 16	1000	S/B/G130H/1.0		
	Y0G40109T		1991 Jan 16	1500	S/B/G130H/0.5		
	Y0G4010BT		1991 Jan 16	1300	S/B/G130H/0.3		
	Y0G4010CT		1991 Jan 16	1300	S/B/G130H/0.3		
	Y0G4010FT		1991 Jan 17	2000	S/B/G130H/0.25X2.0	PK+BIN+PK2	0.025
	Y0G40206T		1991 Jan 14	366	R/A/G190H/4.3	PK+BIN+PK	0.030
	Y0G40207T		1991 Jan 14	705	R/A/G190H/1.0		
	Y0G40209T	1.119	1991 Jan 14	1071	R/A/G190H/0.5		
	Y0G4020BT	1.735	1991 Jan 14	930	R/A/G190H/0.3		
	Y0G4020CT	1.735	1991 Jan 14	930	R/A/G190H/0.3		
	Y0G4020ET	1.828	1991 Jan 15	930	R/A/G270H/0.3		

Table 1—Continued

Target	Rootname	Scale Factor[a]	Observation Date	Exp. Time (s)	FOS Configuration[b]	Targ. Acq. Strategy[c]	Targ. Acq. Uncert.[d] (″)
	Y0G4020FT	1.828	1991 Jan 15	930	R/A/G270H/0.3		
	Y0G4020HT	1.179	1991 Jan 15	1071	R/A/G270H/0.5		
	Y0G4020JT	1.054	1991 Jan 15	705	R/A/G270H/1.0		
	Y0G4020LT	1.054	1991 Jan 15	366	R/A/G270H/4.3		
	Y0G4020NT	1.159	1991 Jan 15	1410	R/A/G270H/0.25X2.0	PK+BIN+PK2	0.025
	Y0G4020PT	1.099	1991 Jan 15	1410	R/A/G190H/0.25X2.0		
NGC 4486	Y15N0303T		1992 Dec 16	1099	S/A/G270H/0.3	BIN+PK	0.05
	Y15N0304T		1992 Dec 16	1099	S/A/G400H/0.3		
	Y15N0305T		1992 Dec 16	1099	S/A/G570H/0.3		
NGC 4486 JET KNOT-A	Y15N0306T		1992 Dec 16	2199	S/A/G270H/1.0	BIN+PK+OFF	0.05
NGC 4486 CLOUD-A	Y15N0307T		1992 Dec 17	1300	S/A/G270H/0.3	BIN+PK+OFF	0.05
	Y15N0308T		1992 Dec 17	1300	S/A/G400H/0.3		
	Y15N0309T		1992 Dec 17	1300	S/A/G570H/0.3		
1229-021	Y0PL0203T		1991 Dec 03	999	S/A/G160L/4.3	BIN	0.12
	Y0ZW0102T		1992 Dec 24	2028	R/B/G160L/1.0	BIN	0.12
	Y0ZW0103T		1992 Dec 24	2028	R/B/G160L/1.0		
1230+097	Y1HI1302T		1993 Jul 21	639	S/A/G190H/4.3	PK	0.4
1241+176	Y10G0403T		1992 Dec 08	2441	R/A/G270H/0.25X2.0	BIN+PK	0.025
1244+324	Y0RV0K02T		1992 Jan 31	1331	R/B/G160L/1.0	BIN	0.12
1246-057	Y1080102T		1992 Nov 26	901	R/B/G160L/4.3	BIN	0.12
	Y1080103T		1992 Nov 26	473	R/B/PRISM/4.3		
	Y1HQ0104T		1993 Aug 02	80	S/A/G270H/1.0	PK3	0.18
	Y1HQ0105T		1993 Aug 02	2289	S/A/G270H/1.0		
	Y1HQ0106T		1993 Aug 02	2289	S/A/G270H/1.0		
	Y1HQ0107T		1993 Aug 02	2289	S/A/G270H/1.0		
1250+568	Y0PE0A02T		1991 Nov 02	1986	S/A/G190H/4.3	BIN	0.12
	Y0PE0A03T		1991 Nov 02	1121	S/A/G270H/4.3		

Table 1—Continued

Target	Rootname	Scale Factor[a]	Observation Date	Exp. Time (s)	FOS Configuration[b]	Targ. Acq. Strategy[c]	Targ. Acq. Uncert.[d] (″)
	Y0PE0A04T		1991 Nov 02	863	S/A/G400H/4.3		
1252+119	Y0RV0Z03T		1992 Mar 19	1828	R/A/G190H/0.25X2.0	BIN+PK	0.034
	Y0RV0Z04T		1992 Mar 19	1828	R/A/G190H/0.25X2.0		
	Y0RV0Z05T		1992 Mar 19	1827	R/A/G190H/0.25X2.0		
	Y0RV0Z06T		1992 Mar 19	1827	R/A/G190H/0.25X2.0		
	Y0RV0Z07T	1.077	1992 Mar 19	1949	R/A/G270H/0.25X2.0		
	Y0RV0Z08T	1.089	1992 Mar 19	853	R/B/G160L/1.0	OFF	
1253-055	Y0PE0B02T		1992 Apr 08	1269	S/A/G190H/4.3	BIN	0.12
	Y0PE0B03T		1992 Apr 08	1279	S/A/G190H/4.3		
	Y0PE0B04T		1992 Apr 08	1278	S/A/G270H/4.3		
	Y0PE0B05T		1992 Apr 08	917	S/A/G400H/4.3		
1254+047	Y1450E03T	1.075	1993 Feb 17	2290	R/A/G190H/0.25X2.0	BIN+PK	0.034
	Y1450E04T	1.075	1993 Feb 17	2290	R/A/G190H/0.25X2.0		
	Y1450E05T	1.075	1993 Feb 17	2290	R/A/G190H/0.25X2.0		
	Y1450E06T	1.075	1993 Feb 17	2290	R/A/G190H/0.25X2.0		
	Y1450E07T	1.075	1993 Feb 17	1992	R/A/G270H/0.25X2.0		
	Y1450E08T		1993 Feb 17	853	R/B/G160L/1.0	OFF	
1257+346	Y1L00203T		1993 Dec 03	601	R/A/G270H/0.25X2.0	BIN+PK	0.034
	Y1L00204T		1993 Dec 03	2216	R/A/G270H/0.25X2.0		
	Y1L00205T		1993 Dec 03	1352	R/A/G270H/0.25X2.0		
1257+286	Y1HI1402T		1993 Jul 15	759	S/B/G130H/4.3	PK	0.4
1259+593	Y0RV1J03T		1991 Dec 27	2398	R/A/G190H/0.25X2.0	BIN+PK	0.034
	Y0RV1J04T		1991 Dec 27	879	R/A/G270H/0.25X2.0		
	Y0VM0303T		1992 Feb 28	2739	R/B/G130H/0.25X2.0	BIN+PK	0.034
	Y0VM0304T		1992 Feb 28	2739	R/B/G130H/0.25X2.0		
	Y0VM0305T		1992 Feb 28	2739	R/B/G130H/0.25X2.0		
	Y0VM0306T		1992 Feb 28	2739	R/B/G130H/0.25X2.0		

Table 1—Continued

Target	Rootname	Scale Factor[a]	Observation Date	Exp. Time (s)	FOS Configuration[b]	Targ. Acq. Strategy[c]	Targ. Acq. Uncert.[d] (″)
	Y0VM0307T		1992 Feb 28	2739	R/B/G130H/0.25X2.0		
	Y0VM0308T		1992 Feb 28	2738	R/B/G130H/0.25X2.0		
	Y0VM0309T		1992 Feb 28	2738	R/B/G130H/0.25X2.0		
1302-102	Y1020103T		1992 Jul 17	2441	R/A/G190H/0.25X2.0	BIN+PK	0.034
	Y1020104T		1992 Jul 17	939	R/A/G270H/0.25X2.0		
1306+303	Y1HI1502T		1993 Jul 17	480	S/B/G160L/4.3	PK	0.4
	Y1HI1602T	1.263	1993 Jul 16	560	S/A/G270H/4.3	PK	0.4
1307+085	Y1HK0102T		1993 Jul 21	480	S/A/G190H/4.3	PK	0.4
1317+277	Y0RV0X03T		1992 Jan 20	1492	R/A/G190H/0.25X2.0	BIN+PK	0.034
	Y0RV0X04T		1992 Jan 20	1492	R/A/G190H/0.25X2.0		
	Y0RV0X05T		1992 Jan 20	1492	R/A/G190H/0.25X2.0		
	Y0RV0X06T		1992 Jan 20	1026	R/A/G270H/0.25X2.0		
	Y0RV0X07T	1.045	1992 Jan 20	797	R/B/G160L/1.0	OFF	
1317+520	Y1HK0402T		1993 Jul 08	480	S/B/G160L/4.3	PK	0.4
	Y1HK0502T		1993 Jul 19	520	S/A/G270H/4.3	PK	0.4
1318+290	Y1550302T		1992 Nov 27	1000	S/B/G160L/1.0	BIN	0.12
1321+294	Y1HK0602T		1993 Jul 15	480	S/B/G160L/4.3	PK	0.4
1328+307	Y0PL0103T		1991 Dec 03	899	S/A/G160L/4.3	BIN	0.12
1332+552	Y1HK0802T		1993 Jul 15	480	S/B/G160L/4.3	PK	0.4
1333+176	Y0RV1103T		1992 Feb 12	1633	R/A/G190H/0.25X2.0	BIN+PK	0.034
	Y0RV1104T		1992 Feb 12	1633	R/A/G190H/0.25X2.0		
	Y0RV1105T		1992 Feb 13	1092	R/A/G270H/0.25X2.0		
	Y0RV1106T		1992 Feb 13	530	R/B/G160L/1.0	OFF	
1334-005	Y1290102T		1993 Feb 06	1126	R/B/G160L/4.3	BIN	0.12
	Y1290103T		1993 Feb 06	563	R/B/PRISM/4.3		
1338+416	Y0RV1K03T		1992 Feb 15	1060	R/A/G270H/0.25X2.0	BIN+PK	0.034
	Y0RV1K04T		1992 Feb 15	797	R/B/G160L/1.0	OFF	

Table 1—Continued

Target	Rootname	Scale Factor[a]	Observation Date	Exp. Time (s)	FOS Configuration[b]	Targ. Acq. Strategy[c]	Targ. Acq. Uncert.[d] (″)
1340+606	Y12B0702T		1993 Apr 06	883	S/A/G270H/4.3	BIN	0.12
	Y12B0703T		1993 Apr 06	879	S/A/G270H/4.3		
1340+289	Y0RV0L02T		1992 Feb 03	1060	R/B/G160L/1.0	BIN	0.12
1347+539	Y0RV1D02T		1991 Dec 27	1538	R/B/G160L/1.0	BIN	0.12
1349+001	Y1HK0A02T		1993 Jul 25	480	S/B/G160L/4.3	PK	0.4
1351+640	Y0P80303T		1991 Sep 05	1599	S/B/G130H/0.25X2.0	BIN+PK	0.025
	Y0P80304T		1991 Sep 05	1599	S/B/G130H/0.25X2.0		
	Y0P80305T		1991 Sep 05	1400	S/B/G270H/0.25X2.0		
	Y0P80306T		1991 Sep 05	1500	S/B/G190H/0.25X2.0		
	Y0P80307T		1991 Sep 05	1500	S/B/G190H/0.25X2.0		
1352+011	Y0RV0A03T		1991 Dec 14	1768	R/A/G190H/0.25X2.0	BIN+PK	0.034
	Y0RV0A04T		1991 Dec 14	1768	R/A/G190H/0.25X2.0		
	Y0RV0A05T		1991 Dec 14	1768	R/A/G190H/0.25X2.0		
	Y0RV0A06T	1.033	1991 Dec 14	1167	R/A/G270H/0.25X2.0		
	Y0RV0A07T	1.033	1991 Dec 14	530	R/B/G160L/1.0	OFF	
1354+195	Y0RV1303T		1992 Feb 26	1758	R/A/G190H/0.25X2.0	BIN+PK	0.034
	Y0RV1304T		1992 Feb 26	1758	R/A/G190H/0.25X2.0		
	Y0RV1305T		1992 Feb 26	1077	R/A/G270H/0.25X2.0		
	Y0RV1306T		1992 Feb 27	530	R/B/G160L/1.0	OFF	
	Y12B0802T	1.224	1993 Apr 29	492	S/A/G190H/4.3	BIN	0.12
	Y12B0803T	1.224	1993 Apr 29	221	S/A/G270H/4.3		
	Y12B0804T	1.224	1993 Apr 29	173	S/A/G400H/4.3		
1355-416	Y1HK0B02T		1993 Jul 15	639	S/A/G190H/4.3	PK	0.4
1356+581	Y1F90602T		1993 Aug 09	659	S/A/G270H/4.3	BIN	0.12
1401+098	Y1HK0D02T		1993 Jul 25	639	S/A/G190H/4.3	PK	0.4
1402+261	Y1HK0E02T		1993 Jul 19	560	S/A/G190H/4.3	PK	0.4
1407+265	Y0RV0C03T		1992 Mar 08	2134	R/A/G190H/0.25X2.0	BIN+PK	0.034

Table 1—Continued

Target	Rootname	Scale Factor[a]	Observation Date	Exp. Time (s)	FOS Configuration[b]	Targ. Acq. Strategy[c]	Targ. Acq. Uncert.[d] (″)
	Y0RV0C04T		1992 Mar 08	2134	R/A/G190H/0.25X2.0		
	Y0RV0C05T		1992 Mar 08	1126	R/A/G270H/0.25X2.0		
	Y0RV0C06T	1.064	1992 Mar 08	676	R/B/G160L/1.0	OFF	
PG 1411+442	Y11U0103T	1.064	1992 Oct 03	751	R/A/G270H/0.25X2.0	BIN+PK	0.025
	Y11U0104T		1992 Oct 03	1878	R/A/G190H/0.25X2.0		
	Y11U0202T		1992 Oct 03	2593	R/B/G130H/0.25X2.0	BIN+PK+OFF+PK	0.034
	Y11U0203T		1992 Oct 03	2592	R/B/G130H/0.25X2.0		
	Y11U0204T		1992 Oct 03	2592	R/B/G130H/0.25X2.0		
1413+117A	Y1FB0203T		1993 Jun 23	1760	S/A/G570H/0.5	INT+PK	0.055
	Y1FB0204T		1993 Jun 23	1759	S/A/G570H/0.5		
1413+117D	Y1FB0206T		1993 Jun 23	1200	S/A/G570H/0.5	PK	0.055
	Y1FB0207T		1993 Jun 23	709	S/A/G570H/0.5		
	Y1FB0208T		1993 Jun 23	2109	S/A/G570H/0.5		
	Y1FB020AT		1993 Jun 23	1699	S/A/G570H/0.5	PK	0.055
1413+117B	Y1FB0303T		1993 Jun 27	2227	S/A/G570H/0.5	INT+PK	0.055
	Y1FB0304T		1993 Jun 27	2219	S/A/G570H/0.5		
1413+117C	Y1FB0306T		1993 Jun 27	1320	S/A/G570H/0.5	PK	0.055
	Y1FB0307T		1993 Jun 27	650	S/A/G570H/0.5		
	Y1FB0308T		1993 Jun 27	2169	S/A/G570H/0.5		
	Y1FB030AT		1993 Jun 27	999	S/A/G570H/0.5	PK	0.055
1415+451	Y10Q0203T		1992 Sep 06	1502	R/A/G270H/0.25X2.0	BIN+PK	0.025
1415+172	Y0RV1X02T		1992 Feb 11	1519	R/B/G160L/1.0	BIN	0.12
NGC 5548 (Low Flux)	Y0YA0202T		1992 Jul 05	1649	S/B/G130H/1.0	BIN	0.12
	Y0YA0203T		1992 Jul 05	1649	S/B/G130H/1.0		
	Y0YA0204T		1992 Jul 05	1200	S/B/G190H/1.0		
	Y0YA0205T		1992 Jul 05	480	S/B/G270H/1.0		
NGC 5548	Y1BP0104T		1993 Apr 19	1295	S/B/G190H/4.3	PK3	0.18

Table 1—Continued

Target	Rootname	Scale Factor[a]	Observation Date	Exp. Time (s)	FOS Configuration[b]	Targ. Acq. Strategy[c]	Targ. Acq. Uncert.[d] (″)
	Y1BP0105T	1.082	1993 Apr 19	1750	S/B/G130H/4.3		
	Y1BP0204T		1993 Apr 20	1295	S/B/G190H/4.3	PK3	0.18
	Y1BP0205T	1.082	1993 Apr 20	1750	S/B/G130H/4.3		
	Y1BP0304T		1993 Apr 21	1295	S/B/G190H/4.3	PK3	0.18
	Y1BP0305T	1.082	1993 Apr 21	1750	S/B/G130H/4.3		
	Y1BP0404T		1993 Apr 22	1295	S/B/G190H/4.3	PK3	0.18
	Y1BP0405T	1.082	1993 Apr 22	1750	S/B/G130H/4.3		
	Y1BP0504T		1993 Apr 23	1295	S/B/G190H/4.3	PK3	0.18
	Y1BP0505T	1.082	1993 Apr 23	1750	S/B/G130H/4.3		
	Y1BP0604T		1993 Apr 24	1295	S/B/G190H/4.3	PK3	0.18
	Y1BP0605T	1.082	1993 Apr 24	1750	S/B/G130H/4.3		
	Y1BP0704T		1993 Apr 25	1295	S/B/G190H/4.3	PK3	0.18
	Y1BP0705T	1.082	1993 Apr 25	1750	S/B/G130H/4.3		
	Y1BP0804T		1993 Apr 26	1295	S/B/G190H/4.3	PK3	0.18
	Y1BP0805T	1.082	1993 Apr 26	1750	S/B/G130H/4.3		
	Y1BP0904T		1993 Apr 27	1295	S/B/G190H/4.3	PK3	0.18
	Y1BP0905T	1.082	1993 Apr 27	1750	S/B/G130H/4.3		
	Y1BP0A04T		1993 Apr 28	1295	S/B/G190H/4.3	PK3	0.18
	Y1BP0A05T	1.082	1993 Apr 28	1750	S/B/G130H/4.3		
	Y1BP0B04M		1993 Apr 29	1295	S/B/G190H/4.3	PK3	0.18
	Y1BP0B05T	1.082	1993 Apr 29	1750	S/B/G130H/4.3		
	Y1BP0C04T		1993 Apr 30	1295	S/B/G190H/4.3	PK3	0.18
	Y1BP0C05T	1.082	1993 Apr 30	1750	S/B/G130H/4.3		
	Y1BP0D04T		1993 May 01	1295	S/B/G190H/4.3	PK3	0.18
	Y1BP0D05T	1.082	1993 May 01	1750	S/B/G130H/4.3		
	Y1BP0E04T		1993 May 02	1295	S/B/G190H/4.3	PK3	0.18
	Y1BP0E05T	1.082	1993 May 02	1750	S/B/G130H/4.3		

Table 1—Continued

Target	Rootname	Scale Factor[a]	Observation Date	Exp. Time (s)	FOS Configuration[b]	Targ. Acq. Strategy[c]	Targ. Acq. Uncert.[d] (″)
	Y1BP0F04T		1993 May 03	1295	S/B/G190H/4.3	PK3	0.18
	Y1BP0F05T	1.082	1993 May 03	1750	S/B/G130H/4.3		
	Y1BP0G04T		1993 May 04	1295	S/B/G190H/4.3	PK3	0.18
	Y1BP0G05T	1.082	1993 May 04	1750	S/B/G130H/4.3		
	Y1BP0H04T		1993 May 05	1295	S/B/G190H/4.3	PK3	0.18
	Y1BP0H05T	1.082	1993 May 05	1750	S/B/G130H/4.3		
	Y1BP0I04T		1993 May 06	1295	S/B/G190H/4.3	PK3	0.18
	Y1BP0I05T	1.082	1993 May 06	1750	S/B/G130H/4.3		
	Y1BP0J04T		1993 May 07	1295	S/B/G190H/4.3	PK3	0.18
	Y1BP0J05T	1.082	1993 May 07	1750	S/B/G130H/4.3		
	Y1BP0K04T		1993 May 08	1295	S/B/G190H/4.3	PK3	0.18
	Y1BP0K05T	1.082	1993 May 08	1750	S/B/G130H/4.3		
	Y1BP0L04T		1993 May 09	1295	S/B/G190H/4.3	PK3	0.18
	Y1BP0L05T	1.082	1993 May 09	1750	S/B/G130H/4.3		
	Y1BP0M04T		1993 May 10	1295	S/B/G190H/4.3	PK3	0.18
	Y1BP0M05T	1.082	1993 May 10	1750	S/B/G130H/4.3		
	Y1BP0N04T		1993 May 11	1295	S/B/G190H/4.3	PK3	0.18
	Y1BP0N05T	1.082	1993 May 11	1750	S/B/G130H/4.3		
	Y1BP0O04T		1993 May 12	1295	S/B/G190H/4.3	PK3	0.18
	Y1BP0O05T	1.082	1993 May 12	1750	S/B/G130H/4.3		
	Y1BP0P04T		1993 May 13	1295	S/B/G190H/4.3	PK3	0.18
	Y1BP0P05T	1.082	1993 May 13	1750	S/B/G130H/4.3		
	Y1BP0Q04T		1993 May 14	1295	S/B/G190H/4.3	PK3	0.18
	Y1BP0Q05M	1.082	1993 May 14	1750	S/B/G130H/4.3		
	Y1BP0R04T		1993 May 15	1295	S/B/G190H/4.3	PK3	0.18
	Y1BP0R05T	1.082	1993 May 15	1750	S/B/G130H/4.3		
	Y1BP0S04T		1993 May 16	1295	S/B/G190H/4.3	PK3	0.18

Table 1—Continued

Target	Rootname	Scale Factor[a]	Observation Date	Exp. Time (s)	FOS Configuration[b]	Targ. Acq. Strategy[c]	Targ. Acq. Uncert.[d] (″)
	Y1BP0S05T	1.082	1993 May 16	1750	S/B/G130H/4.3		
	Y1BP0T04T		1993 May 17	1295	S/B/G190H/4.3	PK3	0.18
	Y1BP0T05T	1.082	1993 May 17	1750	S/B/G130H/4.3		
	Y1BP0U04T		1993 May 18	1295	S/B/G190H/4.3	PK3	0.18
	Y1BP0U05T	1.082	1993 May 18	1750	S/B/G130H/4.3		
	Y1BP0V04T		1993 May 19	1295	S/B/G190H/4.3	PK3	0.18
	Y1BP0V05T	1.082	1993 May 19	1750	S/B/G130H/4.3		
	Y1BP0W04T		1993 May 20	1295	S/B/G190H/4.3	PK3	0.18
	Y1BP0W05T	1.082	1993 May 20	1750	S/B/G130H/4.3		
	Y1BP0X04T		1993 May 21	1295	S/B/G190H/4.3	PK3	0.18
	Y1BP0X05T	1.082	1993 May 21	1750	S/B/G130H/4.3		
	Y1BP0Y04T		1993 May 22	1295	S/B/G190H/4.3	PK3	0.18
	Y1BP0Y05T	1.082	1993 May 22	1750	S/B/G130H/4.3		
	Y1BP0Z04T		1993 May 23	1295	S/B/G190H/4.3	PK3	0.18
	Y1BP0Z05T	1.082	1993 May 23	1750	S/B/G130H/4.3		
	Y1BP1004T		1993 May 24	1295	S/B/G190H/4.3	PK3	0.18
	Y1BP1005T	1.082	1993 May 24	1750	S/B/G130H/4.3		
	Y1BP1104T		1993 May 25	1295	S/B/G190H/4.3	PK3	0.18
	Y1BP1105T	1.082	1993 May 25	1750	S/B/G130H/4.3		
	Y1BP1204T		1993 May 26	1295	S/B/G190H/4.3	PK3	0.18
	Y1BP1205T	1.082	1993 May 26	1750	S/B/G130H/4.3		
	Y1BP1304T		1993 May 27	1295	S/B/G190H/4.3	PK3	0.18
	Y1BP1305T	1.082	1993 May 27	1750	S/B/G130H/4.3		
1424-118	Y0RV1503T		1992 Mar 13	1654	R/A/G190H/0.25X2.0	BIN+PK	0.034
	Y0RV1504T		1992 Mar 13	1654	R/A/G190H/0.25X2.0		
	Y0RV1505T		1992 Mar 13	1654	R/A/G190H/0.25X2.0		
	Y0RV1506T		1992 Mar 13	1653	R/A/G190H/0.25X2.0		

Table 1—Continued

Target	Rootname	Scale Factor[a]	Observation Date	Exp. Time (s)	FOS Configuration[b]	Targ. Acq. Strategy[c]	Targ. Acq. Uncert.[d] (″)
	Y0RV1507T		1992 Mar 13	1893	R/A/G270H/0.25X2.0		
	Y0RV1508T		1992 Mar 13	563	R/B/G160L/1.0	OFF	
1425+200	Y1HK0F02T		1993 Jul 07	560	S/A/G190H/4.3	BIN	0.12
1435-015	Y1HK0K02T		1993 Jul 19	360	S/B/G160L/4.3	BIN	0.12
1435+638	Y0D95103T		1991 Nov 02	1591	R/A/G270H/0.25X2.0	BIN+PK	0.025
	Y0D95104T		1991 Nov 03	1591	R/A/G270H/0.25X2.0		
MRK 478	Y1HK0L02T		1993 Aug 01	679	S/A/G190H/4.3	PK	0.4
1442+101	Y0LF0303T		1991 Jun 06	50	S/B/G160L/4.3	BIN	0.12
	Y0LF0304T		1991 Jun 06	1200	S/B/G160L/4.3		
	Y0LF0305T		1991 Jun 06	50	S/B/G160L/4.3		
	Y0LF0306T		1991 Jun 06	600	S/B/PRISM/4.3		
1444+407	Y10Q0303T		1992 Sep 05	1314	R/A/G270H/0.25X2.0	BIN+PK	0.025
	Y10Q0304T		1992 Sep 05	1690	R/A/G190H/0.25X2.0		
	Y10Q0305T		1992 Sep 05	1690	R/A/G190H/0.25X2.0		
1451-375	Y1IP0504T		1993 Aug 06	220	S/B/G190H/1.0	PK3	0.18
	Y1IP0505T		1993 Aug 06	2469	S/B/G190H/1.0		
	Y1IP0506T		1993 Aug 06	637	S/B/G190H/1.0		
1512+370	Y0RV1703T		1992 Jan 26	1449	R/A/G190H/0.25X2.0	BIN+PK	0.034
	Y0RV1704T		1992 Jan 26	1449	R/A/G190H/0.25X2.0		
	Y0RV1705T		1992 Jan 26	1449	R/A/G190H/0.25X2.0		
	Y0RV1706T		1992 Jan 26	1379	R/A/G270H/0.25X2.0		
1522+101	Y0UW0102T		1992 Mar 14	100	S/A/G270H/4.3	BIN	0.12
	Y0UW0103T		1992 Mar 14	1318	R/A/G270H/1.0		
	Y0UW0104T		1992 Mar 14	1318	R/A/G270H/1.0		
	Y0UW0105T		1992 Mar 14	2371	R/A/G190H/1.0		
	Y0UW0106T		1992 Mar 14	2371	R/A/G190H/1.0		
	Y0UW0107T		1992 Mar 14	2371	R/A/G190H/1.0		

Table 1—Continued

Target	Rootname	Scale Factor[a]	Observation Date	Exp. Time (s)	FOS Configuration[b]	Targ. Acq. Strategy[c]	Targ. Acq. Uncert.[d] (″)
	Y0UW0108T		1992 Mar 14	2371	R/A/G190H/1.0		
	Y0UW0109T	1.058	1992 Mar 14	1878	R/B/G160L/1.0	OFF	
	Y0UW010AT	1.058	1992 Mar 14	1878	R/B/G160L/1.0		
	Y0UW010BT	1.058	1992 Mar 14	1878	R/B/G160L/1.0		
	Y0UW010CT	1.058	1992 Mar 14	100	S/B/G160L/4.3		
1538+477	Y11U0303T		1992 Sep 25	1878	R/A/G270H/0.25X2.0	BIN+PK	0.025
	Y1450G03T	1.206	1993 Apr 13	2441	R/A/G190H/0.25X2.0	BIN+PK	0.034
	Y1450G04T	1.206	1993 Apr 13	2441	R/A/G190H/0.25X2.0		
	Y1450G05T	1.206	1993 Apr 13	2441	R/A/G190H/0.25X2.0		
	Y1450G06T	1.308	1993 Apr 13	563	R/B/G160L/1.0	OFF	
1543+489	Y1HK0O02T		1993 Jul 07	759	S/B/G130H/4.3	PK	0.4
1545+210	Y0PE0C02T		1992 Apr 10	1149	S/B/G130H/4.3	BIN	0.12
	Y0PE0C03T		1992 Apr 10	1160	S/B/G130H/4.3		
	Y0PE0D02T		1992 Apr 08	383	S/A/G190H/4.3	BIN	0.12
	Y0PE0D03T		1992 Apr 08	224	S/A/G270H/4.3		
	Y0PE0D04T		1992 Apr 08	156	S/A/G400H/4.3		
1555+332	Y12B0902T		1993 May 22	1017	S/A/G270H/4.3	BIN	0.12
1611+343	Y0PE0F02T		1992 Apr 04	875	S/A/G270H/4.3	BIN	0.12
	Y0PE0F03T		1992 Apr 04	689	S/A/G400H/4.3		
1612+261	Y1HK0P02T		1993 Jul 23	639	S/A/G190H/4.3	PK	0.4
1618+177	Y0PE0G02T	1.345	1991 Sep 07	648	S/A/G190H/4.3	BIN	0.12
	Y0PE0G03T	1.276	1991 Sep 07	344	S/A/G270H/4.3		
	Y0PE0G04T	1.317	1991 Sep 07	252	S/A/G400H/4.3		
	Y0RV0E03T		1992 Apr 03	1824	R/A/G190H/0.25X2.0	BIN+PK	0.034
	Y0RV0E04T		1992 Apr 03	1824	R/A/G190H/0.25X2.0		
	Y0RV0E05T		1992 Apr 03	1824	R/A/G190H/0.25X2.0		
	Y0RV0E06T	1.062	1992 Apr 03	1838	R/A/G270H/0.25X2.0		

Table 1—Continued

Target	Rootname	Scale Factor[a]	Observation Date	Exp. Time (s)	FOS Configuration[b]	Targ. Acq. Strategy[c]	Targ. Acq. Uncert.[d] (″)
	Y0RV0E07T		1992 Apr 03	563	R/B/G160L/1.0	OFF	
1628.5+3808	Y1550402M		1992 Oct 27	1000	S/B/G160L/1.0	BIN	0.12
1628.6+3806	Y1550502T		1992 Nov 01	1000	S/B/G160L/1.0	BIN	0.12
1631+395	Y1HK0R02T		1993 Jul 21	399	S/A/G270H/4.3	PK	0.4
1634+706	Y0D95203T		1991 Nov 03	1414	R/A/G270H/0.25X2.0	BIN+PK	0.025
	Y0D95204T		1991 Nov 03	1414	R/A/G270H/0.25X2.0		
1637+574	Y1170502T		1992 Aug 11	1313	S/A/G190H/4.3	BIN	0.12
	Y1170503T		1992 Aug 11	563	S/A/G270H/4.3		
	Y1170504T		1992 Aug 11	450	S/A/G400H/4.3		
1641+399	Y0PE0I02T		1992 Jun 07	425	S/A/G190H/4.3	BIN	0.12
	Y0PE0I03T		1992 Jun 07	224	S/A/G270H/4.3		
	Y0PE0I04T		1992 Jun 07	189	S/A/G400H/4.3		
1656+053	Y0RV1Y02T		1992 Feb 19	1060	R/B/G160L/1.0	BIN	0.12
1700+518	Y1020203T		1992 Aug 17	2499	R/B/G130H/0.25X2.0	BIN+PK	0.034
	Y1020204T		1992 Aug 17	2499	R/B/G130H/0.25X2.0		
	Y1020205T		1992 Aug 18	2498	R/B/G130H/0.25X2.0		
	Y1020206T		1992 Aug 18	2498	R/B/G130H/0.25X2.0		
	Y1020207T		1992 Aug 18	2498	R/B/G130H/0.25X2.0		
	Y1020208T		1992 Aug 18	2498	R/B/G130H/0.25X2.0		
	Y1450H03T		1992 Dec 12	2026	R/A/G190H/0.25X2.0	BIN+PK	0.034
	Y1450H04T		1992 Dec 12	859	R/A/G270H/0.25X2.0		
1700+642	Y0TK0103T		1992 Feb 13	2799	S/B/G130H/0.25X2.0	BIN+PK	0.028
	Y0TK0104T		1992 Feb 14	2809	S/B/G130H/0.25X2.0		
	Y0TK0105T		1992 Feb 14	2809	S/B/G130H/0.25X2.0		
	Y0TK0106T		1992 Feb 14	2809	S/B/G130H/0.25X2.0		
	Y0TK0107T		1992 Feb 14	2809	S/B/G130H/0.25X2.0		
	Y0TK0203T		1991 Dec 13	2679	S/A/G190H/0.25X2.0	BIN+PK	0.028

Table 1—Continued

Target	Rootname	Scale Factor[a]	Observation Date	Exp. Time (s)	FOS Configuration[b]	Targ. Acq. Strategy[c]	Targ. Acq. Uncert.[d] (″)
	Y0TK0204T		1991 Dec 13	2679	S/A/G190H/0.25X2.0		
	Y0TK0205T		1991 Dec 13	2689	S/A/G190H/0.25X2.0		
	Y0TK0206T		1991 Dec 13	2689	S/A/G190H/0.25X2.0		
	Y0TK0207T		1991 Dec 13	2689	S/A/G190H/0.25X2.0		
	Y0TK0208T		1991 Dec 14	2689	S/A/G190H/0.25X2.0		
	Y0TK0209T		1991 Dec 14	2249	S/A/G270H/0.25X2.0		
	Y0TK020AT		1991 Dec 14	2249	S/A/G270H/0.25X2.0		
	Y0TK020BT		1991 Dec 14	2249	S/A/G270H/0.25X2.0		
	Y0TK020CT		1991 Dec 14	2249	S/A/G270H/0.25X2.0		
1704+608	Y0RV0G03T		1991 Oct 22	1884	R/A/G190H/0.25X2.0	BIN+PK	0.034
	Y0RV0G04T		1991 Oct 22	697	R/A/G270H/0.25X2.0		
	Y0VM0103T		1992 Feb 15	2652	R/B/G130H/0.25X2.0	BIN+PK	0.034
	Y0VM0104T		1992 Feb 15	2652	R/B/G130H/0.25X2.0		
	Y0VM0105T		1992 Feb 15	2652	R/B/G130H/0.25X2.0		
	Y0VM0106T		1992 Feb 15	2652	R/B/G130H/0.25X2.0		
	Y0VM0107T		1992 Feb 15	2652	R/B/G130H/0.25X2.0		
	Y0VM0108T		1992 Feb 15	2652	R/B/G130H/0.25X2.0		
1716+5010	Y1460902T		1992 Sep 28	1399	S/A/G190H/4.3	BIN	0.12
	Y1460903T		1992 Sep 28	1399	S/A/G190H/4.3		
	Y1460904T		1992 Sep 28	1399	S/A/G190H/4.3		
	Y1460905T		1992 Sep 28	1399	S/A/G190H/4.3		
	Y1460A02T		1992 Sep 28	1399	S/A/G190H/4.3	BIN	0.12
	Y1460A03T		1992 Sep 28	1399	S/A/G190H/4.3		
	Y1460A04T		1992 Sep 28	1399	S/A/G190H/4.3		
	Y1460A05T		1992 Sep 28	1399	S/A/G190H/4.3		
1718+481	Y1C30303T		1993 May 13	2579	R/A/G190H/0.25X2.0	BIN+PK	0.034
	Y1C30304T		1993 May 13	1126	R/A/G270H/0.25X2.0		

Table 1—Continued

Target	Rootname	Scale Factor[a]	Observation Date	Exp. Time (s)	FOS Configuration[b]	Targ. Acq. Strategy[c]	Targ. Acq. Uncert.[d] (″)
1821+643	Y0NT0303T		1991 Jul 08	1520	R/A/G190H/0.25X2.0	BIN+PK	0.025
	Y0NT0305T		1991 Jul 08	2121	R/A/G270H/0.25X2.0		
	Y0D90303T		1991 Jul 22	1659	S/B/G130H/0.25X2.0	BIN+PK	0.025
	Y0D90304T		1991 Jul 22	1669	S/B/G130H/0.25X2.0		
	Y0D90305T		1991 Jul 22	1669	S/B/G130H/0.25X2.0		
1928+738	Y10G0603T		1992 Oct 12	1540	R/A/G270H/0.25X2.0	BIN+PK	0.025
	Y10G0604T		1992 Oct 12	2066	R/A/G190H/0.25X2.0		
	Y10G0605T		1992 Oct 12	2066	R/A/G190H/0.25X2.0		
3C 405	Y1BF0102T		1993 May 23	1905	S/B/G160L/4.3	BIN+OFF	0.12
	Y1BF0103T		1993 May 23	1899	S/B/G160L/4.3		
	Y1BF0104T		1993 May 23	1909	S/B/G160L/4.3		
	Y1BF0105T		1993 May 23	1905	S/A/G270H/4.3	OFF	
	Y1BF0106T		1993 May 23	1899	S/A/G270H/4.3		
	Y1BF0107T		1993 May 23	1909	S/A/G270H/4.3		
MRK 509	Y0YA0302T		1992 Jun 21	2099	S/B/G130H/1.0	BIN	0.12
	Y0YA0303T		1992 Jun 21	2099	S/B/G130H/1.0		
	Y0YA0304T		1992 Jun 21	1620	S/B/G190H/1.0		
	Y0YA0305T	1.029	1992 Jun 21	600	S/B/G270H/1.0		
2112+059	Y10G0203T		1992 Sep 19	2371	R/A/G190H/0.25X2.0	BIN+PK	0.025
	Y10G0204T		1992 Sep 19	2371	R/A/G190H/0.25X2.0		
	Y10G0205T		1992 Sep 19	1690	R/A/G270H/0.25X2.0		
2128-123	Y1HE0F03T		1993 Nov 02	864	R/A/G190H/0.25X2.0	BIN+PK	0.034
	Y1HE0F04T		1993 Nov 02	2404	R/A/G190H/0.25X2.0		
	Y1HE0F05T		1993 Nov 02	1953	R/A/G190H/0.25X2.0		
	Y1HE0F06T		1993 Nov 02	150	R/A/G270H/0.25X2.0		
	Y1HE0F07T		1993 Nov 02	1690	R/A/G270H/0.25X2.0		
2135-147	Y10F0102T		1992 Sep 13	2369	R/B/G130H/1.0	BIN	0.12

Table 1—Continued

Target	Rootname	Scale Factor[a]	Observation Date	Exp. Time (s)	FOS Configuration[b]	Targ. Acq. Strategy[c]	Targ. Acq. Uncert.[d] (″)
	Y10F0103T		1992 Sep 13	2419	R/B/G130H/1.0		
	Y10F0104T		1992 Sep 13	2181	R/A/G190H/1.0		
2141+175	Y0UE0103T		1992 Jan 07	2042	R/B/G130H/1.0	BIN	0.12
	Y0UE0104T		1992 Jan 07	2042	R/B/G130H/1.0		
	Y0UE0105T	1.055	1992 Jan 07	1046	R/A/G270H/1.0	OFF	
	Y0UE0106T		1992 Jan 07	1001	R/A/G190H/1.0		
	Y0UE0107T		1992 Jan 07	100	S/A/G190H/4.3		
2145+067	Y0RV0M03T		1991 Oct 22	1485	R/A/G190H/0.25X2.0	BIN+PK	0.034
	Y0RV0M04T		1991 Oct 22	1485	R/A/G190H/0.25X2.0		
	Y0RV0M05T	1.103	1991 Oct 22	904	R/A/G270H/0.25X2.0		
2155-304	Y0NB0207T		1991 Jul 10	1500	S/B/G130H/1.0	BIN	0.12
2201+315	Y0PE0J02T		1991 Sep 07	1389	S/B/G130H/4.3	BIN	0.12
	Y0PE0J03T		1991 Sep 07	1400	S/B/G130H/4.3		
	Y0PE0J04T		1991 Sep 07	1103	S/B/G190H/4.3		
	Y0PE0K02T	1.055	1991 Sep 06	221	S/A/G270H/4.3	BIN	0.12
	Y0PE0K03T	1.055	1991 Sep 06	131	S/A/G400H/4.3		
2215-037	Y1HK0W02T		1993 Jul 09	759	S/B/G130H/4.3	PK	0.4
2216-038	Y1EM0102P		1993 Oct 03	665	S/A/G190H/4.3	BIN	0.12
	Y1EM0103P		1993 Oct 03	486	S/A/G270H/4.3		
	Y1EM0104P		1993 Oct 03	294	S/A/G400H/4.3		
2223-052	Y0PE0M02T		1991 Sep 11	966	S/A/G270H/4.3	BIN	0.12
	Y0PE0M03T		1991 Sep 11	960	S/A/G270H/4.3		
	Y0PE0M04T		1991 Sep 11	147	S/A/G400H/4.3		
2230+114	Y0PE0N02T		1991 Sep 12	953	S/A/G270H/4.3	BIN	0.12
	Y0PE0N03T		1991 Sep 12	648	S/A/G400H/4.3		
2243-123	Y1450J03T		1993 Oct 09	2281	R/A/G190H/0.25X2.0	BIN+PK	0.034
	Y1450J04T		1993 Oct 09	2281	R/A/G190H/0.25X2.0		

Table 1—Continued

Target	Rootname	Scale Factor[a]	Observation Date	Exp. Time (s)	FOS Configuration[b]	Targ. Acq. Strategy[c]	Targ. Acq. Uncert.[d] (″)
	Y1450J05T		1993 Oct 09	2281	R/A/G190H/0.25X2.0		
	Y1450J06T		1993 Oct 09	2192	R/A/G270H/0.25X2.0		
	Y1450J07T		1993 Oct 09	563	R/B/G160L/1.0	OFF	
2251+158 (Low Flux)	Y0PE0002T		1991 Sep 11	504	S/A/G190H/4.3	BIN	0.12
	Y0PE0003T		1991 Sep 11	953	S/A/G270H/4.3		
	Y0PE0004T		1991 Sep 12	648	S/A/G400H/4.3		
2251+158	Y0RV1M03T		1991 Nov 15	1531	R/A/G190H/0.25X2.0	BIN+PK	0.034
	Y0RV1M04T		1991 Nov 15	1531	R/A/G190H/0.25X2.0		
	Y0RV1M05T		1991 Nov 15	1531	R/A/G190H/0.25X2.0		
	Y0RV1M06T		1991 Nov 15	1244	R/A/G270H/0.25X2.0		
	Y0RV1N01T		1991 Nov 15	530	R/B/G160L/1.0	OFF	
2251+113	Y0PE0P02T		1991 Sep 06	1980	S/B/G130H/4.3	BIN	0.12
	Y0PE0P03T		1991 Sep 06	731	S/B/G190H/4.3		
	Y0PE0Q02T		1991 Sep 06	162	S/A/G270H/4.3	BIN	0.12
	Y0PE0Q03T		1991 Sep 06	140	S/A/G400H/4.3		
	Y0RV0H03T		1991 Oct 23	1769	R/A/G190H/0.25X2.0	BIN+PK	0.034
	Y0RV0H04T		1991 Oct 23	1769	R/A/G190H/0.25X2.0		
	Y0RV0H05T		1991 Oct 23	1769	R/A/G190H/0.25X2.0		
	Y0RV0H06T		1991 Oct 23	1368	R/A/G270H/0.25X2.0		
	Y1450K03T		1992 Dec 04	2538	R/B/G130H/0.25X2.0	BIN+PK	0.034
	Y1450K04T		1992 Dec 04	2538	R/B/G130H/0.25X2.0		
	Y1450K05T		1992 Dec 04	2537	R/B/G130H/0.25X2.0		
	Y1450K06T		1992 Dec 04	2537	R/B/G130H/0.25X2.0		
	Y1450K07T		1992 Dec 04	2537	R/B/G130H/0.25X2.0		
	Y1450K08T		1992 Dec 04	2537	R/B/G130H/0.25X2.0		
	Y1450K09T		1992 Dec 04	2537	R/B/G130H/0.25X2.0		
2300-683	Y0RV1003T		1992 Jun 16	2613	R/A/G190H/0.25X2.0	BIN+PK	0.034

Table 1—Continued

Target	Rootname	Scale Factor[a]	Observation Date	Exp. Time (s)	FOS Configuration[b]	Targ. Acq. Strategy[c]	Targ. Acq. Uncert.[d] (″)
	Y0RV1004T		1992 Jun 16	2613	R/A/G190H/0.25X2.0		
	Y0RV1005T		1992 Jun 16	1782	R/A/G270H/0.25X2.0		
	Y0RV1006T		1992 Jun 16	563	R/B/G160L/1.0		
2308+098	Y14K0202T		1992 Oct 12	995	R/A/G270H/1.0	BIN	0.12
	Y14K0203T		1992 Oct 12	1878	R/A/G190H/1.0		
	Y14K0204T		1992 Oct 12	1878	R/A/G190H/1.0		
	Y1HK0Z02T		1993 Jul 07	480	S/B/G130H/4.3	PK	0.4
2340-036	Y0RV1Q03T		1991 Oct 28	1363	R/A/G190H/0.25X2.0	BIN+PK	0.034
	Y0RV1Q04T		1991 Oct 28	1363	R/A/G190H/0.25X2.0		
	Y0RV1Q05T		1991 Oct 28	1363	R/A/G190H/0.25X2.0		
	Y0WR6103T	1.197	1993 Jan 18	1308	R/A/G270H/0.25X2.0	BIN+PK	0.034
	Y0WR6104T	1.124	1993 Jan 18	563	R/B/G160L/1.0		
2344+092	Y1450L03T		1992 Oct 07	2561	R/A/G190H/0.25X2.0	BIN+PK	0.034
	Y1450L04T		1992 Oct 07	2561	R/A/G190H/0.25X2.0		
	Y1450L05T		1992 Oct 07	1656	R/A/G270H/0.25X2.0		
	Y1450L06T		1992 Oct 07	563	R/B/G160L/1.0	OFF	
2349-014	Y1HK1002T		1993 Jul 09	480	S/A/G190H/4.3	PK	0.4
2352-342	Y0RV1S03T		1992 Jun 24	1726	R/A/G190H/0.25X2.0	BIN+PK	0.034
	Y0RV1S04T		1992 Jun 24	1726	R/A/G190H/0.25X2.0		
	Y0RV1S05T		1992 Jun 24	1726	R/A/G190H/0.25X2.0		
	Y0RV1S06T		1992 Jun 24	1632	R/A/G270H/0.25X2.0		
	Y0RV1S07T		1992 Jun 24	563	R/B/G160L/1.0		

[a]Multiplicative scale factor applied to dataset flux values, as described in section 4.3.4.

[b]Groundmode (R = RAPID-READOUT, S = SPECTROSCOPY)/Detector (A = AMBER, B = BLUE)/Disperser/Aperture.

[c]BIN = Binary Search, BLIND = Blind Pointing (no target acquisition), INT = Interactive Acquisition, OFF = Offset (from previous pointing, or sideswitch), PK(n) = Peakup (n-stage) (*e.g.*, BIN+PK+OFF+PK represents a target acquisition sequence consisting of a binary search followed by a peakup, an offset from the peakup position, and another peakup after the offset.

[d]*Nominal* uncertainty of the final step of the target acquisition strategy in arcseconds.

Table 2. FOS Disperser Overlap Region Statistics

Dispersers	Mean Ratio[a]	Standard Deviation[a]	Median Ratio[a]
All	0.976 (0.920)	0.065 (0.221)	0.975 (0.971)
High resolution	0.971 (0.937)	0.054 (0.160)	0.973 (0.970)
High resolution (RD/RD)	0.972 (0.946)	0.052 (0.145)	0.973 (0.972)
High resolution (BL/BL)	0.969 (0.927)	0.067 (0.132)	0.976 (0.971)
High resolution (BL/RD)	0.956 (0.802)	0.070 (0.333)	0.951 (0.948)
High/low resolution[b]	1.000 (0.978)	0.090 (0.202)	1.006 (1.006)
NGC 5548 sample[c]	1.023 (1.150)	0.025 (0.384)	1.026 (1.029)

[a]The values listed first are for the "good" overlaps which range from 0.8 to 1.25; the corresponding values for the entire sample are given in parentheses.

[b]The low resolution dispersers include the G160L and G650L grating and the PRISM.

[c]This is a uniform sample of 39 observations consisting of G130H and G190H spectra of the nucleus of NGC 5548 obtained with the *FOS* blue detector. A three stage peakup target acquisition strategy was used for each observation.